LA-6926-C

Conference Proceedings

UC-34c

Issued: August 1977

c.3

Lectures from the

LAMPF Summer School

On Nuclear Structure with Pions and Protons

June 22—24, 1977

Compiled by

R. L. Burman
B. F. Gibson, V

los alamos
scientific laboratory
of the University of California
LOS ALAMOS, NEW MEXICO 87545

An Affirmative Action/Equal Opportunity Employer

In the interest of time, these papers are reproduced as submitted by the authors.

FOREWORD

The Summer School on Nuclear Structure with Pions and Protons grew out of the previous LAMPF Users Meeting, where it was felt that the organizational and inclusive nature of the users meeting did not allow time for detailed examination of the basic physics involved in the LAMPF experiments. A Summer School, on the other hand, could focus on the particular physics of interest and could operate in a relaxed atmosphere conducive to learning. We chose to cover only a fraction of the research done at LAMPF, that involving the study of nuclear structure using pions or high-energy protons as probes.

It was apparent that recent high-quality data have already had a significant influence on our understanding of pion and high-energy proton reactions. Although the speakers were nominally balanced between theorists and experimentalists, a great deal of overlap occurred as these Proceedings will show. An amusing highlight of the school occurred when just-released copies of preliminary data were eagerly grabbed up by theorists.

We appreciate the promptness with which these manuscripts were submitted by the speakers, thus allowing rapid publication of the Proceedings. We would like to thank Harold Agnew (Director of the Laboratory) for making available the new National Security and Resource Study Center which was especially useful in fostering both informal and semi-formal discussions among the Conference participants, and Louis Rosen (Director of LAMPF) for his support in making the Summer School possible. We also wish to thank Carl Cuntz, Floyd Archuleta, and Molly Maveety at the Study Center and Eleanor Dunn of MP Division for their help in making the Summer School operation go smoothly. We wish to acknowledge Darragh Nagle for his opening remarks and M. Cooper, R. Silbar, B. Zeidman, G. Emery, E. Rost, and J. Ginocchio for serving ably as session chairmen. Finally, we express our grateful appreciation to Linda Robinson for her efforts in preparation for and attending to the details of the Summer School, as well as typing of the manuscripts in this volume.

Organizing Committee:

R. L. Burman (LASL)
B. F. Gibson (LASL)
E. Rost (University of Colorado)
R. J. Peterson (University of Colorado)

CONTENTS

THE PION-NUCLEUS MANY-BODY PROBLEM

G. E. Brown

Department of Physics
State University of New York

1. INTRODUCTION

The scattering of low-energy pions by nuclei has traditionally been discussed within the framework of pions interacting with and scattering between scattering centers, fixed or moving. This is a very restricted description of the richness of particle-nucleon interactions within the nucleus, and opening up this description brings in new features, especially those connected with exchange of virtual ρ-mesons[1-3], which turn out to be crucial for an understanding of low-energy pion-nucleus interactions. These new features provide important clues for the description of what would otherwise be surprising features of low-energy (∿50 MeV) pion-nucleus scattering.

One can label these new features as arising from short-range correlations. Whereas this is true, the ρ-exchange effects are particularly important because they provide a spin- and isospin-dependent interaction so that, so to speak, a pion can be absorbed by one nucleon, emitted by another, the relevant spin and isospin degrees of freedom being transmitted by the virtual ρ-meson being exchanged between the two nucleons. This is shown graphically in Fig. 1.
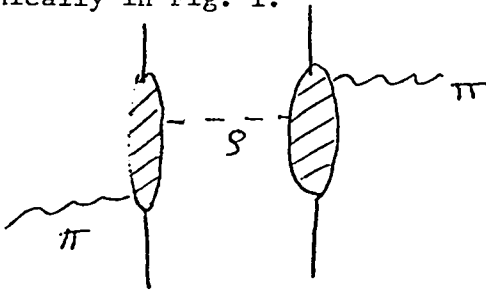

Fig. 1. A scattering, mediated by ρ-meson exchange, involving
two nucleons.

In this figure, the cross-hatched areas represent all possibilities of particles and interactions but, as we shall see later, nucleons and the $\Delta(1230)$-isobar play a special role.

At this state we should note that in so far as processes such as shown in Fig. 1 are important, Bég's theorem[5] is violated, although it holds, or course, for those processes involving only intermediate pions. The satisfaction of conditions for this theorem require the distance between nucleons to be greater than the range of interaction. In the nature of things, interactions seen from only the pionic point of view proceeding through virtual ρ-meson exchange involve two nucleons and must necessarily have range equal to the distance between nucleons.

As we shall see, processes like that shown in Fig. 1 are coherent with, and of opposite sign to, the processes involving a pion between the two nucleons, at least in the low-energy regime. Thus, nuclei even as heavy as Pb^{208}, are sufficiently transparent to π-mesons that there is a good chance of a 50 MeV incident meson traversing the whole nucleus. This opens up the exciting prospect of using low-energy pions to investigate many features of nuclear structure. Ironically, this transparency arises just because the dominant pion-nucleon interaction is strong and of short-range, as we shall see.

2. SCHEMATIC MODEL OF π-NUCLEUS SCATTERING

We begin by studying the double scattering terms, using a schematic model. This model consists of allowing only nucleon intermediate states, and only uncrossed meson exchanges. Whereas the crossed meson exchanges are just as important as the uncrossed ones for low-energy incident pions – and, within the static approximation, cancel them[6,7] – we shall see that our schematic model can later be generalized to include isobars, which give the dominant contributions.

Our model describes the scattering as shown in Fig. 2.

Fig. 2. Double Scattering Terms in the Model.
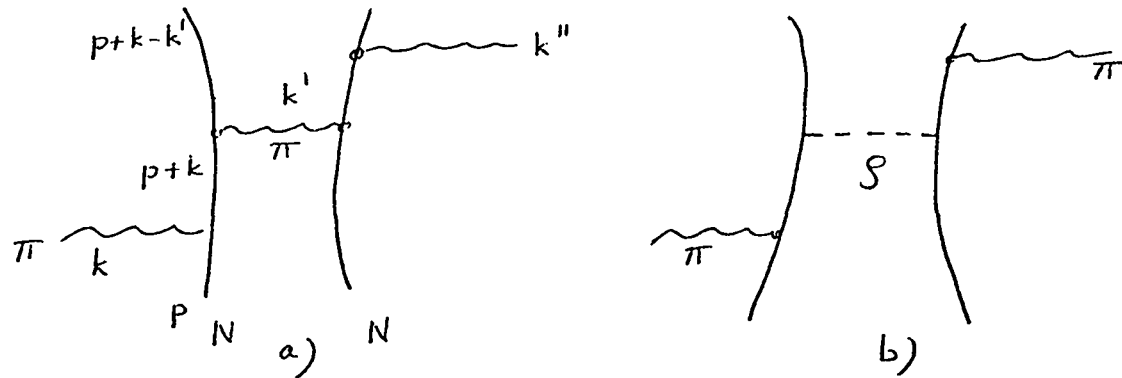
We shall consistently neglect nucleon energies (static approximation). We take the canonical pion-nucleon and rho-nucleon interactions[7]

$$\delta H_\pi = \frac{f_\pi}{m_\pi} \, \bar\psi \, \sigma \cdot \nabla (\vec{\tau} \cdot \vec{\phi}_\pi) \psi(x) \quad .$$

$$\delta H_\rho = \frac{f_\rho}{m_\rho} \, \bar\psi \, [\sigma \times \nabla](\vec{\tau} \cdot \vec{\rho}) \psi(x) \tag{1}$$

where $(f_\pi^2/4\pi) = 0.08$ and, whereas f_ρ is less well determined, the quantity of importance

$$\frac{f_\pi^2}{m_\pi^2} < \frac{f_\rho^2}{m_\rho^2} < 2.5 \, \frac{f_\pi^2}{m_\pi^2} \, . \tag{1.1}$$

It should be noted that within an optical model description, the processes, Figs. 2a) and b), are treated on a different footing. The process a) would, together with all higher terms in multiple scattering, be included by inserting the pion-nucleon elastic scattering amplitude as an optical model potential, and then solving an optical-model equation. Process b) can be included[1] as a modification, of Lorentz-Lorenz form, to this potential, but it will be more convenient for our later purposes to consider both as double scatterings, as shown in Fig. 2.

The exchange of pion and virtual rho mesons in Fig. 2 gives rise to the interactions[7,8],

$$V_\pi = - \frac{f_\pi^2}{m_\pi^2} \, (\vec{\tau}_1 \cdot \vec{\tau}_2) \, \frac{\sigma_1 \cdot k \; \sigma_2 \cdot k}{k^2 + m_\pi^2 - \omega^2} \, ,$$

$$V_\rho = - \frac{f_\rho^2}{m_\rho^2} \, (\vec{\tau}_1 \cdot \vec{\tau}_2) \, \frac{[\sigma_1 \times k][\sigma_2 \times k]}{k^2 + m_\rho^2 - \omega^2} \, , \tag{2}$$

the modification from the incident energy ω^2 carried by the incoming pion being the ω^2 term in the denominator.

It is convenient to decompose V_π and V_ρ into irreducible tensors

$$V_\pi = - \frac{f_\pi^2}{m_\pi^2} (\vec{\tau}_1 \cdot \vec{\tau}_2) \{ \frac{\sigma_1 \cdot k\, \sigma_2 \cdot k - \frac{1}{3} \sigma_1 \cdot \sigma_2\, k^2}{k^2 + m_\pi^2 - \omega^2}$$

$$+ \frac{1}{3} \sigma_1 \cdot \sigma_2 - \frac{1}{3} \sigma_1 \cdot \sigma_2 \frac{m_\pi^2 - \omega^2}{k^2 + m_\pi^2 - \omega^2} \}$$

$$(2.1)$$

$$V_\rho = - \frac{f_\rho^2}{m_\rho^2} (\vec{\tau}_1 \cdot \vec{\tau}_2) \{ - \frac{[\sigma_1 \cdot k\, \sigma_2 \cdot k - \frac{1}{3} \sigma_1 \cdot \sigma_2\, k^2]}{k^2 + m_\rho^2 - \omega^2}$$

$$+ \frac{2}{3} \sigma_1 \cdot \sigma_2 - \frac{2}{3} \sigma_1 \cdot \sigma_2 \frac{m_\rho^2 - \omega^2}{k^2 + m_\rho^2 - \omega^2} \} .$$

The first term in each pair of brackets gives rise to a tensor-like inter-
action; the second term, when Fourier transformed, will behave like

$\sigma_1 \cdot \sigma_2 (\vec{\tau}_1 \cdot \vec{\tau}_2) \delta(r_1 - r_2)$ in configuration space, and the third term is

Yukawa in nature.

Let us now assume that, in addition to the π- and ρ-exchanges shown

in Fig. 2, the two nucleons exchange any number of ω-mesons. The ω-mesons

are coupled very strongly to the nucleons, with[9] an effective coupling

constant given by $(g_\omega^2/4\pi) \sim 10$ to 20, and their exchange provides a

short-range repulsion, strong enough to keep nucleons apart from one another*.

Thus, we drop the δ-function terms in (2.1). Dropping the δ-function piece

in V_π is equivalent to making[6] the Ericson-Ericson, Lorentz-Lorenz correction[10]

to this order.

---

* From the empirical behavior of the electromagnetic form-factor, it is
  known that vector-meson exchange must be modified at short distances;
  we really assume here only that the nucleons be kept apart. This same
  feature would be expected to persist in the quark model, or whatever
  model is used for the short distance behavior.

There has been considerable controversy about whether the δ-function piece in V_π can be dropped[11,12]; introduction of a finite-range π-nucleon vertex allows this δ-function to "leak out" beyond the short-range correlations induced by the hard core. Careful evaluations[13] of this interaction seem to give a range somewhat smaller than assumed by these authors. In any case, we shall see that the ρ-meson exchange provides terms of the same nature and sign, and somewhat larger than the Lorentz-Lorenz correction.

Let us consider the terms in V_ρ in detail. The δ-function term has already been discarded. The tensor term is relatively ineffective in finite nuclei; its main effect is to couple S-states of relative motion of the two interacting nucleons to D-states, and these are suppressed at such short distances as $\hbar/m_\rho c$ by the centrifugal barrier. In shell-model calculations[14] in Pb^{208}, these terms contributed only negligibly. Thus, we are left with only the last term in eq. (2.1) which, when Fourier transformed becomes

$$V_\rho = \frac{2}{3} \frac{f_\rho^2}{4\pi} (\sigma_1 \cdot \sigma_2)(\vec{\tau}_1 \cdot \vec{\tau}_2) \frac{e^{-m_\rho r}}{r}. \tag{3}$$

So far, we have taken no account of the modifications due to ω-exchange; these are considerable, since the range of the ρ-exchange interaction is not much larger than that of the hard core repulsion. We can define[14] in a fairly obvious way an effective interaction

$$\hat{V}_\rho = \frac{2}{3} \frac{f_\rho^2}{4\pi} \, m_\rho \quad (\underset{\sim}{\sigma}_1 \cdot \underset{\sim}{\sigma}_2)(\vec{\tau}_1 \cdot \vec{\tau}_2) \frac{e^{-m_\rho r}}{m_\rho r} g(r) \qquad (4)$$

where $g(r)$ is the two-body correlation function of the two nucleons. We assume $g(r)$ to be independent of spin and isospin; this should be a good approximation if $g(r)$ results from ω-exchange.

Since V_ρ or $\hat{V}_\rho$ are short range, it often is a good approximation to make a zero-range approximation[2]

$$\hat{V}_\rho \simeq \frac{2}{3} \frac{f_\rho^2}{4\pi} \quad m_\rho \quad \underset{\sim}{\sigma}_1 \cdot \underset{\sim}{\sigma}_2 (\vec{\tau}_1 \cdot \vec{\tau}_2)(A/m_\rho^3)\delta(\underset{\sim}{r}_{12}), \qquad (5)$$

with

$$\frac{A}{m_\rho^3} = \int \frac{e^{-m_\rho r}}{m_\rho r} [g(r) - g(o)]d^3r. \qquad (5.1)$$

The $g(o)$ includes the effect from the δ-function piece of V_ρ, eq. (2.1), just in case $g(o) \neq 0$.

We have now reduced the problem of short-range correlations to its ultimate simplicity, relevant effective interactions being approximated by δ-functions. Taking into account the double scattering terms, Fig. 2, implies removing the $\delta(\underset{\sim}{r}_{12})$-piece from the pion propogator, and inserting the effective δ-function representing the effects of ρ-exchange. (Both of these modifications go in the same direction.) It is thus seen that contributions to the double scattering from short-range correlations will enter the double scattering through a ρ^2 terms, where ρ is the nucleon density; i.e., both nucleons will be at the same spatial point.

In fact, one can now see that ρ-exchange will contribute to the optical-model potential not only in order ρ^2, but also in order ρ^3 and ρ^4. The series must break off here, at least in our approximation of the ρ-exchange as zero range, because not more than four fermions can be

together at the same point. On the other hand, the δ-functions associated with pion exchange should be removed in all orders of ρ, since assuming short-range correlations to be effective in holding the nucleons apart, they shouldn't be there in the first place. We shall, therefore, later handle the two effects on a different footing.

Were we to stop in order ρ^2 in expansion of the optical-model potential, we would have

$$2\omega V_{opt} \cong -4\pi a(\omega) \; \nabla\rho\{1-C_2 \frac{4\pi}{3} a(\omega)\rho\}\nabla \tag{6}$$

where^2

$$C_2 = (1 + \frac{2f_\rho^2 m_\pi^2}{m_\rho^2 f_\pi^2} A) \tag{6.1}$$

with A given by (5.1).

The work of refs. 11 and 12 is addressed to cutting down the 1 on the right-hand side, replacing it by $\S_\pi$, where $0 < \S_\pi < 1$, as a result of the finite range of the pion-nucleon interaction. The work of ref. 3 calculates modifications from antisymmetry of the nucleons, but does not take into account exchange of σ, ω, etc. mesons in the exchange terms; these modify the conclusions of ref. 3.

3. CONTACT WITH REALITY
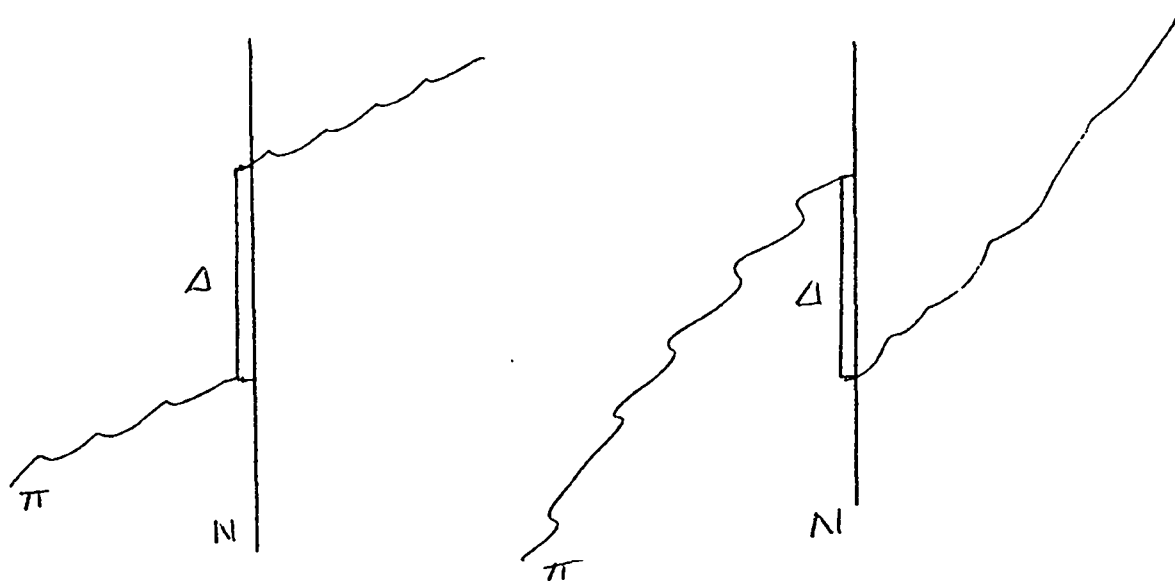
Fig. 3. Contributions of the Δ(1230) Resonance to Pion-Nucleon
Scattering.

In reality, the pion-nucleus scattering is given mainly by scattering

through the Δ(1230) isobar, as shown in fig. 3. Known properties of the

isobars will produce a lowest-order pion-nucleus scattering amplitude of

the Kisslinger[15] form

$$2\omega\, V_{opt} = -4\pi a(\omega)\nabla\rho\nabla \tag{7}$$

with appropriate values for $a(\omega)$ (see ref. 15).

The intermediate states in the double-scattering process, Fig. 2,

will also be isobars. With the assumption that the Δ(1230) isobar is

described in the same multiplet as the nucleon by the constituent quark

model (assumption of SU(4) symmetry for the quarks), all of our preceding

arguments will go through[7] except that

$$f_\pi{}^2 \to f_\pi{}^{*2}, \quad f_\rho{}^2 \to f_\rho{}^{*2},$$

where $f_\pi{}^{*2}$ is the $\pi N\Delta$ coupling constant,

$$\frac{f_\pi{}^{*2}}{4\pi} = \frac{72}{32}\; \frac{f_\pi{}^2}{4\pi} \tag{7.1}$$

and, in particular

$$f_\rho{}^{*2}/f_\rho{}^2 = f_\pi{}^{*2}/f_\pi{}^2. \tag{7.2}$$

These coupling constants are not given accurately by the quark model; it is known that the "Chew-Low value" for $f_\pi{}^{*2}$,

$$\frac{f_\pi{}^{*2}}{4\pi} = 4\; \frac{f_\pi{}^2}{4\pi} \tag{7.3}$$

fits the properties of the isobar better than the quark-model value (7.1), but we expect $f_\rho{}^*$ to be roughly given by (7.2). From the similarity of the ρ-field operator to the isovector electromagnetic current, we expect the ratio $f_\rho{}^*/f_\rho$ to be given fairly well by the quark model, which reproduces[16] to within 20-30% the photoproduction of the Δ-isobar.

4. MORE GENERAL CONSIDERATIONS

By this stage, the reader must feel that we are making a lot of formalism go only a little way. Following the refs. 11 and 3, let us show more generally what is going on.

Suppose we put the Kisslinger V_{opt} into a Klein-Gordon equation and iterate it in powers of V_{opt}, rather than solve the equation by direct numerical methods. We would then encounter first, second, etc. scatterings of the type shown in Fig. 4. Here

Single Scattering   Double Scattering   Triple Scattering
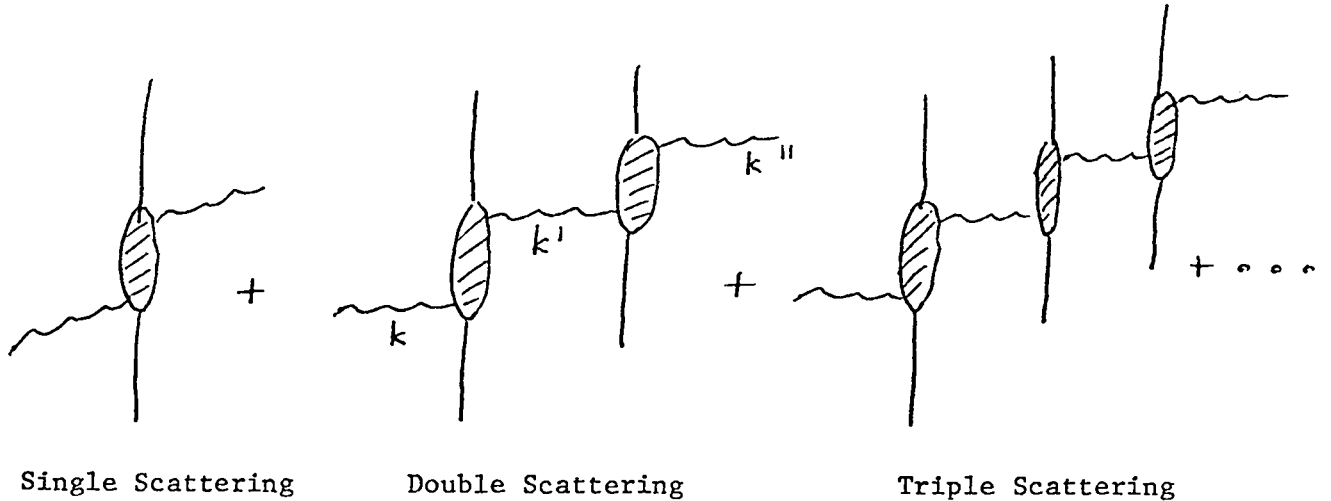
Fig. 4. Multiple Scattering Expansion Encountered in Solution of the Optical-Model Equation.

each blob represents the optical model potential. Thus, the double scattering is represented by

$$M_2 = 4\pi a(\omega)^2 \underset{\sim}{k} \cdot \underset{\sim}{k}' \frac{1}{k'^2 + m_\pi^2 - \omega^2} \underset{\sim}{k}' \cdot \underset{\sim}{k}''. \tag{8}$$

For simplicity, let us consider low-energy scattering where $\omega^2 \simeq m_\pi^2$. We can again decompose the double scattering into invariants,

$$\underset{\sim}{k} \cdot \underset{\sim}{k}' \, \frac{1}{k'^2} \, \underset{\sim}{k}' \cdot \underset{\sim}{k}'' = \frac{\underset{\sim}{k} \cdot \underset{\sim}{k}' \, \underset{\sim}{k}' \cdot \underset{\sim}{k} - \frac{1}{3} k \cdot k'' \, k'^2}{k'^2} + \frac{1}{3} \, k \cdot k'', \qquad (9)$$

consisting of a tensor and a δ-function. The term $(1/3)k \cdot k''$ does not

contain the variable k', and therefore will be multiplied by $\delta(\underset{\sim}{r}_1 - \underset{\sim}{r}_2)$

upon Fourier transforming. Now, as the energy of the pion goes to

zero – in practice, as $k/m_\pi \ll 1$ – the tensor term will go out, because

there is no preferred direction. Thus, we come to the simple, but

important, conclusion, that: Iteration of the Kisslinger potential

produces successive powers of δ-functions; i.e., of ρ^n terms. Any

short-range correlations which hold the nucleons apart will make these

terms inoperable.

Thus, in the above picture which includes only pions in zero-range

interaction with nucleons and some agency which holds nucleons apart

(literally, the picture of ref. 10), single scattering – i.e., impulse

approximation – should be good for small $k \ll m_\pi$, even though the inter-

action is strong. In practice, this seems to be true for light nuclei

still at 50 MeV as we shall discuss.

5. ANTISYMMETRY AND FINITE RANGE EFFECTS

Effects of antisymmetry have been discussed by Delorme and Ericson[17] for double scattering involving only pions, and by Thies[3] for pions and mesons. We shall see that their conclusions are strongly modified when other mesons, esp. the σ and ω, are included.

We first put the considerations of Delorme and Ericson into another language, as in ref. 7. In our intermediate isobar model of scattering, the direct and exchange double scattering terms would be as shown in fig. 5.
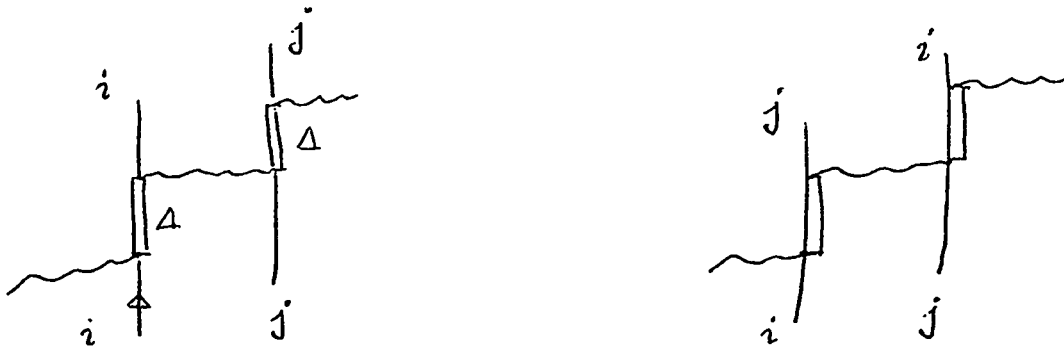
a) direct   b) exchange

Fig. 5. Double Scattering Terms.

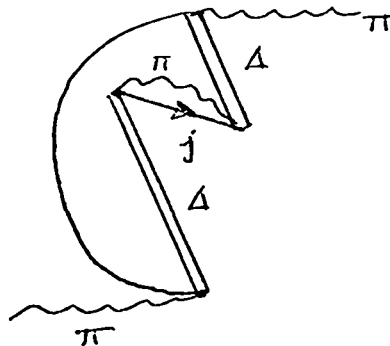The exchange diagram, fig. 5b) can be redrawn[16] as shown in Fig. 6.

Fig. 6. The exchange graph, fig. 5b, redrawn as an isobar
self-energy insertion.

The point about redrawing the graph is to realize that this is just one

of many self-energy insertions.   In particular, a ρ-meson could replace the internal

π in fig. 6, and this is known[7] to cancel most of the effect from the virtual pion.

In addition to the Fock type self-energy insertion shown in fig. 6, other

mesons can participate in Hartree-type self-energy insertions.   Calculation

of all of these insertions[7] shows considerable cancellation among them,

and that the net effect is opposite to that of the process, fig. 6.

Such considerations show it to be useful to look at the pion propagation

systematically within the framework of many-body theory.   The direct graph,

fig. 5a), will be as shown in fig. 7a).
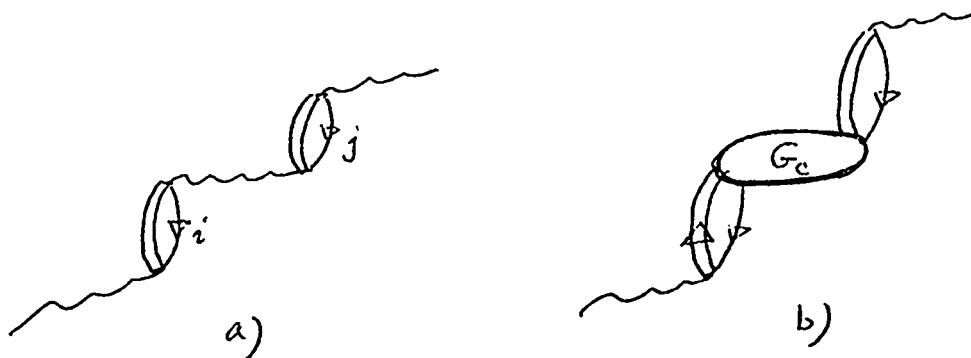
Fig. 7.   The double scattering in many-body language.
          a) represents the reducible pion self-energy,
             with an intermediate pion.
          b) G_c represents everything else.

We find it convenient to collect all modifications to the purely pionic

double scattering into a G_c, as shown in b).   We shall show that G_c is

closely related to the parameter g_o', the coefficient of the $\vec{\sigma}_1 \cdot \vec{\sigma}_2 \, \vec{\tau}_1 \cdot \vec{\tau}_2$

force in the Migdal theory of finite Fermi systems.

For pion exchange, the effective interaction is

$$\hat{V}_\pi(r,t) = V_\pi(r,t)\, g(r) \tag{10}$$

where $V_\pi(r)$ is the Fourier transform of $V_\pi(k)$, eq. (2.1), and $g(r)$ is the two-body correlation function, determined mainly by ω-meson exchange, and assumed here to be independent of spin and isospin. Since the expression representing fig. 7a) contains only V_π, the correction

$$\delta\hat{V}_\pi(r,t) = (g(r)-1)\, V_\pi(r,t) \tag{10.1}$$

should be considered in G_o, fig. 7b). Now $(g(r)-1)$ is a short-ranged function of r, and the tensor and Yukawa pieces of $\hat{V}_\pi(r,t)$ are of range $\hbar/m_\pi c$, so that practically, only the δ-function part enters into $\delta\hat{V}_\pi(r,t)$. Assuming $g(0) = 0$ we find that,

$$\delta\hat{V}_\pi \cong (g(r)-1)\left(-\frac{1}{3}\frac{f_\pi^2}{m_\pi^2}(\sigma_1\cdot\sigma_2)\vec{\tau}_1\cdot\vec{\tau}_2\,\delta(r_1-r_2)\right)$$

$$= +\frac{1}{3}\frac{f_\pi^2}{m_\pi^2}(\sigma_1\cdot\sigma_2)\,\vec{\tau}_1\cdot\vec{\tau}_2\,\delta(r_1-r_2). \tag{11}$$

The matrix element involving $\delta\hat{V}_\pi$ is the "passive" contribution to G_c, passive in that we remove a δ-function term in $V_\pi(r,t)$ which will be rendered inoperable by short-range correlation which hold two nucleons apart.

Within the framework of our model, §2, the ρ-meson exchange is the "active" contribution. Thus, $\hat{V}_\rho$ of eq. (5) will enter into G_c; in fact, within the framework of this model, the total interaction entering into G_c is $\delta\hat{V}_\pi + \hat{V}_\rho$. Note that both terms have the same sign; removing the δ-function from the pion exchange potential contributes in the same way as adding the Yukawa in the ρ-exchange potential. Yet, there is an important

difference. Assuming $g(0) = 0$, the δ-function in the pionic exchange shouldn't be there in the first place, so it must be removed to all orders. (We have discussed only second-order scattering here, but can imagine the scattering to all orders.) On the other hand, upon inclusion of exchange terms, the active contribution can act only through 4th-order in the series for the scattering amplitude, because not more than four nucleons can be at the same place at the same time. Thus, the following parameterization of V_{opt} would appear more appropriate than eq. (6).

$$2\omega V_{opt} = -4\pi a(\omega)\nabla\rho\left\{\frac{1}{1 + \frac{4\pi a(\omega)}{3}\rho[1-B_2\frac{4\pi}{3}a(\omega)\rho+B_3(\frac{4\pi}{3}a(\omega)\rho)^2-B_4(\frac{4\pi}{3}a(\omega)\rho)^3]}\right.$$

$$\times\left.[1 - B_2\frac{4\pi}{3}a(\omega)\rho + B_3(\frac{4\pi}{3}a(\omega)\rho)^2 - B_4(\frac{4\pi}{3}a(\omega)\rho)^3]\right\}\nabla . \qquad (12)$$

Up to this point, we have assumed the pion-nucleon and $\pi N\Delta$ interaction to be of zero range, as assumed in the original Ericson-Ericson work[10]. The contribution of what we call $\delta\hat{V}_\pi$, eq. (11), has been shown to be particularly sensitive to the range of the $\pi N\Delta$ vertex, even for very short ranges of $\sim \hbar/mc$, where m is the nucleon mass. Introduction of vertex functions Γ will lead to an additional term in $\delta\hat{V}_\pi$

$$(\delta\hat{V}_\pi)_{active} = -\frac{1}{3}\frac{f_\pi^2}{m_\pi^2}(\sigma_1\cdot\sigma_2)(\vec{\tau}_1\cdot\vec{\tau}_2)\int d^3r_1' \, d^3r_2' \, g(r_{12})$$

$$\Gamma(|r_1-r_1'|)\Gamma(|r_2-r_2'|)\delta(|r_1'-r_2'|) \qquad (12.1)$$

where Γ is the vertex function, and we have added the subscript "active" to this piece of $\delta\hat{V}_\pi$ because it enters as an additional interaction, in the same way as $\hat{V}_\rho$. Even though the interaction $(\delta\hat{V}_\pi)_{active}$ is somewhat spread out by the range of the vertex functions, it is still short compared

- 16 -

with the interparticle spacing, and it is appropriate to make a zero-range approximation

$$(\hat{\delta V}_\pi)_{active} = -\frac{1}{3}\frac{f_\pi^2}{m_\pi^2}(\underset{\sim}{\sigma}_1 \cdot \underset{\sim}{\sigma}_2)(\vec{\tau}\cdot\vec{\tau})(1-\xi_\pi)\delta(r_{12}).$$ (12.2)

In Appendix II, we present a calculation of ξ within the framework of a schematic model of the two-body correlation function. This model is accurate enough to give semiquantitative features of the variation of ξ with the range of the correlation defining the parameter ξ_π.

Going from our simple model over to the isobar model of §3, we find that the B_2, B_3 and B_4 in eq. (12) now contain effects from both ρ-exchange and from the finite range of the $\pi N\Delta$ interaction, viz

$$B_2 \underset{\sim}{\cong} (\xi_\pi-1 + \frac{2f_\rho^2 m_\pi^2}{m_\rho^2 f_\pi^2}A),$$ (12.3)

and $B_3 \underset{\sim}{\cong} B_2$, $B_4 \underset{\sim}{\cong} B_2$ in the considerations, neglecting effects of antisymmetry.

Note from (12.2) that finite-range effects in the $\pi N\Delta$ couplind and the strength of $\rho N\Delta$ coupling are inextricably bound up in the Lorentz-Lorenz effect. A longer range of the $\pi N\Delta$ coupling can be compensated for by a stronger $\rho N\Delta$ coupling. A similar situation exists in π absorption by the deuteron, $\pi + d \rightarrow p+p$[1].

Our numerical fits to π-nucleus scattering, to be discussed later, suggest that $B_2 \sim 0$; noting that even for nuclear matter densities $\rho_0 \sim 0.16$ particles/fm, $\frac{4\pi}{3}a(\omega)\rho_0 \simeq 0.4$ for low-energy pions, we see that the series in eq. (12) seems to converge rapidly, and that, practically, it should be sufficient to stop with B_2, setting B_3 and B_4 zero.

W.A. Friedman and A.T. Hess[19] have commented on the different character of the results given by the first and second terms in curly brackets in Eq. (12). We are happy to furnish them with both types of terms. Later, Rosenthal et al.[20] showed, however, that when S-wave terms and the Coulomb interaction are included, results calculated with the two expressions $\{1+4 a(\omega)\rho/3\}^{-1}$ and $\{1-4\pi a(\omega)\rho/3\}$ replacing our curly brackets were close, except for the lightest nuclei.

Thus far we have considered mainly π- and ρ-meson exchange, but, as noted in §5, antisymmetry brings in other mesons. Let us concentrate now on the ρ^2 term prefixed by B_2 in eq. (12). All possible active contributions to G_c, fig. 7, enter here. Some of the possible processes are shown in fig. 8, where we have now included exchange terms. In addition to these, we have also $(\delta \dot{V}_\pi)_{active}$ of eq. (12.1)
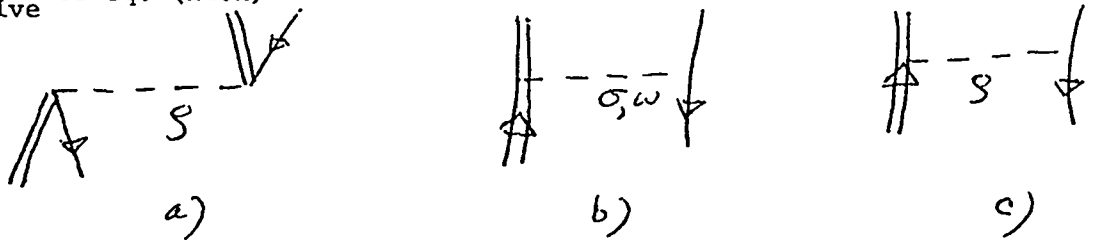

Fig. 8. "Active" processes contributing to G_c; it is to be understood that an arbitrary number of ω-exchanges can accompany any of these processes.

Note that in the exchange terms, the exchanged meson does not have to carry spin or isospin. Such exchange terms, as well as ρ-exchange, were not included in the considerations of ref. 17; yet according to our estimates they are as important, or more important, than the exchange process considered there.

The ρ^3 terms will involve more exchanges and will be difficult to calculate, but just from the fact that two fermions must be in nearly the same place in the ρ^2 term, three must be close together for the ρ^3 term, etc., we might expect that

$$B_3 \cong \frac{1}{2} B_2^2, \quad B_4 \cong \frac{1}{2} \frac{1}{4} B_2^3$$

with account of the effects from antisymmetry. We thus expect a rapid convergence in the B's, and shall neglect B_3 and B_4 in eq. (12).

6. CONNECTION WITH THE MIGDAL THEORY OF FINITE FERMI SYSTEMS

The Migdal theory[21] of finite Fermi systems is based on the Landau theory of Fermi liquids, which deals with effective interaction in the long-wavelength limit; that is, as $k \to 0$. Since $V_\pi \to 0$ as $k \to 0$, the spin, isospin dependent interaction in this limit is just

$$\hat{\delta V}(r_{12}) + \hat{V}_\rho^\varepsilon(r_{12}),$$

both pieces having a $\delta(r_{12})$ behavior, as discussed in the last section.

Migdal and collaborators[21] employ a spin-isospin dependent interaction

$$F_{ot} = g_o{}' \; \vec{\sigma}_1 \cdot \vec{\sigma}_2 \; \vec{\tau}_1 \cdot \vec{\tau}_2 \; \delta(\vec{r}_{12}) \tag{13}$$

where $g_o{}'$ is $2k_f m^*/\pi^2$ times[*] the strength of the δ-function interaction.

Assuming, again, an approximate SU(4) invariance, as discussed in §3, we can get an idea of the sizes of the contributions $\hat{\delta V}_\pi$ and $\hat{V}_\rho$ by looking at the $g_o{}'$ found from nuclear spectra, where, in the main, only nucleons, rather than intermediate isobars, are involved. There, $g_o{}'$ is found[22] to be 1.8. Of this, $\hat{\delta V}_\pi$ would contribute[23,24]

$$\frac{2k_f m^*}{\pi^2} \; \frac{f_\pi{}^2}{3 m_\pi{}^2} \sim 0.9 \tag{14}$$

---

[*] In fact, Migdal and collaborators often multiply by $k_f m^*/\pi^2$; but this is the density of states appropriate to liquid He^3. Here m^* is the effective mass of the nucleon at the Fermi surface, k_f is the Fermi momentum.

and the rest must come from the "active" contribution to G_c. In fact[14], in calculations of G_c, the "active" contribution comes out to be sufficient to account for $g_o' \sim 1.6$ all by itself, the pionic pieces not contributing to the relevant states in Pb^{208} appreciably. Be that as it may, we can foresee either the scenario in which $\delta\hat{V}_\pi$ contributes appreciably to g_o', which would then argue that we should take $\xi_\pi = 1$ in eq. (12) (which assumes that the range of the $\pi N\Delta$ vertex is not appreciably larger than that of the πNN vertex, in line with our assumption of SU(4) invariance), and that B_2 is of order unity, so that the "active" contribution provides roughly half of the total, or the scenario in which $\xi_\pi \sim 0$ and B_2 provides nearly all of the double-scattering term. With our prejudices[13] about the short range of the vertex, we would prefer the former.

It must be admitted that our arguments based on SU(4) invariance should be considered more suggestive than quantitative, and that the final values for ξ_π and the B's must come from fitting experiment. However, we believe eq. (12) to be a useful parameterization, and that our models give us an idea about reasonable values of these parameters. (Were we to allow the four parameters in eq. (12) to range completely freely, we should be able to fit nearly anything.)

7. LABORATORY - CENTRE OF MASS TRANSFORMATION

In this section we will consider the effects of the laboratory-centre of mass transformation and see that when it is considered simultaneously with short-range correlations a new term appears. Although this transformation introduces new terms of only order ω/M and $(\omega/M)^2$, which are small quantities, we shall see that the new terms are not negligible, and, therefore, this transformation must be effected with care.

Let us begin by considering the simple first order Kisslinger[15] potential given by:

$$2\omega \, U(\underset{\sim}{k},\underset{\sim}{k}') = -4\pi b_0 \, \rho(\underset{\sim}{k}-\underset{\sim}{k}') - 4\pi c_0 \underset{\sim}{k}\cdot\underset{\sim}{k}'\rho(\underset{\sim}{k}-\underset{\sim}{k}') \tag{15}$$

for spin zero, N=Z, nuclei. The laboratory-centre of mass transformation shows up in two places. First the ω on the left-hand side of eq. (15) be replaced by the reduced energy, $\omega_r = \omega/(1 + \frac{\omega}{M})$ where M is the nucleon mass. This just gives a well known[27] factor of $(1 + \frac{\omega}{M})$. More importantly the factor $k \cdot k'$ is changed to $k_{cm} \cdot k'_{cm}$ where:

$$\underset{\sim}{k}_{cm} = \frac{M\underset{\sim}{k}-\omega\underset{\sim}{P}}{M+\omega} = \frac{\underset{\sim}{k}-\epsilon\underset{\sim}{P}}{1+\epsilon}$$

$$\underset{\sim}{k}'_{cm} = \frac{M\underset{\sim}{k}'-\omega\underset{\sim}{P}'}{M+\omega} = \frac{\underset{\sim}{k}'-\epsilon\underset{\sim}{P}'}{1+\epsilon} \quad . \tag{16}$$

Here P and P' are nucleon momenta before and after the scattering respectively, and $\epsilon = \omega/M$. If we assume P=0 (nucleon initially at rest) we get:

$$\underset{\sim}{k}_{cm} \cdot \underset{\sim}{k}'_{cm} = \frac{\underset{\sim}{k}\cdot\underset{\sim}{k}'}{1+\epsilon} - \frac{\epsilon}{(1+\epsilon)^2}\underset{\sim}{k}^2 \tag{17}$$

which has the disadvantage of being non-hermitian. A more reasonable approach is to average P over the Fermi motion[25]. This means that the

last term of eq. (15) is replaced by:

$$-\frac{4\pi c_o}{(1+\epsilon)} \sum_i \int \frac{d^3P d^3P'}{(2\pi)^3} \phi_i^*(P')(k-\epsilon P)(k'-\epsilon P')\delta(P+k-P'-k')\phi_i(P) \tag{18}$$

where $\phi_i(P)$ are the single nucleon wave functions and the sum on i goes over all occupied states. Making a change of variables eq. (18) becomes

$$-\frac{4\pi c_o}{(1+\epsilon)} \frac{1}{(2\pi)^3} \sum_i \int d^3P \, \phi_i^*(P + \tfrac{1}{2}(k-k'))[k-\epsilon(P-\tfrac{1}{2}(k-k'))]$$

$$[k' - \epsilon(P + \tfrac{1}{2}(k-k'))]\phi_i(P - \tfrac{1}{2}(k-k')). \tag{19}$$

If the nuclear wave function is time reversal invariant, the terms linear in P vanish upon integration. This term gives:

$$2\omega \, U(k,k') = -4\pi b_o(1+\epsilon)\rho(k-k') - \frac{4\pi c_o}{(1+\epsilon)} [(1+\epsilon) \, k\cdot k'$$

$$-\frac{\epsilon}{2}(k^2+k'^2)] \, \rho(k-k') - \frac{4\pi c_o \epsilon^2}{(1+\epsilon)} \sum_i \frac{d^3p}{(2\pi)} \phi_i^*(P + \tfrac{1}{2}(k-k'))$$

$$[P - \tfrac{1}{2}(k-k')]\cdot[P + \tfrac{1}{2}(k-k')]\phi_i(P - \tfrac{1}{2}(k-k')) \tag{20}$$

The last term in this equation is proportional to the nuclear kinetic energy density. To see this let us write

$$\phi_i(P) = \int d^3r \psi_i(r) \, e^{-iP\cdot r}, \tag{21}$$

where $\psi_i(r)$ is the nuclear wave function in r-space. Substituting this into the last term of eq. (20) we obtain

$$-\frac{4\pi c_o \epsilon^2}{(1+\epsilon)} \sum_i \int d^3r \, d^3r' \, \psi_i^*(r) \, \psi_i(r') \, \nabla_r\cdot\nabla_{r'} \int \frac{d^3P}{(2\pi)^3} e^{i(P-\frac{1}{2}(k-k'))r'}$$

$$e^{-i(P+\frac{1}{2}(k-k'))\cdot r}. \tag{22}$$

After integrating by parts and doing the P and r' integrations we obtain:

- 22 -

$$- \frac{4\pi c_o \epsilon^2}{(1+\epsilon)} \sum_i \int d^3r \, [\nabla_r^* \psi_i(r) \cdot \nabla_r \, \psi(r)] \, e^{-i(k-k') \cdot r} \qquad (23)$$

which is thus proportional to the Fourier transform of the kinetic energy density. Although this term is proportional to ϵ^2 it, as we will show later, gives an appreciable contribution.

Let us now consider the effects of short-range correlations. As previously discussed when the optical potential given by eq. (15) is used to generate a multiple scattering series the $k \cdot k'$ term generates terms of zero range which are removed by short-range correlations, giving rise to the Lorentz-Lorenz effect. As pointed out by Thies[25] the k^2 and k'^2 terms in eq. (20) also generate zero range terms which again are removed by short-range correlations. To see this let us first look at the second order term in the T-matrix generated by the optical potential of eq. (20). It is given by:

$$T^2(k-k') = 2\omega \int \frac{d^3k''}{(2\pi)^3} U(k,k'') \frac{1}{k''^2 - \omega^2 + m_\pi^2} U(k'',k') \qquad (24)$$

This expression gives rise to several terms so let us consider explicitly the term

$$T_1^2(k,k') = \frac{1}{2\omega}(-4\pi)^2 b_o c_o \cdot \int d^3k'' \rho(k-k'') \frac{\epsilon}{2} \frac{(k''^2 + k'^2)}{k''^2 - \omega^2 + m_\pi^2} \rho(k''-k'). \qquad (25)$$

As k' is on shell k'^2 can be replaced by $\omega^2 - m_\pi^2$. However, k'' is not on shell so we use:

$$\frac{k''^2}{k''^2 - \omega^2 + m_\pi^2} = 1 + \frac{\omega^2 - m_\pi^2}{k''^2 - \omega^2 + m_\pi^2}$$

$$T_1^2(k,k') = \frac{1}{2\omega}(-4\pi)^2 b_o c_o \cdot \int \frac{d^3k}{(2\pi)^3} \rho(k-k'') [\frac{\epsilon}{2} + \frac{\epsilon(\omega^2 - m_\pi^2)}{k''^2 - \omega^2 + m_\pi^2}] \rho(k''-k') \qquad (26)$$

It is easily recognized that the first term in the square brackets would give a delta function in configuration space and hence would be removed by short-range correlations. This means that the term $\frac{\varepsilon}{2}(k^2+k'^2)$ in the first order optical potential should be replaced by $\varepsilon(\omega^2-m_\pi^2)$. However, if we allow finite range π-N interactions this is no longer true as some of the delta function survives and we get the replacement:

$$\frac{\varepsilon}{2}(k^2+k'^2) \rightarrow \frac{\varepsilon}{2}(k^2+k'^2)(1-\xi_\pi) + \varepsilon(\omega^2-m_\pi^2)\xi_\pi \tag{27}$$

where ξ_π is the same parameter as used in eq. (12.2). In arguing for the replacement, eq. (27), we have considered only one term. This replacement can be shown to be valid for all terms of order ε however for some of the ε^2 and higher order terms it is not valid. Fortunately these terms are small and can be neglected so eq. (27) can be used without loss of accuracy.

It has been argued by Banerjee[28] that the off-shell behavior of the S-wave amplitude, b_o, has some k^2 as well as ω dependence and that this has a significant effect on π-nucleus scattering. Using the same arguments as in the last paragraph we see that short-range correlations will reduce this effect; e.g., for a zero-range pion-nucleon interaction, k^2 gets converted into $\omega^2-m_\pi^2$. Any residual effects will merely change the effective value of ξ_π in eq. (27) and although we will use the symbol ξ_π in this application it should be kept in mind that we really mean an effective ξ_π. Hence this number by itself does not give us a direct measure of the importance of short-range correlations.

8. CALCULATIONS AND RESULTS

In this section we will compare our results with the experimental
π-nucleus cross-sections and discuss the importance of various terms in
the optical potential. The experimental π-nucleus cross-sections will in
most cases be taken from the preliminary results of Preedem et al.[31]. We
will begin with the pure Kisslinger[15] potential and add effects one at a
time and see what effect each has on the cross section. The examples of
Pb^{208} and C^{12} will be discussed in detail while other examples (O^{16}, Si^{28},
Co^{40}, Fe^{56}, Zr^{90}) will be discussed in less detail.

The Kisslinger[15] potential is given by:

$$2\omega U_k(r) = -4\pi b_o k^2 \rho(r) + 4\pi c_o \nabla \rho \nabla + V_{coul} \tag{27}$$

where b_o and c_o are the isoscalar S- and P-wave scattering strengths
which are taken from experimental[30] π-nucleon phase shifts. In our approach
one should use the phase shifts for free π-nucleon scattering, many-body
effects, such as those from the Pauli principle, being added as terms of
higher-order in ρ. For N≠Z nuclei the isovector S and P-wave scattering
strength, b_1 and c_1, are also needed and are again taken from ref. 30.
The coulomb potential includes not only the term linear in e^2 but also
the term proportional to e^4. The latter term was found to have a nonnegligible
effect in heavy nuclei.

The differential cross-section calculated with this optical potential
is shown in figure 1 for Pb^{208}, figure 4, for C^{12}, and by the dashed line
in figures 9-12 for O^{16}, Si^{28}, Ca^{40}, Fe^{56} and Zr^{90}. It is seen that these
cross sections do a very poor job of fitting the experimental results, so
that correction terms are definitely necessary.

Let us first add on the s-wave correction. There are two types of these. The s-wave Pauli effect gives a term[3]:

$$4\pi k^2 (b_o{}^2 + 2b_1{}^2) < \frac{1}{r} > \rho(r),$$

where $< \frac{1}{r} >$ is taken from Thies[3] and has the value $(0,23 + 0,30i)\,fm^{-1}$. The second term, the s-wave absorption and dispersion term, is given by: $-4\pi B_o \rho^2$. The parameter B_o is obtainable from fits to pionic-atom data and is given by Hufner[26] as $0.168(-1+i)\,fm^4$. This value will be modified later when we include the lab-centre of mass transformation but this value is sufficient for now. The effect of these two terms is shown for Pb^{208} and C^{12} in figures 1 and 4 respectively. It is seen that although these two terms give an appreciable effect the results still are not near the experimental points.

Next we will add the lab-centre of mass contribution as discussed in the last section. To illustrate the effect we will first consider the case $\xi_\pi = 0$ (no short range correlations). For the kinetic energy density we will use the Thomas-Fermi approximation:

$$\sum_i |\nabla \psi_i(r)|^2 = \frac{3}{5} (\frac{3}{2} \pi^2)^{2/3} \, \rho^{5/3} \qquad (28)$$

where we have assumed the neutron and proton densities to be proportional to each other and have neglected terms of order $[(N-Z)/A]^2$. This term (eq. (28)) will give a contribution quite similar to the ρ^2 term so if we keep this term we must adjust the coefficient, B_o, of the ρ^2 term. This is because B_o was fitted using an optical potential which didn't include the term proportional $\rho^{5/3}$.

To estimate the change in B_o we assume ρ has the nuclear matter value $0.16\,fm^{-3}$ and see how much B_o must be changed to compensate for this

term. The adjusted value of B_o is $(-0.291 + 0.149i)fm^4$. This is the value that should be compared with theoretically calculated S-wave dispersion and absorption terms. It is also the value we will use in our optical potential. The difference between the ρ^2 and $\rho^{5/3}$ terms is unimportant for heavy nuclei but for lighter nuclear which are mostly surface ($\rho \neq 0.16$) the difference is significant. The results for ^{208}Pb and C^{12} including CM corrections are given in figures 2 and 5, respectively. The results are now more or less in qualitative agreement with the experimental results.

To get qualitative agreement with the data it is necessary to include the Lorentz-Lorenz effect and the effect of the short-range correlations on the κ^2 terms (set $\xi_\pi \neq 0$).

The Lorentz-Lorenz is given by eq. (12). In the present examples B_3 and B_4 will be set equal to zero. As discussed previously this is a good approximation as B_3 and B_4 are less than B_2 which as we shall show is reasonably small. For ^{208}Pb and ^{12}C we show the cases $B_2=0.0$, $\xi_\pi=0.0$; $B_2=0.0$, $\xi_\pi=0.5$; $B_2=-0.25$, $\xi_\pi=0.5$; $B_2=0.0$, $\xi_\pi=1.0$ and $B_2=0.25$, $\xi_\pi=0.5$, while for the other nuclei we show the cases: $B_2=0.0$, $\xi_\pi=0.5$ and $B_2=0.0$, $\xi_\pi=0.5$. The best fits are with $\xi_\pi=0.5$ and $0 \geq B_2 \geq -0.25$ with the lower value being slightly favored. For heavy nuclei the fits to the data are quite good. For ^{208}Pb it is necessary to have $\xi_\pi=0.5$ in order to fit the back angles. (A smaller ξ_π lowers the back angles.) With this value of ξ_π, B_2 must be slightly negative to get the right depth at the minimum. For lighter nuclei, particularly ^{16}O, the backward-angle cross-section is too low for all reasonable values of B_2 and ξ_π.

Although our optical potential was derived for a many particle system it is interesting to see what happens for a light nucleus like He^4. In figure 16 we show the results for $\xi_\pi=0.5$, $B_2=0.0$ and $\xi_\pi=0.5$, $B_2=-0.25$. We see that the agreement even here is not too bad; no worse than in ^{12}C. In He^4 the terms of order $1/A$, which are unimportant for heavier nuclei, may have an effect.

In recent papers (ref. 19 and 20) there has been some debate on whether it is sufficient to include the Lorentz-Lorenz effect only to second order or whether one should include it to all orders. While we agree with Rosenthal et al.[20] that including corrections such as the lab-cm transformation reduces the sensitivity to this truncation, there is still a 20% effect at places like the forward angles of ^{12}C and at the interference minimum in ^{208}Pb where the cross-section is particularly sensitive to the Lorentz-Lorenz effect. This is shown in figure 17 where we compare the cross sections with the full Lorentz-Lorenz and with the second order Lorentz-Lorenz effect. The size of this effect is comparable to that found by Rosenthal et al.[20]. However, we believe one should be careful about neglecting 20% effects.
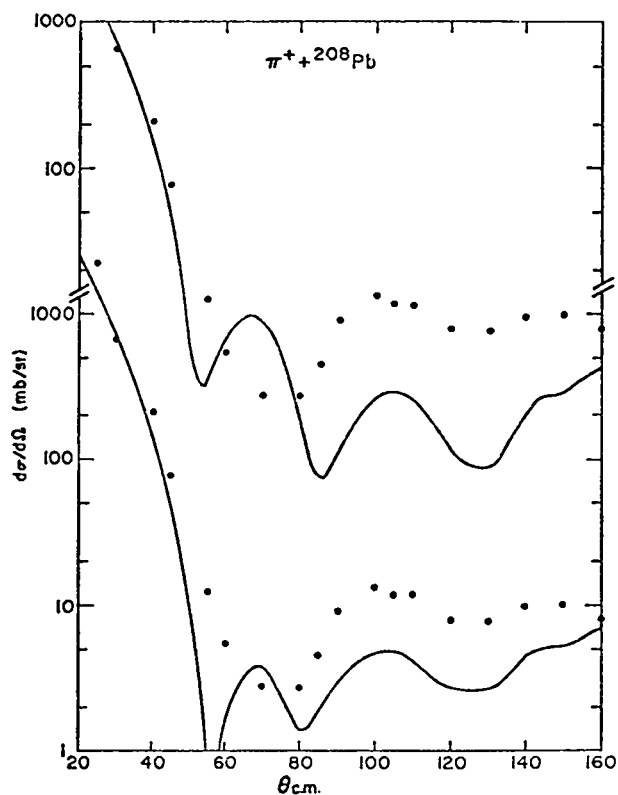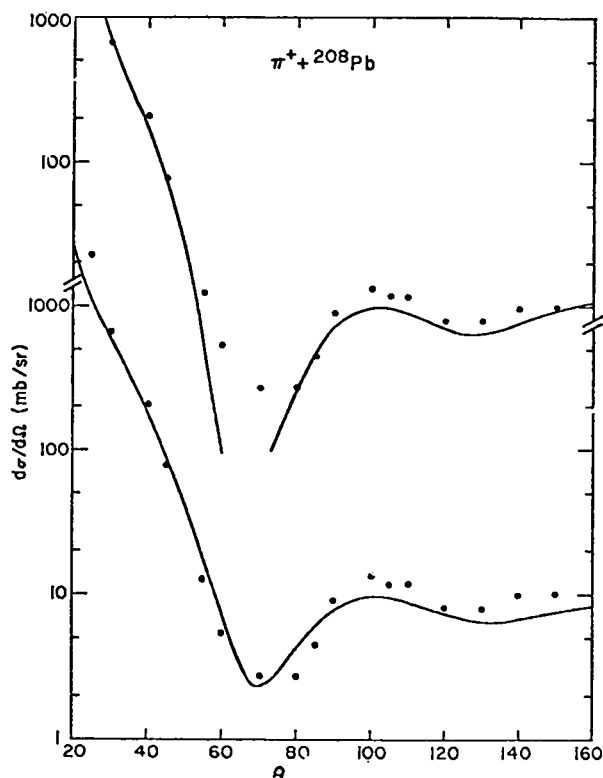
Figure 1

Elastic scattering cross section for 50 MeV π^+ on ^{208}Pb. The upper curve is calculated with a pure Kisslinger plus Coulomb optical potential (eq. (27)) while the lower curve includes also the s-wave dispersion and absorption terms and the s-wave Pauli effects. In both cases the dots are experimental results from ref. 31.

Figure 2

Elastic scattering cross section for 50 MeV π^+ on ^{208}Pb. The upper curve includes the lab-centre of mass tranformation as well as the s-wave correction terms. The lower curve includes as well the Lorentz-Lorenz effect ($B_2=0.0$, $\xi_\pi=0.0$). The dots are the experimental results from ref. 31.
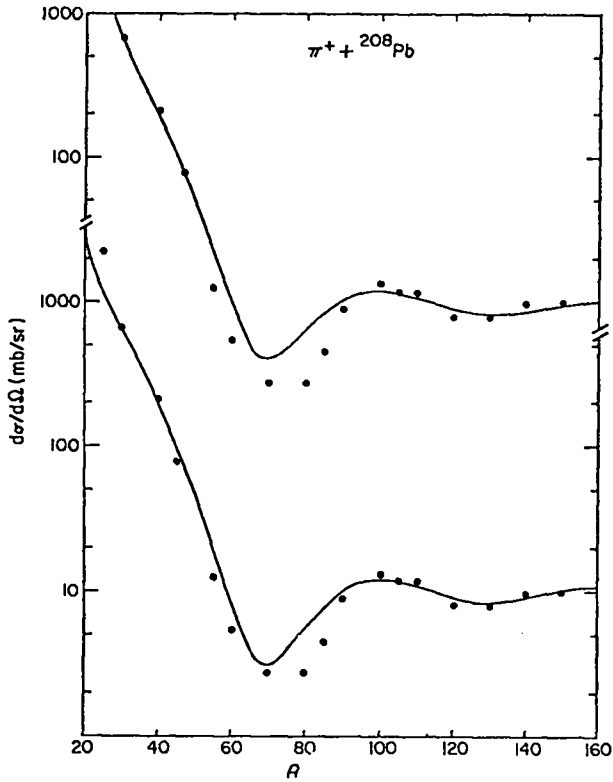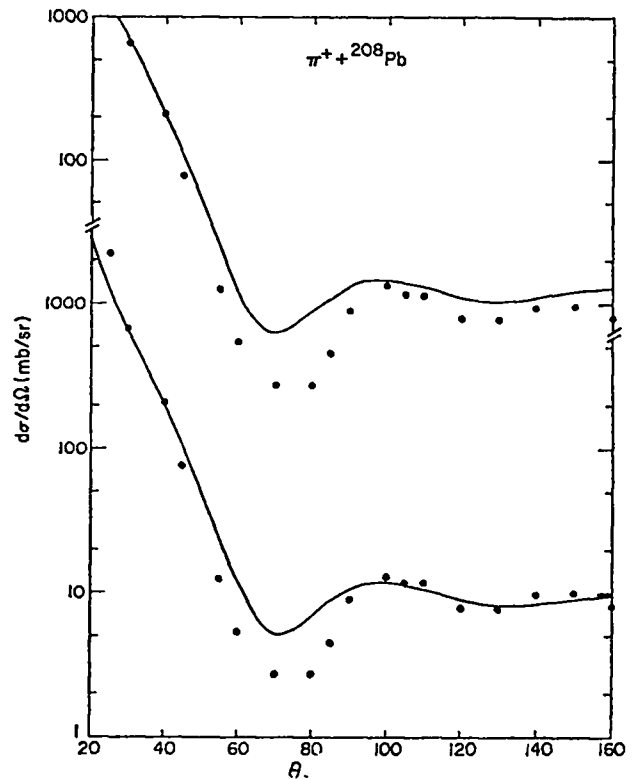
Figure 3
Same as figure 2 except the Lorentz-
Lorenz effect is included with
$B_2=0.0$, $\xi_\pi=0.5$ (upper curve) and
$B_2=-0.25$, $\xi_\pi=0.5$ (lower curve).

Figure 4
Same as figure 2 except the Lorentz-
Lorenz effect is included with
$B_2=0.0$, $\xi_\pi=1.0$ (upper curve) and
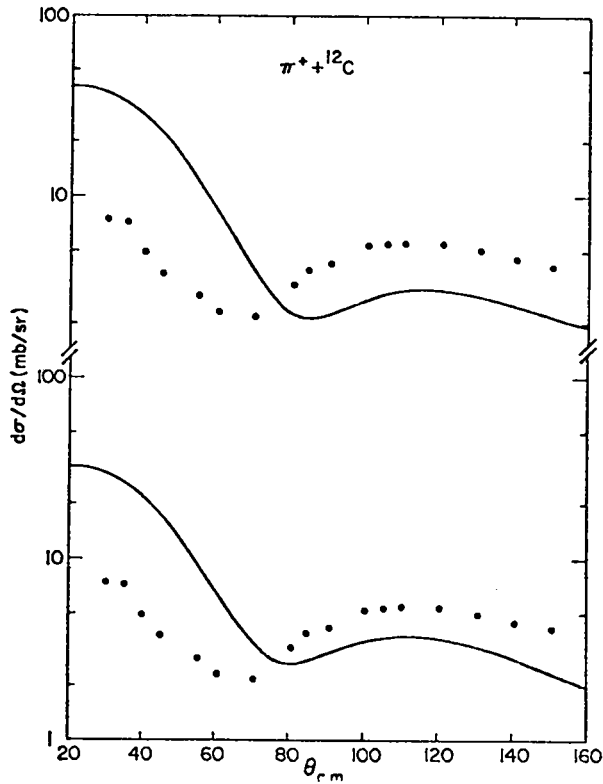$B_2=0.25$, $\xi_\pi=0.5$ (lower curve).
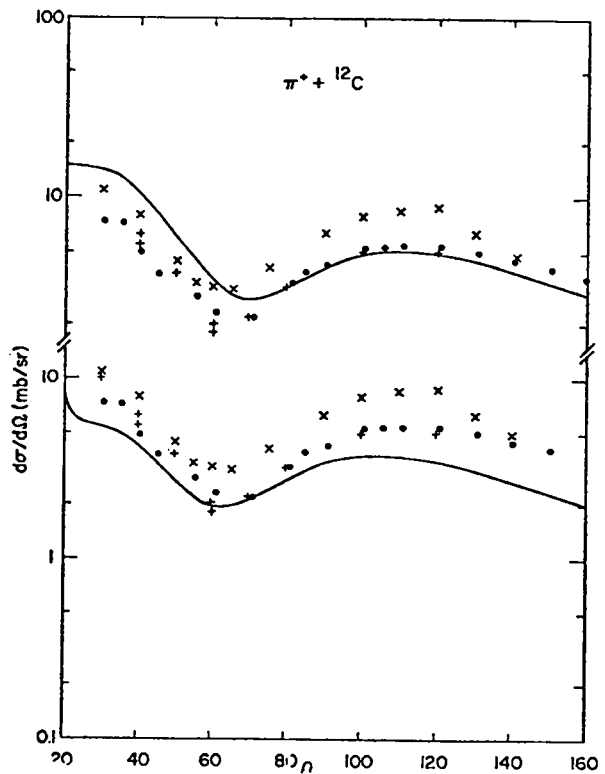
$\pi^+ + {}^{12}C$

Figure 5
Same as figure 1 except for ^{12}C.

Figure 6
Same as figure 2 except for ^{12}C. The x's are the experimental results from ref. 32; the +'s experimental results from ref. 33 and the dots experimental results from ref. 31.

Figure 7
Same as figure 6 except Lorentz-Lorenz effect is included with $B_2 = 0.0$, $\xi_\pi = 0.5$ (upper curve) and $B_2 = -0.25$, $\xi_\pi = 0.5$ (lower curve).
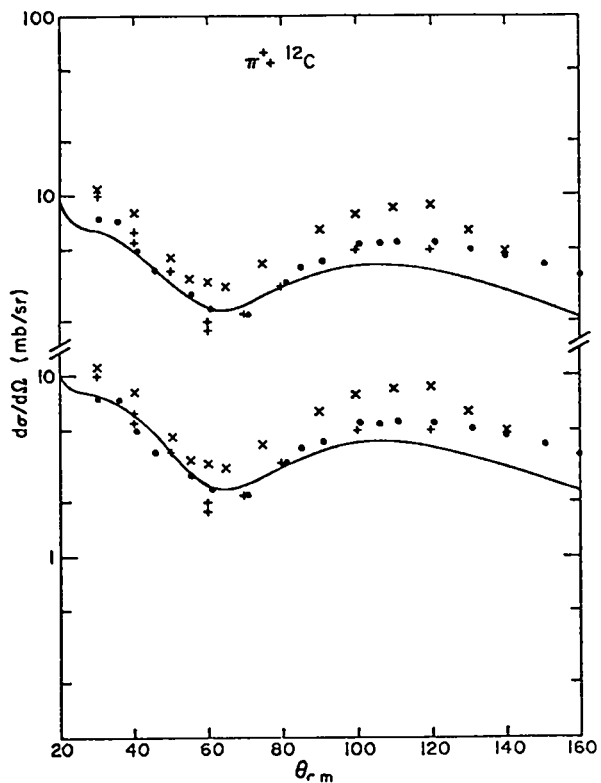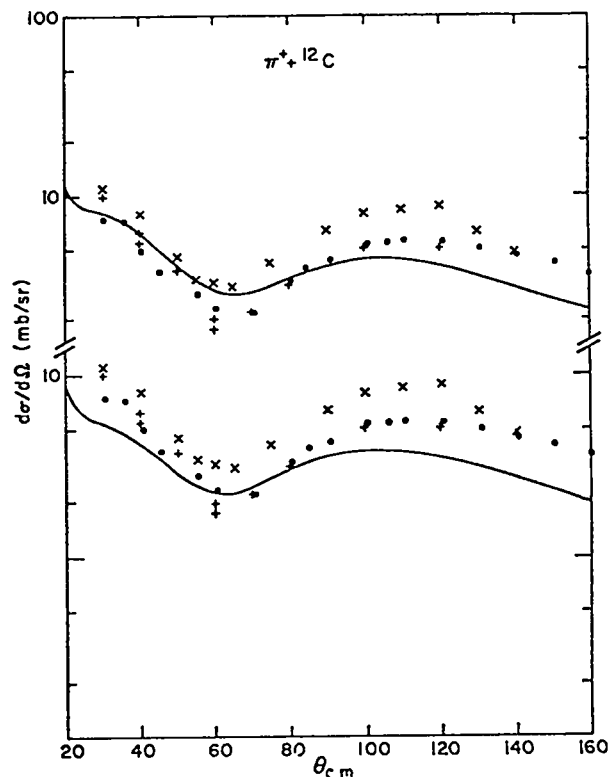
Figure 8
Same as figure 6 except Lorentz-Lorenz effect is included with $B_2 = 0.0$, $\xi_\pi = 1.0$ (upper curve) and $B_2 = 0.25$, $\xi_\pi = 0.5$ (lower curve).

π⁺ ELASTIC SCATTERING

$d\sigma/d\Omega$ (mb/sr)

^{16}O

^{28}Si

θ
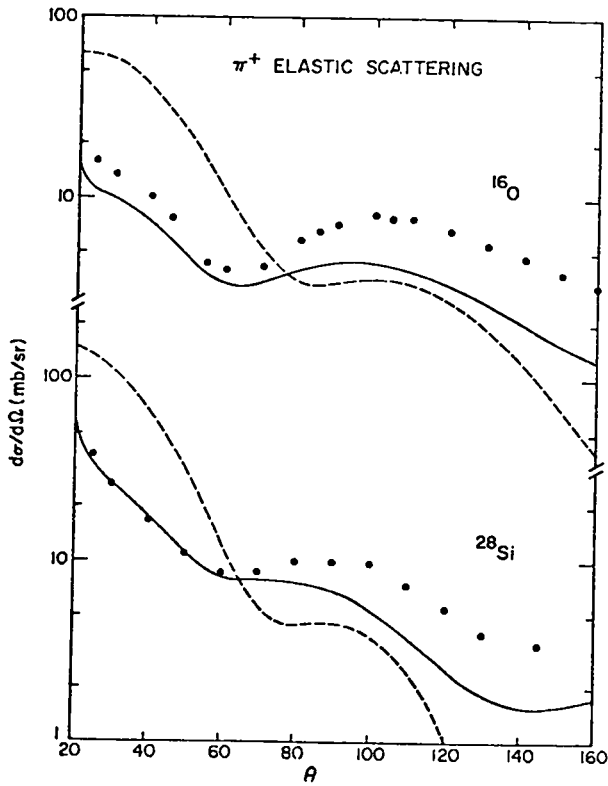
Figure 9
Elastic π^+ scattering cross section.
The dashed curves are calculated using
only the Kisslinger plus Coulomb optical
potential (eq. (27)). The solid curves
include also the s-wave terms, lab-c.m.
tranformation and the Lorentz-Lorenz
effect (B_2=0.0, ξ_π=0.5). The top
curves are for ^{16}O while the bottom
curves are for ^{28}Si.

$\pi^+ + {}^{40}Ca$

$d\sigma/d\Omega$ (mb/sr)

θ

Figure 10
Same as figure 9 except for ^{40}Ca.
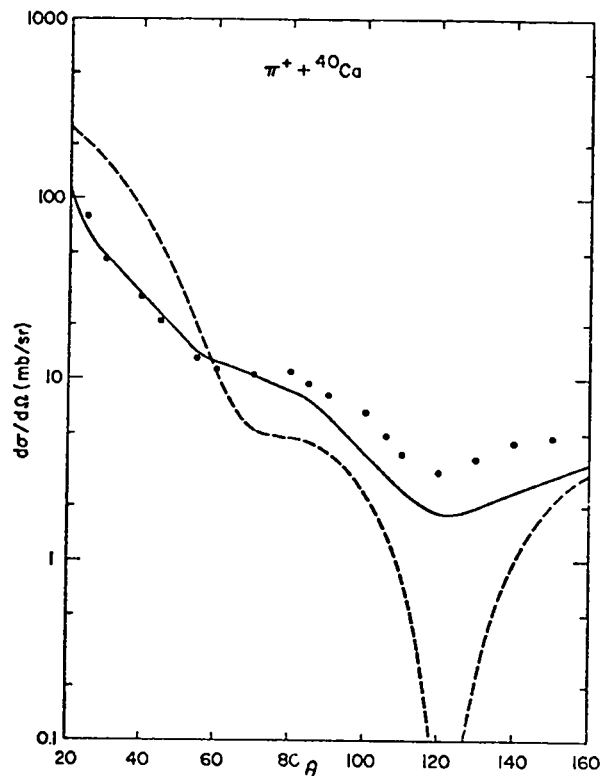
Figure 11

Same as figure 9 except for ^{56}Fe.
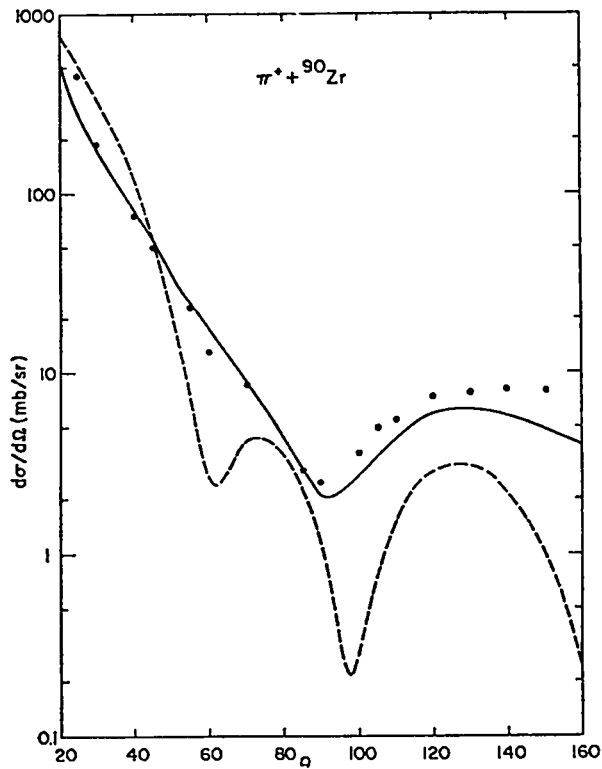
Figure 12

Same as figure 9 except for ^{90}Zr.
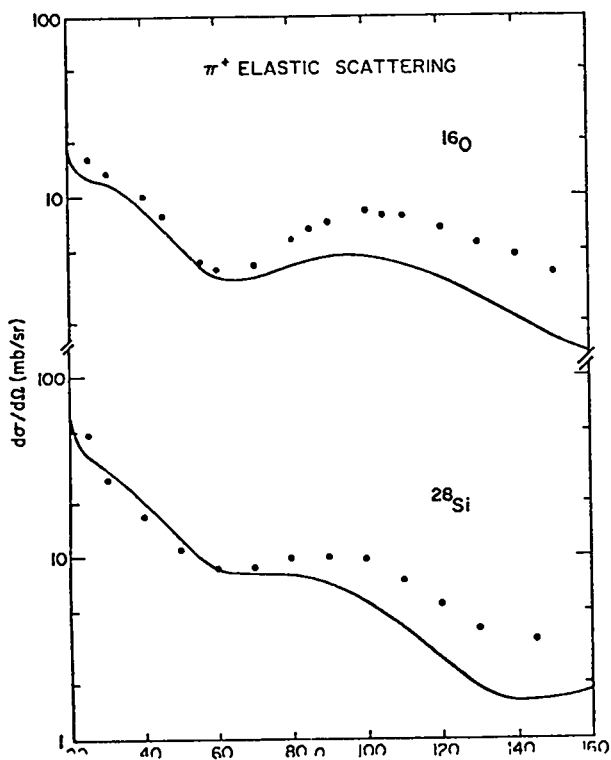
Figure 13

Same as figure 9 except curves are given for B_2=-0.25 and ξ_π=0.0.
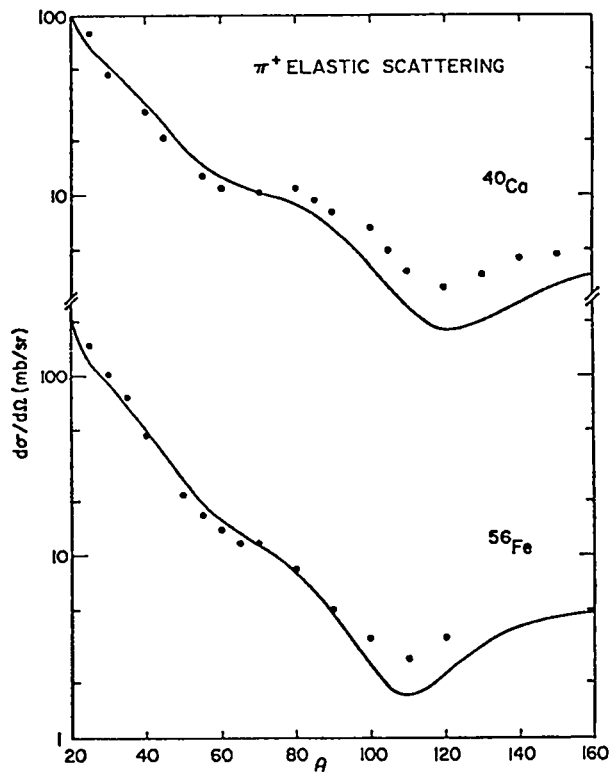
Figure 14

Same as figure 13 except for ^{40}Ca (upper curve) and ^{56}Fe (lower curve).
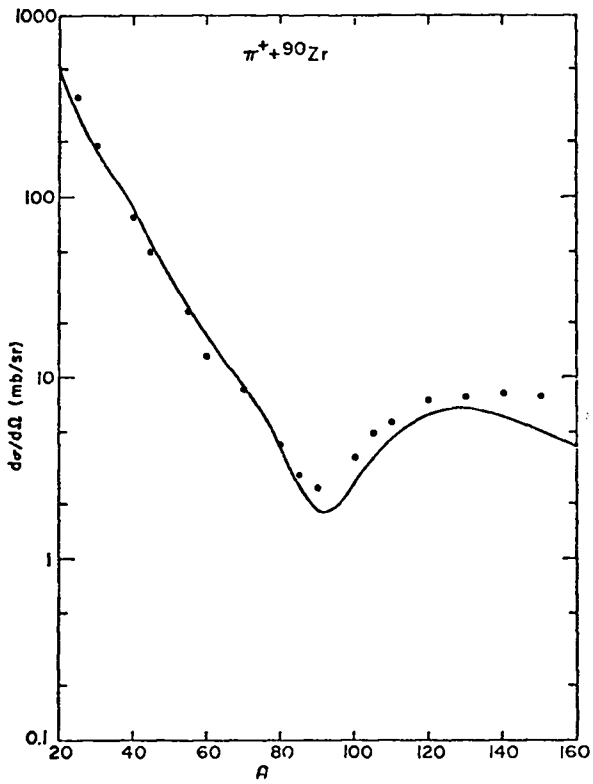
Figure 15

Same as figure 13 except for ^{90}Zr.
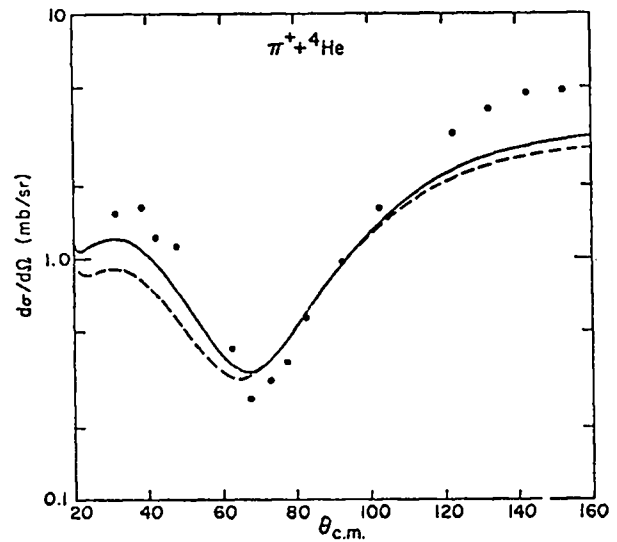
Figure 16

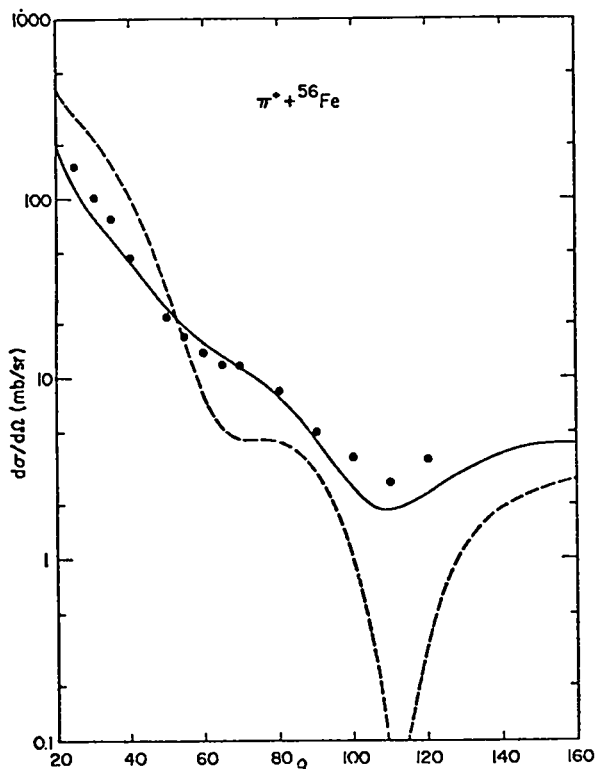Elastic π^+ scattering on ^{4}He. The differential cross section for ^{4}He calculated using the complete optical potential with B_2=0.0, ξ_π=0.5 (dashed line) and B_2=-0.25, ξ_π=0.5 (solid line). The dots are experimental results from ref. 37.
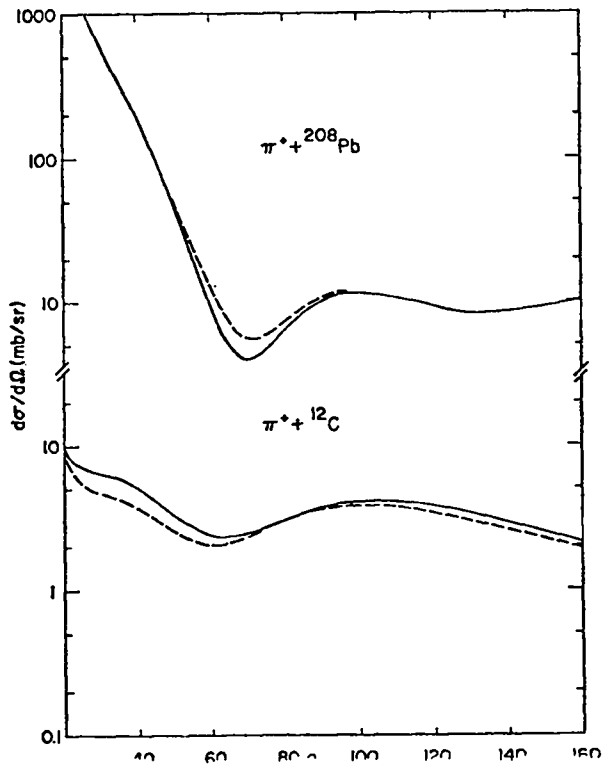
Figure 17

Effect of Truncating the Lorentz-Lorenz effect. The solid curve is the cross section calculated using the full Lorentz-Lorenz effect (B_2=0.0, ξ_π=0.5) while the dashed curve includes only the second order Lorentz-Lorenz effect. The upper curve is for ^{208}Pb while the lower curve is for ^{12}C.

APPENDIX I: THE G-MATRIX FORMULA FOR G_c

For the case where the intermediate particles in the double scattering, fig. 7b) are nucleons, it is straightforward to show, within a certain approximation, that

$$G_c \cong G - \langle V_\pi(r,t) \rangle \qquad\qquad I(1)$$

where G is the G-matrix, (see for example, ref. 35) (often called t-matrix) and V_π is the relevant matrix element of V_π. Furthermore it is a good approximation to set G equal to the usual static G-matrix encountered in nuclear structure.
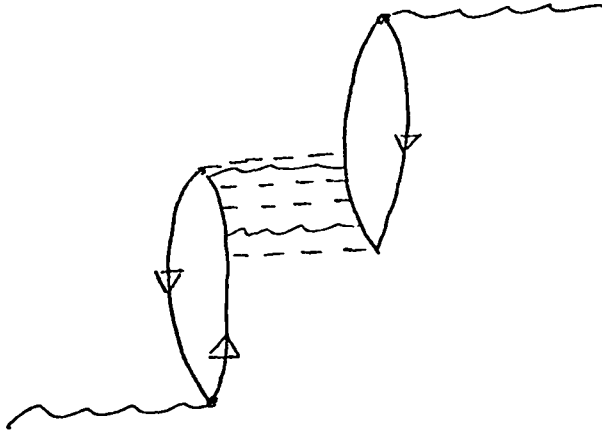
Fig. A.   Types of processes summed in the G-matrix approximation. In our convention, the wavy lines denote pions, the dashed lines, ρ -, ω- or σ-mesons.

Assumption of SU(4) invariance is then needed to apply the results calculated for intermediate nucleons to those relevant to intermediate isobars.

Processes involving only one intermediate pion are included in the reducible graphs of the type, fig. 7a), so we are here dealing with exchanges of two or more pions, one pion and any number of other mesons, or any number of other mesons. In any case, all interactions entering into fig. A are short range in character, and will predominantly lead to high-energy intermediate states. Thus, it should be a good approximation to sum over only intermediate particle states, as shown in fig. A, and which brings us back to the usual Brueckner G-matrix.

Whether this G-matrix is calculated for the correct incoming ω, or for $\omega = 0$ should not make much difference as long as $\omega \sim m_\pi$, because the total mass in the crossed t-channel exchanges is at least $2m_\pi$, and the frequency ω enters in the denominator of the propagator for the exchanges, as

$$\frac{1}{k^2 + m_t^2 - \omega^2}$$

where m_t is the t-channel exchange.

In fact, the weighting function for two-pion exchange is small for t-channel masses $\sim 2m_\pi$ (see ref. 8), so that the static approximation will generally be much better than neglect of ω^2 compared with $4m_\pi^2$. Bäckman and Weise have used the above formalism in calculating G_c for pion condensates, an equivalent problem. The reader can find the relevant formulae for the partial-wave decomposition of G_c there.

We next show that, with neglect of nucleon exchanges,

$$G_c \simeq <\delta\hat{V}_\pi(r)> + \hat{V}_\rho(r) \tag{I(2)}$$

as used in §6. To make this connection, we note that the ω-meson is coupled far more strongly than any other mesons, and make the approximation of splitting the total interaction into strong and weak pieces,

$$V = V_S + V_W. \qquad\qquad I(3)$$

where V_W is the sum of π- and ρ-exchange potentials; i.e., V_S is strong and independent of spin and isospin, the $\underset{\sim}{\sigma}_1 \cdot \underset{\sim}{\sigma}_2$ $(\vec{t}_1 \cdot \vec{t}_2)$ part being completely in V_W. We find then, the total G-matrix for the problem to be [*]

$$G = G_S + \Omega_S^\dagger V_W \Omega_S + \dots \qquad\qquad I(4)$$

where G_S is the G-matrix for V_S, Ω_S is the wave operator. Now Ω_S is, in general, energy dependent and nonlocal, but in the case where the dominant strong interaction is a short-range repulsive potential, it is a good approximation to take Ω_S as local. This is realized, for example, in the reference spectrum formalism . In this case, one can make the replacement

$$\Omega_S^\dagger V_W \Omega_S \cong g(r) V_W \qquad\qquad I(5)$$

where $g(r)$ is the two-body correlation function arising from ω-exchange (effects of σ-exchange can also be included). We have used this approximation in our models in the body of the article.

---

[*] See §V.B. of ref. 8.

- 38 -

When the assumption of a zero-range π-nucleon vertex is dropped the
Lorentz-Lorenz is reduced[11,12]. Here we will consider a simple schematic
model to estimate this effect. More detailed calculations can be found,
for example, in ref. 36.

If we include the effects of finite-range π-nucleon interaction the
pion exchange interaction of eq. (2) is changed to:

$$V_\pi(k) = - \frac{f_\pi^2}{m_\pi^2} (\tau_1 \cdot \tau_2) \frac{\sigma_1 \cdot k \; \sigma_2 \cdot k}{k^2 + m_\pi^2 - \omega^2} |\Gamma(k^2)|^2 \qquad \text{II(1)}$$

where $\Gamma(k^2)$ is the π-nucleon form factor which we assume to have the
form:

$$\Gamma(k^2) = \frac{\Lambda^2 - m_\pi^2}{\Lambda^2 + k^2} \qquad \text{II(2)}$$

with Λ being the cut-off momentum. Considering only the spin-spin
piece (the tensor piece vanishing as $k \to 0$) we have:

$$V_\pi = - \frac{1}{3} \frac{f_\pi^2}{m_\pi^2} \tau_1 \cdot \tau_2 \; \sigma_1 \cdot \sigma_2 \frac{k^2}{k^2 + m_\pi^2} |\Gamma(k^2)|^2 \qquad \text{II(3)}$$

From eq. (10.1) the contribution to G_o from the pion is:

$$\delta V_\pi(r) = (g(r) - 1) V_\pi(r). \qquad \text{II(4)}$$

In this example we will take the correlation function, $g(r)$ to have the
simplified form:

$$g(r) - 1 = -j_o(q_c r) \qquad \text{II(5)}$$

where j_o is a spherical Bessel function and if c determines the range of
the correlations. Transforming eq. II(4) to momentum space we have the

convolution integral:

$$\delta V_{\pi}(\underset{\sim}{k}) = - \int \frac{d^3q}{(2\pi)^3} \frac{(2\pi)^2}{|\underset{\sim}{k}+\underset{\sim}{q}|^2} \; \delta(|\underset{\sim}{k}+\underset{\sim}{q}|-q_c) \; V_{\pi}(q).$$

II(6)

In the limit $k \to 0$ (near threshold) this reduces to

$$\delta V_{\pi}(k=0) = + \frac{1}{3} \frac{f_{\pi}^2}{m_{\pi}^2} \tau_1 \cdot \tau_2 \; \underset{\sim}{\sigma_1} \cdot \underset{\sim}{\sigma_2} \int \frac{d^3q}{(2\pi)^3} \frac{2\pi^2}{q^2} \delta(q-q_c) \frac{q^2}{q^2} \Gamma^2(q^2)$$

$$= \frac{1}{3} \frac{f_{\pi}^2}{m_{\pi}^2} \tau_1 \cdot \tau_2 \; \underset{\sim}{\sigma_1} \cdot \underset{\sim}{\sigma_2} \; \Gamma^2(q_c^2)$$

II(7)

and hence using the definition of ξ_{π} (eq. 11, 12.1, 12.2) we obtain[25]:

$$\xi_{\pi} = \Gamma^2(q_c^2)$$

II(8)

To estimate this we take Λ to be about 1 GeV.[18] Then $\Lambda^2 \gg m_{\pi}^2$ and we have:

$$\xi_{\pi} = \frac{1}{(1 + g_c^2/\Lambda^2)}$$

II(9)

and so we need only the ratio q_c^2/Λ^2. A reasonable estimate for q_c is $\sim$700 MeV giving $\xi_{\pi} \sim 0.45$.

APPENDIX III: THE KISSLINGER CATASTROPHE

It has been emphasized by Bethe and Johnson[38] that the Kisslinger potential leads to an anomalous behavior of the optical model potential for densities of the order of nuclear matter density. We can easily see this by taking only the P-wave part of the optical-model potential, without Lorentz-Lorenz corrections,

$$2\omega \ V_{opt} = -4\pi a(\omega) \ \nabla\rho\nabla \qquad\qquad III(1)$$

Near threshold, $a(\omega)$ should be replaced by the scattering volume

$$a(\omega) \rightarrow c_o \cong 0.21 \ (h/m_\pi c) \ . \qquad\qquad III(2)$$

In infinite nuclear matter, ∇ can be replaced by k, which should be obtained self-consistently from the equation

$$k^2 = \omega^2 - m_\pi^2 - 2\omega \ V_{opt}(k,\omega) \qquad\qquad III(3)$$

with

$$2\omega \ V_{opt}(k,\omega) = -4\pi c_o k^2 \rho \ . \qquad\qquad III(3.1)$$

Solving for k^2, we find

$$k^2 = \frac{\omega^2 - m_\pi^{\ 2}}{1 - 4\pi c_o \rho} \ . \qquad\qquad III(4)$$

Since, at nuclear-matter density, $\rho = \rho_o = \frac{1}{2} /(h/m_\pi c)^3$, we see that for densities smaller than this, the denominator will go through a zero, and k^2, consequently, through a pole. This physically unacceptable

situation in which $k \to \infty$ is known as the Kisslinger catastrophe[*].

Introduction of the Lorentz-Lorenz correction is sufficient to cure this. For $\ell = 1$, the Ericson-Ericson, Lorentz-Lorenz, $4\pi c_o \rho$ in eq. (4) $\to 4\pi c_o \rho / (1 + \frac{4\pi}{3} c_o \rho)$ and at nuclear-matter densities, the denominator becomes

$$\text{Den.} = 1 - \frac{4\pi c_o \rho_o}{1 + \frac{4\pi}{3} c_o \rho_o} = .08 \qquad \text{III(5)}$$

Whereas this may seem small, it should be remembered that:

i)   nuclear-matter densities are reached only in the center of nuclei,

ii)   the s-wave π-nucleus interaction is repulsive, and will help to inhibit reaching the Kisslinger catastrophe so we believe that "a miss is as good as a mile."

It should be remarked that the sensitivity of the theoretical results to the inclusion of the Lorentz-Lorenz correction in heavy nuclei is undoubtedly due to the nearness of the situation to catastrophical.

REFERENCES

1. G. Baym and G.E. Brown, Nuclear Physics $\underline{A247}$ (1975) 395.

2. G.E. Brown, Meson-Nuclear Physics - 1976 (Carnegie-Mellon Conf.) AIP Conf. Proc. No. 33.

3. M. Thies, Phys. Letts. $\underline{63B}$ (1976) 43.

4. M.D. Cooper and R.A. Eisenstein, Phys. Rev. $\underline{C13}$ (1976) 1334.

5. M.A.B. Bég, Ann. of Phys. $\underline{13}$ (1961) 110.

6. S. Barshay, G.E. Brown and M. Rho, Phys. Rev. Lett. $\underline{32}$ (1974) 787.

7. G.E. Brown and W. Weise, Phys. Repts. $\underline{22C}$ (280) 1975.

8. See, for example, §I.B of G.E. Brown and A.D. Jackson, The Nucleon-Nucleon Interaction, North Holland Publ. Co., (1976).

9. See G.E. Brown, J. Durso, A.D. Jackson and M. Saarela, Nuclear Physics A, to be published.

10. M. Ericson and T.E.O. Ericson, Annals of Physics $\underline{36}$ (1966) 323.

11. J.M. Eisenberg, J. Hüfner and E. Moniz, Phys. Letts. $\underline{47B}$ (1974) 381.

12. J. Hüfner, Proc. of Symposium on Interaction Studies in Nuclei, Mainz, Feb. 1975, North Holland Publ. Co. (1975) 709.

13. J. Durso and A.D. Jackson, to be published; M. Brack and M. Dillig, to be published.

14. M.A. Anastasio and G.E. Brown, to be published.

15. L. Kisslinger, Phys. Rev. $\underline{98}$ (1955) 761.

16. R.P. Feynmann, M. Kisslinger and F. Ravndal, Phys. Rev. $\underline{D3}$ (1971) 2706.

17. J. Delorem and M. Ericson, Phys. Lett. $\underline{60B}$ (1976) 451.

18. M. Brack, D.O. Riska and W. Weise, to be published.

19. W.A. Friedman and A.T. Hess, Phys. Lett. $\underline{67B}$ (1977) 285.

20. A.S. Rosenthal, E. Rost, D.A. Sparrow and N.J. DiGiacomi, to be published.

21. A.B. Migdal, Theory of Finite Fermi Systems and Applications to Atomic Nuclei, Interscience Publishers (1967).

22. R. Bauer, J. Speth, V. Klemt, P. Ring, E. Werner and T. Yamazaki, Nucl. Phys. A209 (1973) 535.

23. G. Baym and E. Flowers, Nucl. Phys. A222 (1974) 29.

24. S.O. Bäckman, G.E. Brown, E. Oset and W. Weise, to be published.

25. M. Thies, preprint.

26. J. Hüfner, Phys. Reports 21C (1975) 1.

27. M. Krell and T.E.D. Ericson, Nucl. Phys. B11 (1969) 521.

28. M.K. Banerjee, Meson-Nuclear Physics (Carnegie-Mellon Conference), ed. by P.D. Barnes et al., AIP, New York, 1976, p. 119.

29. N.J. DiGiacomi, A.S. Rosenthal, E. Rose and D.A. Sparrow, Phys. Lett. B66 (1977) 421.

30. Particle Data Group, πN partial wave amplitudes (1970) p.77.

31. B. Preedem et al., private communication.

32. S.A. Dytman, J.F. Amann, P.D. Barnes, J.N. Craig, K.G.R. Doss, R.A. Eisenstein, R.J. Peterson, G.R. Burleson, S.L. Verbeck and H.A. Thiessen, Phys. Rev. Lett. 38 (1977) 1059.

33. J. Amann et al., Phys. Rev. Lett. 35 (1975) 426.

34. G.E. Brown, Unified Theory of Nuclear Models and Forces, 2nd ed., North Holland Publ. Co. (1971) Ch. XI.

35. H.A. Bethe, B. Brandow and A.G. Petschek, Phys. Rev. 129 (1963) 225.

36. W. Weise, Nucl. Phys. A278 (1977) 402.

37. K.M. Crowe, A. Fainberg, F. Miller and A.S.L. Parsons, Phys. Rev. 180 (1969) 1349.

38. H.A. Bethe and M.B. Johnson, Los Alamos Internal Report LA-4R-76-1844 (1974).

EXPERIMENTS ON PION-NUCLEUS SCATTERING

J. P. Egger

Institut de Physique
Neuchatel, Switzerland

I.   INTRODUCTION

The SIN pion spectrometer was built to carry out a number of experiments on pion-nucleus interactions in the momentum range of 150-650 MeV/c. It was designed to cover a broad momentum acceptance (± 18% dp/p) with a large solid angle (16 msr) and an overall momentum resolution, including the contribution from the pion channel, of 7 x 10^{-4} dp/p FWHM. Although the design resolution has been achieved under special conditions, the working resolution is approximately dp/p = 1.5 x 10^{-3} FWHM with a thin target at 200 MeV. A description of the SIN ¶M1 beam and pion spectrometer system (a modified Saclay design) is given in ref. 1.

After a tune-up the research program was started in spring 1976. Two subgroups were formed in order to operate the facility more efficiently. To date, group A[*] has received beam time for the following experiments:

R-71-04.6 : Pion carbon scattering,

R-71-04.10: Double charge exchange,

R-71-04.11: Pion scattering on ^{40}Ca and ^{48}Ca,

R-71-04.14: Inelastic states in ^{18}O, ^{28}Si, ^{50}Ti and ^{52}Cr.

Group B[*] concentrated on

R-71-04.8 : Elastic scattering on ^{16}O, ^{40}Ca, ^{208}Pb

R-71-04.12: Deep inelastic scattering on ^{16}O.

---

[*]In 1977 group A consisted of R. Corfu, J. P. Egger, P. Gretillat, C. Lunke, C. Perrin, J. Piffaretti, B. M. Preedom and E. Schwarz. Group B consisted of J. Arvieux, J. Bolger, E. Boschitz, Q. Ingram, L. Pflug, C. Wiedner and J. Zichy. J. P. Albanèse and J. Jansen participated in experiments of both groups.

Future plans include beam time for a third group headed by J. Domingo to measure pion-deuterium scattering (R-71-04.13) and tune up of an additional magnet to do 180° scattering (R-71-04.7).

The following is a detailed discussion of the above-mentioned experiments.

A.   PION-CARBON SCATTERING

In order to test the system and gain valuable experience, a tune-up experiment was performed by studying elastic and inelastic scattering of both π^+ and π^- from ^{12}C, which was chosen because some accurate data already exists (2).

The experiment was done with a standard layout with five MWPC; two of them were in the beam line with a fast digital read-out (3) to allow the determination of the incident momentum. Change-over from π^- to π^+ was achieved by reversing polarity of all beam and spectrometer elements. Protons in the beam were removed with an electrostatic separator. Muons and electrons were accounted for by a beam sampling method allowing continuous monitoring of the beam composition. Muons from π - decay in the spectrometer were largely rejected by imposing ion optical conditions on each particle trajectory. Typical running conditions with a primary proton beam of $\simeq$ 30 μ A were 4×10^6 π^+/s and 5×10^5 π^-/s incident on a 350 mg cm^{-2} natural carbon target. Overall relative momentum resolution was 2×10^{-3} FWHM which allowed a clear separation of the elastic, the 4.44 MeV (2^+), 7.66 MeV (0^+) and 9.64 MeV (3^-) states. In addition, levels up to excitation energies of 20 MeV were seen.

Typical spectra are shown in fig. 1 and 2. So far angular distributions with π^+ and π^- were measured at 148, 162 and 226 MeV. The 148 MeV results have been published (4). The comparison of the π^+ and π^- elastic differential
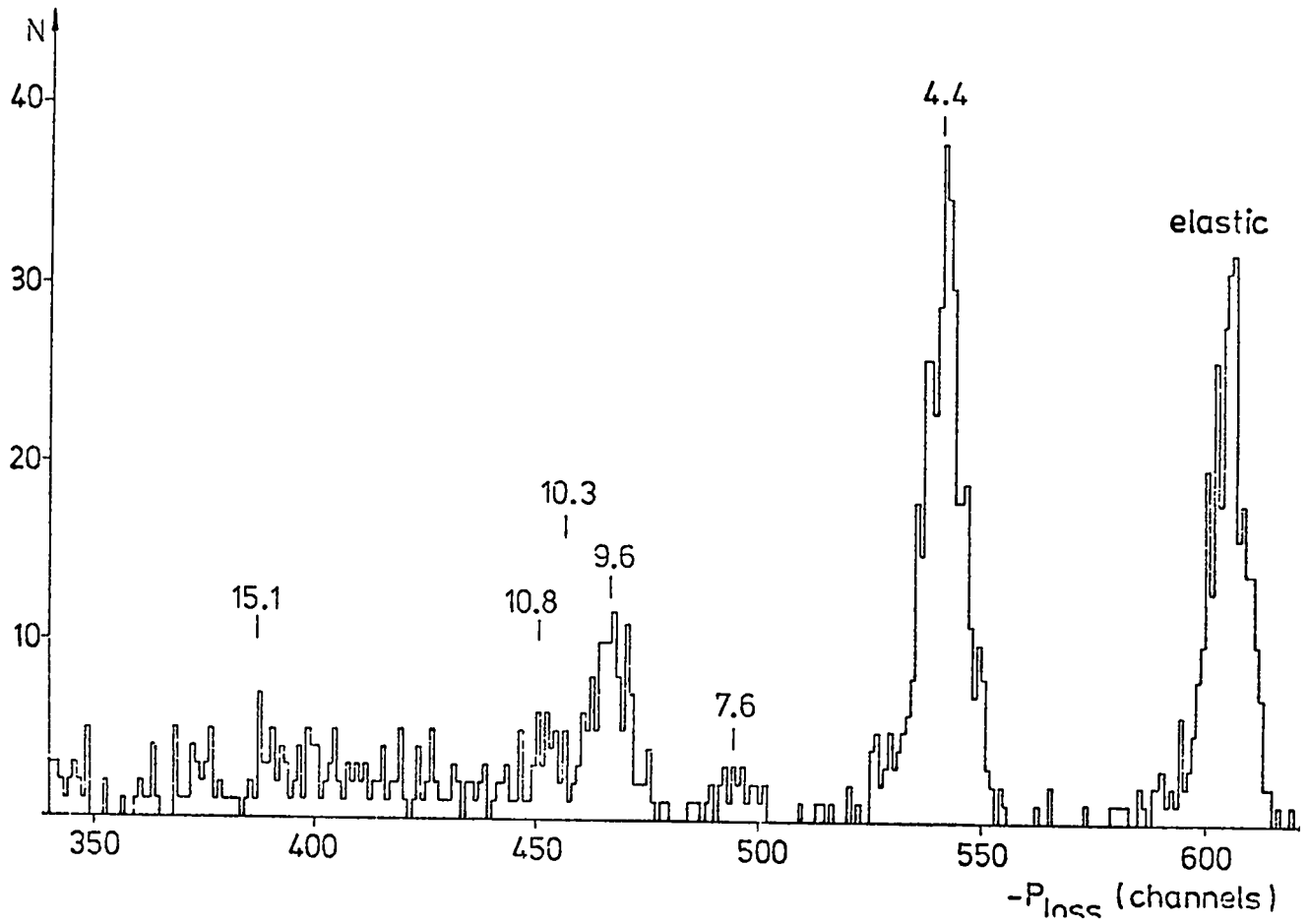
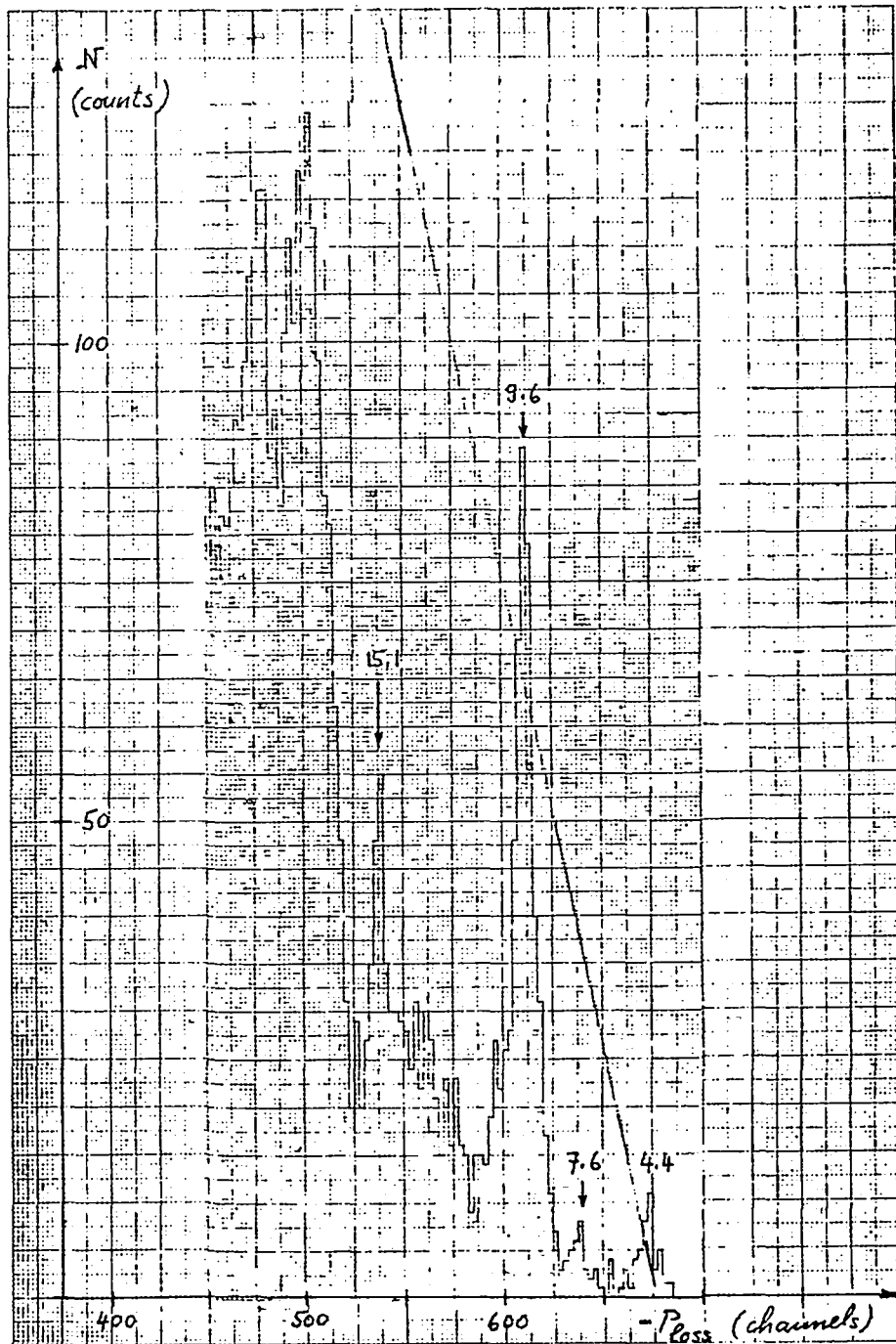Fig. 1   Pion-carbon scattering spectrum for 162 MeV π^- at a lab angle of 85°.

Fig. 2 Pion-carbon scattering spectrum for 148 MeV π^+ at a lab angle of 58°. This spectrum was shifted along the focal plane of the spectrometer and not corrected for spectrometer acceptance which is approximately rendered by the solid line. Although the 15.1 MeV (1^+) state is generally excited very weakly, it is clearly separated here.

cross sections shows strong differences in the vicinity of the diffraction

minima. This effect, which was seen for the first time in this experiment,

is energy dependent; below the (3,3) resonance the minima are deeper for π^+,

whereas above they are deeper for π^-. The elastic scattering results are shown

in fig. 3. In a recent paper (5), Germond and Wilkin explain this difference

in terms of Coulomb distortion. First they fitted the π^+ and π^- data separately

with a scattering amplitude of the form

$$F(q) = F(0) \left(1 - \frac{q^2}{q_1^2}\right) \left(1 - \frac{q^2}{q_2^2}\right) e^{-1/2 \, \beta^2 q^2}$$

which depends on the nearby complex zeros q_i^2, the forward scattering amplitude

$F(0)$ and a slope parameter β. The obtained parameters were then averaged to

determine $F_N(q)$, the nuclear scattering amplitude. Assuming the nuclear and

Coulomb phases can be added in impact parameter representation,

$$F(q) = F_C(q) + e^{i X_C(0)} F_{CN}(q)$$

with $F_C(q)$ = pure Coulomb amplitude and

$\qquad F_{CN}(q)$ = Coulomb distorded nuclear amplitude

a good fit was obtained for the π^+ and π^- data (see fig. 3) in the vicinity

of the first diffraction minimum. In addition the change of sign of the cross

section differences at the first minimum was quite well predicted (fig. 4).

Inelastic data (fig. 5) show very little π^+/ π^- difference, agreeing with

the Germond and Wilkin prediction except at 162 MeV for the 4.4 MeV state at

large angles. This, in addition to the large angle behavior of the elastic

cross sections, is not yet understood. Therefore further measurements will be

performed on ^{12}C at very small angles and large angles up to 180°.

PION-CARBON ELASTIC SCATTERING
AT 148 MeV

o PI-MINUS
+ PI-PLUS

Fig. 3A

Comparison of π^+ and π^- - ^{12}C elastic scattering differential cross sections at 148 MeV versus the pion scattering angle. The curves result from a fit by a formula given in the text.
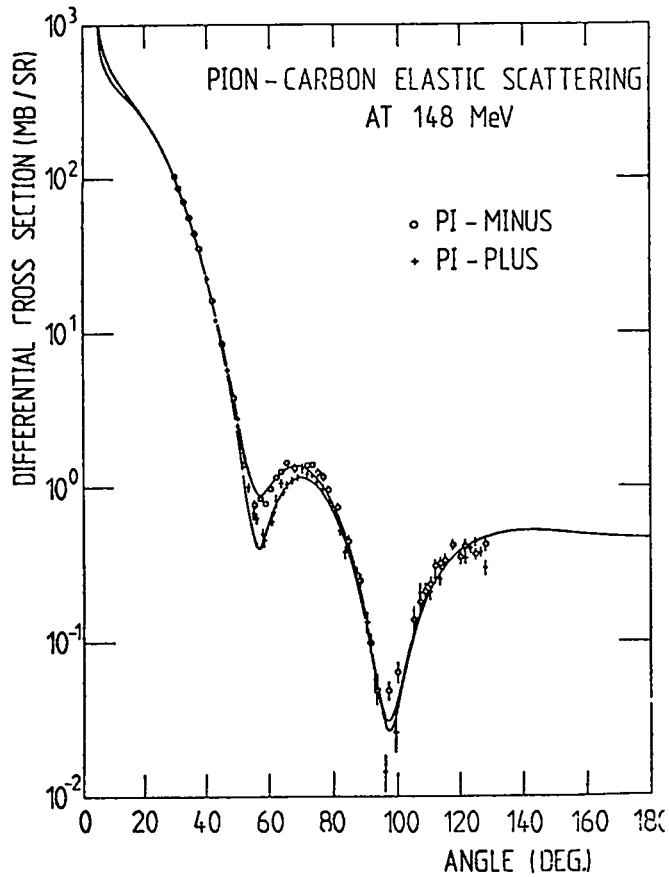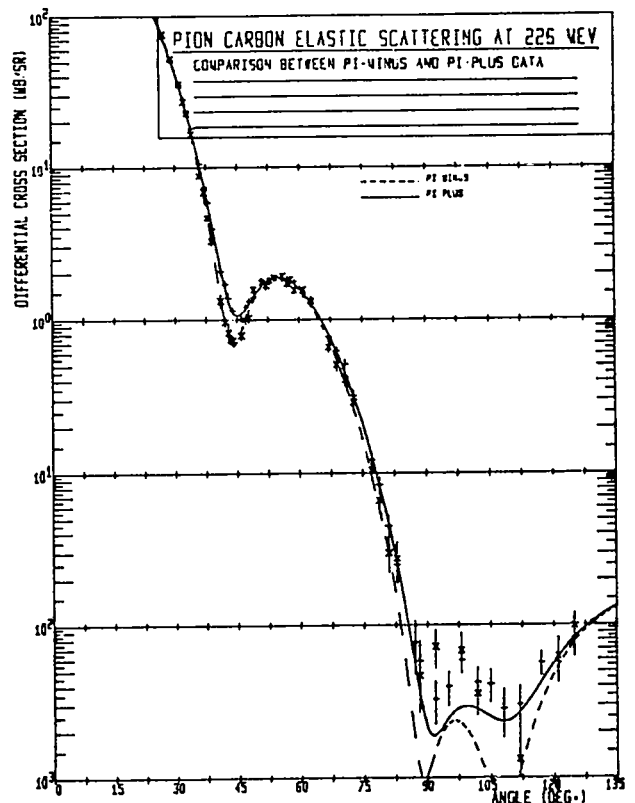
Fig. 3B

Comparison of π^+ and π^- - ^{12}C elastic scattering differential cross sections at 226 MeV versus the pion scattering angle. The curves result from a fit by a formula given in the text.

PION CARBON ELASTIC SCATTERING AT 225 MEV
COMPARISON BETWEEN PI-MINUS AND PI-PLUS DATA

PI MINUS
PI PLUS
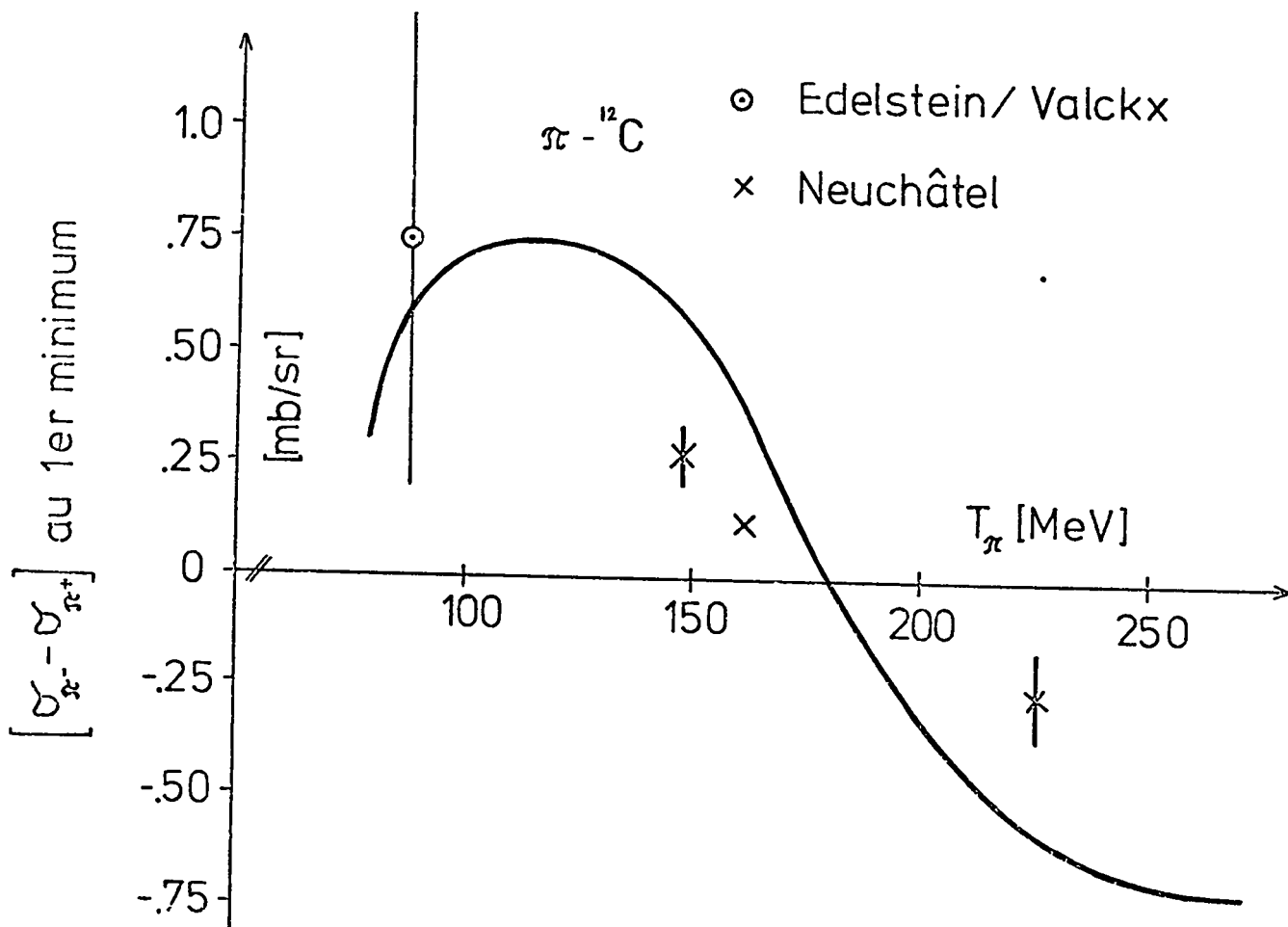
Fig. 4   Cross section difference between π^- and π^+ elastic scattering in the vicinity of the first diffraction minimum as a function of the pion kinetic energy. The theoretical curve is calculated from equations given in the text. Experimental crosses are from the Neuchâtel carbon data. The point at 87 MeV represents the combined results of older work (18). In all cases only statistical errors are represented.

Fig. 5 Comparison of π^+ and π^- - ^{12}C inelastic cross sections at 148 MeV for the 4.4 MeV (2^+), 7.66 MeV (0^+) and 9.64 MeV (3^-) states versus the scattering angle.

B. PION DOUBLE CHARGE EXCHANGE

Pion double charge exchange

$$_Z^A X \; (\pi^{\pm}, \pi^{\mp}) \; _{Z\pm2}^A X'$$

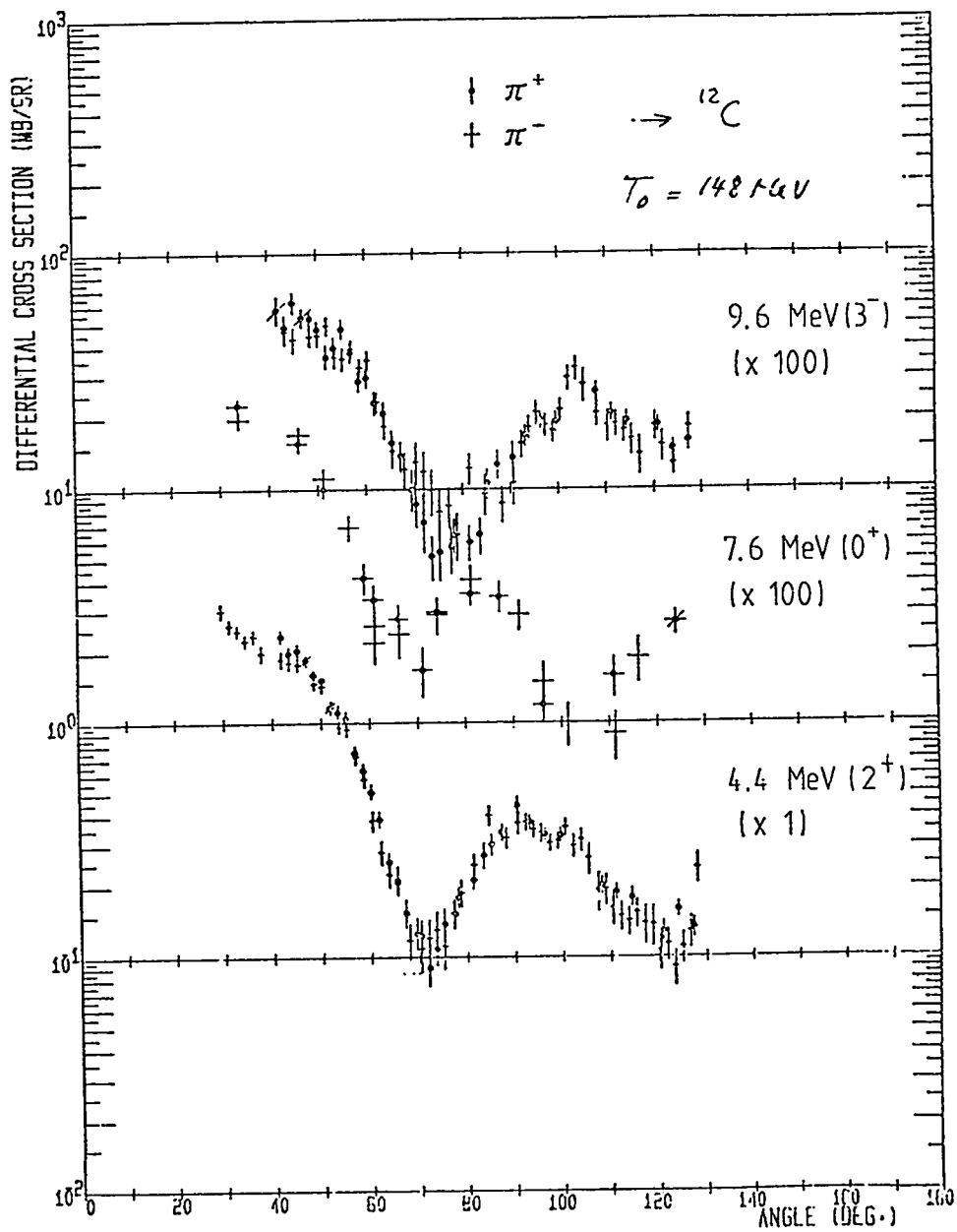has long been regarded as a process of interest due to the dynamics involved and nuclear structure research possibilities. The reaction is usually assumed to take place in two steps, a charge exchange on one nucleon followed by another (6). However other mechanisms via delta production (7) or scattering from a virtual pion (8) could also be involved.

At SIN we carried out a high-resolution measurement of the pion double-charge-exchange (DCE) reaction $^{18}O \; (\pi^+, \pi^-)^{18}Ne$ and observed the ^{18}Ne ground state which is a $\Delta T_Z = 2$ isobaric analog state of the ^{18}O ground state. Numerous experiments (9) were performed over the last 13 years in an attempt to identify specific final states without producing convincing evidence for them. Recently a group from Los Alamos (10) reported a clear peak at the location of the ^{18}Ne ground state in the $^{18}O \; (\pi^+, \pi^-)^{18}Ne$ DCE reaction at 139 MeV and 0°. Since their resolution was 4 MeV FWHM and the first ^{18}Ne excited state ($T^P = 2^+$, 1.89 MeV) is probably negligible with respect to the ground state at 0°, they attributed the entire peak to the ^{18}Ne ground state. With a typical resolution of 1 MeV FWHM, we were able to identify the 1.89 MeV state in principle, depending only on its cross section. In addition, we determined a value for the differential cross section, integrated over the DCE continuum and the excited states of ^{18}Ne up to 20 MeV excitation energy.

For the experiment the channel was tuned for a π^+ beam and the spectrometer for the opposite polarity. Measurements were taken at 148 MeV and 187 MeV. For the 148 MeV data, a 5 mm liquid $H_2{}^{18}O$ (98%) target was used. Because of very low count rates, the 187 MeV data were obtained with the above target

plus a 10 mm liquid D_2 ^{18}O (95%) target. Resolution was 0.7 MeV and 1.1 MeV

FWHM, respectively. The spectrometer was set at a fixed 18° scattering angle

to avoid the direct beam. This is the smallest angle compatible with low back-

ground. During the experiment, the incident pion flux was approximately

4×10^6 π^+/s corresponding to a primary proton beam of 40 μ A.

The detection apparatus is shown in fig. 6. In addition to the standard

layout used in the carbon experiment, a scintillator S1 monitored the beam

together with the fast MWPC C1 and C2. Muons and erratic particles in the

spectrometer were rejected through ion optics and time of flight between counter

S3 and the 50 MHz signal.

The TOF resolution was 1 ns FWHM for the channel and 1.5 ns FWHM for the

spectrometer which resulted in decisive electron rejection. The DCE candidates

were identified by the logic trigger requirement

(p.C1.C2.S1) * (C3.S2.S3) * anti (V1 or V2)

Chambers C2, C3 and C4 were used for projection onto the scattering target

and calculation of the scattering angle. Thus events which did not pass through

the target were rejected; C3 was also useful for rejection of γ -rays from π°

decay. The histograms of fig. 7 passed the following tests:

- TOF in the πM1 channel
- target position
- scattering angle
- optics in the spectrometer
- TOF in the spectrometer

The field in the spectrometer magnets was adjusted to fill approximately

75% (Δ p/p) of the focal plane with DCE events and the remaining 25% provided

a background measurement and a good test for the rejection conditions mentioned

above. For calibration purposes and extraction of an absolute cross section,
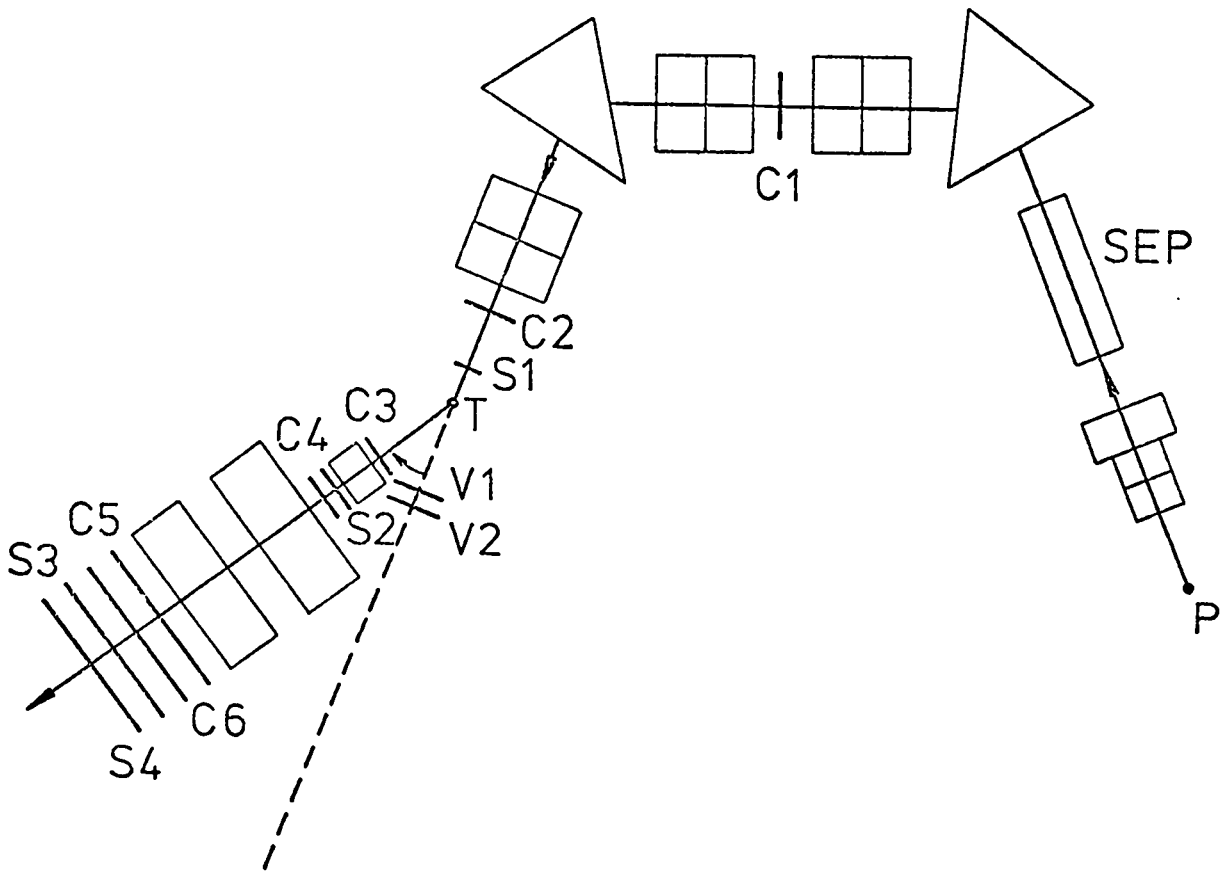
Fig. 6   Schematic layout of the SIN πM1 channel and pion spectrometer for
           double charge exchange measurements. C1 - C6 are MWPC's. C1 and
           C2 have a fast digital readout and in C3 to C6 delay lines are used.
           S1 - S4 are scintillators and V1 - V2 veto counters.

elastic scattering spectra on ^{18}O and ^{12}C were taken at 18° and a polyethylene [(CH$_2$)n] target was used at 45°.

In fig. 7 we present our two DCE spectra. There is no background and the ^{18}Ne g.s. is clearly separated from the DCE continuum which starts at about 4.5 MeV excitation energy. The full spectrometer acceptance of 8° FWHM was used and no angular binning was done. The ^{12}C elastic scattering data was normalized with the value of 293 mb/sr for the lab differential pion-carbon elastic cross section at 18° and 148 MeV (303 mb/sr at 18° and 187 MeV) obtained from our carbon data (4). This normalization then contains the solid angle acceptance of the spectrometer, the transmission through the spectrometer, the focal plane acceptance, etc. It was then used to normalize the DCE spectra yielding a lab differential cross section for the ^{18}O (π^+,π^-)^{18}Ne ground state of

$$\frac{d\sigma}{d\Omega}_{lab} (18°, 148 \text{ MeV}) = 0.30 \pm 0.10 \ \mu b/sr$$

$$\frac{d\sigma}{d\Omega}_{lab} (18°, 187 \text{ MeV}) = 0.21 \pm 0.08 \ \mu b/sr.$$

The quoted error is obviously dominated by statistical uncertainties. A cross check of the [(CH$_2$)n] spectra against the known hydrogen cross section (11) produces consistent results. Due to the lack of statistics for the transition to the first excited state of ^{18}Ne, only an upper limit can be presented for the differential cross section at 148 MeV, $\frac{d\sigma}{d\Omega}_{lab}$ (18°, 148 MeV) $\leq$ 70 nb/sr. At 187 MeV the cross section was estimated as $\frac{d\sigma}{d\Omega}_{lab}$ (18°, 187 MeV) $\simeq$ 120 nb/sr. The important DCE contribution for strongly excited and unbound states is easily observed because of the large momentum acceptance of the spectrometer. Integration over the DCE continuum and the excited states of ^{18}Ne up to 20 MeV excitation energy, yields a lab differential cross section of
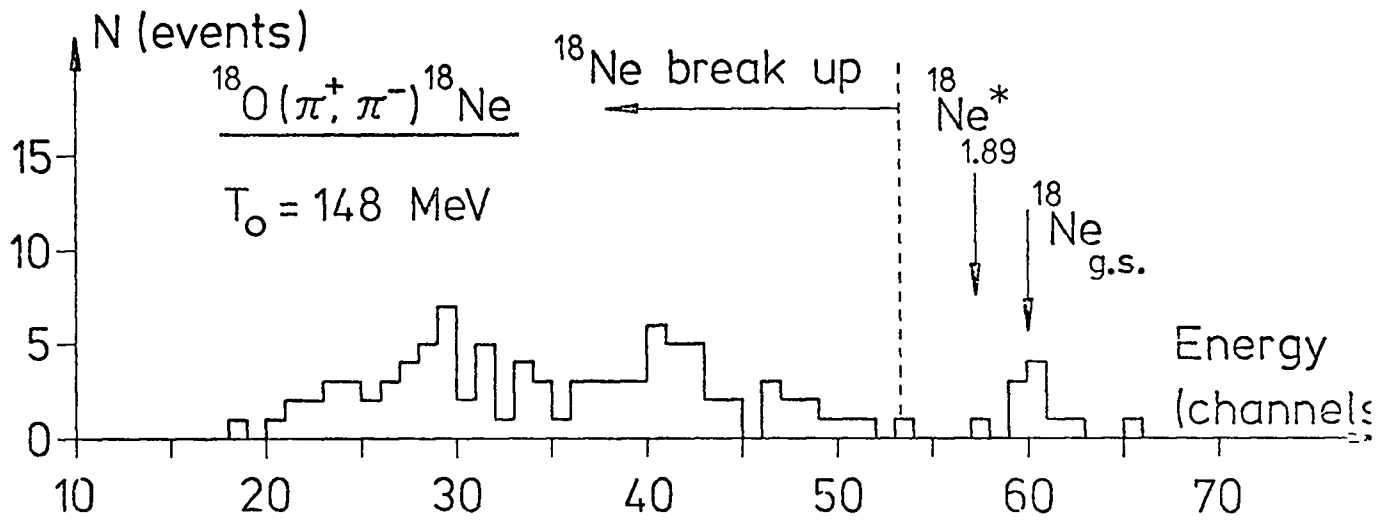
Fig. 7A ^{18}O (π^+, π^-) ^{18}Ne spectrum obtained at an incident pion energy of 148 MeV and a spectrometer angle of 18° for events surviving the tests described in the text. The DCE continuum was not corrected for spectrometer transmission.
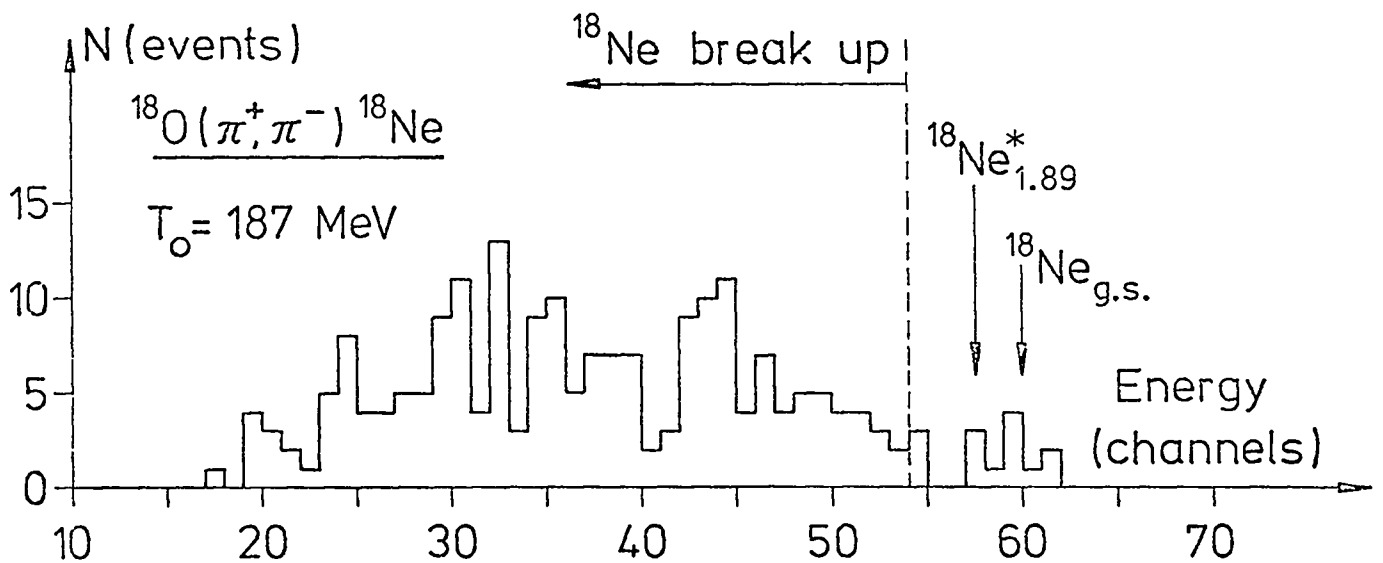

Fig. 7B ^{18}O (π^+, π^-) ^{18}Ne spectrum obtained at a 187 MeV pion energy with identical conditions than for fig. 7A.

$$\int_{E_x = 4.5 \text{ MeV}}^{E_x = 20 \text{ MeV}} \frac{d^2\sigma}{d\Omega\, dE_x} (18°)\, dE_x = 3.8 \pm 0.7 \ \mu b/sr \text{ and } 3.0 \pm 0.5 \ \mu b/sr,$$

at E_π = 148 and 187 MeV, respectively.

The quoted error includes statistics and uncertainties due to spectrometer transmission.

The comparison of our results with the value of 1.78 ± 0.30 $\mu b/sr$ at 0° and 139 MeV given in ref. 10 probably shows a significant angular dependence of the cross section. Recently, several theoretical calculations (6) have been performed, based on multiple scattering theory. It is interesting to note that the prediction of Liu and Franco, for example, is in qualitative agreement with both our results and those of ref. 10.

66 shifts are scheduled for further DCE measurements this summer. These include data on ^{18}O at energies above 200 MeV (if spectrometer TOF resolution is sufficient); at zero degrees (if background levels are not too high) and larger angles (if count rates are sufficient). In addition some measurements on other nuclei are planned.

C.   PION SCATTERING ON ^{40}Ca and ^{48}Ca

A comparison of π^+ and π^- scattering in the region of the πN (3,3) resonance is an ideal tool for investigating neutron radii of nuclei, since π^+ are believed to interact preferentially with the protons and π^- with the neutrons of the nucleus. The comparison of elastic π^+ and π^- data at 130 MeV on ^{48}Ca and ^{40}Ca revealed large π^+/π^- cross section differences for ^{48}Ca at the minima of the angular distributions. However π^+/π^- differences in ^{40}Ca were less pronounced and can be explained by Coulomb distortion effects similar to those introduced by Germond and Wilkin to explain our ^{12}C data. It should be noted however that the π^+/π^- differences seen in ^{40}Ca were

already predicted years ago by Burman and Kisslinger (13). The remaining dis-
crepancies between the π^+ and π^- scattering off ^{48}Ca, together with the
charge radius obtained from electron scattering data (12) should permit extraction
of a neutron radius for ^{48}Ca. It is interesting to note that the electron
scattering experiment of ref. 12 found a very small ^{48}Ca - ^{40}Ca charge radius
difference (-0.5%) in contradiction with the $A^{1/3}$ rule (standard isotopic shift).
This rule which has been verified experimentally in electron scattering experi-
ments for many nuclei with $A \geq 12$ predicts 0.22 fm (+6.3%) for the ^{48}Ca - ^{40}Ca
charge radius difference. Presuming the matter radii also follow the $A^{1/3}$ rule,
the neutron radius of ^{48}Ca would exceed the measured charge radius by 0.4 fm
which is in agreement with some theoretical works based on shell model calcu-
lations (14). However Hartree- Fock calculations predict lower values between
0.1 and 0.2 fm (15).

The experiment involved a layout similar to the one used for pion-carbon
scattering. Typical running conditions with a primary proton beam of $\simeq 40\ \mu$ A
were $2 \times 10^6\ \pi^+$/s and $2 \times 10^5\ \pi^-$/s incident on a 250 mg cm^{-2} 92% enriched
^{48}Ca target and on a 300 mg cm^{-2} natural calcium target. A typical spectrum
is shown in fig. 8.

The results of our analysis yield preliminary elastic angular distributions
for ^{40}Ca and ^{48}Ca. Since the spectrometer has an angular acceptance of 8° FWHM,
the data was divided into angular bins of 2°. Because the minima in the cross
section are relatively deep, a finite angle correction was performed which is
similar to the FAC introduced in ref. 2. Measurements were taken at 6° inter-
vals, thus giving overlapping bins. The relative differences of 2 bins at the
same scattering angle for 2 spectrometer positions were consistently compatible
with statistics. Relative normalization between π^+ and π^- data was obtained
by taking beam composition into account. For normalization purposes, measure-
ments were also gathered with a polyethylene [$(CH_2)n$] target. Scaling our
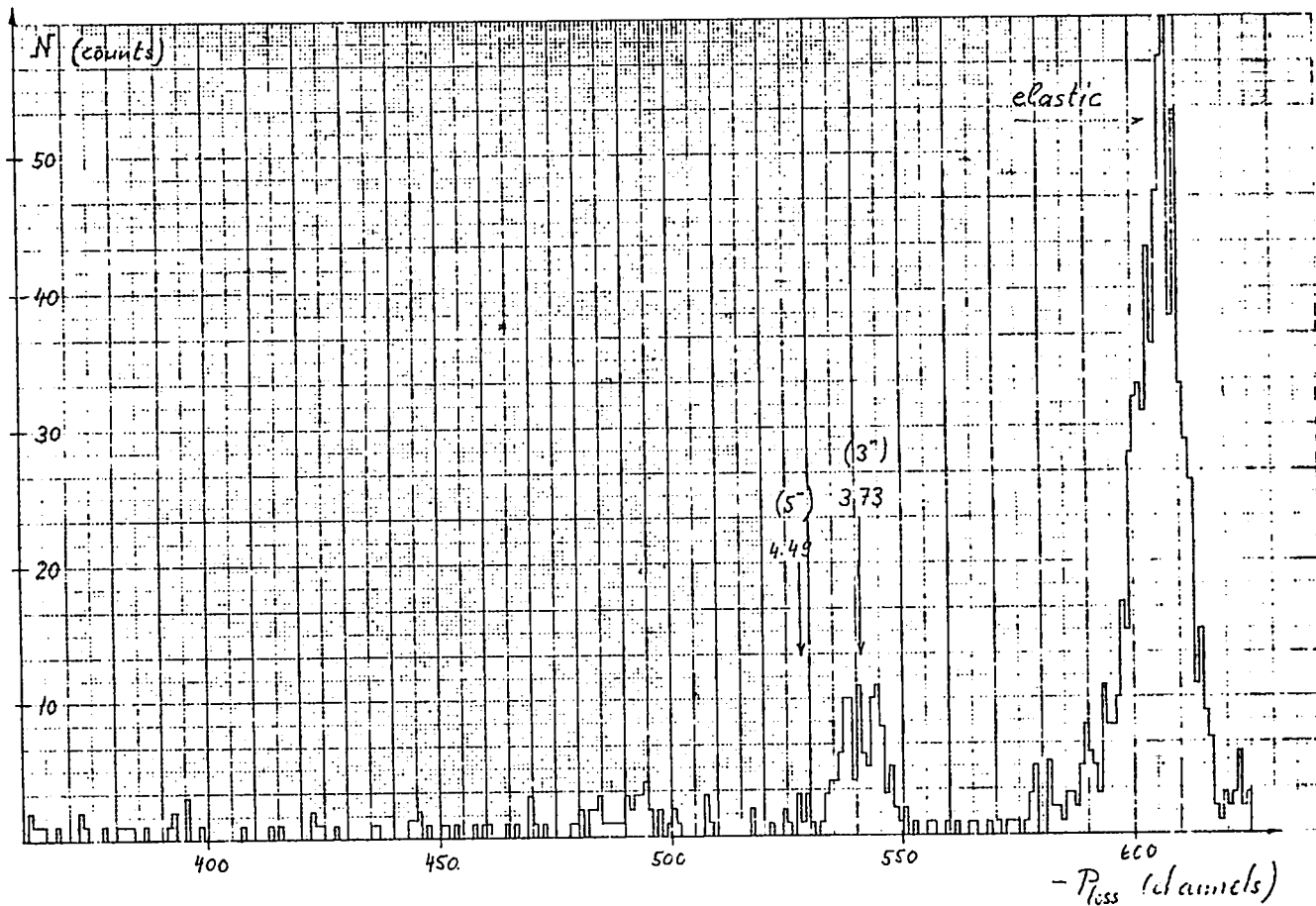
Fig. 8   Pion - ^{40}Ca scattering spectrum for 130 MeV π^- at a lab angle of 45°.

data against the known hydrogen (11) and carbon (2,4) cross sections yielded the cross section values presented. The preliminary angular distributions are given in fig. 9. No subtraction of background was required; error bars are statistical. In the case of ^{48}Ca the π^+/π^- cross sections near the minima of the angular distributions differ up to a factor 4. In addition, the position of the first minimum is shifted by $\simeq 5°$ towards smaller angles for π^-. The shift is $\simeq 6°$ for the position of the second minimum. These shifts as well as the important cross section differences are believed to be due partially to the larger neutron distribution in ^{48}Ca. The ^{40}Ca angular distributions show smaller differences and a smaller shift of the minima ($\simeq 2°$ for the first minimum).

Further measurements on ^{40}Ca and ^{48}Ca are planned this fall at energies where Coulomb distortion effects should be reduced.

D.   INELASTIC STATES IN ^{18}O, ^{28}Si, ^{50}Ti and ^{52}Cr

In order to test possible mechanisms for the excitation of nuclear states by pion inelastic scattering, it is necessary to choose targets whose ground state and excited state wave functions are well known. Given this condition, it may be possible to isolate effects resulting from the reaction mechanism. Types of states that have been studied in sufficient detail both experimentally and theoretically can be placed into three categories; specifically these are (a) states whose wave functions contain a minimum number of shell model configurations, (b) collective states characterized by rotations of a rigid rotor or vibration of a viscous sphere, and (c) continuum states which appear as multipole resonances. In the first group of low-lying states ^{18}O (involving neutrons) and ^{50}Ti and ^{52}Cr (involving protons) were chosen. ^{28}Si was selected as a typical example for the second group.

We have measured the elastic and inelastic scattering of both π^+ and π^- from ^{28}Si. The measurements were taken with a 2 mm thick natural Silicon target

Fig. 9A   Comparison of π^+ and π^- - ^{40}Ca elastic scattering lab differential
cross sections at 130 MeV versus the pion scattering angle. The
curves are the results of a calculation with an α-particle model
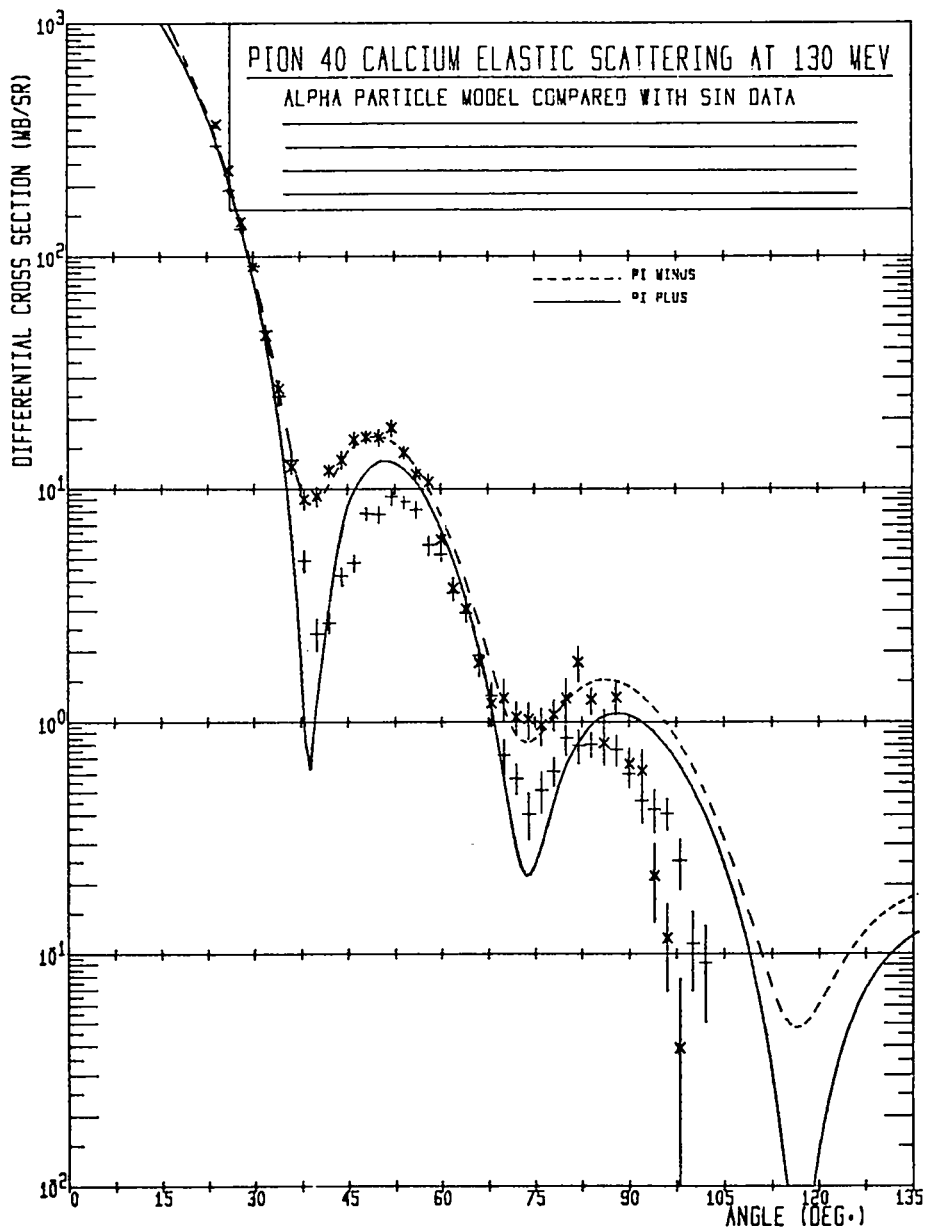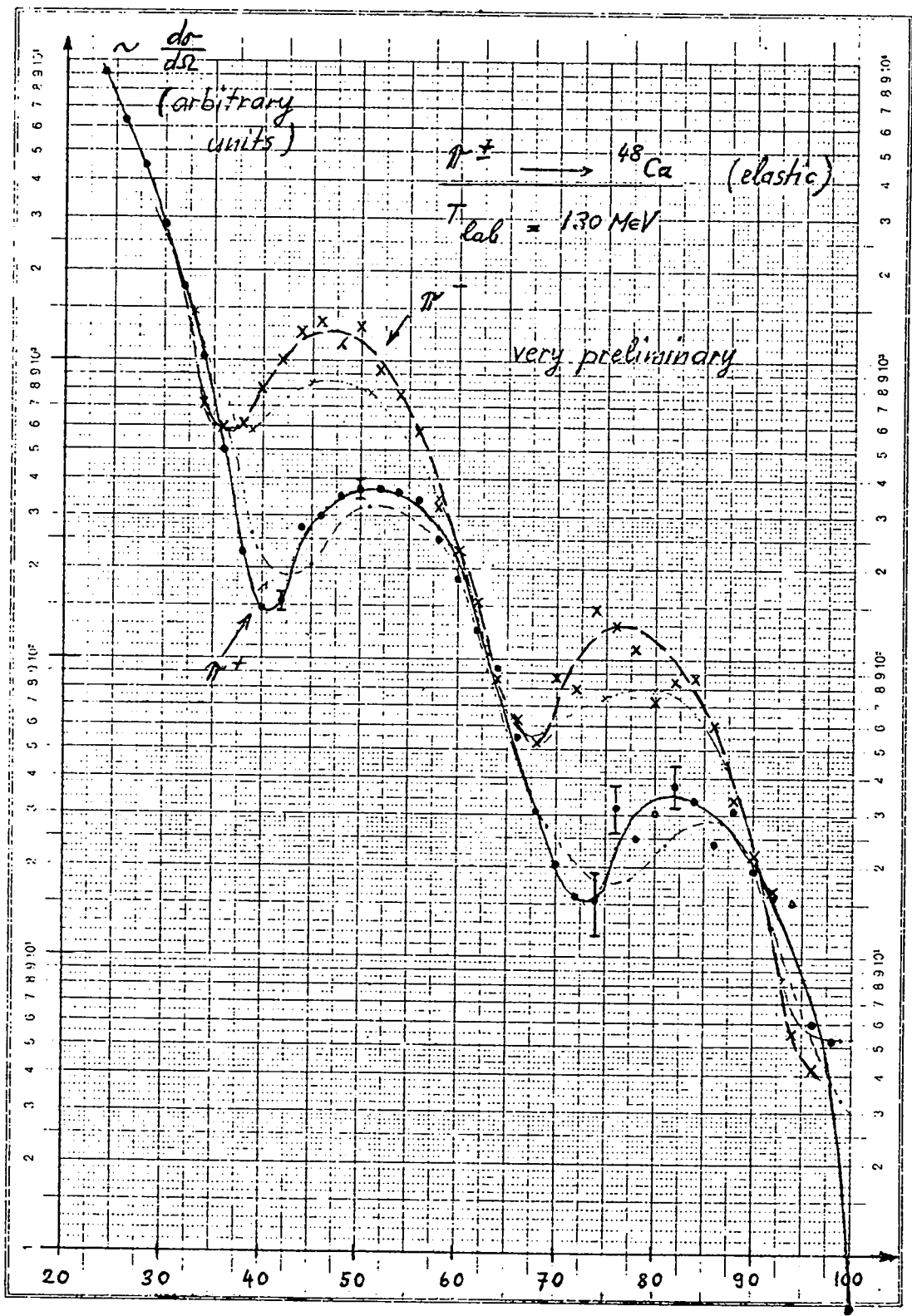(16) by Germond and Wilkin.

Fig. 9B   Preliminary comparison of π^+ and π^- - ^{48}Ca elastic lab scattering
differential cross sections at 130 MeV versus the pion scattering
angle. Normalization is arbitrary. Analysis is still in progress.

(92.2% ^{28}Si). Differential cross sections were obtained over the angular region from 27° to 87° for both polarities. The resolution was approximately 600 KeV (FWHM). A spectrum for π^+ taken at 81° is shown in fig. 10.

Preliminary analysis of the data shows no major differences between the two angular distributions for the excitation of the first 2^+ state (1.78 MeV). Differences in the elastic scattering are similar to those observed at 148 MeV for ^{12}C (4).

Plans are to increase the angular range of the ^{28}Si data and to start measurements on ^{18}O.

E.   ELASTIC SCATTERING ON ^{16}O, ^{40}Ca AND ^{208}Pb

Since the understanding of elastic scattering of pions from nuclei is important for the study of more complicated processes such as quasi-elastic scattering or double charge exchange, it was decided to perform a survey experiment on elastic scattering off ^{16}O, ^{40}Ca and ^{208}Pb. Relatively thick targets could be used since the best resolution of the system was not needed, as elastic and the first excited states are easy to separate in the above nuclei. In addition the amount of material in the beam line was not very critical which allowed the introduction of scintillators instead of MWPC into the trigger. It was therefore possible to accumulate data with good statistics in a relatively short time.

Data were taken at 5 energies on ^{16}O (80,115,163,240 and 345 MeV) with π^+ and at 3 energies (115, 163, 240 MeV) with π^-. On ^{40}Ca, measurements were obtained at 115 and 163 MeV with both polarities. In addition a measurement with both π^+ and π^- was performed on ^{208}Pb at 115 MeV. Preliminary angular distributions are presented in fig. 11 and 12. The curves given for the ^{40}Ca data are a calculation by Germond and Wilkin with an α-particle model (16) where π - ^{4}He data (17) were used as input. The results on ^{16}O and ^{40}Ca
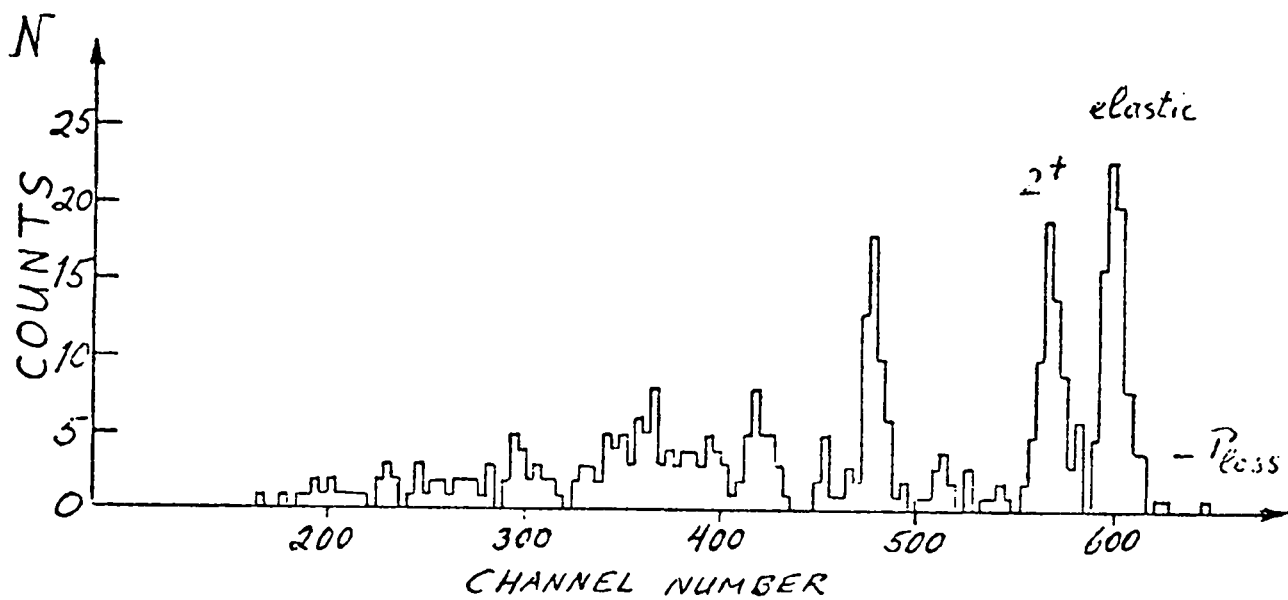
Fig. 10   Pion - ^{28}Si scattering spectrum for 130 MeV π^+ at a lab angle of 81°.
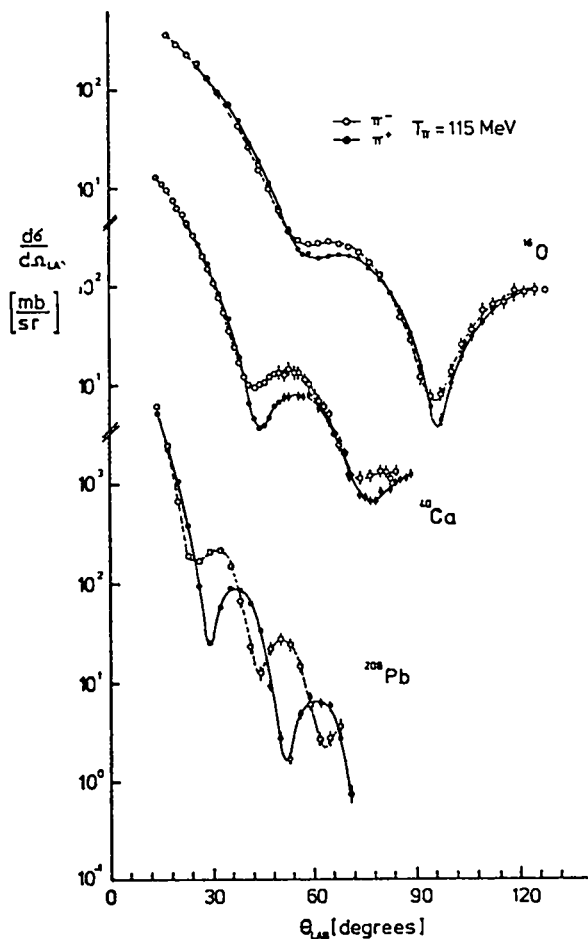
Fig. 11A
Comparison of π^+ and π^- elastic lab scattering differential cross sections at 115 MeV on ^{16}O, ^{40}Ca and ^{208}Pb versus the pion scattering angle. The curves do not result from a fit but are a simple guide to the eye. No finite angle correction was performed.

Fig. 11B
π^+ elastic lab scattering differential cross sections at 5 energies versus the pion scattering angle. No finite angle correction was performed.
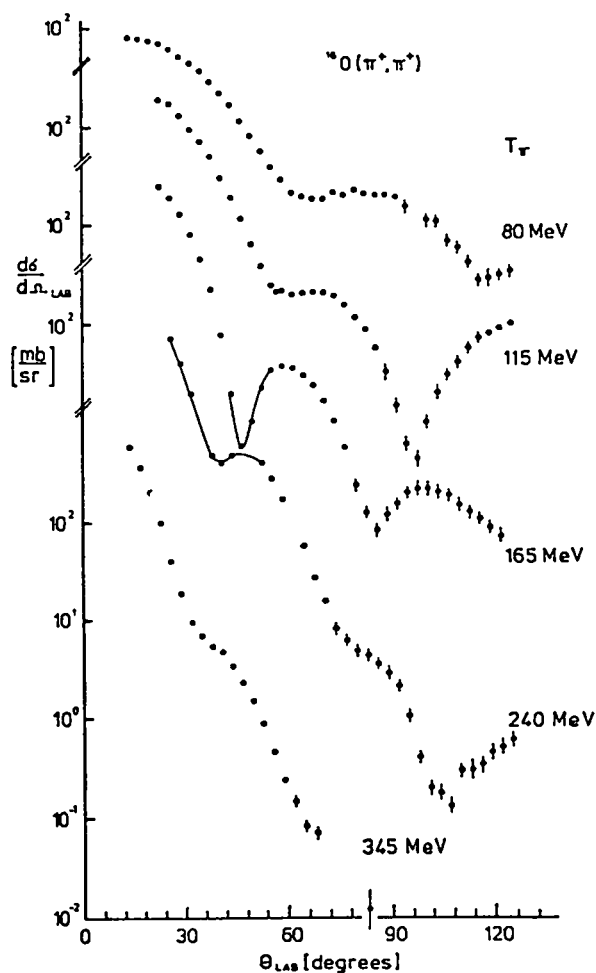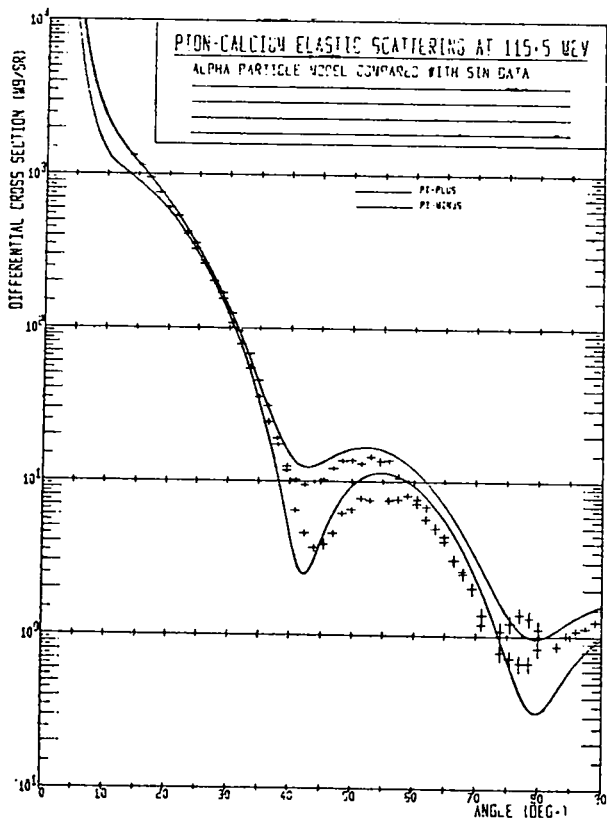
Fig. 12A
This figure is identical to
figure 9A except that the data
was taken at 115 MeV and no
finite angle correction was
performed.
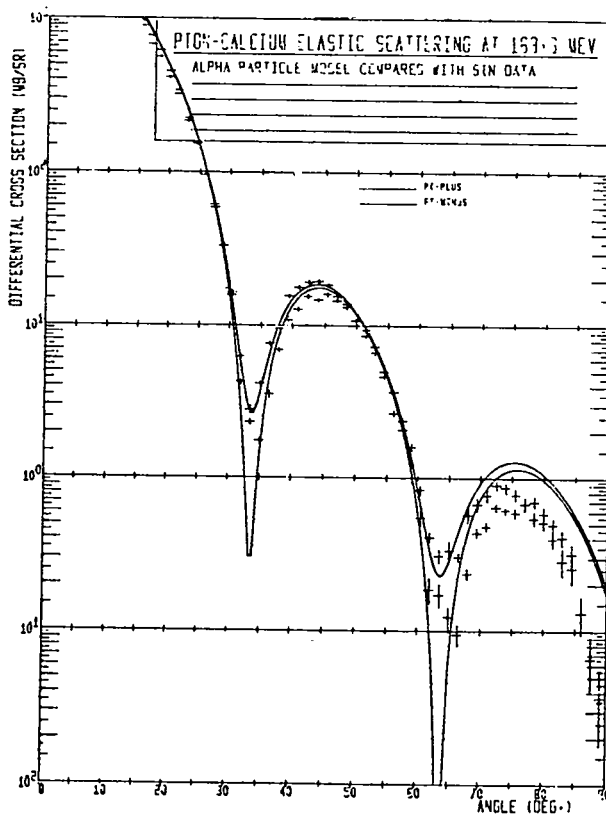
Fig. 12B
π - ^{40}Ca angular distributions
obtained at 163 MeV with identical
conditions than for figure 12 A.

confirm the elastic scattering behavior measured on ^{12}C and ^{28}Si. Cross sections of $\pi - {}^{40}$Ca elastic scattering at 115 and 163 MeV are consistent with the 130 MeV data of group A. The significant π^+/π^- differences measured on ^{208}Pb are probably only due in part to Coulomb effects and reflect the larger neutron distribution in this nucleus.

F.   DEEP INELASTIC SCATTERING ON ^{16}O

This experiment has just begun and some test runs have been made. With the completion of the new 2.4 meter long focal plane MWPC this summer, it will be possible to use the full ± 18% Δp/p momentum acceptance of the spectrometer. This condition, in addition to the 100% macro duty cycle of the SIN machine will render quasi free scattering and similar one arm and coincidence experiments very attractive.

CONCULSION

I believe that beautiful data is now coming out in pion-nucleus scattering in the region of the (3,3) resonance and that with the help of EPICS, LEP and SUSI and good theories, progress will be rapid and exciting in this wide open field of pion-nucleus physics.

NOTE

All unpublished data presented in this report should still be considered preliminary.

REFERENCES

1) J. P. Albanèse, J. Arvieux, E. Boschitz, R. Corfu, J. P. Egger, P. Gretillat,
    Q. Ingram, C. Lunke, E. Pedroni, C. Perrin, L. Pflug, J. Piffaretti,
    E. Schwarz, C. Wiedner and J. Zichy, Nucl. Inst. and Meth., to be published
    and Proc. of the Carnegie-Mellon Conf. on Meson-Nucl. Phys. 1976, page 724.

2) F. Binon, P. Duteil, J. P. Garron, J. Gorres, L. Hugon, J. P. Peigneux,
    C. Schmit, M. Spighel and J. P. Stroot, Nucl. Phys. $\underline{B17}$, 168 (1970).

3) R. Foglio, C. Perrin, J. Pouxe, U. Bart and E. Schwarz, Proc. of 2nd Ispra
    Nucl. Electronics Symposium, 1975, page 129.

4) J. Piffaretti, R. Corfu, J. P. Egger, P. Gretillat, C. Lunke, E. Schwarz
    and C. Perrin, Phys. Lett. $\underline{67B}$, 289 (1977).

5) J. F. Germond and C. Wilkin, Phys. Lett. (in press).

6) L. C. Liu and V. Franco, Phys. Rev. $\underline{C11}$, 760 (1975).
    W. B. Kaufman, J. C. Jackson and W. R. Gibbs, Phys. Rev. $\underline{C9}$, 1340 (1974).
    G. A. Miller and J. E. Spencer, Phys. Lett. $\underline{53B}$, 329 (1974) and Ann. Phys.
    $\underline{100}$, 562 (1976).

7) O. D. Dal'karov and I. S. Shapiro, Phys. Lett. $\underline{26B}$, 706 (1968).

8) J. F. Germond and C. Wilkin, Nuovo Cimento Lett. $\underline{13}$, 605 (1975).

9) L. Gilly, M. Jean, R. Meunier, M. Spighel, J. P. Stroot, P. Duteil and
    A. Rode, Phys. Lett. $\underline{11}$, 244 (1964) and Phys. Lett. $\underline{19}$, 335 (1965);
    P. E. Boynton, T. J. Devlin, J. Solomon and V. Perez-Mendez, Phys. Rev.
    $\underline{174}$, 1083 (1968); C. J. Cook, M. E. Nordberg and R. L. Burman, Phys. Rev.
    $\underline{174}$, 1374 (1968); J. Sperinde, D. Fredrickson, R. Hinkins, V. Perez-Mendez
    and B. Smith, Phys. Lett. $\underline{32B}$, 185 (1970).

10) T. Marks, M. P. Baker, R. L. Burman, M. D. Cooper, R. H. Heffner, R. J. Holt,
    D. M. Lee, D. J. Malbrough, B. M. Preedom, R. P. Redwine, J. E. Spencer
    and B. Zeidman, Phys. Rev. Lett. $\underline{38}$, 149 (1977).

11) J. Ashkin, J. P. Blaser, F. Feiner and M. O. Stern, Phys. Rev. 101, 1149 (1956).
P. J. Bussey, J. R. Carter, D. R. Dance, D. V. Bugg, A. A. Carter and A. M. Smith, Nucl, Phys. B58, 363 (1973).

12) R. F. Frosch, R. Hofstadter, J. S. McCarthy, G. K. Noldeke, K. J. van Oostr M. R. Yearian, B. C. Clark, R. Herman and D. G. Ravenhall, Phys. Rev. 174, 1380 (1968).

13) L. S. Kisslinger, R. L. Burman, J. H. Koch and M. M. Sternheim, Los Alamos Report LA-4969-MS and Phys. Rev. C6, 469 (1972).

14) L. R. Elton and A. Swift, Nucl. Phys. A94, 52 (1967); C. J. Batty, and G. W. Greenless, Nucl. Phys. A133, 673 (1969).

15) D. Vautherin and D. M. Brink, Phys. Lett. 32B, 149 (1970); H. C. Lee and R. Y. Cusson, Nucl. Phys. A170, 429 (1971); R. J. Lombard, Phys. Lett. 32B, 652 (1970).

16) J. F. Germond and C. Wilkin, Nucl. Phys. A249, 457 (1975).

17) F. Binon, P. Duteil, M. Gouanère, L. Hugon, J. Jansen, J. P. Lagnaux, H. Palevsky, J. P. Peigneux, M. Spighel, and J. P. Stroot, Phys. Rev. Lett. 35, 145 (1975).

18) R. M. Edelstein et al., Phys. Rev. 122, 252 (1961), F. P. G. Valckx et al., Nuovo Cim. 23, 1005 (1962).

PION INDUCED NUCLEON REMOVAL FROM LIGHT NUCLEI

R. J. Peterson
Department of Physics and Astrophysics
University of Colorado

Elastic and inelastic scattering studies have been one of the standard tools of low-energy nuclear physics, but more valuable yet have been the nucleon transfer reactions. For single nucleon stripping or pickup, the interaction between the projectile and the bound nucleon is tractable -- to the extent of being treated as a delta function. The question I am planning to address is the utility of pi meson beams to induce nucleon transfer reactions, primarily single nucleon, with a few examples of two or four nucleon removal. The experimental problems with pions are obvious -- even a meson factory is not a truly good source for a pion beam, and there is no bound final state for the ejectile. The opportunity is that the interaction between the pion and the to-be-picked-up nucleon is not merely a delta function, and moreover has a well-understood energy dependence. An understanding of the reaction mechanism could provide view points on nuclear structure not otherwise available.

The basic reaction is A $(\pi^{\pm},\pi N)$ A - 1, and we really don't even measure the sign of the outgoing pion or nucleon in most of the experiments. It is safe to ignore the A (π,N) A - 1 reaction to a discrete state in the A - 1 system because of its very small yield. With a three (or more) body final state, difficult coincidence experiments with good resolution are needed to specify exactly what reaction happened and to measure the angular dependence. I'll mention the few experiments I know about, but these are not too useful to unravel the structure of complex nuclei because of the very poor resolution. A bubble chamber experiment[1] has provided much information on states with several emerging protons, but with poor resolution and statistics.

The larger set of data is obtained by observation of the final nucleus, A - 1, earliest by counting the radioactive decay to measure the dependence of the total cross section to all bound final states as a function of pion kinetic energy.[2,3,4,5] A more sophisticated scheme is to detect the prompt gamma decay lines in the A - 1 nucleus. This must be performed in the pion beam, which often provides terrific backgrounds of other gamma radiation. With good resolution, some kinematic information is gained from the Doppler shift seen in the gamma ray, which measures the mean momentum of the (A - 1) nucleus as it recoils from the exitting nucleon.[6,7,8,9,10] Often, however, a variety of gamma ray feedings produce the spectrum, and again one isn't sure of the yield to discrete states.[11,12,13] For a few light nuclei, single nucleon removal provides only one gamma ray,[14] or so few that feedings can be unravelled. Some such data are published, and an extensive set of experiments have been done here at LAMPF, but the results are largely unpublished. Since these results are the most complete and systematic available, I'll go over the experiment a bit. The data were taken by a collaboration from the Universities of Colorado, Texas and Virginia.

The beams of π^+ and π^- was from the EPICS channel, last summer before the large spectrometer was installed. Figure 1 shows a view of the setup. A crossed field separation removed most of the protons from the π^+ beam. The flux was monitored by a calibrated ion chamber for some runs, and normalization for all runs was done with direct counting of minimum ionizing particles incident upon the target at $S\phi$. The fraction of pions in this beam is known.[15] The detectors were large, heavily shielded NaI crystals with anti-coincidence plastic detectors to eliminate particle events. These detectors were at 90^0 and 125^0. Their efficiencies were determined directly with a calibrated Co^{56} source up to 3 MeV, then extrapolated with the aid of Monte Carlo calculations. The time difference between the beam counter $S\phi$ and the gamma counter was used to specify

a proper event, and to measure backgrounds. Figure 2 shows such a time spectrum, with a resolution of better than 3 nsec. Sample gamma spectra are shown with background subtracted -- on time minus off time -- for a target of ^{7}Li (Fig. 3) to the 0^+ T = 1 state. The decay scheme of ^{6}Li is indicated. Figure 4 shows a spectrum for proton removal from ^{9}Be to ^{8}Li. Similar data were taken for targets of ^{12}C, ^{13}C , and ^{16}O.[16]

The pi-induced cross section for producing any sort of nucleon are large, and in the thick targets there is the possibility of sequential processes, such as $(\pi,2p) \rightarrow (p,p')$. For a low-energy transition in ^{55}Mn, this has been shown to be the dominant mechanism.[17] The signature of a sequential process is a yield quadratically dependent on target thickness. The data in figure 5 show the yield of 4.4 MeV gamma from a ^{12}C target, divided by the number of beam particles, plotted against the target thickness. The line is a least-squares fit, and shows a dependence linearly dependent on the target thickness, inter-cepting at zero. Similar results are found at other pion energies on ^{12}C and for the ^{7}Li target. We are assured then that we have only a one-step process in the one inch targets used for most of the data.

The energy dependence of the gamma ray yields is quite striking. The data of figure 6 for ^{7}Li are published[14]. The curves are the total cross sections for $\pi^{\pm}$ - neutron scattering, scaled down to the observed magnitude. The rest are new, from ^{9}Be (figure 7), ^{13}C to 2^+, T = 0 state of ^{12}C (figure 8) and to the 1^+, T = 1 state of ^{12}C (figure 9). The yield for a prominent line to be discussed in more detail for the ^{12}C target also have the resonant shape (figure 10). This same energy dependence is noted in the radioactivity ex-periments[3,4]. Note the size of the observed cross sections. For the 2^+ state of ^{12}C (figure 8), the 40 mb cross section to this one state is almost 10% of the 680 mb total cross section on natural carbon.[18]
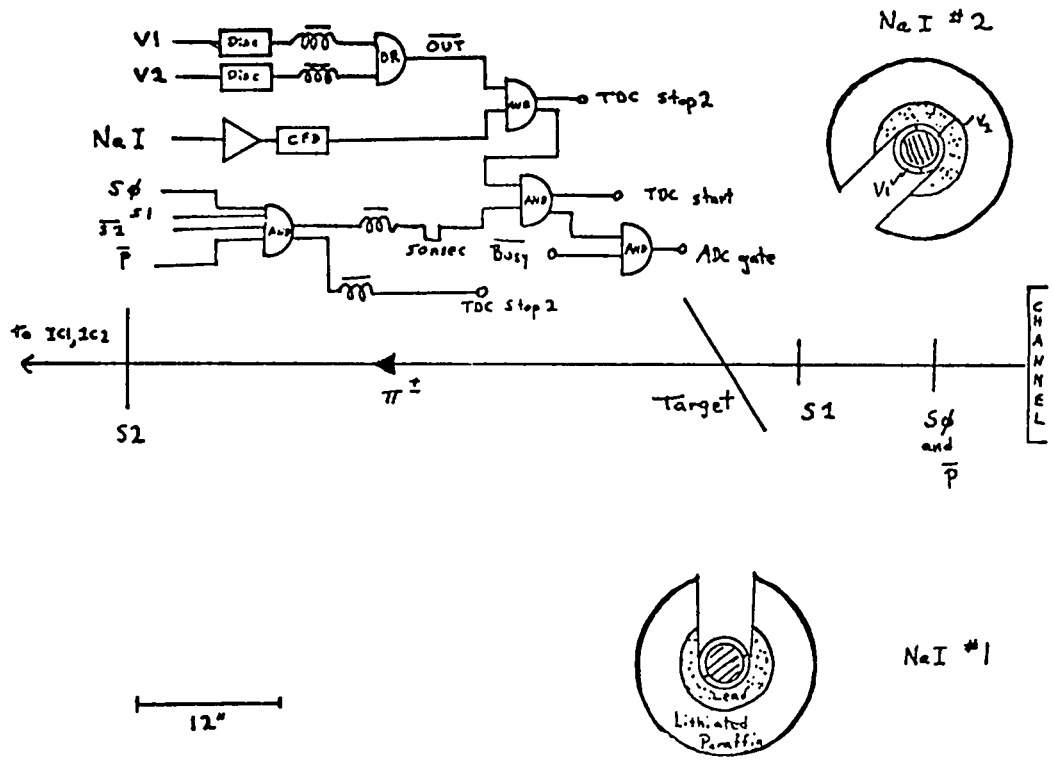
1. An overhead view of the setup used for in beam gamma experiments on the EPICS channel at LAMPF. The sketch shows the logic to select valid gamma ray events.
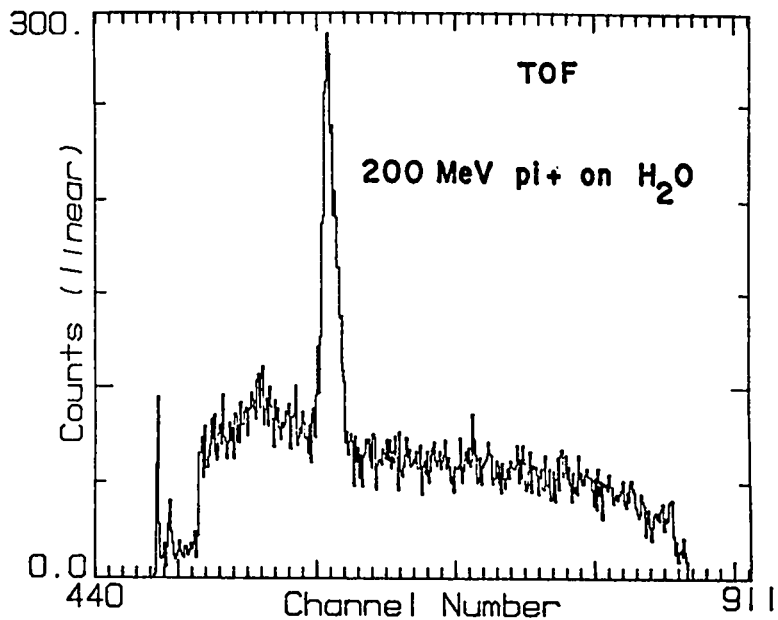
2. The time difference between events in the plastic scintillater Sϕ and a NaI crystal is plotted. A gate on the sharp (better than 3 nsec) peak selected the prompt events. Background was subtracted by an off-time window.
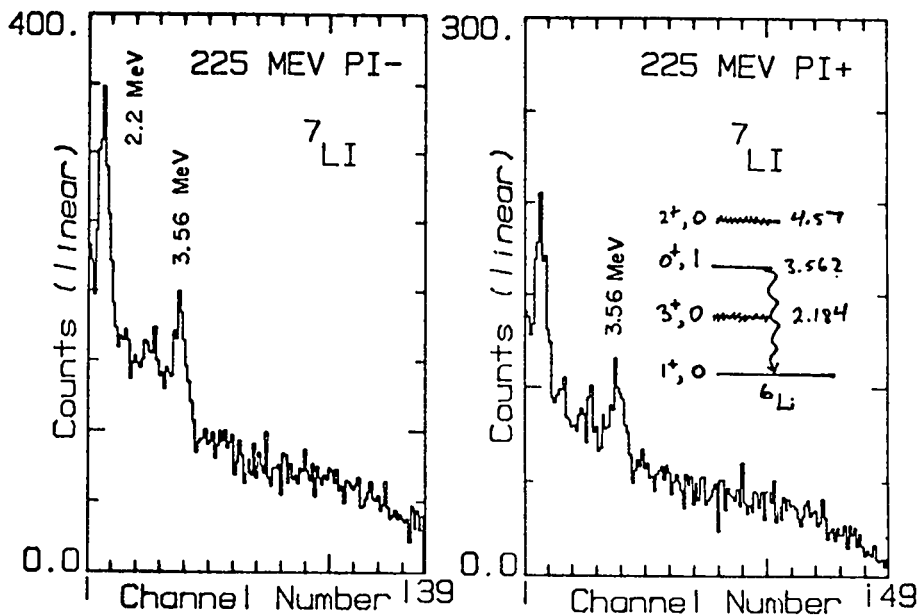
3. Gamma ray spectra from pion bombardment of ^{7}Li. The 3.56 MeV line is seen to be a unique signature for neutron removal to the 0^+, T = 1 state in ^{6}Li.
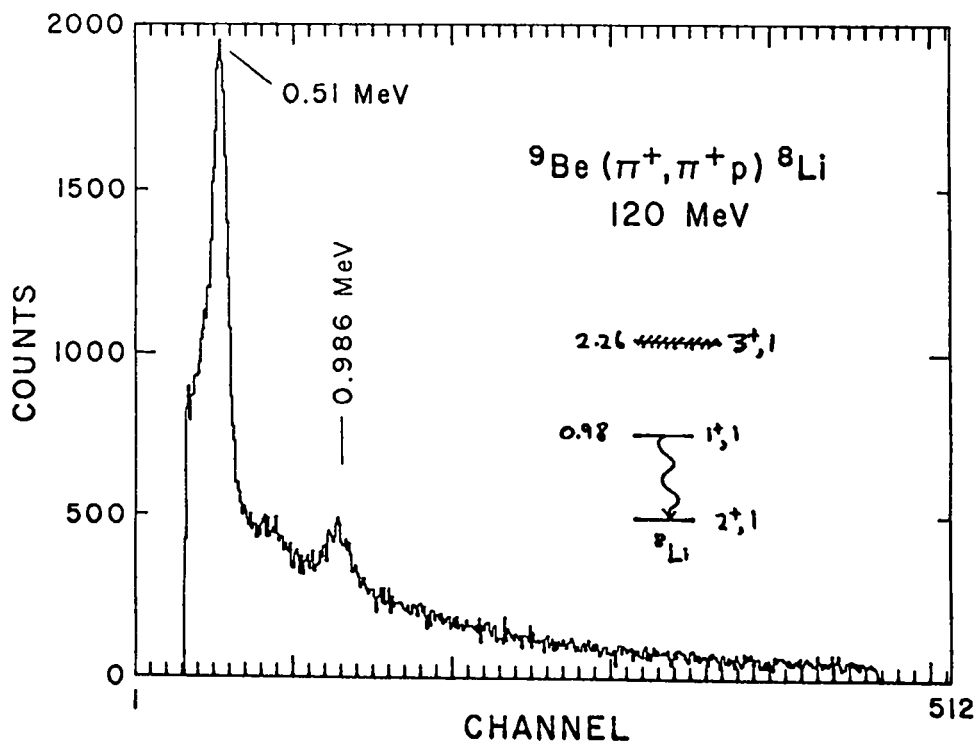
4. A gamma ray spectrum from π^+ bombardment of ^{9}Be. The 0.986 MeV line is a unique signature for proton removal to the 1^+, T = 1 state at 0.986 MeV. No other gamma emitting states are found in ^{8}Li.

100 MeV π^+ on $^{nat.}C$

Counts / Beam (IC1)

fit to $a + bT$

$a = 0.09$
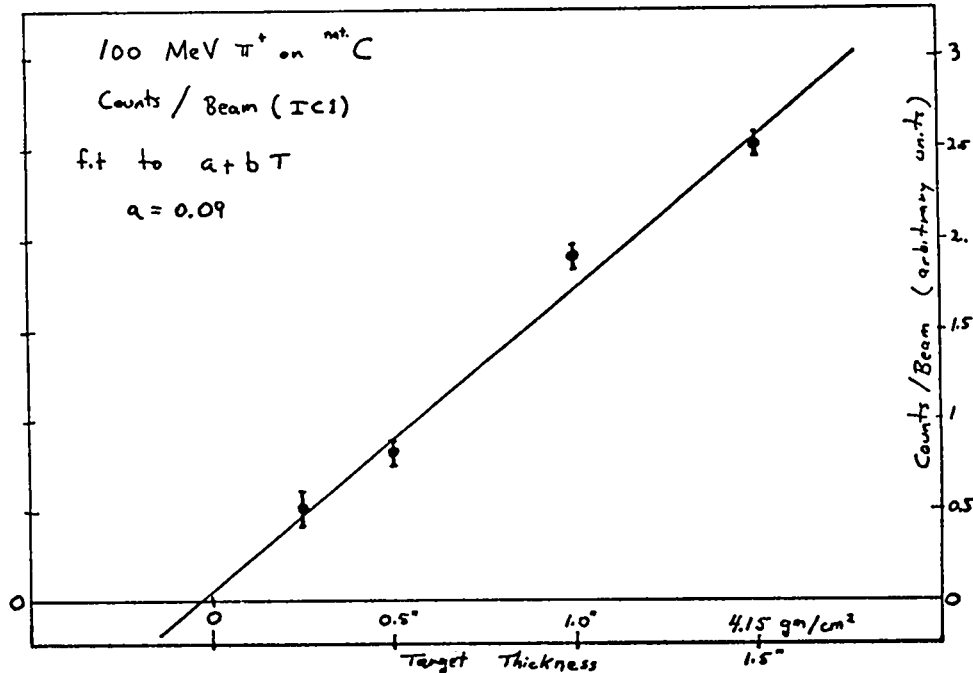
5.   The yield of 4.4 MeV gamma rays from π^+ bombardment of a carbon target is divided by the pion flux and plotted against the target thickness. The least-squares fit shown indicates that sequential, thick target effects are small. The one inch target was used for all data runs.

$^7Li \, (\pi, \pi N) \, ^6Li$
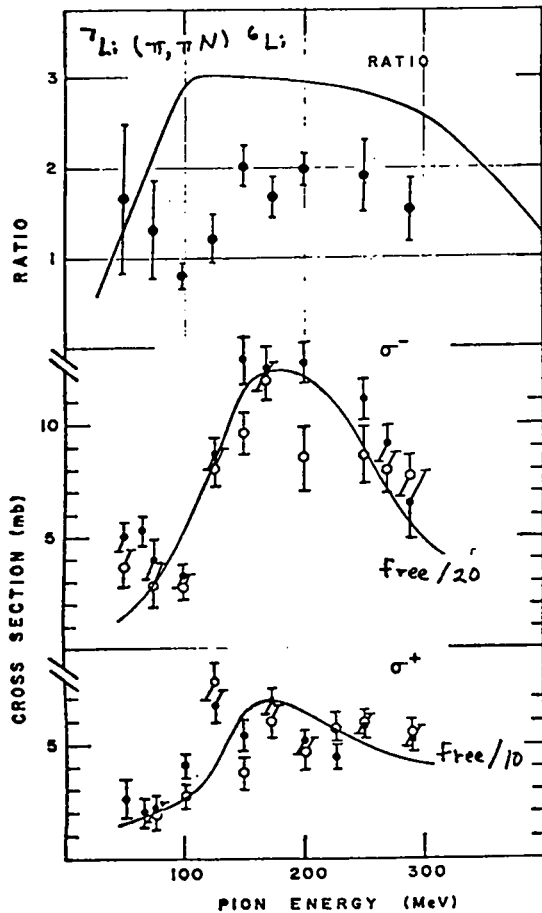
6.   The cross sections for production of the 0^+, $T = 1$ state of ^6Li by pions are plotted against the pion lab energy. The curves are the free pion-neutron cross sections, scaled by 1/20 for the π^- and 1/10 for the π^+ results. The ratio at the yields, $R = \sigma-/\sigma+$ is plotted at the top, compared to the ratio of free pion-neutron cross sections. The open circles are from the 90 degree counter, the solid circles from 125 degrees.

7. The cross sections for populating the 0.98 MeV 1^+, T = 1 state of ^{8}Li by pion bombardment of ^{9}Be are plotted as a function of the pion energy. The curves are scaled free pion-proton cross sections. At the bottom are shown the ratios of π^+ to π^- yields. The open circles are from the 90 deg. counter, the solid circles are from 125 deg.
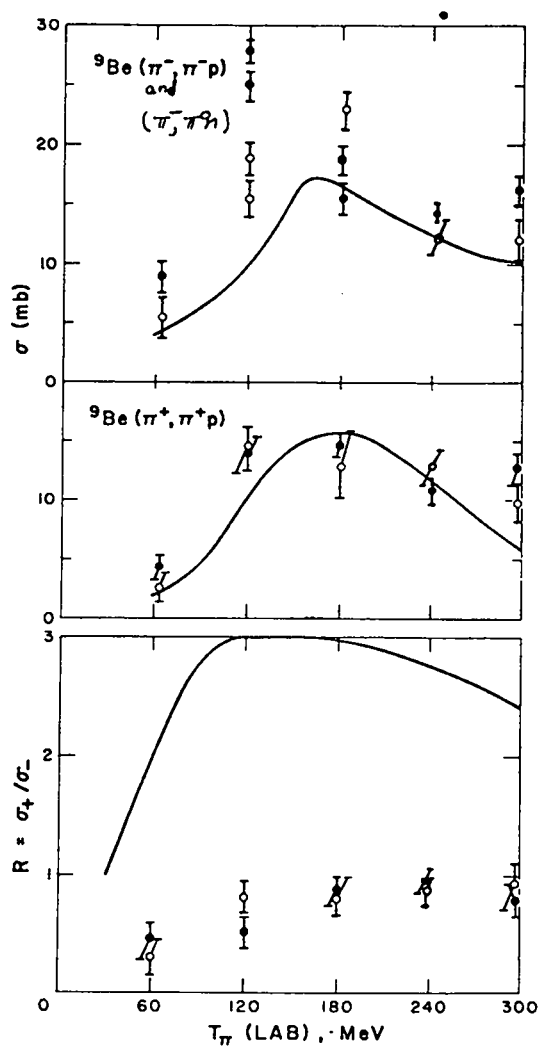
8. The yields to 2^+, T = 0 state of ^{12}C at 4.44 MeV as found from pion bombardment of ^{13}C, plotted and compared as in figure 7.

- 77 -
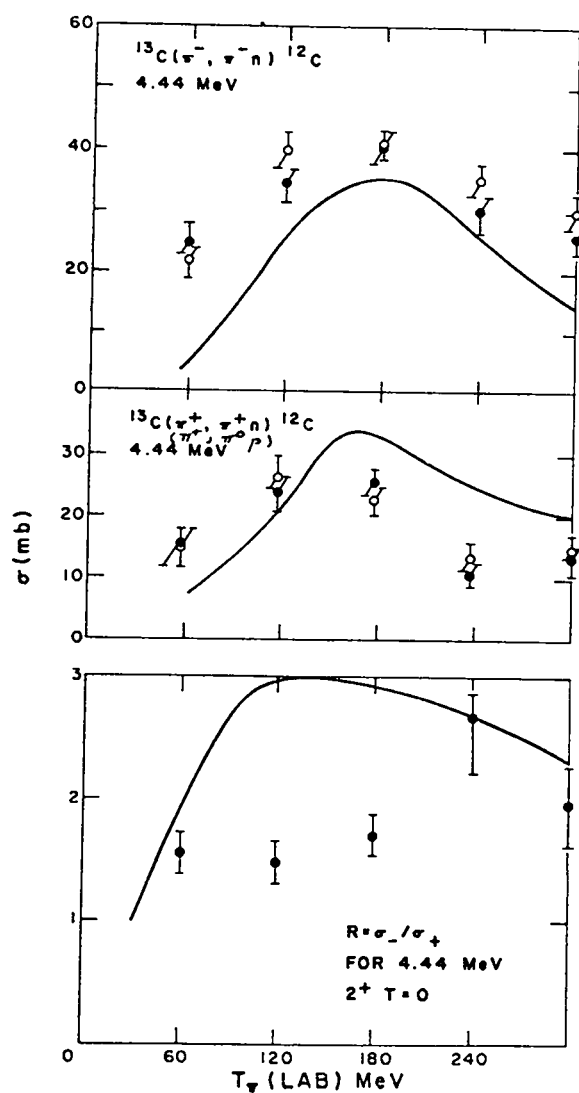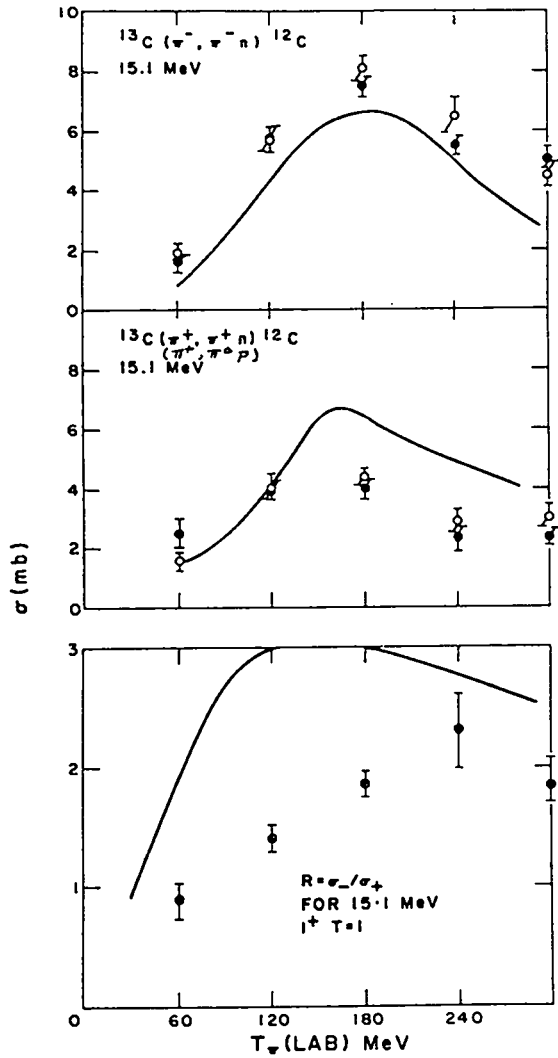
9. The yields to the 1^+, $T = 0$ state of ^{12}C at 15.1 MeV as found from pion bombardment of ^{13}C, plotted and compared as in figure 7.

10.

The yield for π^+ induced nucleon removal from ^{12}C to the $5/2^-$ states in A = 11 near 4.4 MeV is plotted. The solid curve is the scaled free π^+ - proton cross section, and the broken curve is the observed yield for inelastic scattering on ^{12}C to the 4.44 MeV 2^+ state.
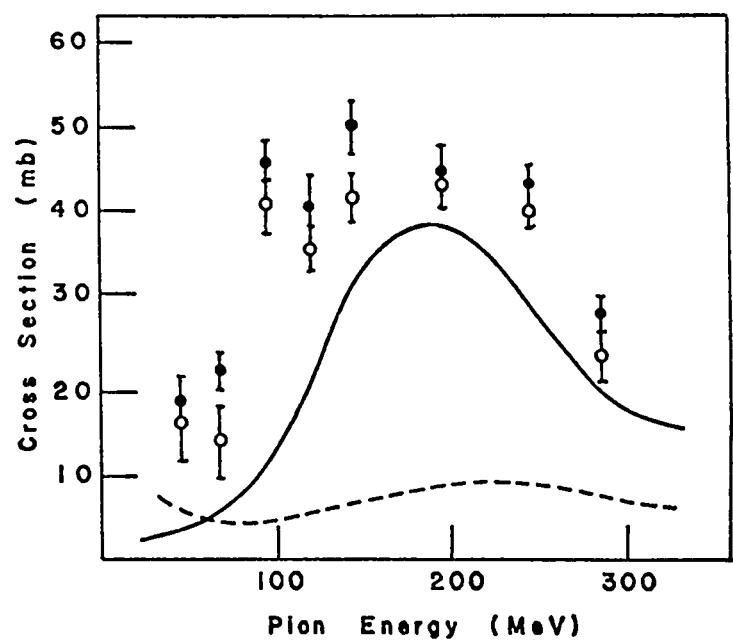
These large, energy dependent yields are emphasized by comparison to those for inelastic scattering or charge exchange reaction by pion beams. Figure 11 shows the data for several transitions known from low energy nuclear physics to be very collective -- scattering to the rotational state of ^{12}C,[12,19,20] analog charge exchange yields on two targets,[22] and non analog charge exchange on ^{10}B. The biggest yield, for ^{12}C, is taken from DWBA fits to the data of Binon[19] and Dytman.[20] This is still much less than the weakest nucleon removal yields. The 3 - 3 resonance, so prominent in the nucleon removal data, is absent for these direct reaction cross sections.

We might also compare the pion induced yields to discrete final states to the spectroscopic factors for direct pickup to the same states. In Table 1 we see no simple relation. For the radioactivity study of ^{13}N, only the ground state is bound, and so this result may be included.[2] The arguments for the population of the A = 13 and A = 15 states are involved, requiring a detailed study of the final level schemes and the gamma ray spectra. The assignments of the transitions are quite secure, but too involved to go into here.

Table 1 demonstrates that no simple scaling accounts for the two sets of data, nor for electron-induced knockout.[21] The outstanding example is that for the 5/2⁻ state in the A = 11 mirror nuclei. This 5/2⁻ state cannot be any sort of hole state, and is not made in pickup reactions. This is a dramatic new effect for pions, and is just what we've been looking for. I will return to this after comparing some theoretical results to the data.

The most reliable data from the early days were the ratios of single nucleon removal by π^+ and π^-. In a quasifree picture, for neutron removal to ^{11}C, for instance:

$$\pi^- + {}^{12}C \rightarrow \pi^- + n + {}^{11}C$$
$$\pi^+ + {}^{12}C \rightarrow \pi^+ + n + {}^{11}C$$
$$\rightarrow \pi^0 + p + {}^{11}C$$
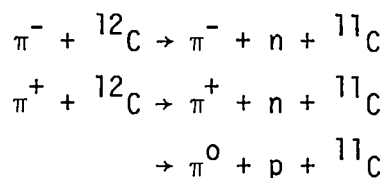
TABLE I[16)]

Final State	$(\pi,\pi N)$ Yield (mb)	Spectroscopic Factor (norm. to 2j + 1)
$^{6}Li(0^{+},1)$	12	1.0
$^{8}Li(1^{+},1)$	15	0.63
$^{11}C(5/2^{-},1/2)$	28	0.005
$^{12}C(2^{+},0)$	42	1.2
$^{12}C(1^{+},1)$	8.3	1.0
$^{13}N(1/2^{-},1/2)$	15	0.7
$^{15}N(3/2^{-},1/2)$	17	3.7
$^{15}O(3/2^{-},1/2)$	16	2.6

The last process is present because we only observe the ^{11}C, not the nucleon. On the pi-nucleon 3 - 3 resonance, the amplitudes for these three reactions, treated as quasifree, are proportional to the Clebsch-Gordon coefficients:

$$(1 \quad 1 \ 1/2 \ 1/2 \ |3/2 \ 3/2)^2 = 1$$

$$(1 - 1 \ 1/2 \ 1/2 \ |3/2 \ - \ 1/2)^2 = 1/3$$

$$(1 - 1 \ 1/2 \ 1/2 \ |3/2 \ - \ 1/2)(1 \ 0 \ 1/2 \ - \ 1/2| \ 3/2 \ - \ 1/2) = \sqrt{\tfrac{2}{9}},$$

or, since the incoherent sum of squares determines the ratios of cross section

$$\sigma(\pi^-)/\sigma(\pi^+) = 3.$$

If the experiment detects the nucleon as well, the ratio is 9.

This is not at all the case, as seen in figures 6 - 9, and is a long standing question from the radioactivity work as well.[2] The ^{11}C ratio from $\pi^\pm$ bombardment of ^{12}C is also about 1.7 on the resonance.[3] By charge independence one expects the π^+ induced proton to neutron removal cross sections from ^{12}C to be 1.7 as well. This is found.[1] These observations were an early indication that reactions of high energy pions were sensitive to nuclear structure. The nucleus was something other than merely a collection of free nucleons.

A simplest way to include the nuclear structure is to note that analog charge exchange cross sections are large in the p + ^{11}C system, and these modify the ratios of $\pi^\pm$ data strongly.[23,24,25] The data of figure 11 tell us that the pion charge exchange is weak. If P is the probability for analog charge exchange, the same for ^{11}C (n,p) ^{11}B and ^{11}B (p,n) ^{11}C, the charge exchanges are:

$$\pi^- + {}^{12}C \to \pi^- + n + {}^{11}C \to \pi^- + p + {}^{11}B$$
$$\to \pi^- + p + {}^{11}B \to \pi^- + n + {}^{11}C$$
$$\pi^+ + {}^{12}C \to \pi^+ + n + {}^{11}C \to \pi^+ + p + {}^{11}B$$
$$\to \pi^+ + p + {}^{11}B \to \pi^+ + n + {}^{11}C$$
$$\to \pi^0 + p + {}^{11}C$$
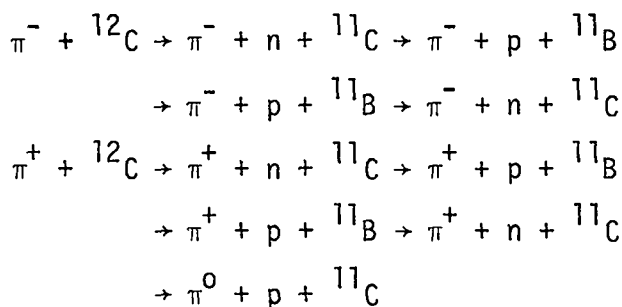
By counting the terms adding and subtracting to the yield of ^{11}C, with the 3 - 3 amplitudes, one finds

$$R = \sigma-/\sigma+ = \frac{9N(1 - P) + zP}{N(1 - P) + 2N + 9zP}$$

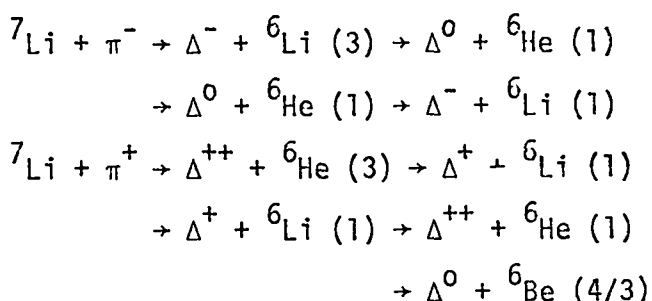with N and z the number of valence neutrons and protons, since the final states in the light nuclei are formed mainly from only the p shell. If P were around 0.25 the ratio would be 1.4, quite near the experimental value. The weakness of the picture is of course that P can vary with nucleon energy (and hence the pion energy) in some unknown way. We may also make an experimental test of this model.

From a ^{13}C target, neutron removal produces two gamma ray lines, as shown in the spectrum of figure 12. These are from the 2^+, T = 0 state and the 1^+, T = 1 state. As above, analog nucleon charge exchange is allowed for the T = 1 state, but clearly not for the T = 0 state. The ratio data for the 1^+, T = 1 state are seen in figure 9, and, as usual, a value of P near 0.25 isn't too bad. However, for the T = 0 state, for which P would have to be much smaller, figure 8 shows just the same ratio. It would appear that this simplest model fails the test.[25]

If the reaction proceeds by the formation of an explicit Δ, this excited nucleon could also charge exchange.

$$^7\text{Li} + \pi^- \rightarrow \Delta^- + {}^6\text{Li} \ (3) \rightarrow \Delta^0 + {}^6\text{He} \ (1)$$
$$\rightarrow \Delta^0 + {}^6\text{He} \ (1) \rightarrow \Delta^- + {}^6\text{Li} \ (1)$$
$$^7\text{Li} + \pi^+ \rightarrow \Delta^{++} + {}^6\text{He} \ (3) \rightarrow \Delta^+ + {}^6\text{Li} \ (1)$$
$$\rightarrow \Delta^+ + {}^6\text{Li} \ (1) \rightarrow \Delta^{++} + {}^6\text{He} \ (1)$$
$$\rightarrow \Delta^0 + {}^6\text{Be} \ (4/3)$$

with the isospin weights calculated on the 3 - 3 resonance. In the simplest picture, the ratio is still 3. For ^{7}Li, with 2 valence neutrons and one proton,
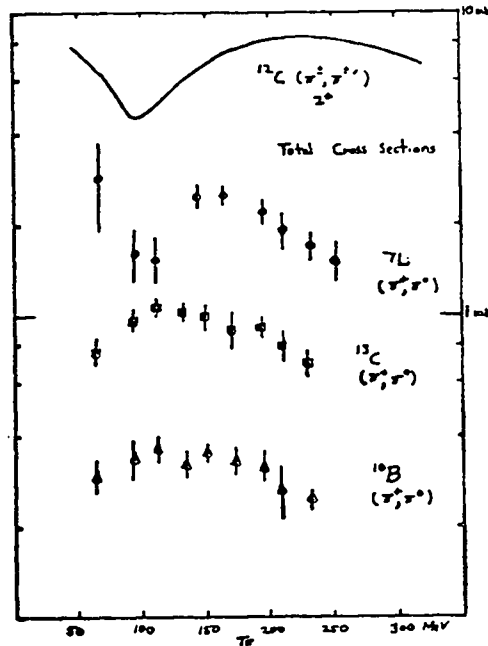
11. Total cross sections for pion induced direct reactions are plotted as a
function of pion energy. At the top is a representation of the $\pi^{\pm}$ inelastic
scattering to the ^{12}C 2^+ state at 4.44 MeV. The single charge exchange
reaction on ^7Li and ^{13}C proceed to analog states, while only a non-analog
charge exchange is available for the ^{10}B target.
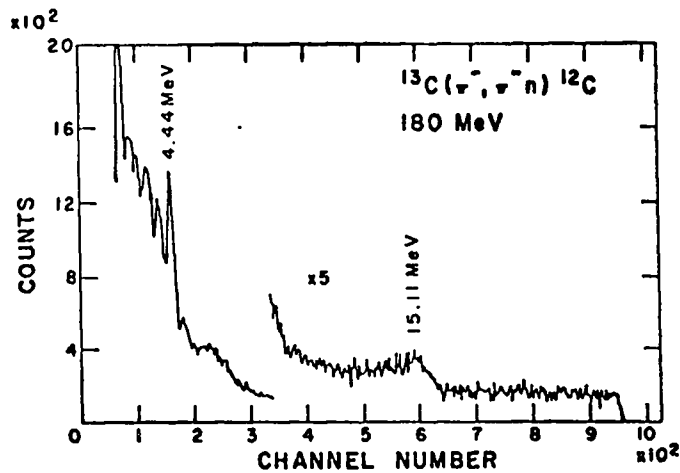
12. A spectrum of gamma rays from π^- bombardment of ^{13}C. Prominent transitions
to the 2^+, T = 0 state at 4.44 MeV and the 1^+, T = 1 state at 15.11 MeV
are noted.

the ratio, even with charge exchange of the nucleon isobar, is $R = \sigma(-)/\sigma(+) = 3$, exactly. The test is less sensitive for other targets, since the Δ charge exchange probability is unknown. This model must be rejected by comparison to the ^{7}Li data, as noted in figure 6.

And no impulse approximation, no matter what it does to the ejected nucleon, can produce other than hole states in the final nucleus. On general grounds then, the strong excitation of the $5/2^-$ state in $A = 11$ is inconsistent with any such model. There are no other such unexpected transitions to search for by the gamma-ray method, so further tests are not simple.

Of course, for a truly quasifree reaction, as identified by the full kinematics at the final state, all the arguments would still hold. I'm only comparing to the large yields measured by the de-excitation gammas, summing over all nucleon states. In a kinematically determined experiment demanding high energy protons, Swenson, et al[26] detected coincidences between the pion and proton. On targets of ^{27}Al and ^{208}Pb, they measure $R = \sigma(\pi^+)/\sigma(\pi^-)$ equal to 7.2 and 4.5 respectively. On ^{12}C, the ratio is about 8.[27] A value of nine is expected from the quasifree models. Modifications to the quasifree expectations are discussed in ref. 23. In the bubble chamber experiment on ^{12}C[1], again demanding fairly high energy protons, the ration of the cross sections for $(\pi^+, \pi^+ p)$ to $(\pi^+, \pi^0 p)$ is 3.7 ± 1.2, in agreement with the expected 4.5. So indeed, quasifree models work for quasifree experiments.

We're not the only ones who perform in beam gamma ray experiments. In the light nuclei, the same experiments have been done with photons on ^{12}C[29] and ^{16}O,[30] for instance. A realistic calculation and some data are available[31] for a ^{13}C target. On ^{12}C, for instance, the $5/2^-$ state is seen with a few percent of the ground state yield. From both ^{12}C and ^{16}O, positive parity final states are noted by neutron or proton removal. In the photonuclear business,

no one dreams of a quasifree mechanism. What happens is the photo absorption into the isovector giant dipole state, from which the one particle - one hole portion decays by emitting the particle to produce the final hole ground state. Either configuration mixing or rescattering in the compound state is invoked for the other states. With all that's known of single-nucleon spectrosopic factors, the configuration mixing is less than thought to be the case a few years ago. Many of the weaker cross sections in the (p,d) reaction, for instance, are now known to be due to multistep reaction mechanisms. The rescattering is essentially that of the nucleon that absorbed the photon with the rest of those in the target. The coherent sum of these coupled to $T = 1$, $J^\pi = 1^-$ form the classical liquid drop oscillation, with a very large cross section. This is shown schematically in figure 13. The rescattering may also mix the isospin of the giant resonance, explaining ratio experiments done by the photonuclear folks.[32]

This collective process may also be applied to pion induced nucleon removal. Let us first list some typical decay widths:

Δ (3 - 3 Resonance) $\simeq$ 100 MeV

Γ (Width of Dipole Resonance) $\simeq$ 3 MeV

γ (photon absorption) $\simeq$ 100 meV.

These last two tell us why the photon is rarely re-emitted, as nuclear Raman scattering.[33] If a pion is absorbed on a nucleon, the simple probabilities indicate that the pion is re-emitted before the nucleon decay, and the re-scattering after the pion emission is much as the photonuclear case. This pion reaction is then much like Raman scattering of photons on molecules. A dipole field of the same form that binds the target entity is absorbed and re-emitted. Hüfner[34] has demonstrated that much of the p-wave pion absorption proceeds through such a process. The first rescattering, with the pion in the nucleus, is just what we heard about from Gerry Brown this morning. The two

rescatterings of course give a new spectrum of final gamma-emitting states, not merely the hole state. These may be continuum or unbound collective giant resonance states.

First, let's deal with the $5/2^-$ states seen from the ^{12}C target. If the initial and final wave functions are written in L - S coupling, the dominant terms are[35]

$| \ ^{12}C$ g.s. $> \ = -0.840 \ | \ [44]$ L = 0, S = 0, J = 0 $>$

$< \ ^{11}C$ g.s. $| \ = 0.678 \ < \ [43]$ L = 1, S = 1/2, J = 3/2$|$

$< \ ^{11}C \ 5/2^- \ | \ = -0.893 < \ [43]$ L = 2, S = 1/2, J = 5/2$|$

$< \ ^{11}C \ 7/2^- \ | \ = -0.891 < \ [43]$ L = 3, S = 1/2, J = 7/2$|$.

Absorption and re-emission of a pion through the p-wave (1 = 1) 3 - 3 resonance can alter the orbital nuclear angular momentum by as much as $\Delta L = 2$, but not $\Delta L = 3$. Hence we are allowed to produce the $5/2^-$ but not the $7/2^-$ state, as observed. The decay of the $7/2^-$ state provides a clean gamma ray signature, which we don't see at all. Comparison of the absolute yields of the ^{11}C activation experiment[3] and the present gamma ray results indicates that about half the transitions from ^{12}C go to the ground state and half to the $5/2^-$ state. On ^{16}O, the pion induced, high resolution data of ref. 6 indicate that positive parity final states are seen, just as noted in photonuclear reactions.[30] Such states are readily formed by rescattering during the pion's transit, but our resolution was too poor to allow a systematic study of the yields.

Without a dynamic theory, we can still compute some useful ratios by isospin Clebsch-Gordon coefficients, based only on the asymptotic observables. The terminology for this analogy to molecular Raman scattering is established in figure 13. Seki[36] pursued arguments such as will follow several years ago, when less experimental information was available, and the concept is mentioned by Hewson.[23] We observe only the final nucleus T_f, T_{fz}. On a $T_i = 0$ target,

for instance, T^* may be 0, 1 or 2. On a $T_i = 1/2$ target, we assume a $T = 3/2$ super-compound state upon pion capture (remember the resonant energy dependence of the gamma ray yields). For $T_f = 0$, the predicted ratio is simply 1.55 compared to an observed value of 1.7 ± 0.4 for the 4.4 MeV state of ^{12}C. For $T_f = 1$, the ratio is

$$R(T = 1) = \left| \frac{\frac{1}{\sqrt{240}} \sum (3/2||T_1||3/2)(3/2||t_{1/2}||1) + \frac{1}{\sqrt{96}} \sum (3/2||T_1||1/2)(1/2||t_{1/2}||1)}{\frac{1+\sqrt{8}}{\sqrt{12 \times 360}} \sum (3/2||T_1||3/2)(3/2||t_{1/2}||1) + (\frac{1-\sqrt{2}}{\sqrt{12 \times 72}}) \sum (3/2||T_1||1/2)(1/2||t_{1/2}||1)} \right|^2$$

The first reduced matrix element is that for pion decay of the super compound state to T^*, the second that for nucleon decay to T_f. Since both $T^* = 1/2$ and 3/2 are present, we are somewhat stuck. If only $T^* = 3/2$ were allowed, the ratio would be 1.23. This is a bit below the experimental results of 1.7 ± 0.4 for ^{13}C and 1.8 ± 0.4 for ^{7}Li.

For the ratio of $T_f = 0$ to $T_f = 1$ from the ^{13}C target, if only the $T^* = 3/2$ channel were active, a value of 7.5 is predicted for π^-, 6.0 for π^+. The experimental result is 5.6 ± 1.2, the same for both pion beams.

Similarly, for the proton removal from ^{9}Be to ^{8}Li, $T^* = 3/2$ dominance leads to $R = 3.44$, while for $T^* = 1/2$ only, $R = 0.11$. Neither is near the observed ratio of 0.85 at $T_\pi = 180$ MeV. All of these results on $T_i = 1/2$ targets are valid only near this energy, since the isospin of the super compound system is taken to be 3/2.

To return to the original question on the ratio of π^- to π^+ induced ^{11}C production the compound model may be useful. On the $T = 0$ target, both isospin $T^* = 0$ and 1 are allowed. The ratio of pi$^-$ to pi$^+$ ^{11}C production is

$$R(C^{11}) = \frac{\sigma(\pi^-)}{\sigma(\pi^+)} = \frac{\left| \frac{1}{\sqrt{6}} \Sigma(1||T_1||0)(0||t_{1/2}||1/2) + \frac{1}{\sqrt{36}} \Sigma(1||T_1||1)(1||t_{1/2}||1/2) \right|^2}{\left| \frac{1}{\sqrt{6}} \Sigma(1||T_1||0)(0||t_{1/2}||1/2) + (\frac{\sqrt{2}-1}{\sqrt{36}}) \frac{1}{\sqrt{36}} \Sigma(1||T_1||1)(1||t_{1/2}||1/2) \right|^2}$$

To study the energy dependence, write the ratio of sums of reduced matrix elements as f:

$$R(^{11}C) = \left| \frac{\frac{1}{\sqrt{6}} + \frac{1}{\sqrt{36}} f}{\frac{1}{\sqrt{6}} + \frac{\sqrt{2}-1}{\sqrt{36}} f} \right|^2$$

This ratio f may be found for each energy. The ratios for ^{14}N, ^{16}O and ^{19}F are similar to this one from ^{12}C, all detected by their radioactivity. The results for f are plotted in figure 14. This is nothing fundamental, only a ratio of all the unknown dynamics. Both solutions are smoothly dependent on the beam energy. The left hand solution has a fascinating zero near 100 MeV.

Now I'll turn to the gamma ray yields for multinucleon removal. The spectrum of figure 15 is from π^+ bombardment of ^{16}O.[37] The four-nucleon removal to the $T_f = 0$ state of ^{12}C is very strong -- about 12 mb. This value agrees fairly well with that for production of the same state by 230 MeV π^- bombardment of ^{16}O.[6,8] Also, large cross sections for alpha-particle removal are noted in heavy nuclei.[12,13] In figure 15 it is noted that the 15.1 MeV state of ^{12}C is not seen; the yield cannot be more than a few percent of that to the $T_f = 0$ state. If the four removed nucleons were a simple alpha particle, and the reaction were $(\pi,\pi\alpha)$, this lack of a $T_f = 1$ state implies the dominance of compound states $T^* = 0$. This is of course directly opposite to the case for photon induced alpha particle removal from ^{16}O.[30] The energy dependence of the 4.4 MeV gamma ray yield is seen in figure 16 No 3 - 3 resonance is seen, indicating a mechanism different from that for single-nucleon removal.
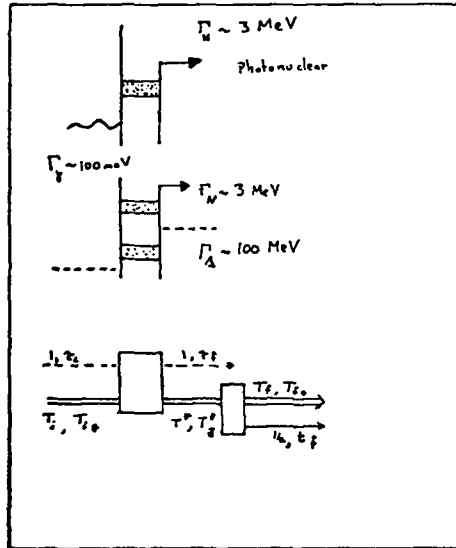
13. At the top is a representation of the photonuclear absorption. The photon absorbs on a nucleon, which may rescatter before nucleon emission. The analogous process for absorption again including nucleon rescattering. At the bottom the terminology for isospin in the pion-induced nucleon removal picture is summarized.
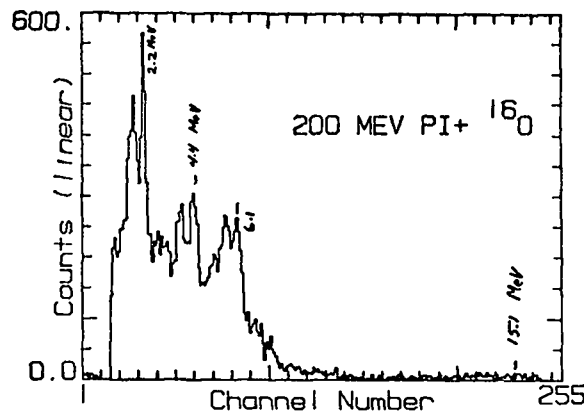
14. In the pionic Raman scattering model, the ration of π^- to π^+ neutron removal cross sections may be written as a ratio of isospin-weighted matrix elements. In turn, the ratio of matrix elements is written as

$$f = \frac{\sum(1||T_1||0)(0||t_{1/2}||1/2)}{\sum(1||T_1||1)(1||t_{1/2}||1/2)}$$

The terms on top are the density of compound states of isospin zero, the matrix element for decay of the supercompound system to a compound system of isospin zero, and the matrix element for nucleon decay of that compound system. In this figure, the ^{11}C production ratio is fitted by the form shown, and the two solutions for the factors f are plotted against the pion energy.

There are a few inclusive cases for two nucleon removal. Some data are shown in figure 17. The top shows the π^+ induced cross section to the 2^+, T = 0 state at 3.59 MeV in ^{10}B.[37] This could proceed by the quasi-deuteron process (π^+, 2p). No other clean signatures of such reactions have been seen systematically in gamma ray experiments. A similar reaction on ^{16}O is noted at one energy[8], but our resolution was not good enough to see it. On ^{12}C, the resolution of an experiment[40] observing the two protons was good enough to show that states near 4 MeV, not the ground state were populated. Also shown in figure 17 are the ^{16}N radioactivity yields from π^+ bombardment of ^{18}O. The energy dependence for these two is not remotely like that for the true reaction on deuterium, shown as the solid line. Again, we cannot be seeing any simple direct reaction in the two nucleon removal.

Recent data to support a LAMPF proposal compare the ^{11}C radioactivity from π^+ bombardment of ^{12}C and ^{13}C.[41] From 100 to 250 MeV the yield from ^{13}C is about 25% of that for one neutron removal from ^{12}C. This is π^+ induced removal of two neutrons, and cannot be any sort of quasi-deuteron reaction, yet has a very large yield.

The lack of an obvious 3 - 3 resonance in 2 and 4 nucleon removal emphasizes the importance of the strong energy dependence seen in the single nucleon removal. No resonance is noted for the direct reaction data in figure 11 either. In the Raman scattering model sketched in figure 13 for pion absorption, each pion-nucleon vertex has the 3 - 3 resonant structure.[34] The more rescattering there is before the pion is emitted, the more sharply peaked we may expect the cross section to be. For two or four nucleon removal, this simple feature is lost in the data, as it is for the direct reactions, such as inelastic scattering and charge exchange.

If then, the pionic Raman scattering is a valid picture, most of the scattering experiments done to date on low-lying states are not appropriate tests. The
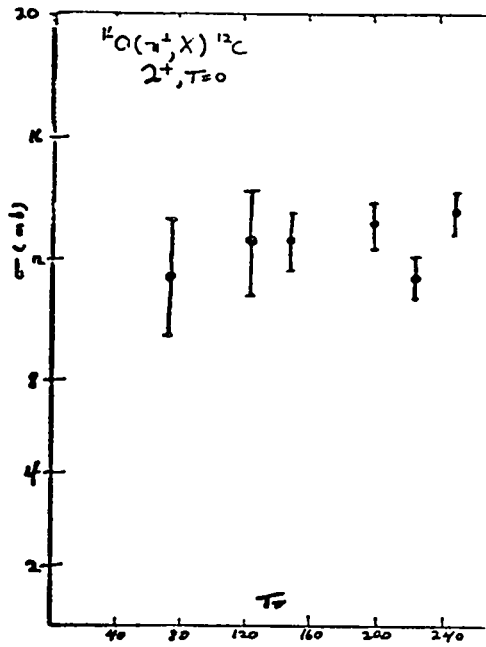
15. Gamma rays for π^+ induced reactions on ^{16}O. Prominent lines to the $3/2^-$ 6.1 MeV states in A = 15 and to the 2^+ 4.44 MeV state of ^{12}C are noted. The latter is evidence for four-nucleon removal. Note the absence of any strength to the 15.1 MeV T = 1 state of ^{12}C.
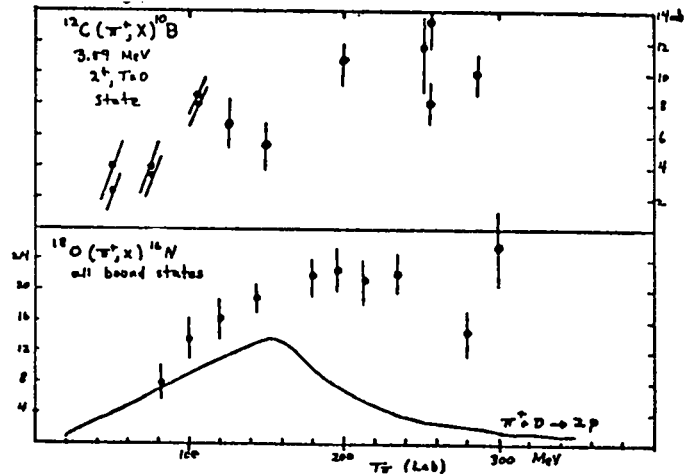
16. The yield for π^+ induced four nucleon removal from ^{16}O is plotted as a function of pion energy. In contrast to the single-nucleon removal in figures 6 - 9, no striking 3 - 3 resonance is noted.
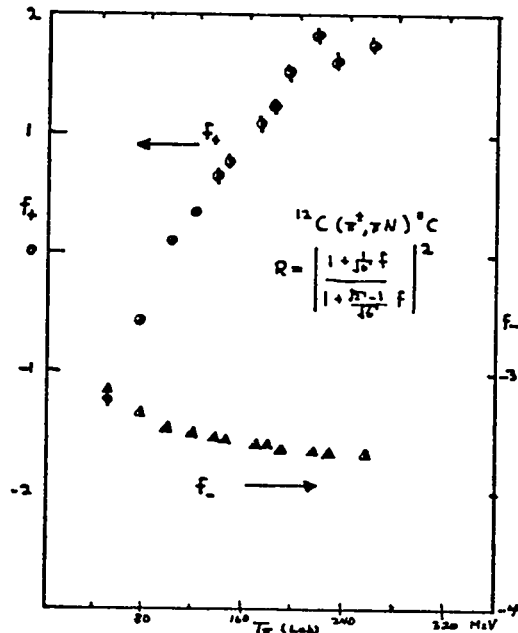
17. Inclusive cross sections for two-nucleon removal from ^{12}C and ^{18}O are shown. The ^{18}O data are from a measurement of the ^{16}N radioactivity. The solid curve is the deuteron absorption, which shows a resonance not noted in the gamma ray or radioactivity results.

- 91 -

compound states T^* had to have $T^* = 1$ for photonuclear experiments on $T_i = 0$ targets. For pions, $T^* = 0$, 1 or 2. The ^{16}O data leading to the $T = 0$ state of ^{12}C demands a large fraction at $T^* = 0$. The strong spin-flip in the pion-nucleon amplitude allows unnatural parity states or continuum. Two p-wave interactions allow $\Delta L = 2$. So we may have $\Delta J = 0$, 1, 2, 3, of either parity, although the 1^-, $T = 0$ choice cannot be a collective oscillation. We then should be more interested in the giant resonance states. Several calculations have been published on π^- [42] and μ^- [43] absorption through these states. It is also known that the (π^-,γ) reaction on light nuclei proceeds largely to giant spin-isospin states.[42] In the present picture, as in figure 13, these correspond to the T^* states, with appropriate changes in isospin projection. The pion reactions are thus selectively populating the bulk degrees of freedom in the nucleus. This would also occur in a direct reaction, since the operator is much like that for electron scattering, which is known to populate collective states.

There are two means to do new experiments touching the question of pions and giant resonances. The first is simple inelastic scattering to the high excitation regions. We should expect to see the giant resonance bumps seen in other experiments, plus new ones from the more general selection rules. Also, as suggested from the nucleon removal data, this scattering yield should be more strongly dependent upon beam energy than is found for low-lying excitations.

A different approach is to play the photonuclear game with pions. The yield for nucleon removal, for instance, should be strongly dependent on the pion energy as it is stepped from ten to thirty MeV across the doorway giant resonance states. At the upper range, interference with the 3 - 3 resonance would provide yet more information.

So, I've shown a lot of data for pion-induced nucleon removal, and used this to test several quasifree reaction mechanisms. These largely failed for

the radioactivity and gamma ray data. In contrast to the direct reaction theories, a compound reaction model indicated several encouraging successes, even without detailed calculations. We have only a taste of two or four nucleon removal data from light nuclei, and no understanding at all of the results.

Perhaps now we've seen the end of experiments of the type covered here. With more modern tools more sophisticated experiments are possible -- no longer are we stuck with radioactivity as our only observable. But the experiments served a purpose in posing a question as to the mechanism of pion-nucleus interactions, and our groping for an answer has suggested what should be done in the next generation of experiments to examine the mechanism for pions on complex nuclei.

REFERENCES

1. E. Bellotti et al, Nuevo Cimento, 14A, 567 (1973).

2. D.T. Chivers et al, Nucl. Phys. A126, 129 (1969).

3. B.J. Dropesky et al, Phys. Rev. Lett. 34, 821 (1975).
    L.H. Batist et al, Nucl. Phys. A254, 480 (1975).

4. N.P. Jacob and S.S. Markowitz, Phys. Rev. C13, 754 (1976).

5. H.S. Plendl et al, Nucl. Phys. B44, 413 (1972).

6. B.J. Lieb et al, Phys. Rev. Lett. 34, 965 (1975).

7. B.J. Lieb and H.O. Funsten, in "High Energy Physics and Nuclear Structure",
    ed. by S. Devons, Plenum Press, New York (1970).

8. B.J. Lieb and H.O. Funsten, Phys. Rev. C10, 1753 (1974).

9. M.V. Yester et al, Phys. Lett. 45B, 327 (1973).

10. W.J. Kossler et al, Phys. Rev. C4, 1551 (1971).

11. D. Ashery et al, Phys. Rev. Lett. 32, 943 (1974).

12. H.E. Jackson et al, Phys. Rev. Lett. 31, 1353 (1973).

13. V.G. Lind et al, Phys. Rev. Lett. 32, 479 (1974).

14. J.E. Bolger et al, Phys. Rev. Lett. 37, 1206 (1976).

15. H.A. Thiessen et al, Los Alamos Informal Report LA-6663-MS (unpublished)
    1977.

16. C.L. Morris et al, to be published.

17. R.A.J. Riddle et al, Nucl. Phys. A260, 349 (1976).

18. A.S. Carroll et al, Phys. Rev. C14, 635 (1976).

19. F.Binon et al, Nucl. Phys. B17, 168 (1970).
    J. Piffaretti et al, Phys Letters 67B, 289 (1977).

20. S.A. Dytman et al, Phys. Rev. Lett. 38, 1059 (1977).

21. A.E.L. Dieperink and T. DeForest, Ann. Rev. Nucl. Sci. 25, 1 (1975).

22. Y. Shamai et al, Phys. Rev. Lett. 36, 82 (1976).

23. P.W. Hewson, Nucl. Phys. A133, 659 (1969).

24.   M.M. Sternheim and R.R. Silbar, Phys. Rev. Lett. 34, 824 (1975).

25.   R.R. Silbar, J.N. Ginocchio and M.M. Sternheim, Phys. Rev. C15, 371 (1977),
2   R.R. Silbar, Phys. Rev. C15, 1158 (1977).

26.   L.W. Swenson et al, to be published.

27.   P. Varghese, private communication.

28.   R.R. Silbar and D.M. Stupin, Phys. Rev. C12, 1089 (1975),
       P. Varghese, R.R. Silbar and M.M. Sternheim, Phys. Rev. C14, 1893 (1976).

29.   H.A. Medicus et al, Nucl.Phys. 156, 257 (1970).

30.   R.O. Owens and J.E.E. Baglin, Phys. Rev. Lett. 17, 1268 (1966).
       J.T. Caldwell, S.C. Fultz and R.L. Brambett, Phys. Rev. Lett. 19, 447
       (1967).

31.   H.R. Kissener et al, Nucl. Phys. A219, 601 (1974).
       K.M. Murray and M.E. Toms, Nuovo C.M. Lett. 1, 571 (1971).

32.   F.C. Barter and A.K. Mann, Ph. 1. Mag. 2, 5 (1957).

33.   H.E. Jackson and K.J. Wetzel, Phys. Rev. Lett. 28, 513 (1972).

34.   J. Hüfner, Phys. Reports 21, 1 (1975).

35.   J.L. Norton, Ph.D. Thesis, University of Kansas (1970).

36.   R. Seki, Nuovo Cimento, 9A, 235 (1972).

37.   G.R. Smith et al, to be published.

38.   Data of B.W. Allardyce et al, as quoted in Reference 36.

39.   T. Bressani et al, Nucl. Phys. B9, 427 (1969).

40.   J. Favier et al, Phys. Letters 25B, 409 (1967).

41.   I. Halpern, spokesman, LAMPF experiment proposal #324.

42.   H.W. Baer et al, Phys. Rev. C12, 921 (1975),
       J.A. Bistirlich et al, Phys. Rev. Lett.

43.   H. Überall, Springer Tracts 71, 1 (1974).

PI-NUCLEUS REACTION PHYSICS

Gerald A. Miller

Department of Physics, University of Washington
Seattle, Washington 98195

I. INTRODUCTION

I'm going to discuss various pi-nucleus reactions, how people calculate cross sections and how reactions might be used to learn about nuclear structure. The basic idea is that if one knows the means by which a reaction proceeds, i.e. the reaction mechanism, one is able to learn about the structure of nuclei. An equally interesting alternative is the possibility of using known nuclear structure information to determine the reaction physics. Of course, there may be unhappy cases in which one knows only a little bit about both the structure and mechanism and has trouble in learning exactly what a given experiment is teaching us.

In order to illustrate and explain these ideas in a talk of finite size I must deal with specific reactions. There have been a multitude of suggestions, both experimental and theoretical, of very interesting reactions. I'm going to limit my talk to elastic pion double charge exchange and pion production and absorption reactions. Both of these reactions are very interesting and both of these reactions have been publicized as having great potential for learning about two-nucleon wave functions in nuclei. However both reactions suffer from a common problem: the information about two-nucleon wave functions comes together and is tied up with information about the off-shell, π-nucleon T-matrix. If we are going to make the best use of the experiments, we are going to have to learn how to handle this problem.

I'd like to explain how this difficulty comes about and make a suggestion on how to handle it. Of course, this is not the only problem, but it is enough to talk about in one lecture.

Several subjects which serve as background information for this talk have been relegated to Appendices.

I.1   PI-NUCLEON OFF-SHELL T-MATRICES

In order to understand the notation about off-shell T-matrices, recall that for elastic pi-nucleon scattering, the T-matrix is given as a function of two variables: the center-of-mass energy and the angle between the initial and final relative momenta. For low energy pi-nucleon scattering only S- and P-waves enter and we write

$$T_E(\cos \theta) = A + C \, k_0^2 \, \cos \theta$$

where A and C are complex energy-dependent functions and k_0^2 is the pi-nucleon relative momentum. For scattering from nuclei we may need to use the T-matrix when the initial and final relative momenta are different in magnitude and have no relation to E . Kisslinger in 1955 introduced the parameterization

$$T_E(\vec{k},\vec{k}') = A + C \, \vec{k}\cdot\vec{k}'$$

which for $|\vec{k}| = |\vec{k}'| = k_0$ exactly reproduces the elastic data. However for fixed $\vec{k}'$ and E and in the limit $k \to \infty$ this expression diverges linearly. Another simple parameterization is

$$T_E(\vec{k},\vec{k}') = A + C [\, k_0^2 - \tfrac{1}{2} \, (\vec{k}-\vec{k}')^2]$$

which is called the local Laplacian because the Fourier transform of the square of the momentum transfer is the Laplacian. This expression diverges quadratically for fixed k' and E as $k \to \infty$.

The above two forms are simple parameterizations. One might want to make a dynamical model such as a separable potential model. In this case one fits the formal potential by means of solving the appropriate integral equation and fitting to elastic π-nucleon data. Then

$$T_E(k,k') = \frac{A \ v_0(k)v_0(k')}{v_0^2(k_0)} + C \ \vec{k}\cdot\vec{k}' \ \frac{v_1(k)v_1(k')}{v_1^2(k_0)}$$

here for fixed k' and E and as $k \to \infty$ the T-matrix smoothly approaches zero.

All of these models could be criticized on the grounds that the necessity for using off-shell T-matrices comes from dealing with the many-body problem and there is no many-body input involved in these equations.

Now to the Physics!

II.1 DOUBLE CHARGE EXCHANGE - QUALITATIVE

The most intriguing thing about this reaction is that, because of charge conservation, it must proceed on two nucleons. The basic process is

$$\pi^+ + nn \to \pi^- + pp \quad .$$
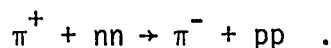
This gives us an opportunity to learn something about the two-nucleon wave function inside the nucleus. Furthermore in elastic double charge exchange the final state is a member of the ground state isospin multiplet. This state, or double analog, is assumed to have the same structure as the target ground state and the question of whether one is observing the two-nucleon wave function in the initial or final state does not come up. In either case, one is observing the ground state wave function.

- 98 -

A representation of what one must calculate is shown in Fig. 1. This is the double charge exchange version of the term which includes the Lorentz-Lorenz effect. We are interested in learning about the two nucleon wave function $\psi(r_1, r_2)$ which is given by

$$\psi(r_1, r_2) = \sum_{a,b} \left(\phi_a(r_1)\phi_b(r_2) - \phi_b(r_1)\phi_a(r_2) \right)\left(1 + f(r_1, r_2) \right)$$

in which the function f represents the deviation from the pure shell model state, ϕ. Various quantities of interest may be obtained from ψ. For example, the two-body density, $\rho^{(2)}(r_1, r_2)$, is given by
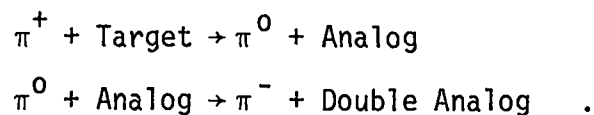
$$\rho^{(2)}(r_1, r_2) = |\psi(r_1, r_2)|^2$$

and the one-body density $\rho(r_1)$ is given by

$$\rho(r_1) = \int d^3r_2 \, \rho^{(2)}(r_1, r_2) \quad .$$

II.2 DOUBLE CHARGE EXCHANGE - STANDARD CALCULATIONS

The simplest means by which the double analog is produced is

$$\pi^+ + \text{Target} \to \pi^0 + \text{Analog}$$
$$\pi^0 + \text{Analog} \to \pi^- + \text{Double Analog} \quad .$$

This process is easily included in coupled channels calculations using the first order optical potential which contains a term proportional to the isospin of the nucleus. The double analog is made in a process involving two actions of the first-order optical potential. The requirement that the intermediate state

be the analog produces too many restrictions on the phase space of the inter-
mediate nucleon and the above process is not expected to be dominant. Thus
one must investigate second-order terms of the optical potential.

In multiple scattering theory, and neglecting the ρ-exchange term, the
second order optical potential is represented by $U^{(2)}$:

$$U^{(2)} = \sum_{i \neq j} t_i GQ\, t_j \quad,$$

where $Q = 1-P$ and P projects on the ground state multiplet and G is the
pi-nucleus Green's function. This is because the GP term is already included
in the coupled-channel calculation.

The potential $U^{(2)}$ is calculated under a set of approximations, the
first of which has been made. In an expansion of the optical potential in
terms of the number of struck nucleons, the second order optical potential should
involve <u>all</u> terms involving two nucleons. The term shown in Fig. 1 is just
the Born approximation to a Fadeev-like series involving various multiple
scatterings on two nucleons.[1]

The next approximation is to neglect nuclear excitation energies in G
and use closure. Here one is calculating a term involving a kind of pion
exchange, but nuclear interactions proceed by similar exchanges. Hence if
second order terms are important, corrections to closure must also be important.
Nevertheless, everybody does it.

Under this closure approximation we have

$$U^{(2)}(\vec{k},\vec{k}') = \int d^3r_1 d^3r_2 \left(\rho^{(2)}(r_1,r_2) - \rho(r_1)\rho(r_2)\right) \int \frac{d^3p}{(2\pi)^3}\, e^{i\vec{k}\cdot\vec{r}_1 - i\vec{k}'\cdot\vec{r}_2}\, e^{i\vec{p}\cdot(\vec{r}_2-\vec{r}_1)}$$

$$\times \frac{t(\vec{k},\vec{p})\,t(\vec{p},\vec{k}')}{E^2 - \mu^2 - \vec{p}^2 + i\eta} \quad.$$

where the isospin operators are not explicitly shown. The above expression contains isoscalar, isovector and isotensor terms. Because of the presence of Q only the difference between the two body density and the product of single particle densities enters (correlation function). In a finite nucleus this function depends on r_1 and r_2 in a non-trivial way. However, the correlation function is usually approximated by

$$\rho^{(2)}(r_1,r_2) - \rho(r_1)\,\rho(r_2) = \rho^2(R)\,C(s)$$

where $\vec{R} = \dfrac{\vec{r}_1 + \vec{r}_2}{2}$ and $\vec{s} = \vec{r}_1 - \vec{r}_2$. This approximation breaks down when R is the order of the nuclear radius.

Under this approximation

$$U^{(2)}(\vec{k},\vec{k}') = \int d^3R\; e^{i\vec{q}\cdot\vec{R}}\,\rho^2(R) \int d^3s\; C(s)\; e^{i\vec{q}\cdot\vec{s} + \frac{1}{2}(\vec{k}+\vec{k}')\cdot\vec{s}} \int \frac{d^3p}{(2\pi)^3}\; \frac{t(\vec{k},\vec{p})t(\vec{p},\vec{k}')}{E^2 - p^2 - \mu^2 + i\eta}$$

By integrating over $\vec{R}$ and $\vec{s}$ we get

$$U^{(2)}(\vec{k},\vec{k}') = F(q)\; \frac{d^3p}{(2\pi)^3}\; \tilde{C}\!\left(\vec{p} + \frac{\vec{k}+\vec{k}'}{2}\right)\; \frac{t(\vec{k},\vec{p})t(\vec{p},\vec{k}')}{E^2 - \vec{p}^2 - \mu^2}$$

where $q = \vec{k} - \vec{k}'$, and F and $\tilde{C}$ are Fourier transforms of $\rho^2(R)$ and $C(s)$. The integral over $\vec{p}$ extends over all space. Because of p-wave dominance the product of the two t-matrices contains the factor $\vec{k}\cdot\vec{p}\;\vec{k}'\cdot\vec{p}$ which emphasizes the large p region. The effects which cause the integral to become finite are very important and come from $\tilde{C}$ and the rest of the momentum dependence of the pi-nucleon t-matrices. Hence the information on correlations is mixed up with information about the unknown off-shell pi-nucleon t-matrix. (It must be off-shell because the integral over $\vec{p}$ necessarily covers regions in which

$\vec{p}^2 \neq E^2 - \mu^2$). The assumptions under which this expression simplifies have been much discussed and the resulting theorem is called Beg's theorem. I prefer not to make any assumptions about the range of the correlation function because I'd like to learn it from experiment. Hence one must deal with this off-shell difficulty.

II.3   A MORE FUNDAMENTAL APPROACH

One might try to improve the treatment of pi-nucleus interactions by considering a more fundamental dynamical model, one in which the basic interaction is given by a single absorption or by emission of a pion from a nucleon. In this case, because one is usually being non-relativistic or in some sense incomplete, one introduces a fundamental pi-nucleon cutoff, $v_F(p)$. It is expected that $v_F(p)$ starts falling off only for momenta greater than about a nucleon mass. The way to calculate the scattering cross section is to sum all of the relevant Feynman graphs. However this is very difficult. For example, one must use the same interaction in constructing the physical nuclear eigenstates and meson scattering states.

I tried to avoid this difficulty by solving the pi-nucleus Low equation.[2] This equation is a fundamental non-linear, non-perturbative equation which is equivalent to the Schroedinger equation. Under certain approximations we were able to solve the Low equation by finding a linear equation, the solution of which is also a solution of the Low equation. Now linear equations are easy to solve, (I'm not going to tell you how I obtained the linear equation, but see Ref. 1) and the result is easy to state. Use the equations of the preceeding section but wherever there was a propagator of the form $\dfrac{1}{E^2 - \vec{p}^2 - \mu^2}$ replace it by $\dfrac{E^2}{\vec{p}^2 + \mu^2} \dfrac{1}{E^2 - \vec{p}^2 - \mu^2}$. The factor $E^2/(\vec{p}^2 + \mu^2)$ is one for on-shell pions but for large $|\vec{p}|$ the field theoretic effective

propagator goes like $\dfrac{1}{|\vec{p}|^4}$ instead of the usual $\dfrac{1}{\vec{p}^2}$.

I'd like to give some plausibility arguments for this result. First consider the mathematical origins of this factor. It specifically arises from the fact that the assumed driving term of the Low equation contains a pole ($\sim 1/E$). This pole is simply the sum over nucleons of the pi-nucleon pole. The factor $E^2/(\vec{p}^2 + \mu^2)$ which occurs in second and higher terms in t prevents the rescattering from destroying the pole because E^2 approaches zero as E approaches zero. Thus the factor $E^2/(p^2 + \mu^2)$ arises as a result of a subtraction to a pole. This means that some terms which seem to contribute to pion scattering are really contributing to the physical mass (binding energy) of the nucleus.

Using the idea of having a subtraction, it is possible to construct a perturbation theory which gives the same result as the Low equation. First observe that by subtracting the static (E=0) one pion exchange propagator from the full pion propagator we get the equivalent propagator of the Low equation i.e.

$$\frac{1}{E^2 - \vec{p}^2 - \mu^2} - \frac{1}{-\vec{p}^2 - \mu^2} = \frac{E^2}{\vec{p}^2 + \mu^2} \quad \frac{1}{E^2 - \vec{p}^2 - \mu^2}$$

We can then set up a perturbation theory in which the unperturbed Hamiltonian includes the nucleon-nucleon interactions via the static pion exchange potential (OPEP). These eigenstates are the usual nuclear wave functions. Then when one calculates various Feynman diagrams one must expand in these eigenfunctions and one must subtract the two-nucleon OPEP. The above argument says that there is a consistent perturbation theory approach which generates the answer of the Low equation.

Let's consider some of the implications of this discussion. The result of using the extra factor $E^2/(\vec{p}^2 + \mu^2)$ is that the high momentum part of the d^3p integral is damped considerably. There is also an essential simplification.

The provided cut-off occurs even if the fundamental pion-nucleon form factor has not cut off. If there is such a cut-off in the fundamental form factor, $v_F(p)$, it is much higher than a pion mass. Hence the $E^2/(\vec{p}^2 + \mu^2)$ term provides the most important cut-off and one does not have to worry about off-shell effects.

The effects of correlations are reduced, in this theory. However they are still there and must be calculated.

II.4 $O^{18}(\pi^+,\pi^-)Ne^{18}$

The elastic double charge exchange reaction was recently observed here at LAMPF by Marks et al.[3] Previous predictions were that strong effects of correlations would show up by having the cross section be proportional to $(N-Z)^2$ at given energy or small range of energies.[4] If this were the case, it would mean that the effects of correlations were beating the inhibiting effects of distortions. Even with the data on one target it is relevant to ask if there are any indications of correlations.

For O^{18} there are two neutrons outside of O^{16} and there are two kinds of nuclear structure physics going on. The two aspects are: (1) how far the center of mass of the two neutrons is from the core, and (2) how does the wave function depend on the relative distance.

Shown in Fig. 2, along with the data, are some first order optical potential calculations with the Kisslinger local Laplacian and LMM[5] models for the off-shell t-matrix. (The LMM calculation gives the same results as the first-order version of the theory of section I.2. This is because the nuclear form factor cuts off high momentum transfer.) These calculations use a neutron density which has the same shape, but different normalization, as the proton density. This choice is in disagreement with the simple shell model which would put two neutrons into the $d_{5/2}$ shell. Putting the neutrons on top of
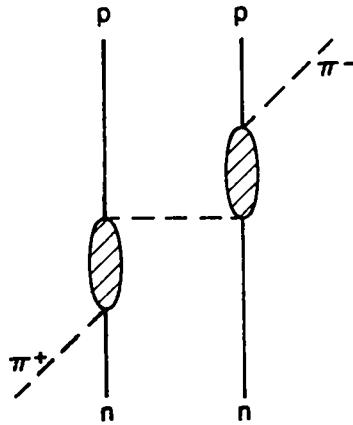
Fig. 1. Double charge exchange process. The intermediate meson can be a
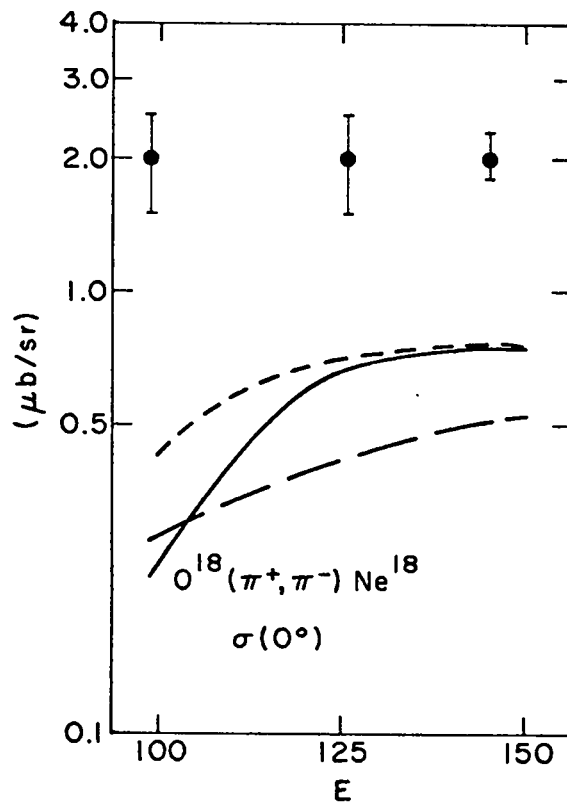π or a ρ. The blob represents the meson-nucleon off-shell
T-matrix.

Fig. 2 First-order optical model calculations. Long dashed curve:
Kisslinger potential; solid curve: local Laplacian; short dashed
curve: LMM model (= my theory).

the protons results in strong suppression due to absorptive effects.

The effects of correlations in the Miller-Spencer[4] theory are shown in Fig. 3. These calculations make use of a first order local Laplacian potential along with a second order potential calculation with πN t-matrices in the forward scattering approximation but with a strong off-shell damping. Significant effects are obtained.

The previous results were predictions. In the following we tried a semi-phenomenological approach. We used a first order optical potential given by the LMM[5] (= my theory) off-shell t-matrix, and tried to see if there is any single neutron density, no matter how unrealistic which explains the energy dependence of the data. Because of strong absorption effects of 150 MeV, pushing the neutrons out increases the cross section. However, at 100 MeV the absorption is not strong and there are different sensitivities. In Fig. 4 we adjusted the excess neutron density to fit the 95 MeV data and could not explain the 145 MeV data point. We also adjusted the excess neutron density to fit the 145 MeV data point but could not explain the low energy point. No attempt has been made to prove that no choice of excess neutron density could be made to work. However these results indicate that something else, probably longer short-range correlations, is going on.

It is very important to calculate the second order effects more carefully. However, I haven't done it yet, so I'm going to get a cup of coffee.

III. MESON PRODUCTION AND ABSORPTION ON NUCLEI

III.1 WHAT IS PION PRODUCTION

In this part of the talk we discuss the reactions

$$p + A \rightleftharpoons \pi + B$$
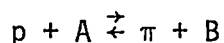
where A and B represent the initial and final nuclear states. The meson production reaction has a simple classical analogy - bremsstrahlung. An electron moving with constant velocity does not radiate. However, an application of an
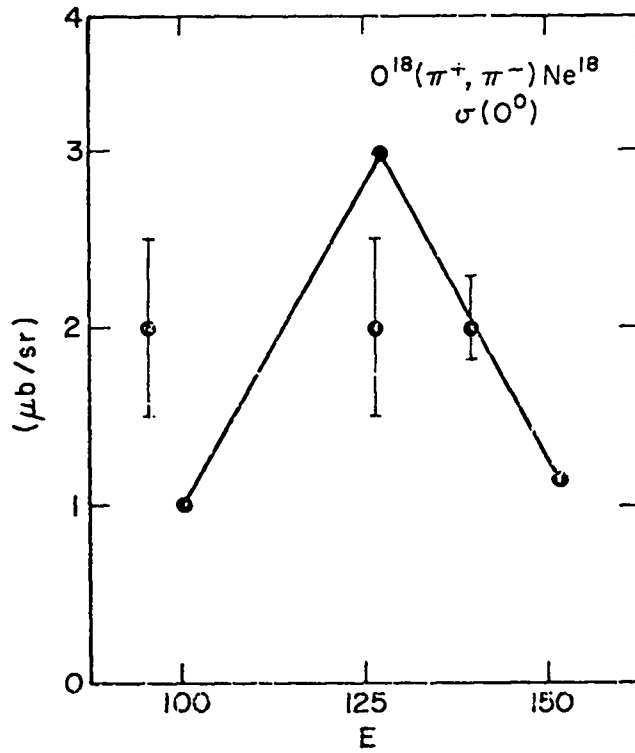
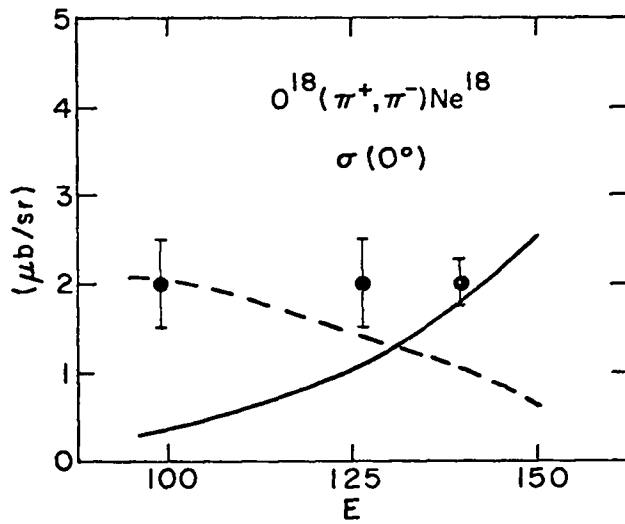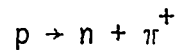Fig. 3.   Effects of correlations on double charge exchange, from ref. 4.

Fig. 4.   Sensitivity to different excess neutron densities. LMM model or
my theory.

electromagnetic field causes an acceleration and photons are produced. Similarly a free proton does not decay into a pion and a nucleon, i.e. the reaction

$$p \rightarrow n + \pi^+$$

cannot take place because energy and momentum cannot be simultaneously conserved. Therefore it is necessary to have a nucleus or another nucleon around to supply the necessary strong field. In this case the strong field may be applied to the incoming proton or outgoing pion and neutron.

Thus it is obvious that <u>the pion production reaction must proceed on at least two nucleons</u>. The name "single nucleon model" is a very bad misnomer because a single nucleon cannot emit a pion. Thus the pion production reaction is similar to the double charge exchange reaction.

The strong field applied by a nucleon or nucleus to the incident proton, for example, causes it to accelerate and acquire momenta different than the free space value. In quantum mechanical language we say that the proton is off-shell, i.e. $\vec{p}^2 \neq E^2 - m^2$. Now an off-shell proton can emit an on-shell pion and neutron and not violate conservation of energy and momentum. Similarly an off-shell pion can be absorbed on an on-shell neutron giving rise to a fast on-shell proton. Thus the appropriate question to ask about a given meson production or absorption reaction is which particle or particles are the most off-shell, and how did they get that way?

In order to ask these questions it is most convenient to divide the reaction into two categories according to the energy of the fast proton. At energies less than about 300 MeV one is in the <u>subthreshold</u> region in which the production reaction on a nucleus is kinematically allowed; but, is forbidden in the interactions of two free nucleons. In this case it is the presence of the entire nucleus which enables the reaction to proceed and one may hope to learn something about the influence of other nucleons on the wave functions of the involved nucleons. At higher energies the two-nucleon production reaction

is allowed and one may think about having the pion produced on a pair and then being affected by the final state interactions.

The rest of this talk concerns the subthreshold region.

III.2 HIGH MOMENTUM TRANSFER

The truly unique aspects of pion production or absorption is that the reaction takes place at very high momentum transfer. For example consider production at threshold. For simplicity we neglect recoil, binding and relativistic corrections to the proton's energy. Then

$$\frac{p^2}{2m} = \mu$$

where m and μ are the proton's and pion's masses respectively. Then the momentum transfer, q, is just the proton's momentum p, and $q = (2m\mu)^{\frac{1}{2}} \approx \left(\frac{2}{7}\right)^{\frac{1}{2}} m \approx 500$ MeV $= 2.5$ fm^{-1}. Although this does not seem much larger than the typical momentum of a nucleon in the nucleus, 1.4 fm^{-1}, it is in fact very, very high. This is because typical nuclear wave functions drop rapidly with momentum at large momenta. Thus the change from 1.4 to 2.5 fm^{-1} gives a decrease of a factor of 10 or more in the wave function. If one considers a model in which the proton and pion are treated as plane waves (Plane Wave Model) the t-matrix is proportioned to the Fourier transform of the wave function of the transfered neutron, $\tilde{\phi}_{LJM}(q)$. In this model only the neutron can be off-shell and because q is large the resulting cross sections are generally too small to account for the experimental data. This statement arises out of experience derived largely from p,π reactions in light nuclei in which the neutron is of low angular momentum and is loosely bound. These wave functions are necessarily small at high momenta. There are some qualifications because

the high momentum region corresponds to the short distance behavior and one

must admit that not much is known about wave functions at short distances in

coordinate space.

Subject to such caveats, one must look for another source of momentum

and we consider next the possibility of having the proton off-shell. In the

previous model one includes final state nucleon-nucleus interactions and one

should also look at initial state interactions. However, in production reactions

the initial nucleon has much higher kinetic energy than the final nucleon.

Thus its real optical potential is smaller than for bound nucleons because

nucleon-nucleon scattering phase shifts (from which the optical potential is

derived) decrease with energy. This means that the proton doesn't get very

far off-shell. Furthermore the proton can tear up the nucleus on its way in.

This results in not observing the definite final state of interest. This de-

creases the cross section. Surely there must be another stronger mechanism.

III.3 REALISTIC MODELS

Indeed, there is a very natural mechanism. Nucleons often exchange

mesons, π's, ρ's, ω's and others. Therefore a one meson exchange model is the

next logical guess. This is shown in Fig. 5, which includes two possibilities.

Either the pion is emitted from the incident projectile or by the target nucleon.

The ρ-meson is not shown explicitly but one could imagine replacing the π by a

ρ . Such terms are important because the exchanged meson helps share the momen-

tum between two nucleons. The blobs indicate the off-shell pi-nucleon t-matrices

These are off-shell because the pion has very different momentum and (Fig. 5a)

very different momentum and energy (Fig. 5b) than in the asymptotic final state.

The blobs are, of course, dominated by the pi-nucleon (3,3) resonance except

for the $pp \rightarrow d\pi^+$ reaction near threshold.

Let us briefly consider the "internal" part of the evaluation of Fig. 5a.

The intermediate pion has momentum $\vec{p}$ and in conventional theories the graph includes a factor

$$\int d^3p \;\; \frac{\vec{\sigma}_1 \cdot \vec{p} \;\; \vec{p} \cdot \vec{k} \;\; v^2(p) e^{i\vec{p} \cdot \vec{s}}}{E^2 - \vec{p}^2 - \mu^2} \;\; .$$

Notice that this is the integral that appeared in Section 1. This means that pion production is similar to double charge exchange. One sees that the factor $v^2(p)$ cuts off the high momentum part of the integral but one must also take the matrix element of the above operator between the initial and final two-nucleon wave functions. Again the short distance behavior or high momentum behavior of the two-nucleon wave functions has crucial effects on the calculated cross sections. Hence we again see that information about the two nucleon wave function is tied up with information about the off-shell t-matrices. Perhaps we can someday use the two reactions to untangle each other.

There are three further observations to be made about these terms.

(1) This reaction mechanism, or some variation of it, explains the $pp \rightarrow d\pi^+$ reaction. However, in the subthreshold region, kinematics <u>forbid</u> the reaction from taking place on free nucleons. Hence the reaction cannot proceed without distortion of the single nucleon wave functions. This means that the reaction is sensitive to details of single nucleon wave functions even in this two-nucleon process.

(2) Because two nucleons are involved, this mechanism can create either a single particle or two-particle one-hole excitations. Hence a great variety of interesting states may be excited.

(3) Both diagrams are important in $pp \rightarrow d\pi^+$ reaction. This is because in the center-of-mass the protons have equal and opposite momenta. However, for reactions in which a single nucleon is deposited in the nucleus the

projectile emission term dominates. This is because in Fig. 5a the rescattering takes place on all of the target nucleons. However, in Fig. 5b the $\vec{\sigma} \cdot \vec{\nabla} \, \tau$ term tends to average to zero in a large nucleus. This is because there are equal numbers of protons and neutrons and equal numbers of spin up and spin down particles. These terms give opposite signs. A similar cancellation takes place for the target ρ-emission term. I won't talk about this term any more.

III.4 TWO METHODS OF CALCULATION - DWBA AND TNM

There are essentially two procedures which have been used to calculate the pion production cross section. The first is to treat the rescattering of the pion in Fig. 5a by using its optical model wave function.[6,7] This is just the DWBA method of nuclear physics. In this model and for a single nucleon transfer the T-matrix is proportional to the integral

$$\int d^3r \;\; \phi_{LJM}(\vec{r}) \;\; [\vec{\sigma} \cdot \vec{\nabla}_\pi \, \phi_\pi^*(\vec{r})] \;\; \psi_p(\vec{r})$$

where $\psi_p(\vec{r})$ is the incident proton's wave function. The pion wave function $\phi_\pi(\vec{r})$ contains the necessary off-shell information. These integrals are obtained by making partial wave decompositions for the proton and pion wave functions, doing the angular integral analytically and performing the radial integrals numerically.

The second method involves an explicit calculation of the production of a pion by two nucleons.[8,9] The one must put in the appropriate initial and final state interactions with the A-2 nucleons. This model is called the two-nucleon model (TNM). In this case one must calculate the integral

$$\sum_{n\ell j} \int d^3r_1 d^3r_2 \;\; \phi_{LJM}^*(r_1) \;\; \phi_{n\ell j}^*(r_2)(f_f(r_1,r_2) + 1) \;\; \phi_\pi^*(r_1) \; H(r_1,r_2)$$

$$x \quad [\psi_p(r_1) \, \phi_{n\ell j}(r_2) - \psi_p(r_2) \, \phi_{n\ell j}(r_1)] \, (1 + f_i(r_1, r_2)$$

where H_2 is a two nucleon production operator containing gradients of the pion wave function and $\phi_{n\ell j}$ represents the single particle wave functions of the target nucleons. The functions f_i , f_f indicate the deviation of the nuclear structure from the pure single particle model in the initial and final states. (In the pure shell model $f_i = f_f = 0$.) This calculation contains more information than the DWBA and is necessarily more difficult.

Although each method has had its proponents, one may simply list the advantages and disadvantages of each.

The advantages of the DWBA model include:

(1) The pion's wave function can be obtained by either phenomenological means or by microscopic theoretical calculations.

(2) The wave function contains more terms than shown in Fig. 5a. The term shown is just the first Born approximation to the wave function.

(3) Calculations of this model can be and have been done exactly with standard numerical techniques.

(4) One may put in excitation of 2 particle-1 hole states or particle-collective states by using coupled-channel pion and proton wave functions.

The disadvantages of the DWBA model include:

(1) Nucleon-nucleon correlations not contained in the proton optical potential and neutron single particle potentials are ignored.

(2) The nucleon-nucleon antisymmetrization term, Fig. 6, is absent.

(3) The ρ-exchange must be put in explicitly.

(4) The target emission term which enters only in the creation of 2 particle-1 hole and particle collective states must be put in explicitly.
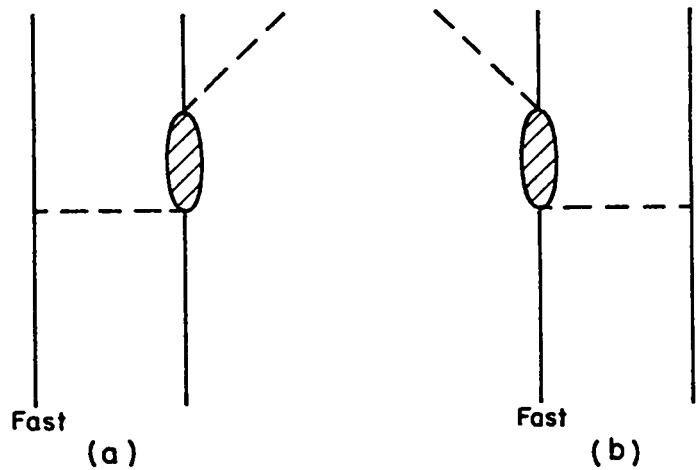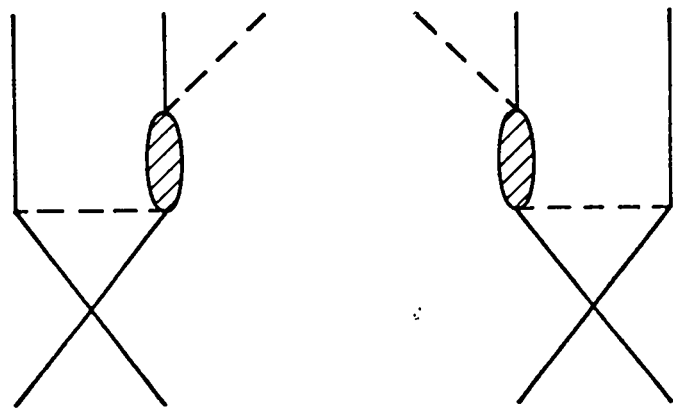
Fig. 5.   Mechanisms for pion production.

Fig. 6.   Effect of antisymmetry on pion production.

The DWBA puts in the pion off-shell information, but in its single particle aspects it ignores two-nucleon effects. Hence the DWBA is guilty of concentrating on off-shell effects and largely ignoring two-nucleon wave function effects.

The advantages of the TNM include:

(1) Two step excitations are included by construction.

(2) The ρ-exchange mechanism is also included.

(3) The target pion emission term is also included.

(4) Nucleon-nucleon correlations are also included.

The disadvantages of the TNM include:

(1) The two-nucleon pion production operator, H_2, is a function of r_1 and r_2 and detailed calculations of the six dimensional integral must be done.

(2) Some part of the optical potential rescattering is contained in the TNM, and care must be taken so as not to overcount.

The TNM model is more ambitious than the DWBA and more calculations using careful evaluations of this model should be done.

Both models need to use good pion wave functions, and I would like to discuss them. Although the Kisslinger singularity and the means for suppressing it have been reviewed in detail by Gerry Brown, I would like to briefly discuss this problem which arises from the attractive nature of the strong p-wave pi-nucleon interaction. In the Kisslinger model

$$t_E(\vec{k},\vec{k}') = b_E \vec{k}\cdot\vec{k}'$$

where b_E is attractive (negative) at energies below the (3,3) resonance. In nuclear matter the pion wave function has the form e^{iKX} where K, the

momentum of the pion in the medium, is determined by the wave equation

$$K^2 + b\rho_0 K^2 = p_0^2$$

where ρ_0 is the density of nuclear matter and p_0^2 is the on-shell momentum of the pion. The solution is

$$K^2 = p_0^2 (1 + b\rho_0)^{-1}$$

and the problem arises because $b\rho_0 \approx -1$ so that K^2 is huge. This gives rise to high momentum components of pion wave functions. For scattering by a finite nucleus, the imaginary part of b presents a barrier so that the effective density is lower than ρ_0, and the problem is mitigated. However, even in situations where the elastic scattering is well described by a potential of the Kisslinger form, the π-nucleus wave functions have kinks inside the nucleus.

As discussed by Brown the singularity is damped by the effects of correlations. In this case the wave equation is modified

$$K^2 + \frac{b\rho K^2}{1 - \frac{b\rho}{3}} = p_0^2$$

and

$$K^2 = p_0^2 \left(1 + \frac{2}{3} b\rho\right)^{-1}$$

and the disaster happens at densities 3/2 as large as that of nuclear matter. However the value of K^2 is still quite large. For $b\rho = -1$, $K^2 = 3p^2$. As we will see, the Lorentz-Lorenz effect is not strong enough to fix things up in pion production.

III.5 CALCULATIONS OF PRODUCTION AND ABSORPTION

The most dramatic example of the effects of the Kisslinger singularity occurs in the $B^{10}(p,\pi^+)$ reaction at 154 MeV (Fig. 7) where the pion is close to threshold and has no momentum of its own so that the virtual momentum is greatly emphasized. The use of the Kisslinger potential gives results that are bigger than the data by a factor of 1000. On the other hand the use of the first order potential obtained from the LMM interaction results in a tolerable fit to the data. A better understanding of this effect may be obtained from considering the pi-nucleus s-wave functions. The kink at about 2 fm causes all the trouble; see Fig. 8.

It has often been claimed that the Lorentz-Lorenz effect removes all high momentum components of the pion wave function. This idea is tested against the Uppsala data in Fig. 9 which is taken from Keating and Wills.[10] The LL reduced the (p,π^+) cross section by about 30% and not the required 35. Jones and Eisenberg[11] were the first to point out that the LL is not sufficient to remove the Kisslinger singularity.

The sensitivity of the results to the neutron bound state wave function is displayed in Fig. 10. There is a significant spread in these results. This is because the nucleus must supply momentum to make the reaction go (even on two nucleons). This _theoretical_ sensitivity to neutron wave functions leads one to hope that someday we will be able to extract information about such wave functions.

Our calculations are not the only ones to give good fits. Grossman, Lenz and Locher[8] acheived good fits using the TNM. The most recent TNM results shown in Fig. 11 are from Dillig and Huber.[9] They use the local Laplacian model to describe the final state pi-nucleus interaction. The model does not fit the pion elastic data. They do include, within their model, the ρ-exchange and nucleon (Pauli) exchange mechanisms. They explain the A dependence of the
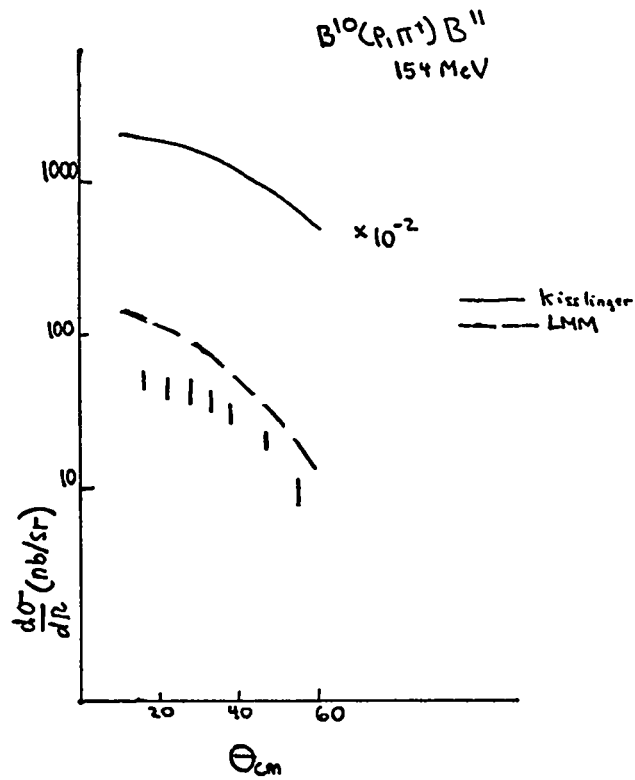
Fig. 7. $B^{10}(p,\pi^+)$ B^{11} at 154 MeV.
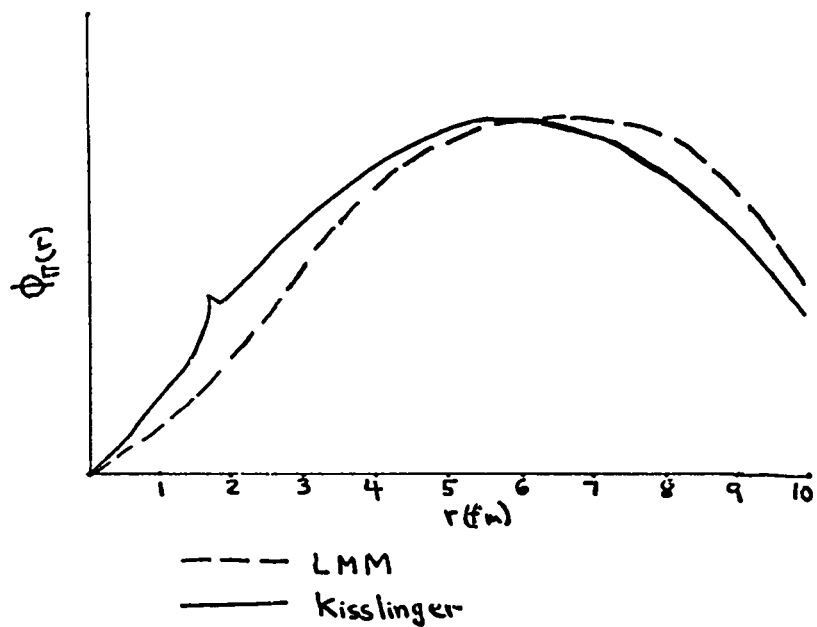

Fig. 8.   S-wave pi-nucleus wave functions near threshold. The solid curve
is obtained from the Kisslinger potential. The dashed curve is
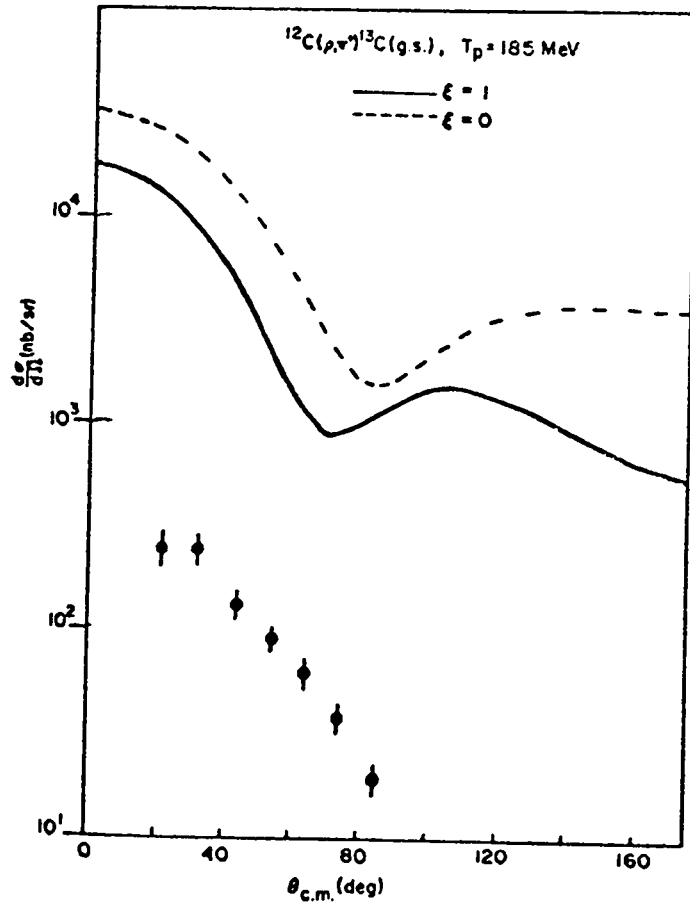obtained from the off-shell model of Ref. 5.

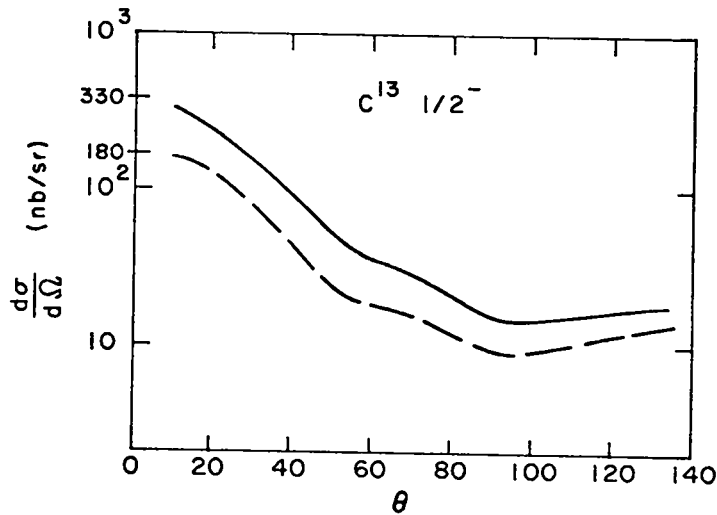Fig. 9.   Effect of the Lorentz-Lorenz potential in pion production.

Fig. 10.   Sensitivity to neutron wave functions. The solid curve is obtained
with r_0 = 1.3 and the dashed curve with r_0 = 1.1. From Ref. 6.

cross section quite well.

Previously in Section 1 we discussed how in a more fundamental treatment of pi-nucleus scattering one could obtain the standard multiple scattering series but with the modified propagator $\dfrac{E^2}{\vec{p}^2 - \mu^2} \dfrac{1}{E^2 - \vec{p}^2 - \mu^2}$. It turns out that a similar thing happens in pion production.

If one solves the Low equation for pion production one finds the same effect and one gets a term $\omega^2/(\vec{p}^2 + \mu^2)$ to damp the $\vec{p}^2$ factor.

I'd like to illustrate this more fundamental approach. Figure 12 shows the $pp \to d\pi^+$ cross section calculated with our propagator modification mentioned above. This is from Alberg, Henley, Miller and Walker.[12] No ρ-meson is needed to fit the data and there are no adjustable parameters. Also shown is the work of Brack, Riska and Wiese[13] (Fig. 13). Brack et al. uses a ρ-meson to reduce the cross section. (The ρ-exchange interferes destructively with the π-exchange.) Both cross sections are too low at small energies because the s-wave rescattering is not included.[1] Previous good fits have also been obtained by Goplen et al.[14]

III.6 CONFIGURATION MIXING

Having discussed the reaction mechanism in detail, I would like to turn to the possibility of using the (p,π^+) reaction to learn about configuration mixing in nuclei. This interesting hope is another consequence of the high momentum transfer nature of the reaction.

We begin with the observation that final neutron wave functions with high angular momentum are preferred. Meson production to a neutron state of high angular momentum is large because these bound states have more high momentum components than the states of small angular momentum. This may be understood by considering harmonic oscillator wave functions of angular momentum ℓ which have the form $r^\ell e^{(-\frac{1}{2}\beta r^2)}$. When one takes the Fourier transform, the $r^\ell e$
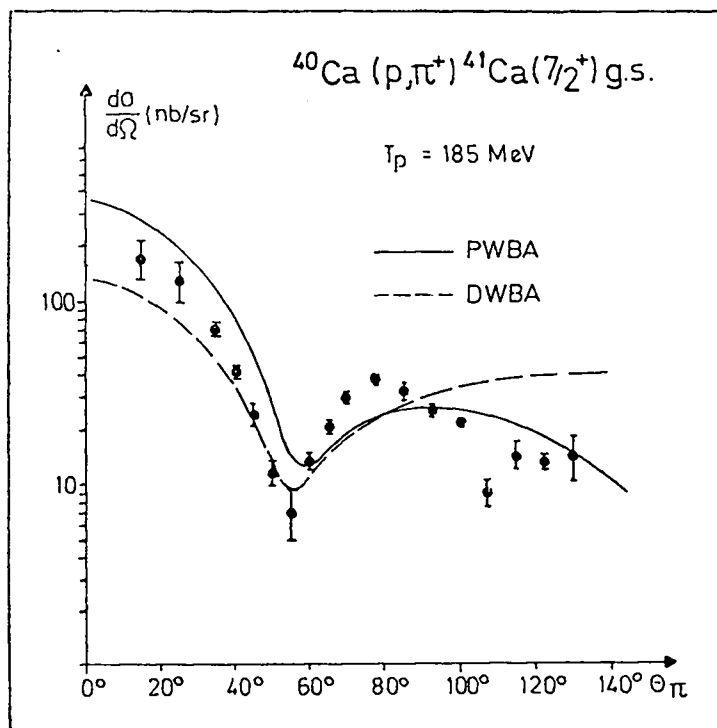
Fig. 11.   TNM calculations of Ref. 9. The notation PWBA and DWBA stands for the wave function of the outgoing π after it has been produced by the pair of neutrons. $^{40}Ca(p,\pi^+)$ ^{41}Ca(ground state).
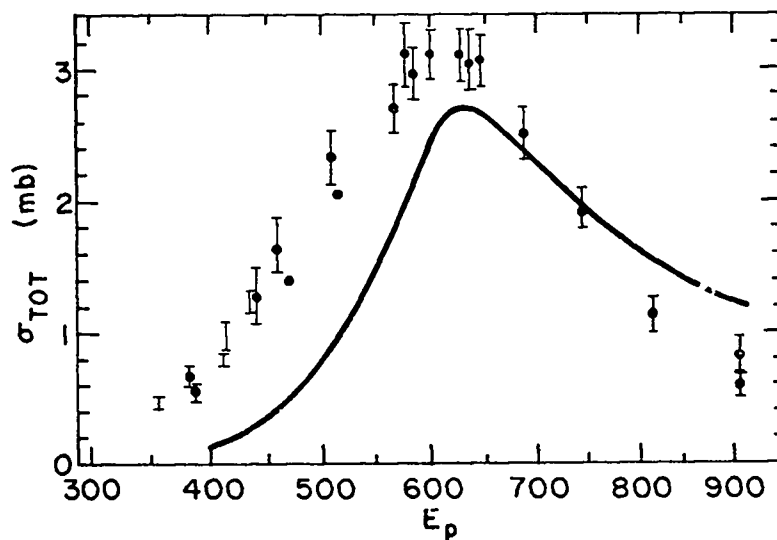

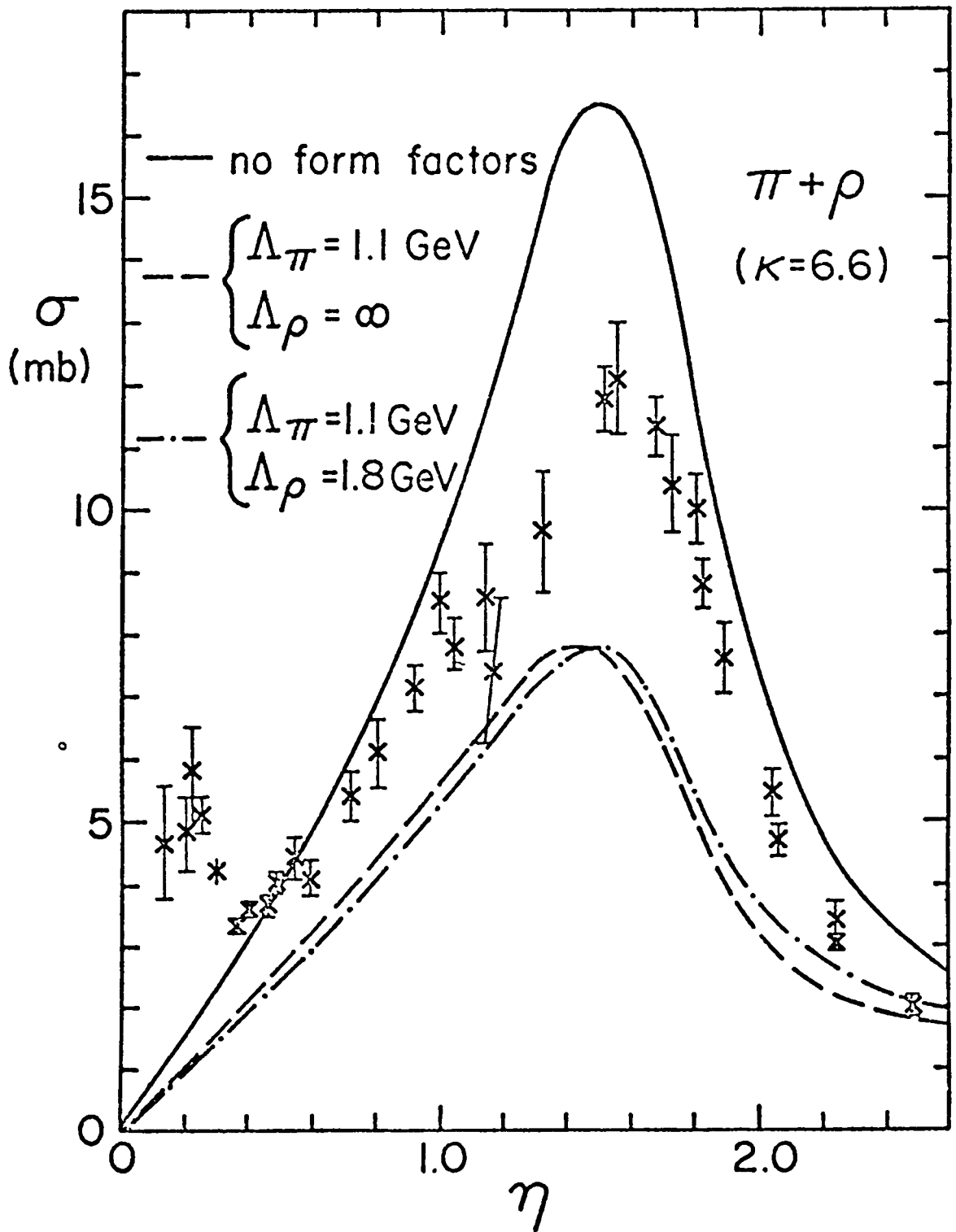Fig. 12.   Total cross section for pp → πd; from Ref. 24.

Fig. 13.   Total cross section for $\pi d \to pp$; from Ref. 19.

term results in a q^ℓ term which enhances the wave function in the high momentum transfer region that is important for this reaction. Alternatively one may express the high momentum transfer in terms of high angular momentum transfer because the angular momentum of the outgoing pion is small. Having a high angular momentum neutron helps make up the angular momentum mismatch.

This effect is exhibited for the (p,π^+) reaction on ^{12}C leading to several high angular momentum single-particle states of ^{13}C in Fig. 14. For example, the stripping cross section to the $1g_{9/2}$ and $1h_{11/2}$ single-particle states for potential II are about 10^3 and 10^4 times as large, respectively, as to the $p_{1/2}$ state.

One must next learn how the high angular momentum enters into the reaction. In the calculations described above we have assumed that the final state wave function consists of a single particle outside the target ground state. While the spectroscopic factors of these single-particle states are close to one, it is interesting to consider the components of the final state wave function that consist of a single-particle state of high angular momentum or high radial quantum number coupled to an excited state of the core. For example, for the $p_{1/2}$ ground state of C^{13} one may write

$$|\psi> = \sqrt{S} \; \phi_{p_{1/2}}|C^{12}>_{GS} + \sum_{LJ,\mathcal{L}} c^{LJ,\mathcal{L}} \left\{ \phi_{LJ}|C^{12}_{\mathcal{L}} > \right\}_{\frac{1}{2}}$$

where S is the spectroscopic factor, ϕ_{LJ} represents the high angular momentum state, and $\mathcal{L}$ is the angular momentum at the excited core state. The values at LJ and $\mathcal{L}$ must couple to $1/2^-$ in this case.

Such components enter into the reaction by two mechanisms. In Fig. 15a the proton emits a pion and goes into a high angular momentum final state. The pion then excites the core. In Fig. 15b the proton excites the core and then
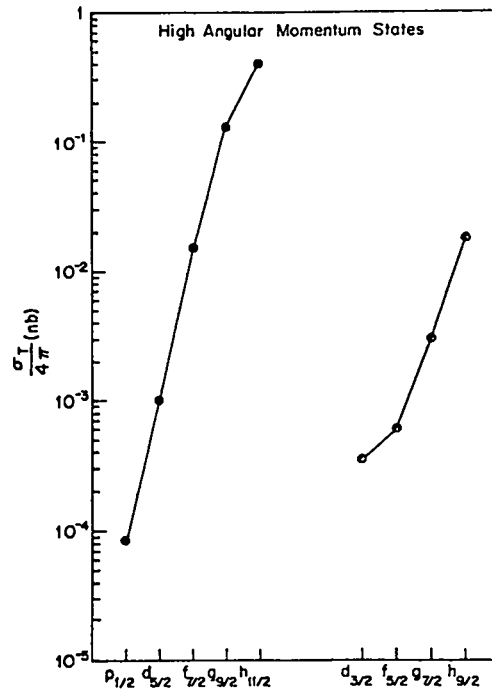
Fig. 14.   The total (p, π^+) cross section, σ_T, to various single-particle states of high angular momentum.
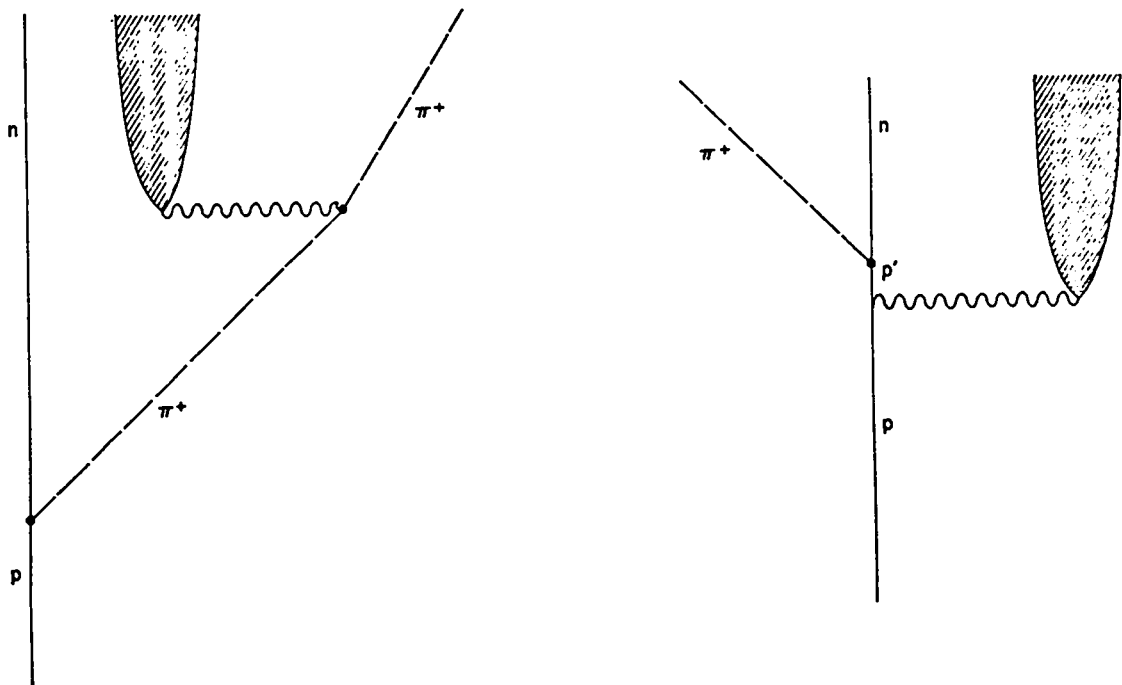

Fig. 15.

a) Pion emission followed by pion inelastic scattering.

b) Inelastic proton scattering followed by pion emission.

- 124 -

emits the pion and goes into the high angular momentum final state.

The calculations have been performed[6] by generalizing the wave equations of the pion and proton into a set of coupled channel equations. These equations are solved to get the necessary wave functions which have a proton or pion coupled to an excited nuclear state.

The results for the transition to the ground state of C^{13} are shown in Fig. 16. We see that the cross section can change considerably even if the spectroscopic factor of the final state is quite large. The transition to the $5/2^+$ excited state at 6.9 MeV is interesting because it is not a single particle state, Fig. 17. The two step mechanisms are able to provide sufficient cross section. In these two cases the effects are dominated by the pion inelastic rescattering term.

IV. SUMMARY

During the course of this talk I have tried to explain three points.

1) In analyzing elastic double charge exchange and pion production reactions make sure to treat both the two-nucleon wave functions and the off-shell pi-nucleon t-matrix carefully. More generally, in any reaction try to clearly understand the separation of the reaction mechanism from the nuclear structure information.

2) In calculations of pion production or absorption do not use the Kisslinger potential or the Lorentz-Lorenz potential. They will surely cause unphysically large cross sections.

3) It is possible to use a field theoretic multiple scattering approach. The only change (for multiple scattering terms) is to use a factor of $E^2/(\vec{p}^2 + \mu^2)$ in the propagator.

I'd like to thank Norman Austern for a critical reading of a preliminary version of this manuscript.
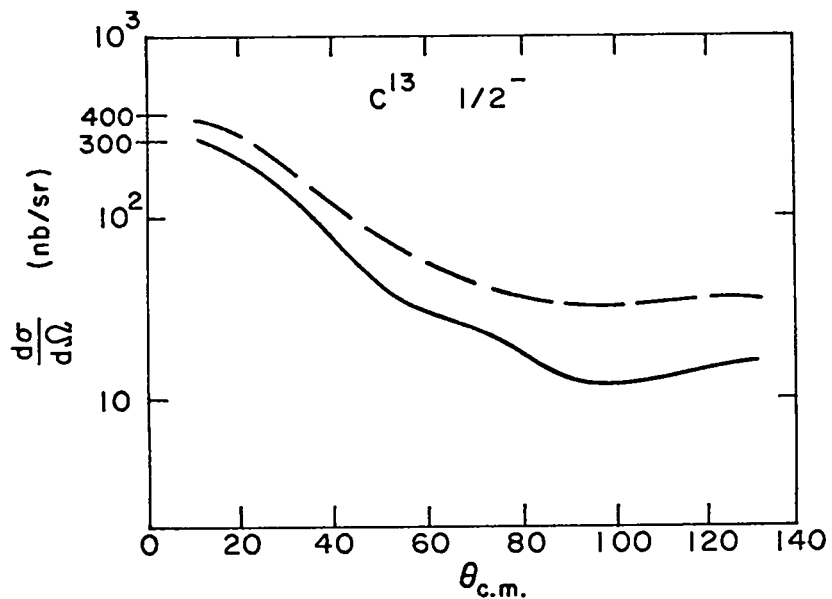
Fig. 16.   Effects of configuration mixing. The dashed curve includes the effects of Fig. 15; the solid curve does not.
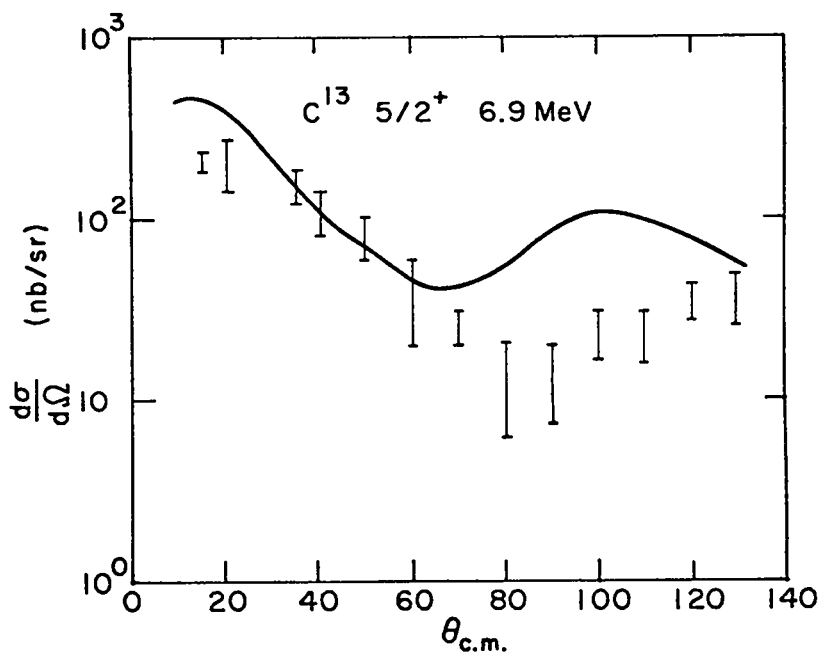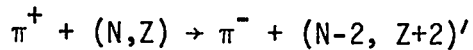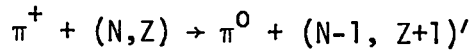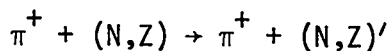

Fig. 17.   The (p,π^+) criss section to the second $5/2^+$ state of ^{13}C. Two-step processes are included.

A.1   WHAT IS CHARGE EXCHANGE?

In the charge-exchange reactions we make use of the fact that the pion has three charge states $(\pi^{\pm}, \pi^{0})$. Thus the reactions

$$\pi^{+} + (N,Z) \to \pi^{0} + (N-1, Z+1)'$$
$$\pi^{+} + (N,Z) \to \pi^{-} + (N-2, Z+2)'$$

are available in addition to the usual

$$\pi^{+} + (N,Z) \to \pi^{+} + (N,Z)'$$

non-charge exchange reactions. Here (N,Z) stands for a nucleus in its ground state with N neutrons and Z protons and the primes designate the ground or excited states.

The main thing to know about charge exchange is that it is not an unusual process. Because the pi-nucleon amplitude has a strong isospin dependence, i.e. the isospin 3/2 channel dominates, charge exchange takes place all the time. To illustrate, let us calculate the ratio of the $\pi^{+} + n \to \pi^{0} + p$ and $\pi^{+}n \to \pi^{+}n$ cross sections in the vicinity of the (3,3) resonance. The T-matrix for each process is simply the product of the probabilities for the initial and final states to have total isospin 3/2. Thus

$$R = \frac{\sigma(\pi^{+} + n \to \pi^{0} + p)}{\sigma(\pi^{+} + n \to \pi^{+} + n)} = \left\{ \frac{\langle 11, \tfrac{1}{2} - \tfrac{1}{2} | \tfrac{3}{2} \tfrac{1}{2} \rangle \langle 0, \tfrac{1}{2} \tfrac{1}{2} | \tfrac{3}{2} \tfrac{1}{2} \rangle}{\langle 11, \tfrac{1}{2} - \tfrac{1}{2} | \tfrac{3}{2} \tfrac{1}{2} \rangle^{2}} \right\}$$

The Clebsch-Gordon coefficients are

$$\langle 11, \tfrac{1}{2} - \tfrac{1}{2} | \tfrac{3}{2} \tfrac{1}{2} \rangle = 1/\sqrt{3}$$

$$\langle 10, \tfrac{1}{2} \tfrac{1}{2} | \tfrac{3}{2} \tfrac{1}{2} \rangle = \sqrt{2/3}$$

so $R = 2$ and charge-exchange is twice as likely as non-charge exchange.

A.2 ELASTIC CHARGE EXCHANGE

In order to be specific I'll only talk about reactions to definite final states and confine myself to _elastic_ charge exchange reactions. To explain elastic charge exchange, let me briefly recall the definitions of isobaric multiplets. States in nuclei, of the same nucleon number, that have the same quantum numbers, nuclear structure, and similar energy except for the change of one or more neutrons into protons are said to be members of an isospin multiplet. Two such states are said to be isobaric analogs of each other. If $|GS\rangle$ represents the ground state, its analog $|A\rangle$ is given by

$$|A\rangle = \frac{1}{\sqrt{N}} \; T_+ \; |GS\rangle$$

where T_+ is the charge raising operator which changes a neutron into a proton and N is a normalization factor. Similarly the double analog is the state that differs by making two neutrons into protons

$$|DA\rangle = \frac{1}{\sqrt{N_2}} \; T_+^2 |GS\rangle \; .$$

Because the nuclear states must be antisymmetrized it is only _excess_ neutrons which can be changed into protons to make the analog.

As an aside I'd like to point out that the representation of analog states as rotations in isospin space neglects the fact that protons feel the Coulomb force of other protons and have different wave functions than the neutrons.

In particular, excess proton wave functions have less binding energy than excess neutron wave functions and have a longer tail outside the nucleus. Most people, or at least me, have been ignoring this effect in their calculations.

The elastic single charge exchange takes a nucleus into its analog and the elastic double charge exchange takes a nucleus into its double analog. Because the reaction proceeds only on _excess_ neutrons one might reasonably hope to obtain quantitative information about the excess neutron density. To understand this let us consider how to calculate cross sections, and begin with the simplest approximation. (We discuss (π^+, π^0) here. Although it is hard to measure it is easy to talk about.)

A.3   SINGLE CHARGE EXCHANGE - PLANE WAVE IMPULSE APPROXIMATION

For the low energies of interest to us $(0 < E < 250$ MeV) pi-nucleon (πN) scattering is dominated by the s and p waves and we may represent the πN elastic and charge exchange data by the relation

$$t = A + B\vec{k}\cdot\vec{k}' + (C + D\vec{k}\cdot\vec{k}')\ \vec{t}_{\pi}\cdot\vec{T}$$

where t is the T-matrix. A, B, C and D are complex energy-dependent functions. The quantities t_{π} and T are the pion and nucleon isospin operators. (One must use the same conventions for isospin in the definition of the analog states and in the definition of t.)

In the plane wave impulse approximation a free π^+ makes a charge exchange reaction on a neutron and the resulting π^0 emerges undistorted. (This model is terrible, but is useful pedantically.) In this case the reaction T-matrix is

$$M = \langle A| \sum_i (C + D\vec{k}\cdot\vec{k}') \, e^{i\vec{q}\cdot\vec{r}_i} \; T_i(+)|GS\rangle \quad \langle \pi^0|t_\pi(-)|\pi^+\rangle$$

where the sum is over target nucleons and $\vec{q}$ is the momentum transfer. Now $T_i(+)|p\rangle = 0$ and $T_i(-)|n\rangle \propto |p\rangle$ if the proton orbital is unoccupied. Thus only the excess neutron density enters and we find

$$M = I(C + D\vec{k}\cdot\vec{k}) \int e^{i\vec{q}\cdot\vec{r}} \left(\rho_n(\vec{r}) - \rho_p(\vec{r})\right) d^3r$$

where I is the isospin factor and we define

$$F_T(q) = \int d^3r \, e^{i\vec{q}\cdot\vec{r}}\left(\rho_n(\vec{r}) - \rho_p(\vec{r})\right) = \int d^3r \, e^{i\vec{q}\cdot\vec{r}}\rho_T(r)$$

Here $\langle t_\pi \cdot T \rangle$ is the isospin matrix element and $\rho_{n,p}$ represent the neutron and proton density. Because $F_T(q = 0)$ is $(N-Z)$ and $e^{iq\cdot r}$ oscillates $F_T(q)$ must be forward peaked. The function $(B + D\vec{k}\cdot\vec{k}')$ is large at back angles and small at forward angles due to s-p interference. In fact at $E \approx 80$ MeV $B \approx -Dk^2$. Because of the Pauli principle the form factor is forward peaked, but the t-matrix is backward peaked and the elastic single charge exchange form factors are peaked at larger q and are not so much inhibited.[15]

A.4   SINGLE CHARGE EXCHANGE-DISTORTED WAVE IMPULSE (DWIA)

Pions in the vicinity of nuclei are not plane waves. Indeed at energies near the resonance the waves are strongly absorbed. To see how the strong absorption situation comes about sonsider the impulse approximation to the optical potential, V ,

$$V = t\rho$$

which is the amount of scattering times the probability of having a scatterer. The pi-nucleon t-matrix near resonance is dominated by the (3,3) phase shift $\delta_{3,3}$ and

$$t \propto \frac{e^{i\delta_{3,3}}\sin \delta_{3,3}}{k} \quad .$$

Near resonance $\delta_{3,3}= \pi/2$ so that t is large and purely imaginary and so is V. The pi-nucleon (π^+p) cross section at resonance is about 200 mb. This large cross section corresponds to a very short mean free path, ~ 1.2 fm. Near the resonance strong absorption physics dominates and <u>surface</u> effects are important, but at low energies the mean free path is quite large and one may be concerned with <u>volume</u> effects. (This presumes that true meson absorption never gives a tremendous imaginary potential.)

One then calculates the cross section by expanding the pion wave function into a complete set of partial waves and solving the Schroedinger or Klein-Gordon equations to obtain the radial wave functions. Then for a given partial wave

$$T_\ell \propto \int dr \left(u_\ell^2(r) \, C\rho_T(r) - \left(\frac{\delta u_\ell}{\delta r} - \frac{u_\ell}{r}\right)^2 D\rho_T(r) \right)$$

or

$$T_\ell \propto \int dr \, u_\ell^2(r) \left\{ (C + Dk^2)\rho_T(r) + \frac{1}{2} D \, \nabla^2 \rho_T(r) \right\}$$

where the Kisslinger and local Laplacian extrapolations are used. For partial waves $\ell < kR$ where R is the strong absorption radius (somewhat larger than

the rms radius), the integrals T_ℓ are very small. This is because for such partial waves u_ℓ is purely incoming and u_ℓ^2 oscillates rapidly to cancel the integral. Thus at energies near the resonance we have a surface reaction. The cross section is very sensitive to changes of $\rho_n - \rho_p$ in the surface region. A typical example[4,15] is shown in Fig. 18. For an explanation of strong absorption physics see N. Austern.[16]

At low energies the optical potential is less well understood and one might think of using the resonance region to determine ρ_T and then using the known ρ_T to learn about pion wave functions at low energies.

A.5   THE PLANE WAVE MODEL OF (p,π^+)

Although the high momentum components of single nucleon wave functions are generally very small, one might be tempted to try a plane wave model. After all, the experimental cross section is also very small. Here we take the non-relativistic model of the pi-nucleon interaction: $H' = \frac{4\pi}{2\omega}\ \frac{f}{\mu}\ \tau\vec{\sigma}\cdot\vec{\nabla}_\pi\phi_\pi(\vec{r})$ where $\phi_\pi(r)$ is the pion's wave function, in this case a plane wave, which includes the creation operator. The form $\vec{\sigma}\cdot\vec{\nabla}_\pi$ comes from the fact that the pion has negative intrinsic parity, i.e. the pion is a pseudoscalar particle. Here the gradient acts only on the pion's wave function and $\vec{\sigma}$ and τ act on the nucleon. I will discuss the non-static corrections to this operator later. In this plane wave model the T-matrix is just

$$T = \sqrt{\frac{4\pi}{2\hbar\omega}}\ \sqrt{2} \int d^3r\ e^{-i\vec{k}\cdot\vec{r}}\ \phi_{LJM}^*(\vec{r})\ e^{i\vec{p}\cdot\vec{r}}\ \chi_{\frac{1}{2}\ m_i}$$

where the initial spin of the nucleon is m_i and the final neutron wave function has orbital and total angular momentum L and J respectively. The factor $\sqrt{2}$ comes from the matrix element of the isospin operator. Because $\vec{q} = \vec{p} - \vec{k}$ is large, the factor $e^{i\vec{q}\cdot\vec{r}}$ oscillates rapidly and tends to cancel the integral
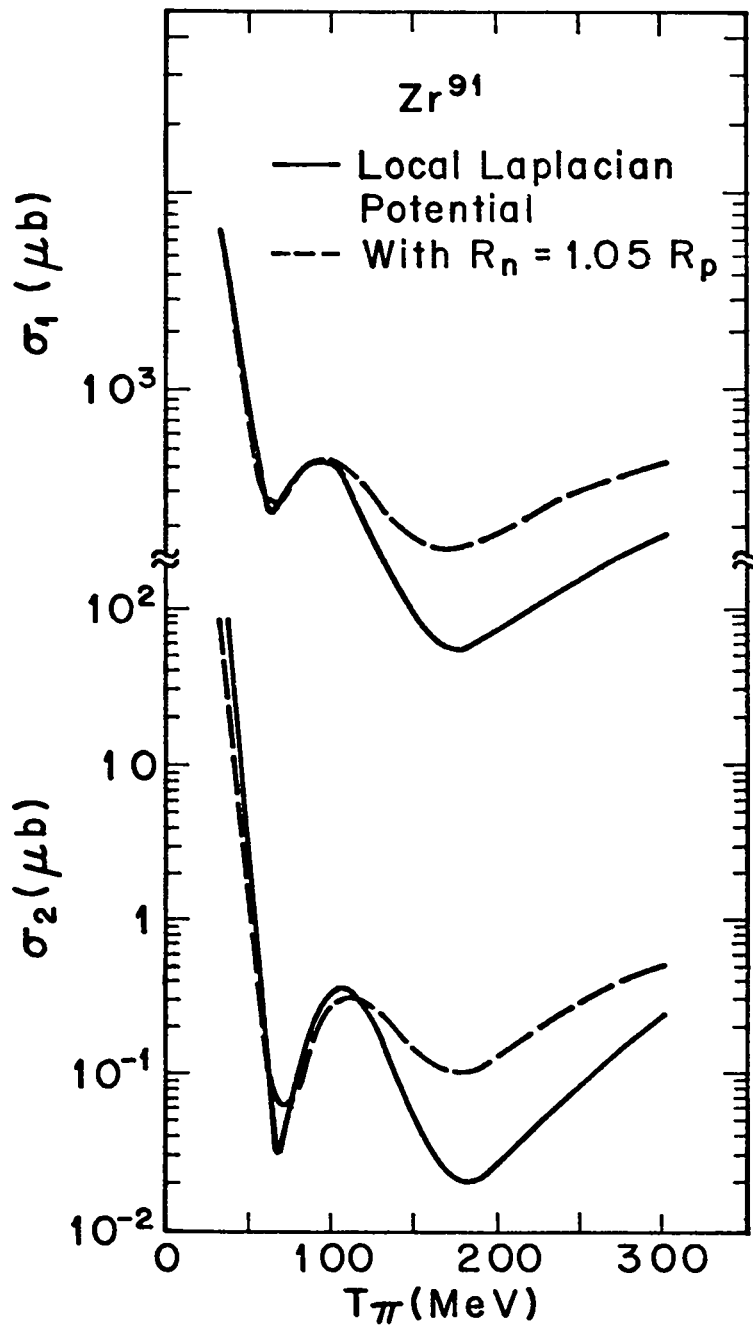
- 132 -

Fig. 18.   Sensitivity of total elastic charge exchange cross sections to changes in neutron density. Solid curve: neutron shape equals proton shape. Dashed curve: neutron radius five percent larger than proton radius.

except where r is small. Hence the small r region is important for this integral.

It is immediately apparent that

$$T = \sqrt{\frac{4\pi}{\hbar\omega}} \quad < \vec{\sigma}\cdot\vec{k} > \tilde{\phi}^{*}_{LJ}(q)$$

A.6   GALLILEAN INVARIANCE OF THE PRODUCTION OPERATOR

I now would like to discuss the Gallilean covariant red herring. There has been a continuing controversy over the form of the non-relativistic pion production operator. This problem arises because the Lorentz-invariant operator is $\gamma_5\tau\phi$ or $\gamma_5\gamma_\mu\partial^\mu\phi\,\tau$ and in order to be used along with typical nuclear wave functions, some non-relativistic reduction must be carried out. If the nucleon's momentum is much less than its mass, the static result $H' \propto \vec{\sigma}\cdot\vec{k}$, where $\vec{k}$ is the momentum of the pion, is a good approximation. This result is not Gallilean invariant, but one knows in which frame one is working so that there is no problem. If one wants to do a better job one keeps terms proportional to the nucleon momentum. A problem occurs in that different methods of doing the Foldy-Woutheysen reduction gives different results. One finds, in first order,[17]

$$H' \propto \vec{\sigma}\cdot\left(\vec{k} - \frac{\lambda}{2m}\mu(\vec{p}_i + \vec{p}_f)\right)$$

where $\vec{p}_i$ and $\vec{p}_f$ are the initial and final momenta of the nucleons. The choice $\lambda = 1$ gives a Gallilean invariant result because one can shift the velocity of the frame and get the same H! However, any value of λ is allowed to first order in p_i and p_f. In pion production $\mu/M\,p_i > k$ so that this ambiguity would appear to be a tremendous problem. In reality this is no problem at all. This is because in the dominant mechanism the pion is virtual and has

- 134 -

a momentum <u>much</u> <u>greater</u> than $\mu\, p_i/m$. Calculations in the TNM or DWBA

calculations which allow the pion to go off-shell show <u>no</u> sensitivity to the

parameter λ . Furthermore, if one follows a simpler reduction procedure

based on Dirac spinors, one finds $\lambda = 1/2$ for the case in which the pion is

off-shell and the nucleons are nearly on-shell. This result has now been ob-

tained by myself,[6] Bolsterli[18] and by Brack <u>et</u> <u>al</u>.[13] Thus cross sections are

not sensitive to λ and, people believe it to be small.

The simplifications of the problem occurs because of the strong rescatter-

ing which is due to the (3,3) resonance. There may be situations, such as very

close to threshold, where the rescattering is not strong. In this case, the

nucleus might be off-shell and the pion on-shell. Then the production operator

must take on a different form. For example, Delacroix and Gross[19] find that

the small components of the deuteron wave function play a significant role in

production of threshold mesons in proton-proton interactions. These authors

use the relativistic pseudovector coupling vertex to do the calculation.

REFERENCES

1) D. J. Ernst, J. T. Londergan, G. A. Miller and R. M. Thaler, Phys. Rev. $\underline{C}$ (in press).

2) G. A. Miller, Phys. Rev. Lett. $\underline{38}$, 753 (1977) and to be published in Phys. Rev. $\underline{C}$.

3) T. Marks, M. P. Baker, R. L. Burman, M. B. Cooper, R. H. Heffner, R. J. Holt, D. M. Lee, D. J. Malbrough, B. M. Preedom, R. P. Redwine, J. E. Spencer and B. Zeidman, Phys. Rev. Lett. $\underline{38}$, 149 (1977).

4) G. A. Miller and J. E. Spencer, Ann. Phys. (N.Y.) $\underline{100}$, 562 (1976).

5) J. T. Londergan, K. W. McVoy and E. J. Moniz, Ann. Phys. (N.Y.), $\underline{86}$, 147 (1974).

6) G. A. Miller, Nucl. Phys. $\underline{A224}$, 269 (1974).

7) G. A. Miller and S. C. Phatak, Phys. Lett. $\underline{51B}$, 129 (1974).

8) Z. Grossman, F. Lenz and M. P. Locher, Ann. Phys. (N.Y.) $\underline{84}$, 348 (1974).

9) M. Dillig and M. G. Huber, Phys. Lett. and Nucl. Phys. (to be published).

10) M. P. Keating and J. G. Wills, Phys. Rev. $\underline{C7}$, 1336 (1973).

11) W. B. Jones and J. M. Eisenberg, Nucl. Phys. $\underline{A154}$, 49 (1970).

12) M. Alberg, E. M. Henley, G. A. Miller, J. E. Walker (to be published).

13) M. Brack, D. O. Riska and W. Weise, Phys. Lett. $\underline{61B}$, 41 (1976); Nucl. Phys. (to be published).

14) B. Goplen, W. R. Gibbs and E. Lomon, Phys. Rev. Lett. $\underline{32}$, 1012 (1974).

15) W. R. Gibbs, B. F. Gibson, A. T. Hess, G. J. Stephenson, Jr. and W. B. Kaufmann, Phys. Rev. Lett. $\underline{36}$, 85 (1976).

16) N. Austern, Direct Nuclear Reaction Theories, Wiley (New York) 1970.

17) M. V. Barnhill, III, Nucl. Phys. $\underline{A131}$, 106 (1969).

18) M. M. Bolsterli, Phys. Rev. $\underline{D14}$, 2008 (1976).

19) E. Delacroix and F. Gross, Phys. Lett. $\underline{66B}$, 337 (1977).

NUCLEAR STRUCTURE WITH PIONIC ATOMS

M. Leon
University of California
Los Alamos Scientific Laboratory

My remarks today will be made up of two fairly disjoint parts: the first will be a survey of what might be called the "classical" pionic atom studies, and the second will describe recent work on using the dynamic E2 effect and nuclear resonances in pionic atoms. There are some very useful reviews on pionic atoms; in particular Backenstoss (1970) presents the basic ideas and the experimental situation as of 1970, and Hüfner (1975) includes a very nice section on pionic atoms in his review of the pion-nucleus interaction. The E2 nuclear resonance effect is discussed in Leon (1976).

I. BASIC PHYSICS OF PIONIC ATOMS

The main reason for studying pionic atoms is for the information they give on the zero-energy pion-nucleus interaction. While for a given nucleus the information is confined to just one or two partial waves, the high precision attainable makes the method very attractive.

The story begins with negative pions stopping in a target. The very slow pions are captured into bound atomic orbits with quite large quantum numbers. This stage and the subsequent one of de-excitation through the electron cloud of the atom have not yet been described both convincingly and quantitatively, but fortunately our ignorance does not significantly affect the strong inter-action information. For this it is enough to know that once inside the electronic k-shell the pionic atom is hydrogenic, and that for low enough quantum numbers (E1) radiative transitions take over from the Auger de-excitation transitions. The population of pions tends to become concentrated in the circular orbits, those with $\ell = n-1$, so that the main sequence x-ray lines are the most intense

ones (see Fig. 1). This sequence comes to an abrupt halt at the last x-ray line, where in the lower level (Fig. 1) the absorption of the pion by the nucleus overwhelms the next radiative transition. It is this last x-ray line that carries all of the strong interaction information. Although the energy eigenvalues are basically hydrogenic at this stage, there are significant corrections for vacuum polarization and some less important electromagnetic effects. The lower level, however, has its energy shifted (from the purely electromagnetic value) by the strong interaction, and is broadened by the absorption. The upper level (Fig. 1), since it has a larger ℓ-value (and hence a stronger centrifugal barrier) has shift and width three orders of magnitude smaller; thus the upper level shift is too small to be detected, but the width can often be measured because the absorption competes with the known radiative transition rate. So by measuring the shift width, and intensity of the last x-ray line, one can extract three pieces of information on the interaction of the π^- with that nucleus.

As we look at a given last line for increasing Z, it grows broader and less intense until it fades out altogether; then the preceding transition becomes the last line. Figure 2 shows which levels have been measured for different Z's; the solid line indicates shift and width measurements (lower level), the dotted line width measurements only (upper level). The relative errors in these measurements tend to be smallest in the middle of each region and get quite large at the extremes. To give you an idea of the quality of the data as of 1970, I show in figures 3-5 the 1s and 2p shifts and the 2p and 3d widths (all taken from Backenstoss, 1970). The most striking fact is that while the 1s shift is repulsive, the 2p and higher waves are attractive. This immediately requires that any potential used to describe the pion-nucleus interaction for a range of Z must be non-local.
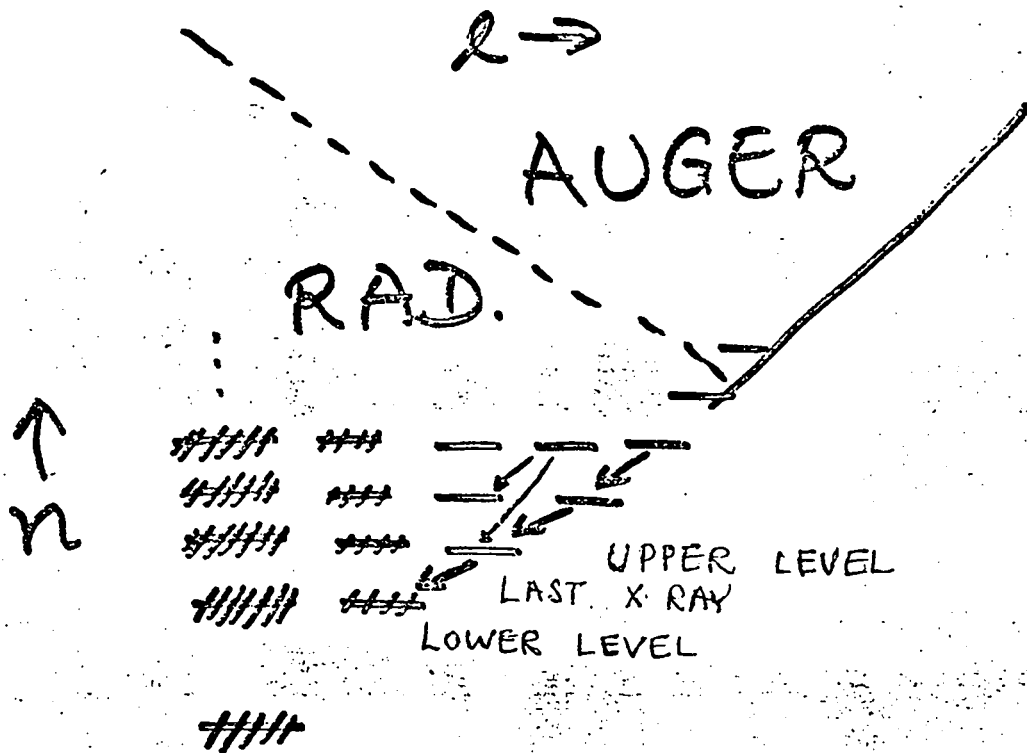
Fig. 1   The interesting states and transitions in pionic atoms.
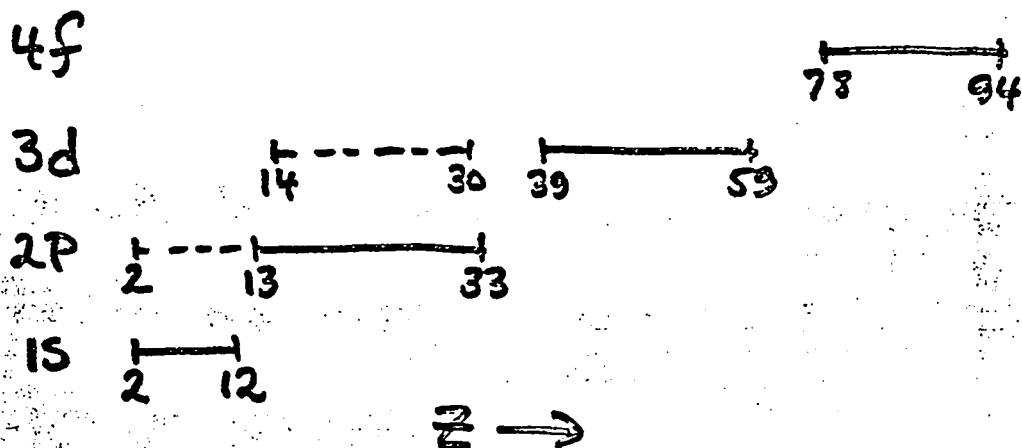

Fig. 2   Z-range of available pionic atom measurements. The solid line indicates shift and width measurements (lower level), the dashed line width measurements only (upper level).
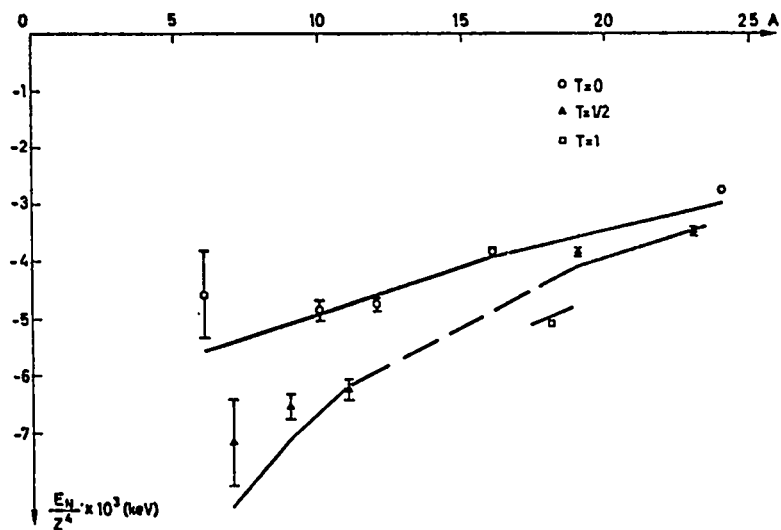
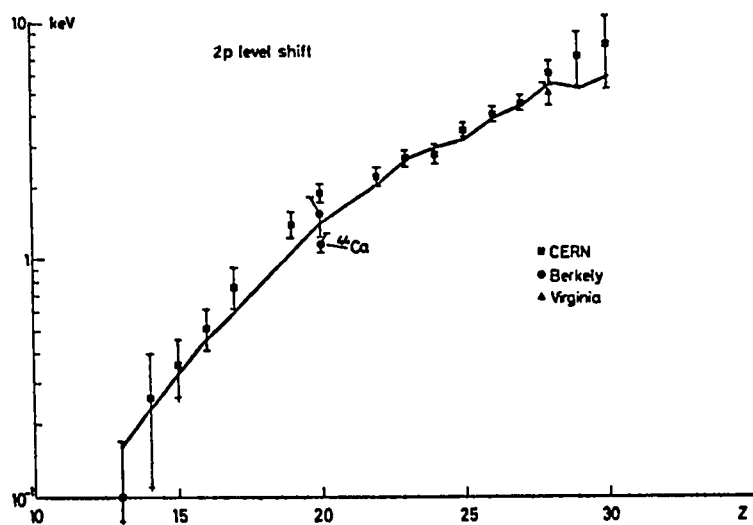Fig. 3   1s shifts (multiplied by $10^3/Z^4$) in keV.
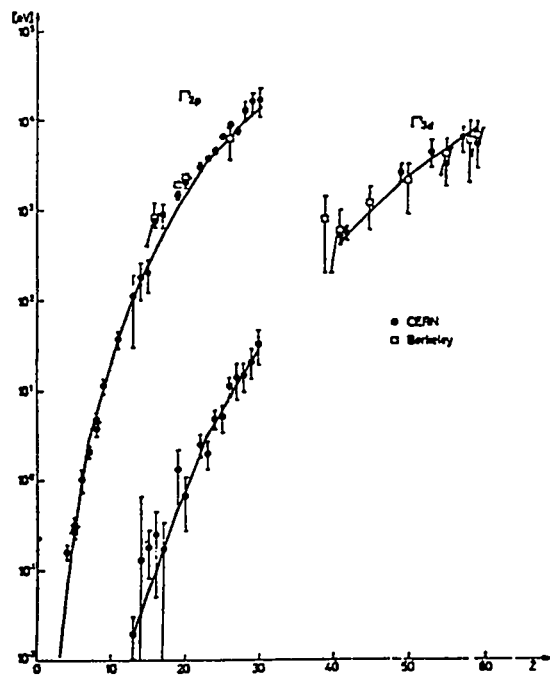

Fig. 4   2p shifts in keV.

Fig. 5   2p and 3d widths in keV.

II. THE PION-NUCLEUS POTENTIAL

A potential gives us a very convenient way of treating the repeated
scattering of the pion by the nucleus. This potential, along with the Coulomb
potential (from the finite, not point, nucleus, and including the vacuum
polarization, etc., contributions) is inserted into the Klein-Gordan equation,
and the energy eigenvalues are found numerically. The form of potential most
often used is that introduced by Ericson and Ericson (1966). This has both
local (s-wave π-nucleon) and non-local (p-wave π-nucleon) parts:

$$U = U^{\ell} + U^{n.\ell.}$$ (1)

Here

$$U^{\ell} = - \frac{4\pi}{2\mu_R} \left\{ b_0\rho(r) + b_1(\rho_n(r) - \rho_p(r)) + B_0\rho^2(r) \right\}$$ (2)

and $\mu_R = \mu/(1 + \mu/M)$. ρ_p and ρ_n are the proton and neutron densities (normalized
to Z and A) and $\rho \equiv \rho_n + \rho_p$, while b_0 and b_1 are the effective (real) isoscalar
and isovector π-nucleon scattering lengths. The free particle value of b_0 is

$$1/2(a_{\pi-p} + a_{\pi-n}) \approx 0,$$ (3)

and multiple scattering corrections then result in a small, negative value of b_0.
This supplies the observed s-wave π-nucleus repulsion. The ρ^2 term is inserted
to express absorption on <u>pairs of nucleons</u> (since it is hard for a single nucleon
to absorb all that energy and no momentum), so Im $B_0 > 0$.

The non-local part was written by Ericson and Ericson as

$$U^{n-\ell} = - \frac{1}{2\mu_R} \nabla \frac{\alpha(r)}{1+1/3\xi\alpha(r)} \nabla$$ (4)

with

$$\alpha(r) \equiv 4\pi\{c_0\rho + c_1(\rho_n - \rho_p) + C_0\rho^2\}.$$

Analogous to the local part, c_0 and c_1 are averages of the p-wave π N scattering
lengths; $c_0 > 0$ to give the p-wave attraction and Im $C_0 > 0$ to produce two-

nucleon absorption. The term in the denominator, $1/3\ \xi\alpha(r)$, is the Lorentz-Lorenz effect for π-nuleus interaction and expresses the effect of the correlations between the nucleons. Stated simply, this effect arises because the pion wave scattered from a given nucleon does not see a _uniform_ distribution of nucleons, but one with that particular nucleon removed; since presumably two nucleons cannot sit at the same point, there is a hole in distribution of the other nucleons at the position of the scattering nucleon. The value of ξ, the Lorentz-Lorenz parameter, depends on the correlation function and the range of π-N interaction. In fact this correction has received a lot of theoretical attention and slightly different forms are now sometimes used (Hüfner, 1975).

This expression represents an expansion in powers of the nuclear density ρ, and because of the weakness of the interaction, the expansion appears to converge. The potential forms a very convenient meeting ground for the experimentalists and the many-body theorists. Unfortunately the determination of the parameters from the experimental data is _not_ clean-cut. The basic problem is that it is hard to separate the ρ and ρ^2 terms, because the ratio of expectation values $<\rho^2>/<\rho>$ does not vary very much for the available shifts and widths. Thus the empirical values of b_0 and ReB_0 are strongly correlated, as are the values of c_0, ReC_0, and ξ (Seki, 1977).

One way of dodging part of this problem is to arbitrarily set $ReB_0 = ReC_0 = 0$. Some fits to the data obtained in this way are shown in Table 1 where the older work of Tauscher (1971) is presented along with some recent unpublished(and preliminary) results of R. Seki. The errors that go along with these results (not shown) are fairly small (mostly 10% of the value or less) but these merely correspond to χ^2 increasing by one. Since the fit is not terribly good - i.e., χ^2/N is significantly greater than 1.0 - these errors probably should not be taken very seriously either. And while $\xi = 1.0$ is preferred over $\xi = 0.0$, this should not be taken

as conclusive evidence. In the last column of Table 1 are shown the theoretical

values of Ericson-Ericson parameters, as quoted by Tauscher (1971). One sees

that the agreement is surprisingly good, except perhaps for ImB_0.

As a cautionary tale, Seki has also done a fit using the Kisslinger potential

i.e., dropping the ρ^2 and the Lorentz-Lorenz terms and making b_0 and c_0 complex

to produce the absorption. At least for a subset of the experimental data

(column one of Table 1) χ^2/N is actually smaller for the Kisslinger form

(3.06 compared to 3.19), even though we all believe that the Ericson-Ericson

potential is a better model! Moral: One should not buy a used car on the basis

of χ^2.

Of course, there is no real reason for $ReB_0 = ReC_0 = 0$. Any theoretical

constraint on these parameters would greatly reduce the uncertainty in the re-

maining free ones and hence is much to be desired. I should mention explicitly

that these analyses assume that $\rho_n(r) \equiv \rho_p(r)$; of course any significant deviation

of the neutron from the proton distribution would be important, especially as

the p-wave interaction with the neutrons is much stronger than with the protons.

In principle, this makes pionic atoms a good probe of the neutron distributions,

but in practice Catch 22 applies: the neutron distributions cannot be extracted

until the potential parameters are known, but determining the potential para-

meters requires a knowledge of the neutron distributions. Here again a lot

of help from theory is needed if we are to disentangle the physics.

At some point along the road to greater experimental precision, the potential

model must break down; after all, nuclei are not simply globs of nuclear matter,

but have individual shell structures which will presumably affect the inter-

action at some level of precision (more than through the nucleon density distri-

butions). It would be very interesting to have a theoretical estimate of these

shell effects, but as far as I know none has been made.

TABLE 1

FITTED AND PREDICTED POTENTIAL PARAMETERS
(R. Seki)

	33 ATOMS (1s,2p) $\xi = 1.0$	59 ATOMS $\xi = 1.0$	59 ATOMS $\xi = 0.0$	TAUSCHER $\xi = 1.0 \pm .1$	THEORY
b_0	-.030	-.030	-.029	-.029	-.025+....
b_1	-.10	-.15	-.15	-.08	-.09
ImB_0	.039	.041	.043	.043	.017
c_0	.22	.24	.018	.23	.19
c_1	.16	.29	.23	.18	.17
ImC_0	.12	.11	.038	.08	.07
χ^2/N	3.19	3.30	3.69	?	

III. THE NUCLEAR RESONANCE EFFECT IN PIONIC ATOMS

Nuclear resonance effects certainly have to do with individual nuclear structure but in a rather different way. These effects occur because of Coulomb excitation of the nucleus during the atomic cascade, and studying them will contribute a modest but still significant amount to our knowledge of the pion-nucleus interaction. This topic has the advantage of being somewhat new and also that of most of the work having been done here at Los Alamos.

Nuclear resonance effects are much more unusual for pionic atoms than for muonic atoms because the muons get very close to (and inside) the nucleus while a pion is absorbed while most of its wave function lies far outside the nucleus. As if to compensate for this, the effect of a resonance is much easier to observe for the pion case just because of the absorption. To see how this goes consider the case of pionic ^{112}Cd. The relevant nuclear and pionic atom levels are shown in Figure 6. The very close matching of the 2^+ excitation energy with the 5g-3d atomic de-excitation energy together with the E2 coupling results in significant configuration mixing, so that the nominal $(5g,0^+)$ state has some $(3d,2^+)$ mixed in, with mixing coefficient $\underline{a}$ being given by the usual second-order perturbation theory expression:

$$a = \frac{<3d,2^+|H_Q|5g,0^+>}{E_{5g,0^+} - E_{3d,2^+}} \tag{5}$$

The mixed 5g state then has an <u>induced width</u>

$$\Gamma_{ind} = |a|^2 \Gamma_{3d}, \tag{6}$$

and while this induced width is much less than the 3d width, it is about the same size as the radiative 5g→4f width. Thus the 5→4 and the subsequent 4→3

transition will be weakened or attenuated by this induced absorption. This effect is easily observed by comparing x-ray intensities from a ^{112}Cd target and a "normal" isotope, e.g. ^{110}Cd, whose E_2^+ is far off resonance. Then using the higher 6→5 transition for normalization, we define the ratios

$$R_\alpha(112) \equiv \frac{[I(5\to 4)/I(6\to 5)]112}{[I(5\to 4)/I(6\to 5)]110},$$

$$R_\beta(112) = \frac{[I(4\to 3)/I(6\to 5)]112}{[I(4\to 3)/I(6\to 5)]110}. \tag{7}$$

As long as we make the two separated isotope targets identical, all the unpleasant corrections for x-ray absorption in the targets, detector efficiency, etc., drop out of these ratios, making the experiment very easy.

To calculate the size of this effect, we need to know (a) the quadrupole matrix element $< H_Q >$, (b) the energy shift and width of the "inner" level (3d in this case), and (c) the nuclear excitation energy. Now $< H_Q >$ contains, aside from some tedious angular momentum factors, the atomic E2 matrix element - which is easily computed using point Coulomb wave functions - and the nuclear E2 matrix element - which comes directly from the B(E2↑) value _measured_ in Coulomb excitation experiments. Furthermore, for Cd the 3d level is directly observable. (Here we are explicitly assuming that the strong interaction of the 3d pion with the 2^+ excited nucleus is identical to that with the nucleus in its ground state, i.e., that any _pionic isomer shift_ is negligible.) Thus the cadmium case is ideally suited for testing these ideas.

The first experimental test (for both ^{112}Cd and ^{111}Cd which also shows the effect) was made here at LAMPF a couple of years ago and more precise measurements were made recently both at Rutherford High Energy Lab and here; the (unpublished) results of the recent experiments are summarized in Table 2. From this data we see that (1) the two laboratories are in very good agreement, and (2) the

agreement with theory is also quite good. I should mention that, as part of their experiment, the Rutherford group made a very precise measurement of the $^{112}Cd_2$+ energy which has been incorporated in the theoretical prediction and which has considerably reduced its error. In fact, the biggest single contributor to this theoretical error in ^{112}Cd is now the error in the spectroscopic quadrupole moment of the 2^+ state; Q_2+ contributes an _electromagnetic_ isomer shift which _is_ significant. Thus if we wanted to, we could turn this measure-ment around and use it to give a value of Q_2+ with smaller error bars than the present adopted value! For ^{111}Cd the biggest contributor is the error in E_2+, so here we could use the nuclear resonance result to get a value of E_2+ with tighter error bars.

However, the most interesting aspect of the nuclear resonance effect is the information it can give about "hidden" levels, i.e., those not normally accessible because they are beyond the last x ray. An especially interesting example of this is in ^{110}Pd, where we can probe the 3p state for this very large Z (46) and test the prediction made years ago by Ericson, Ericson and Krell (1969) that the p-wave pion-nucleus interaction changes from attractive to repulsive as Z in-creases past about 36. To see how this sign change comes about, we can look at the following approximate form for the energy shift:

$$I \simeq const \cdot \int [\bar{a}_s \phi^2(\bar{r}) + 3\bar{a}_p (\nabla\phi(\bar{r}))^2] \rho(\bar{r})d^3\bar{r}. \qquad (8)$$

For a nucleus of very small radius, only the s-wave pion-nucleon interaction (first term) can contribute to the s-wave pion-nucleus interaction, and similarly for the p-wave. As the nuclear radius increases, however, the first term begins to contribute in the p-wave pion-nucleus states, until, at large enough radius, the repulsive first term overwhelms the attractive second term. The predicted behavior along with the experimental p-wave energy shift data plotted by Ericson (1970) is shown in Figure 7. We see that the data faded out just before the

TABLE 2

RUTHERFORD AND LOS ALAMOS RESULTS
FOR
^{112}Cd AND ^{111}Cd COMPARED WITH THEORY

	RHEL	LASL	COMBINED	THEORY
$R_\alpha(112)$	.557 ± .022	.495 ± .029	.534 ± .018	.520 ± .040
$R_\beta(112)$	.678 ± .037	.715 ± .058	.689 ± .031	.633 ± .037
$R_\alpha(111)$	.796 ± .036	.782 ± .037	.789 ± .026	.739 ± .057
$R_\beta(111)$	.914 ± .057	.908 ± .059	.911 ± .041	.807 ± .040
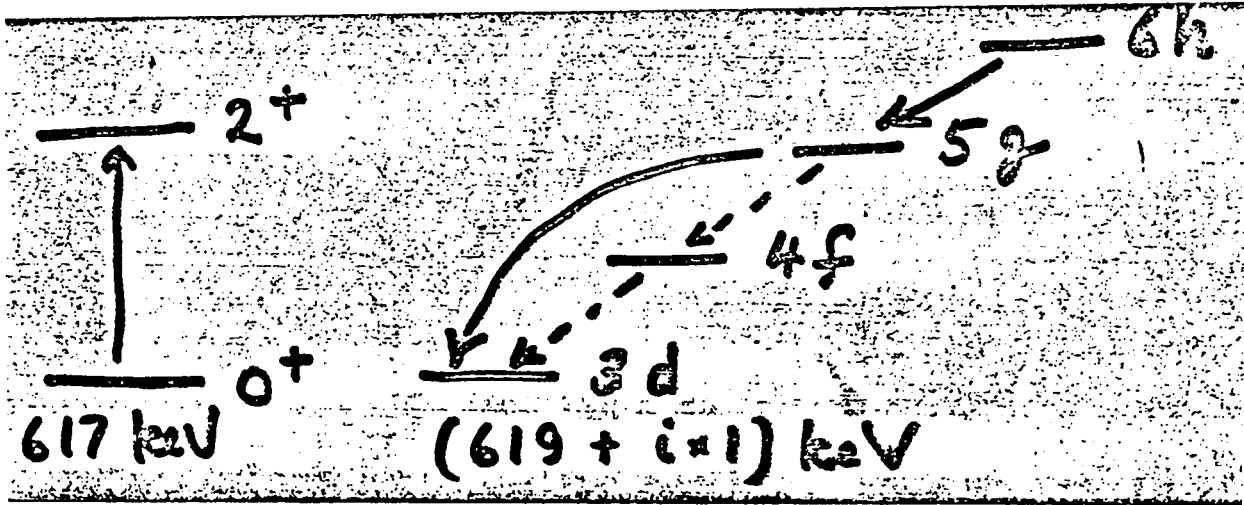
Fig. 6   Nuclear and atomic levels in pionic ^{112}Cd.
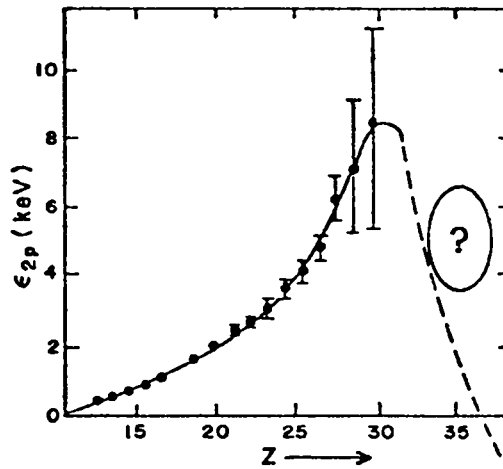
Fig. 7   Observed and predicted behavior of the 2p
shift as a function of Z(Ericson,1970).

predicted down turn; thus this striking prediction remained untested until
our recent LAMPF experiment on ^{110}Pd (Leon et al, 1976a).

The relevant energy levels are shown in Figure 8; the shift and half-width given have been calculated using a standard set of potential parameters. The amount of attenuation (attenuation $A_\alpha \equiv 1 - R_\alpha$) of course depends on the values of both the 3p shift and width; this dependence is explored in Figure 9, where we plot contours of fixed attenuation (which are circles) in the plane of the complex energy denominator of Eq. 5. Since the width and shift of the 4f level are negligible, the choice of 3p width and shift uniquely determines a point in this plane. Suppose first that all of the strong-interaction parameters are set to zero; this corresponds to the intersection of the dashed curve and the abscissa. If we now turn on the absorptive parameters, leaving the real parameters at zero, we trace out the dashed curve. Then the entire region to the left of the dashed curve corresponds to pion-nucleus repulsion, and the region to the right to attraction. The open circle is the region implied by naive extrapolation of Figure 5, i.e., no sign change, while the dot is the actual prediction of the fitted optical potential, therefore including the sign change and lying in the repulsive region.

The experimentally measured attenuation was found to be

$$A_\alpha = (19.4 \pm 2.8)\% \tag{9}$$

which corresponds to the shaded region of Figure 9. Since the shaded region lies well within the repulsive part of the complex energy difference plane, the experiment confirms unambiguously the predicted sign change of Ericson et al(1969)

In fact, it does more than that, since the observed A_α is significantly larger than the predicted value of 11%. This implies that the 3p width must be significantly less than the predicted value of 30 keV; we must have

$$\Gamma_{3p} \leq 21 \text{ keV}. \tag{10}$$

We are now planning an experiment involving the 3p level of ^{104}Ru$(Z = 44)$,

- 150 -
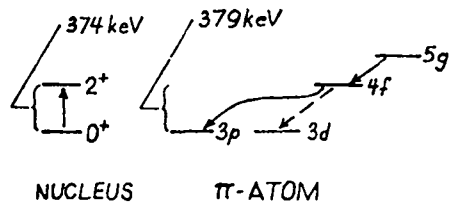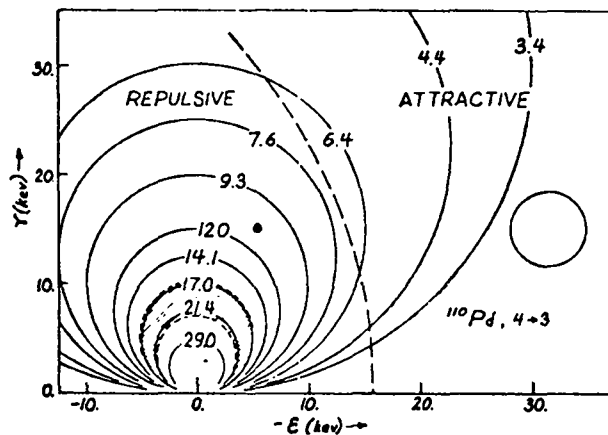
Fig. 8   Levels mixed in pionic ^{110}Pd.

Fig. 9   Attenuation contours in the ΔE plane for pionic ^{110}Pd. The ε is $E_2^+ + E_{3p} - E_0^+ - E_{4f}$, while the γ is $(\Gamma_{3p} + \Gamma_{4f})/2 \simeq \Gamma_{3p}/2$. The broken curve comes from setting the real phenomenological potential parameters to zero while varying the imaginary ones; the region to the left of this curve corresponds to pion-nucleus repulsion, the right to attraction. The solid point is the predicted value while the circle to the right is from naive extrapolation of the data for $Z = 30$. The contours of fixed A_α are marked in percent. The shaded area is the result of this experiment; note that it lies well within the repulsive region.(Leon et al, 1976a).

to see if the same discrepancy shows up there.

In general, experiments on these hidden levels are interesting because the hidden levels have larger strong interaction effects than the usual lower levels; they involve larger values of the ratio $<\rho^2>/<\rho>$ and hence have more "leverage" toward fixing the potential parameters. This is illustrated in Figure 10, again due to R. Seki. The figure shows the 2p level shifts as a function of Z; the potential parameters of the two forms (Ericson- Ericson and Kisslinger) were fitted to the $Z \leq 28$ data. One sees that the sign change is shifted to much higher Z for the Kisslinger form. (Also shown are very recent measurements of Abela et al (1977) for Z = 32 and 33, which seem to confirm the down turn of Figure 7). The 3p shifts and widths in the cross-over region are shown in Figure 11. While the Ericson-Ericson form gives better agreement with the ^{110}Pd shift, both forms are equally bad as far as the width is concerned. (These results of Seki are preliminary and no doubt subject to change.)

In Table 3 we summarize our results to date for hidden levels. One sees that the large error for ^{104}Ru make the measurement nearly useless, while the result for ^{150}Sm agrees quite well with the predicted value. The null result for ^{48}Ti is very interesting and indicates that the 1s level is not where it is predicted to be. We would like to try to find this level by looking in ^{58}Ni - a difficult task, because the 3→2 line is so weak and broad in Ni.

The cases we are planning to look at are also listed in Table 3; the only one not discussed above is ^{125}Te (Z = 52). The expected effect here is just a few percent (because of the large 3p width) and the point is whether there will be a discrepancy as in ^{110}Pd.

In closing, I want to express the hope that the experimentalists will continue to work hard on these pionic atom measurements and will continue to
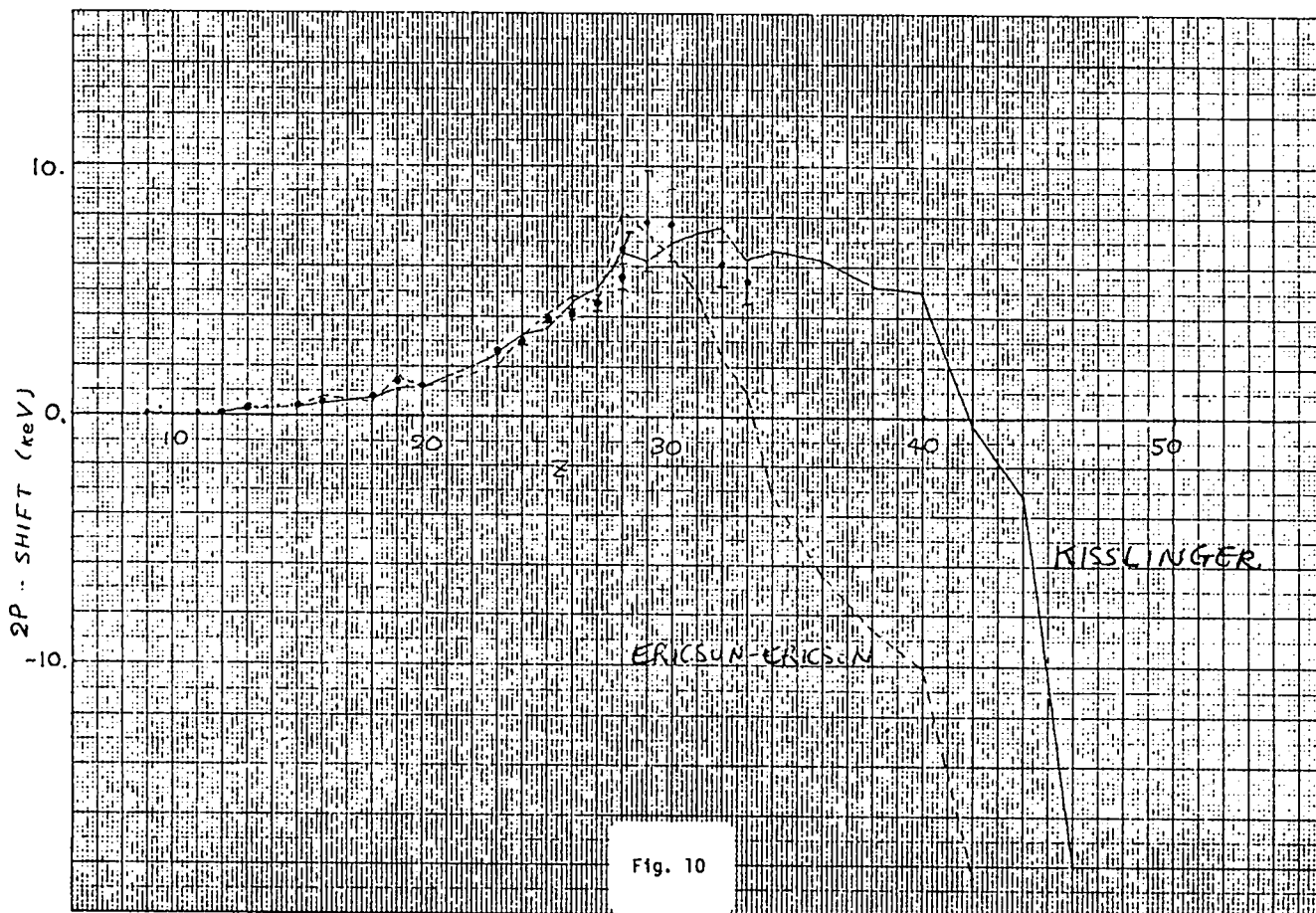
Fig. 10 2p shifts as a function of Z, showing experimental data and fits of the
Ericson-Ericson (dashed curve) and Kisslinger (solid curve) forms.
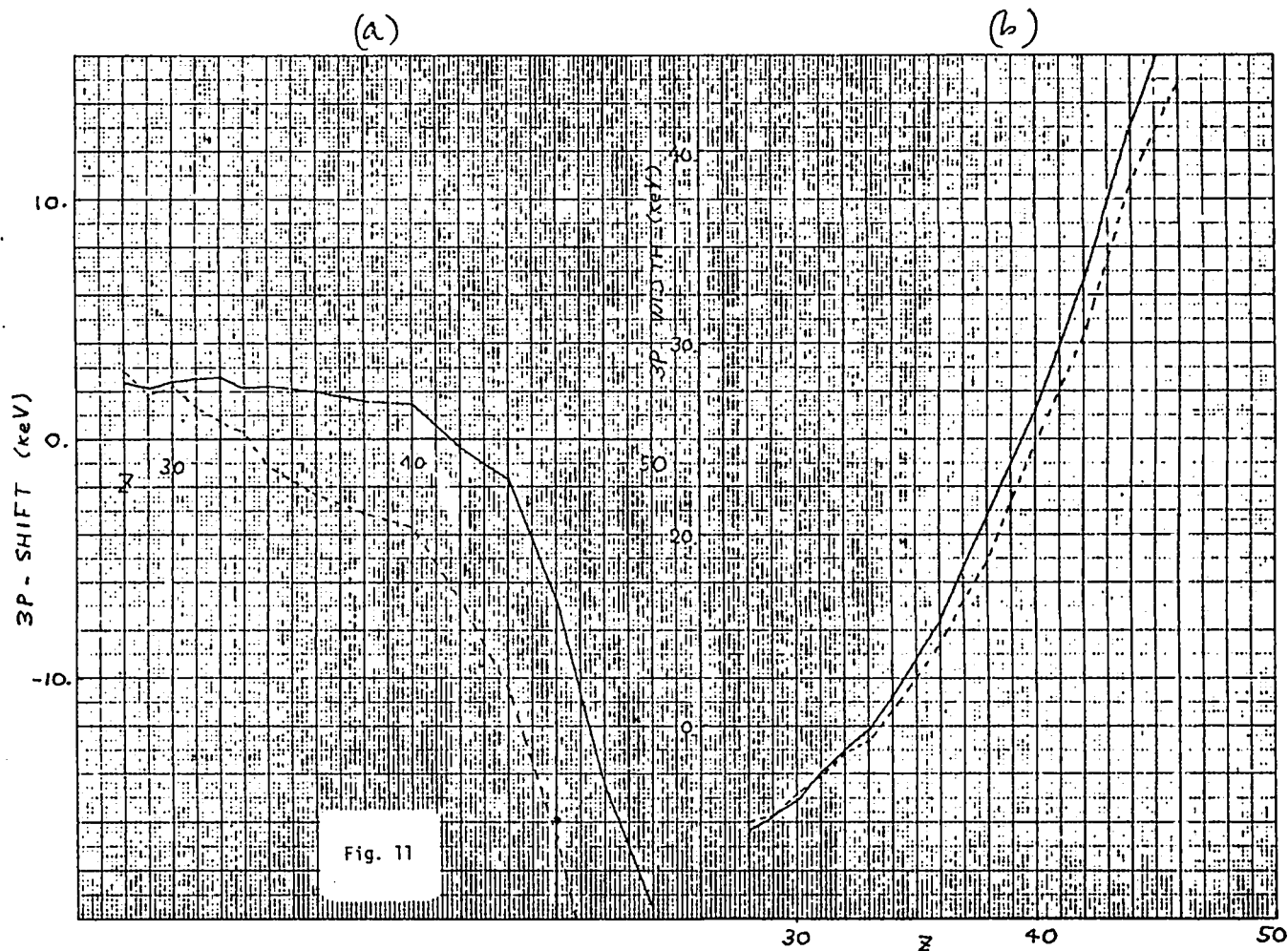Data for Z ≤ 28 were used in the fits. (By R. Seki)

Fig. 11 (a) Predicted 3p shifts using the Ericson-Ericson (dashed curve) and
and Kisslinger (solid curve) forms, and the ^{110}Pd data point.
(b) Predicted 3p width and the ^{110}Pd data point. (By R. Seki)

TABLE 3

ATTENUATION RESULTS AND FUTURE TARGETS

NUCLEUS	LEVEL PROBED	OBSERVED A_α (%)	PREDICTED A_α (%)
^{110}Pd	3p	19.4 ± 2.8	11
^{104}Pd	3p	7.2 ± 10.5	11
^{150}Sm	4d	14.0 ± 3.4	11
^{48}Ti	1s	1.9 ± 3.2	8

FUTURE: 1) 3p: ^{104}Ru, ^{125}Te

          2) 1s: ^{48}Ti, ^{58}Ni

improve the quality of the experimental data. The effort is certainly justified, since the problem of the pion-nucleus interaction lies at the heart of medium-energy physics.

Finally, I want to express my gratitude to R. Seki for many useful discussions and for making available his unpublished results. I am also indebted to C. J. Batty for informing me of the RHEL results prior to publication.

REFERENCES

Abela et al (1977):   To be published.

Backenstoss (1970):   Ann. Rev. Nucl. Sci. 20.

Ericson (1970):   Third Int. Conf. High Energy Physics and
                              Nuclear Structure, ed. S. Devons (Plenum, NY),
                              448.

Ericson & Ericson (1966):   Ann. of Phys. 36, 323.

Ericson, Ericson & Krell (1969):   Phys. Rev. Lett. 22, 1189.

Hüfner (1975):   Phys. Reports 21, 1.

Leon (1976):   Nucl. Phys. A260, 461.

Leon et al (1976a)   Phys. Rev. Lett. 37, 1135.

Seki (1977):   Int. Conf. on Nuclear Structure, Tokyo

Tauscher (1971):   Proc. Int. Sem. on the π-Meson Nucleus
                              Interactions, Strasbourg.

EXPERIMENTS ON PROTON-NUCLEUS SCATTERING

Charles A. Whitten, Jr.

University of California
at Los Angeles

I. INTRODUCTION

In this talk I would like to review some recent work on the study of nuclear structure using medium energy ($\simeq 1$ Gev) protons. In particular the talk will emphasize experimental and theoretical work which bears on the current experimental program at the LAMPF High Resolution Spectrometer (HRS) facility. There will be four main topics. First I will briefly discuss the general characteristics of the HRS facility in its present mode of operation. Second a particular theoretical model for the reaction mechanism will be introduced, the Glauber model; and recent experimental and theoretical work on p-^{4}He elastic scattering around the interference region ($q^2 \simeq 0.25$ GeV^2/c^2) between single and double scattering will be presented. The third topic will be elastic and inelastic scattering on nuclei. Here I will both discuss the extraction of neutron and matter radii from elastic scattering and review current work on the excitation of nuclear collective states at medium energies. The fourth topic will be polarization studies at medium energies where some recent work at the HRS on the measurement of the polarization in elastic scattering will be presented.

II. CHARACTERISTICS OF THE HRS FACILITY

Figure 1 presents a schematic of the current HRS system. An energy analyzed beam (vertical dispersion = 20 cm/%) strikes the target; and the scattered particles enter a spectrometer magnet system run in the energy loss mode. There are a set of decay line chambers -- designed by Chris Morris at LAMPF -- in the focal plane region; and behind these chambers are a set of four scintillators extending over a distance of about 2 meters. A four-fold coincidence between these scintillators

The figure shows a cross-sectional schematic diagram of the HRS facility. Labels within the diagram include:

DETECTOR AND TIME-OF-FLIGHT SYSTEM

S4, S3, S6, S2, Delay Line Chambers

CABLE TRAY SYSTEM

SCATTERING CHAMBER HANDLING CRANE

TARGET TRANSFER MECHANISM

SCATTERING CHAMBER

ℓ BEAM

TARGET POSITION

SLIDING VACUUM SEAL

QUADRUPOLE MAGNET HS-QM-01

BENDING MAGNET HS-BM-02

BENDING MAGNET HS-BM-01

AIR PADS

BEAM DUMP TUNNEL

SECTION HRS FACILITY

0   5   10

GRAPHIC SCALE IN FEET

Fig. 1 - A schematic of the current HRS facility. An event is defined as a four-fold coincidence between scintillation counters S2, S6, S3 and S4 which are behind the focal plane. Energy loss and time of flight information from these four counters determines the particle type, while the position information from the multiwire delay line chambers determines the scattering angle and missing mass represented by the particle through the spectrometer.

- 159 -

provides the event trigger. The missing mass and scattering angle are determined by the particle co-ordinates in the decay line chambers while time-of-flight (tof) and energy loss (dE/dξ) information from the scintillators determines the particle type. Figure 2 presents a typical dE/dξ vs tof plot, demonstrating the excellent particle separation. In figure 3 missing mass spectra at 12° and 15° are presented for elastic and inelastic proton scattering cn ^{58}Ni at 800 MeV. The energy resolution is typically 100 keV. Notice the rather dramatic changes of the relative peak hights, indicating considerable structure in the angular distributions over the range of 3°. Table I presents some general characteristics of the HRS system in its present mode of operation. Table II lists the completed (in the sense of data taking) and in progress experiments at HRS.

III. GLAUBER THEORY AND p-^{4}He ELASTIC SCATTERING IN THE INTERFERENCE REGION AROUND $q^2 \simeq 0.25$ GeV^2/c^2

A. Some Aspects of Glauber Theory

Before discussing the interpretation of experimental data, I would like to introduce and briefly discuss a particular theory of the reaction mechanism, namely Glauber Theory,[1] giving emphasis to the way in which certain terms, the nucleon-nucleon amplitudes and their phases, the nuclear form factors, nuclear correlations, and spin dependence in the nucleon-nucleon amplitudes enter into the theoretical expressions.

In Glauber Theory an eikonal approximation is made in which the wave, within the region of interaction, propagates forward picking up a phase from the interaction. In potential scattering we then have the scattering amplitude:

$$f(\vec{q}) = \frac{k}{2\pi i} \int e^{i\vec{q}\cdot\vec{b}} [e^{i\chi(\vec{b})} - 1] d^2b$$

$$\chi(\vec{b}) = -\frac{1}{\hbar v} \int_{-\infty}^{+\infty} V(\vec{b} + \hat{k}z) dz$$

(1)

PARTICLE ID 800 MeV 20° ^{208}Pb (p.p)
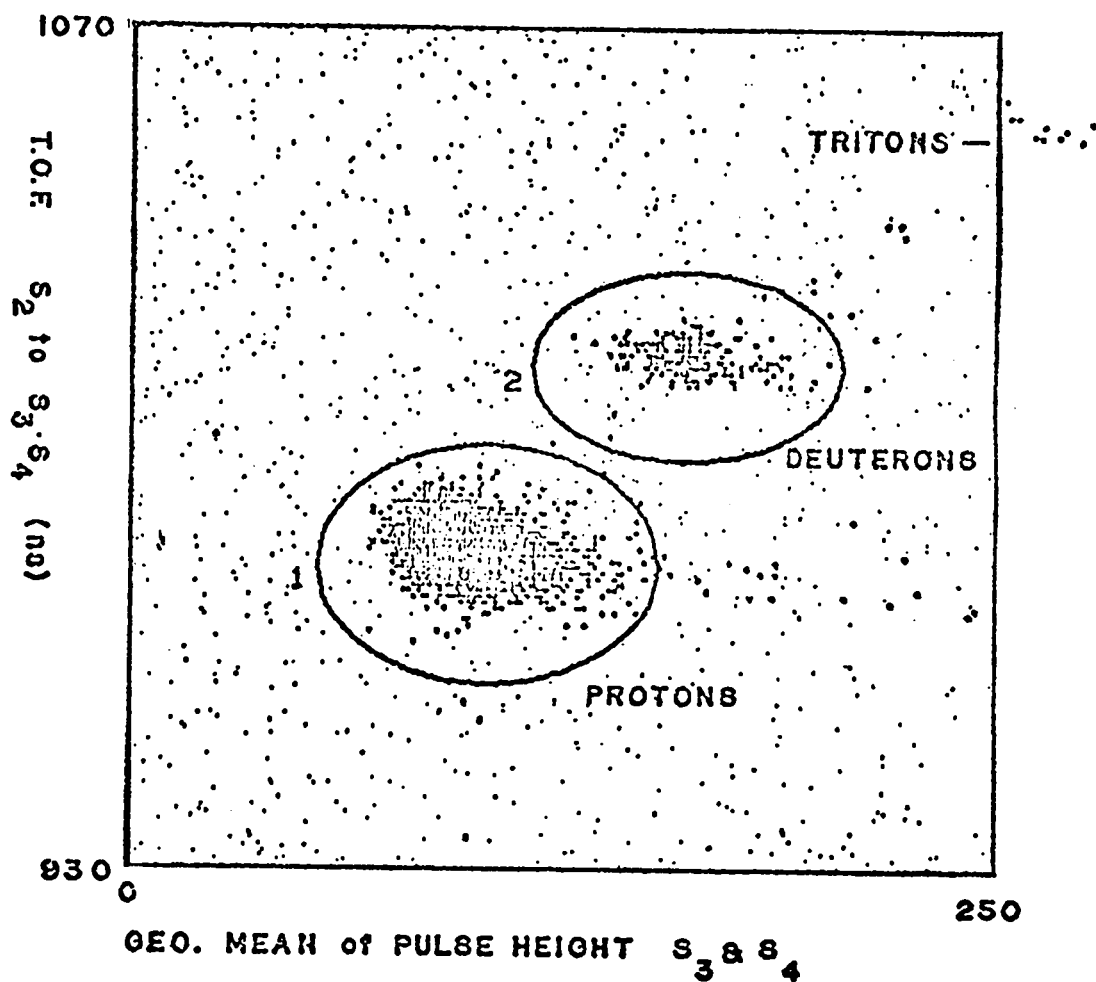
Fig. 2 - The particle identification obtained at HRS by the scintillators be-
hind the focal plane. The geometric mean of the signal pulse heights
in the S_3 and S_4 scintillators is plotted vs the average time of flight
between scintillator S_2 and the scintillators S_3 and S_4. Protons,
deuterons and tritons are easily separated. The small dots are an
artifact of the reproduction process, only the large dots are real
data.
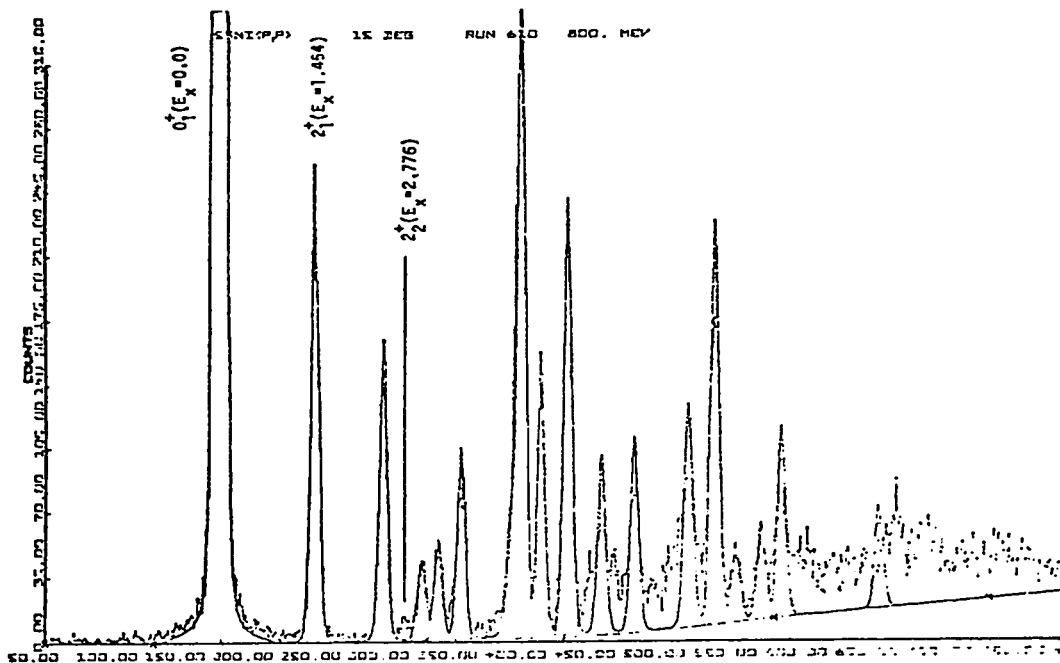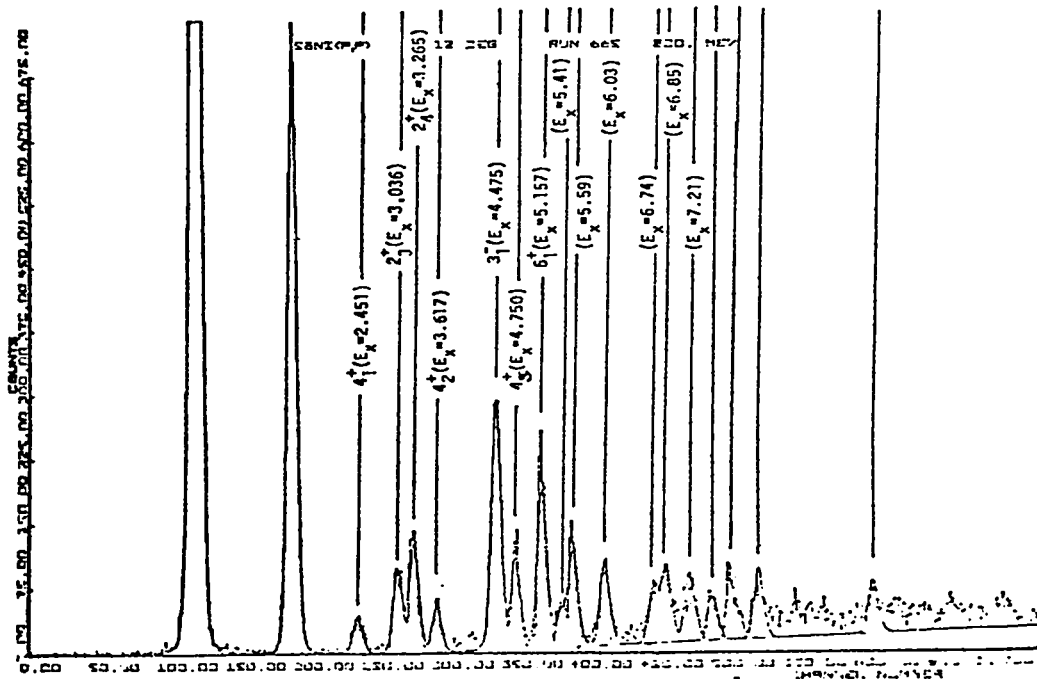
Fig. 3 - Missing mass spectra at 12° and 15° for proton elastic and inelastic scattering on ^{58}Ni at 800 MeV obtained at the HRS facility. The energy resolution is typically 100 KeV.

Table I. General Characteristics of the HRS system

Energy Resolution $\cong$ 80 to 100 KeV for elastic and inelastic proton

scattering $A \gtrsim 40$

Solid angle $\Delta\Omega$ = 2 msr

Angular resolution = $\pm 0.05°$ or ± 1 mrad

I_{max} on target $\cong$ 50nA (limited by dead time in delay live chambers)

Event rate = 1.2×10^3cts/hr/μb/sr for 50 mg/cm^2 ^{58}Ni target with

50nA beam (Event rate is limited to $\sim$ 100 cts/sec by the computer)

Polarized beam is $\sim$ 0.5nA with p $\cong$ 80%

Thus ΔP = ± 0.02 in bins of $\cong 0.2°$ for 2 hr run on 50 mg/cm^2 ^{58}Ni

target with $<\frac{d\sigma}{d\Omega}> \cong 1$ mb/sr

Table II. Experimental Program at HRS

A. Experiments Completed (data taking phase)

Exp. 256 - Inclusive proton-nucleus scattering at backward angles Measured p,d,t spectra at θ_L = 100° and 158° on targets of ^{6}Li, ^{9}Be, ^{12}C and ^{181}Ta

Exp. 4 - p-^{4}He   Elastic Scattering at 800 MeV; $\frac{d\sigma}{d\Omega}$ measured from θ_L = 13° to 165.5°; -t from 0.11 to 4.26 GeV^2/c^2

Exp. 139 - Elastic and Inelastic Proton Scattering Survey Experiment Ex = 0 to $\simeq$ 15 MeV; $\frac{d\sigma}{d\Omega}$ from 4° to 30°; targets ^{12,13}C, ^{58,60,62,64}Ni, ^{208}Pb

B. Experiments in Progress

Exp. 5 - Quasi Elastic Scattering

Exp. 311 - Elastic and Inelastic Proton Scattering Survey Experiment using Polarized Beam.

Participants

Brookhaven National Laboratory: R. Chrien, H. Palevsky, R. Sutter, T. Kozlowski

Los Alamos Scientific Laboratory: G. Hoffman, D. Madland, C. Morris, J. Pratt, J. Spencer, A. Thiesseu, O. van Dyke

Northwestern University: P. Lang, H. Nann, K. Seth

University of California at Los Angeles: T. Bauer, J. Fong, G. J. Igo, G. Pauletta, R. Ridge, R. Rolfe, J. Soukup, C. Whitten Jr.

University of Minnesota: N. Hintz, G. Kyle, M. Oothoudt

University of Oregon: D. McDaniel, P. Varghese

University of Pennsylvania: S. Frankel, W. Fratti

University of Texas at Austin: G. Blanpied, R. Liljestrand

Vassar College: R. Stearns

under the approximations $ka \gg 1$, $V/E \ll$, $ka\,\theta^2 \ll 1$. Here k is the incident wave number, $\vec{q} = \vec{k} - \vec{k}'$ is the momentum transfer, $\vec{b}$ is the impact parameter in the plane $\perp$ to the incident wave, a is the range of the interaction and v is the velocity.

For nucleon-nucleus scattering the approximation is made that the nucleons in the nucleus are "frozen" during the passage of the incident hadron through the nucleus--the fixed scatterer approximation. Also it is assumed that the phases picked up from the interactions with the individual nucleons are additive. Then we have an expression for the scattering amplitude from the nuclear state $|0>$ to the nuclear state $|f>$ of a nucleus with A nucleons

$$F_{fo}(\vec{q}) = \frac{ik}{2\pi} \int d^2b \; e^{i\vec{q}\cdot\vec{b}} \; [\delta_{fo} - S_{fo}(\vec{b})] \tag{2}$$

$$S_{fo}(\vec{b}) = < f| \prod_{j=1}^{A} \{1 - \Gamma_j(\vec{b}-\vec{s}_j)\} \; \underline{\delta(\Sigma\vec{r}_j)}_{A} | \, 0 > \tag{3}$$

where the nuclear co-ordinate, $\vec{r}_j$, of the jth nucleon is given by: $\vec{r}_j = \vec{s}_j + z_j \hat{k}$. Here $\Gamma_j(\vec{b}-\vec{s}_j)$ is the profile function for the interaction and is related to the nucleon-nucleon amplitude $f_j(\vec{q})$ by:

$$\Gamma_j(\vec{b}) = \frac{1}{2\pi i k_0} \int d^2q \; e^{-i\vec{q}\cdot\vec{b}} f_j(q) \tag{4}$$

where k_0 is the wave number in the nucleon-nucleon cm. system. The expansion of $\prod_{j=1}^{A} \{1 - \Gamma_j(\vec{b}-\vec{s}_j)\}$ shows directly the multiple scattering aspect of the theory.

$$\prod_{j=1}^{A} \{1 - \Gamma_j(\vec{b}-\vec{s}_j)\} = 1 - \sum_{j} \Gamma_j(\vec{b}-\vec{s}_j) + \sum_{\substack{j,k \\ j \neq k}} \Gamma_j(\vec{b}-\vec{s}_j)\Gamma_k(\vec{b}-\vec{s}_k) + \ldots \tag{5}$$

Now for small $q^2 (q^2 \gtrsim 0.4 \text{ GeV/c}^2)$ and incident proton energies around 1 GeV/c the spin independent proton-nucleon amplitude may be parametrized as:

$$f_{pN}(q) = \frac{ik_0 \sigma_{PN}}{4\pi} (1 - i\alpha_{PN}) e^{-\frac{1}{2}\beta^2_{PN}q^2} \qquad (6)$$

where σ_{PN} is the P-N total cross section, α_{PN} is the ratio of the real to imaginary forward scattering amplitude and β^2_{PN} is the slope parameter. It should be mentioned that α_{PN} is not well determined experimentally in the ~ 1 GeV region.

The general behavior of the Glauber elastic scattering expression and in particular its sensitivity to α_{PN} can be seen in a closed form expression first derived by Cycz and Lesniak[2]. Let all the A nucleons be in 1s bound states in an harmonic oscillator of range $1/\gamma$. Then:

$$\psi_0^*(\vec{r}_1, ----, \vec{r}_A)\ \psi_0(\vec{r}_1, ----, \vec{r}_A) = \prod_{i=1}^{i=A} \left[(\frac{\gamma^2}{\pi})^{3/2}\ e^{-\gamma^2 r_i^2} \right] \qquad (7)$$

and:

$$F_{00}(q) = (\frac{ik}{2\pi}) \left(\frac{1+\gamma^2\beta^2}{\gamma^2} \right) e^{\frac{q^2}{4A\gamma^2}} \sum_{j=1}^{A} \binom{A}{j} \frac{(-1)^{j+1}}{j} \left[\frac{\sigma(1-i\alpha)\gamma^2}{2\pi(1+2\gamma^2\beta^2)} \right]^j \exp \left[-\frac{(1+2\gamma^2\beta^2)q^2}{4\gamma^2 j} \right]$$

$$(8)$$

Due to the $\exp[-\frac{kq^2}{j}]$ dependence of the individual terms the higher multiple scattering become more important as q^2 increases. In the region where the j and j+1 terms are of approximately equal magnitude the value of α is very important in determining the interference between these terms. For $\alpha=0$ the two terms have opposite sign and a deep minimum can occur.

For elastic scattering, following the derivation of Glauber, we can write:

$$< 0 \mid \prod_{j=1}^{A} \{1 - \Gamma_j(\vec{b}-\vec{s}_j)\} \mid 0 > = e^{i\chi(\vec{b})} \qquad (9)$$

For A nucleons--neutrons and protons identical--we can expand $\chi(\vec{b})$ in the following way:

$$\chi(\vec{b}) = \chi_0(\vec{b}) + \chi_1(\vec{b}) + \dots \quad . \qquad (10)$$

where

$$\chi_0(\vec{b}) = iA \int \Gamma(\vec{b}-\vec{s})\rho(r) \, d\vec{r}^3 \qquad (11)$$

$$\chi_1(\vec{b}) = -\frac{1}{2} iA \int\int [(A-1)\rho_2(\vec{r}_1,\vec{r}_2) - A\rho(\vec{r}_1)\rho(\vec{r}_2)]\Gamma(\vec{b}-\vec{s}_1)\Gamma(\vec{b}-\vec{s}_2)d^3\vec{r}_1 d^3\vec{r}_2 \qquad (12)$$

where $\rho(\vec{r})$ is the one body density $\rho(\vec{r}_1) = \int \psi^*(\vec{r}_1,\text{----}\vec{r}_N)\psi(\vec{r}_1,\text{----}\vec{r}_N)d^3\vec{r}_2\text{---}d^3r_N$ and $\rho(\vec{r}_1,\vec{r}_2)$ is the two body density $\rho(\vec{r}_1,\vec{r}_2) = \int\psi^*(\vec{r}_1,\text{----},\vec{r}_N)\psi(\vec{r}_1\text{----}\vec{r}_N)d^3\vec{r}_3\text{---}d^3r_N$. Thus $\chi_1(\vec{b})$ will be sensitive to two-body correlations in the nuclear wave function. Note that $\chi_i(\vec{b})$ is proportional to the nucleon-nucleon amplitude squared. To take into account the difference between the neutron and proton one body densities and elementary amplities Eq. (11) can be rewritten as:

$$\chi_0(\vec{b}) = iZ \int \Gamma_p(\vec{b}-\vec{s})\rho_p(\vec{r})d^3r + i(A-Z)\int\Gamma_n(\vec{b}-\vec{s})\rho_n(\vec{r})d^3\vec{r}$$

$$= \frac{1}{k_0} \int_0^\infty dq \, q \, J_0(qb) \, [Z \, f_{pp}(q)S_p(q) + (A-Z) \, f_{pn}(q)S_n(q)] \qquad (13)$$

where $S_p(q)$ and $S_n(q)$ are the form factors for the proton and neutron one body densities:

$$S_N(\vec{q}) = \int \rho_N(\vec{r}) \, e^{i\vec{q}\cdot\vec{r}} d^3\vec{r} \qquad (14)$$

It is important to include Coulomb scattering even for light nuclei[3]; and the

inclusion of Coulomb scattering into the formalism is discussed by Glauber and Matthiae[4].

Recent calculations have also indicated that the elastic scattering angular distributions are sensitive to the spin-dependence in the nucleon-nucleon amplitude.[3],[5],[6] To first order for elastic scattering on spin zero target nuclei only two terms need be considered in the amplitude. Following Auger et al.[3] We write

$$f_{PN}(q) = A_{PN}(q) + C_{PN}(q)\vec{\sigma} \cdot \hat{n} \tag{15}$$

where $\vec{\sigma}$ is the spin operator for the incident proton and $\hat{n}$ is the unit vector determined by $\vec{k} \times \vec{k'}$. $A_{PN}(q)$ is given by Eq. (6) while $C_{PN}(q)$ is given by

$$C_{PN}(q) = \frac{\sigma_{PN}k_0}{4\pi} i\left(\frac{q^2}{4m^2}\right)^{\frac{1}{2}} (i + \alpha_{PN}^S) D_S \exp\left(-\frac{1}{2}(\beta_{PN}^S)^2 q^2\right) \tag{16}$$

where α_{PN}^S is the ratio of the real to imaginary part of the amplitude, D_S is the relative strength of the spin-dependent parameter, $(\beta_{PN}^S)^2$ is the slope parameter, and m is the nucleon mass. Following Glauber and Frnaco[7] and Kujawski[8], Auger et al[3] write a new expression for $\int \Gamma(\vec{b}-\vec{s})\rho(\vec{r}) \, d^3\vec{r}$.

$$\int \Gamma(\vec{b}-\vec{s})\rho(\vec{r})d^3\vec{r} = T(b) + \vec{\sigma} \cdot (\hat{b} \times \hat{k}) \, T_S(b) \tag{17}$$

where

$$T(b) = \frac{1}{ik_0} \int J_0(qb)A(q)S(q)q \, dq \tag{18}$$

$$T_S(b) = \frac{1}{k_0} \int J_1(qb)C(q)S(q)q \, dq \tag{19}$$

The elastic scattering amplitude then has two terms:

$$F_{00}(q) = F_1(q) + \vec{\sigma} \cdot \hat{n} \, F_2(q) \tag{20}$$

with the cross section given by:

$$d\sigma/d\Omega = |F_1(q)|^2 + |F_2(q)|^2 \tag{21}$$

and the polarization given by:

$$P = 2 \, \mathrm{Re} \, F_1^* F_2 / \frac{d\sigma}{d\Omega} \tag{22}$$

B. Analysis of p-^{4}He Elastic Scattering in the Interference Region around $q^2 \cong 0.25 \, \mathrm{GeV}^2/c^2$.

A considerable amount of theoretical and experimental work was spurred by the disagreement between the 1967 data of Palevsky et al[9] and the 1974 data of Baker et al[10] as regards the behavior of the p-^{4}He elastic scattering angular distribution at 1 GeV and a momentum transfer, -t , of about 0.25 GeV^2/c^2, where the single and double scattering terms in the Glauber expansion are interfering. This is shown in Fig. 4 where the two data sets are moved relative to one another by 0.5° which is comparable to the combined error in the two data sets. The earlier work[9] showed a much deeper minimum in the interference region than the later experiment[10]. In the past few years a considerable amount of p-^{4}He elastic scattering has been amassed in this region of -t for incident proton energies between 350 and 1,150 MeV--with points at 2.68 and 23.1 GeV-- thus allowing a rather detailed study of the energy dependence in the reaction mechanism. Table III presents a list of the various experiments which have been performed. Fig. 5 presents a selected set of the experimental data between 0.35 and 23.1 GeV where dσ/dt is plotted versus t . Since
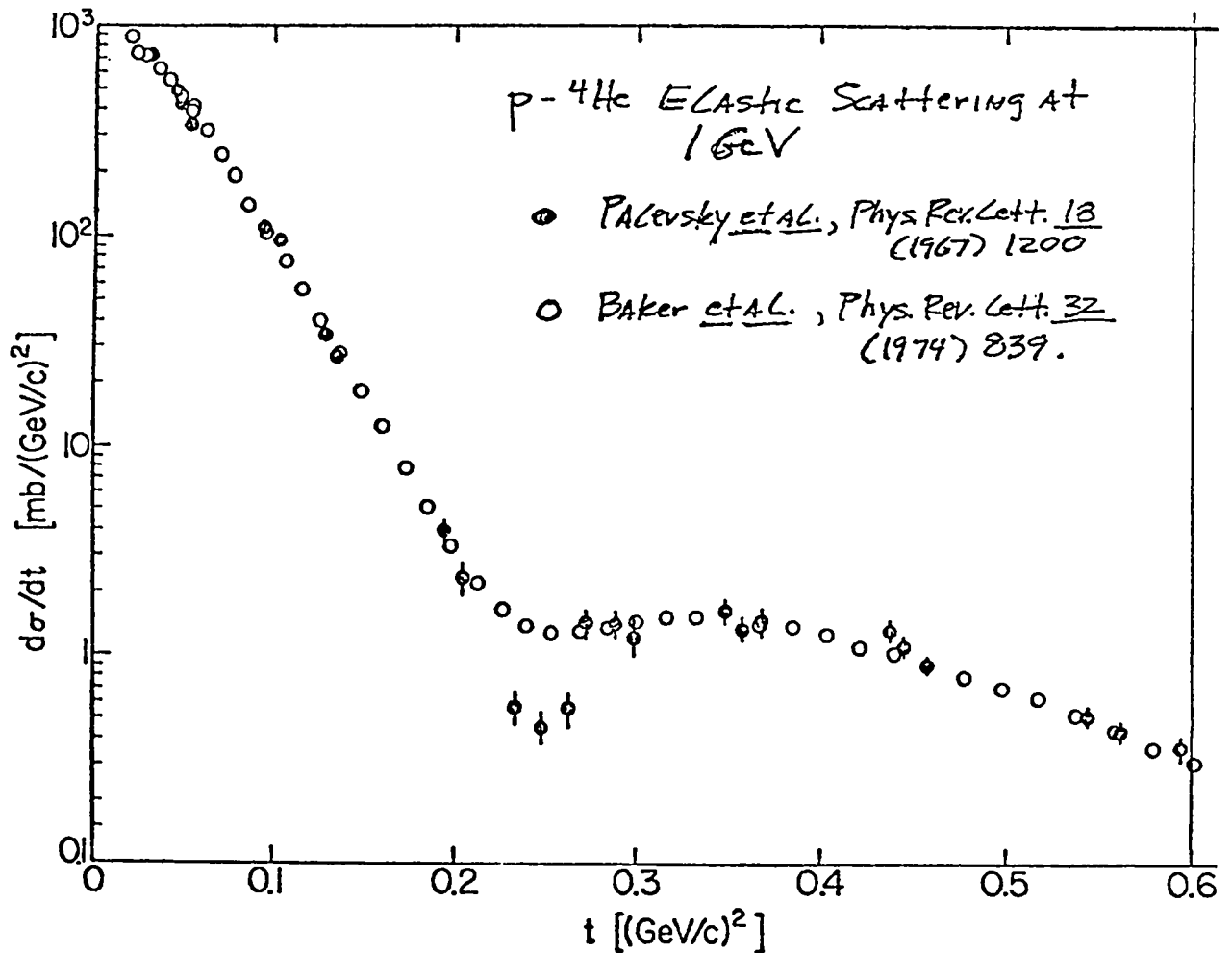
Fig. 4 - Comparison of data sets for p-^{4}He elastic scattering near 1 GeV.
The closed circles are the data of Palevsky et al (ref. 9) while
the open circles are the data of Baker et al (ref. 10). The two data
sets have been moved relative to one another by 0.5°, which is com-
parable to the combined angular error in the two data sets.

Table III. Experimental Work on p - ^{4}He Elastic Scattering
in the Interference Region Around - t $\cong$ 0.25 GeV^2/c^2

E_p(GeV)	Group
0.35, 0.65, 1.05, 1.15	SACLAY - Aslanides et al. Contribition to VI International Conference on High Energy Physics and Nuclear Structure, Santa Fe, New Mexico (1975).
0.59, 0.72	UCLA-LBL - Verbeck et al Phys. Lett. 59B, 339 (1975).
0.58	SREL - Boschitz et al Phys. Rev. C6, 457 (1972).
0.60	CERN - Fain et al Nucl. Phys. A262, 413 (1976).
0.80	UCLA-LAMPF - Exp. 4.
1.00	BNL - Palevsky et al Phys. Rev. Lett. 8, 1200 (1967).
1.05	UCLA-LBL - Geaga et al Phys. Rev. Lett. 38, 1265 (1977).
2.68	UCLA-LBL - Nasser et al preprint (to be published)
23.1	CERN - Berthot et al Contribution to VI International Conference on High Energy Physics and Nuclear Structure, Santa Fe, New Mexico (1975).
0.80	UCLA-LAMPF - Exp. 4.

$[d\sigma/dt] = [\pi/k^2][d\sigma/d\Omega_{cm}] = [\pi/k^2]|F_{00}(q)|^2$, $d\sigma/dt$ takes out the multiplier k in the nucleon-nucleus elastic scattering amplitude (see Eq. 2). Considerable structure is observed around the interference region. The different slope for the 350 MeV data is caused by the fact that the nucleon-nucleon slope parameter β^2 is much smaller at this energy than at the higher energies between 0.6 and 1.15 GeV. The slope of $d\sigma/dt$ before the first minimum is mainly determined by the nuclear form factor since $\frac{1}{\gamma^2} > 2\beta^2$ (see eq. 8). Fig. 6 presents the ratio $R = (d\sigma/dt)_{max}/(d\sigma/dt)_{min}$ and the location of $(d\sigma/dt)_{min}$ as a function p_{inc}(GeV/c). The maximum in R at ~ 1.3 GeV/c can be very qualitatively explained by the fact that α_{pp} is crossing zero in this region thus enhancing the interference between the single and double scattering terms. Auger, Lombard and Gillespie[3] have performed a systematic calculation of p-^{4}He elastic scattering in the range between 0.6 and 23.1 GeV. Their calculations included Coulomb effects and used spin-dependent (except at 23.1 GeV) nucleon-nucleon amplitudes of the type indicated in Eqs. 15 and 16. The parameters in these amplitudes were chosen to fit nucleon-nucleon scattering and polarization data where available. The nuclear one body density chosen, $\rho_p(r) = \rho_n(r)$, provided a reasonable fit to the measured ^{4}He charge form factor out to $q = 4.0$ fm. Fig. 7 presents their theoretical fits to the experimental angular distributions. The fit to the 23.1 GeV data is excellent while the fits to the 0.6 - 1.15 GeV data are qualitatively correct, but the minimum is predicted at too small a value of q and the R ratios are larger than those found experimentally. Fig. 8 presents a more complete picture of the theoretical calculation at 720 MeV. Inclusion of the spin term is very important in filling in the minimum region and Coulomb effects also play a role.

A recent paper by Wallace and Alexander[19] has considered the effect of Δ intermediate states in the context of the Glauber multiple scattering theory
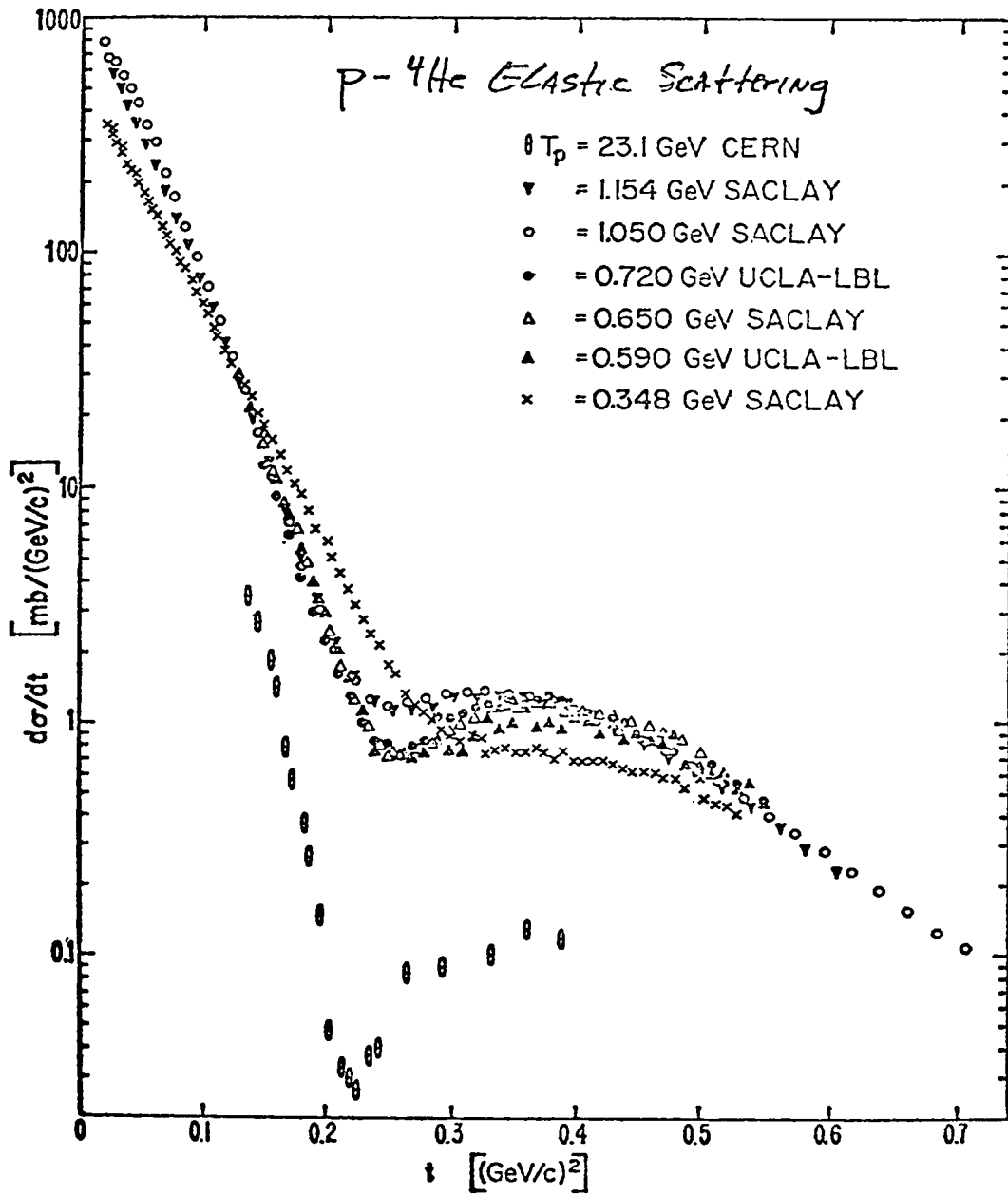
Fig. 5 - Data sets for p-^{4}He elastic scattering in the range of four momentum transfer, -t, from 0.02 to 0.7 GeV^2/c^2 and for incident proton energies between 0.348 and 23.1 GeV: θ - 23.1 GeV ref. 17, ▼ - 1.154 GeV ref. 11, 0 - 1.050 GeV ref. 11, ● - 0.720 GeV ref. 12, Δ - 0.650 GeV ref. 11, ▲ - 0.590 GeV ref. 12 and x - 0.348 GeV ref. 11.

Fig. 6.

Dependence of

$R = (d\sigma/dt)_{max}/(d\sigma/dt)_{min}$
and the position of the
minimum, t_{min}, as a
function of the incident
momentum in p-^{4}He elastic
scattering.

Fig. 7.

Comparison of the Glauber
calculations of Auger, Gillespie
and Lombard (ref. 3) which use
spin dependent nucleon-nucleon
amplitudes with experimental
data for p-^{4}He elastic scatter-
ing: a) 23.1 GeV ref. 17;
b) 1.15 GeV ref. 11; c) near
1 GeV ● ref. 9, ▲ ref. 10;
d) near 0.7 GeV O ref. 12,
■ ref. 43; e) near 0.6 GeV
● ref. 13, ▲ ref. 11, 0 ref. 12.
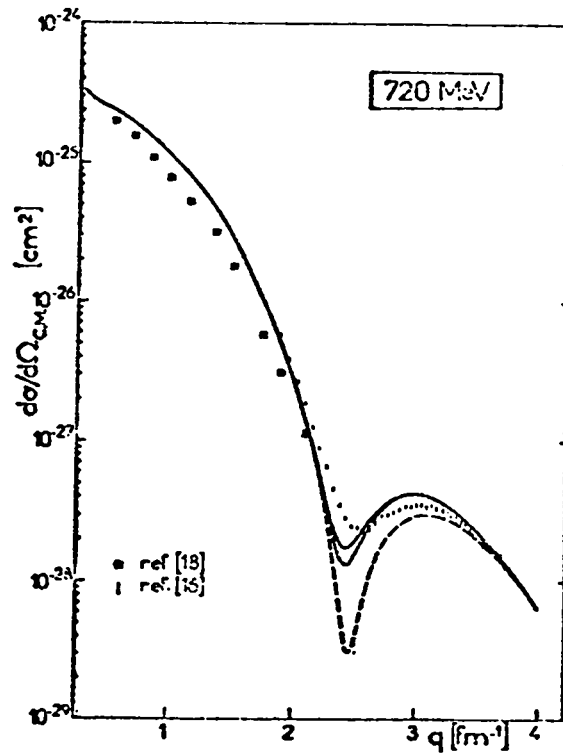
Fig. 8 - Comparison of the Glauber calculations of Auger, Gillespie and Lombard
(ref. 3) with the experimental data - ■ ref. 43, ♦ ref. 12 - for p-^{4}He
elastic scattering at 720 MeV. The solid line represents the full
calculation; the dashed curve represents the calculation with no
Coulomb interaction ans spin independent nucleon-nucleon amplitudes;
and the dotted curve represents the calculation with no Coulomb in-
teraction.

and included this effect in a calculation of p-^{4}He elastic scattering around
1 GeV. Here the incident proton becomes a Δ in one scattering $p+N\rightarrow\Delta+N$
and the Δ becomes a proton in a second scattering $\Delta+N\rightarrow p+N$. One reason
for investigating this process is that Δ production is known to be a large
part of the total proton-nucleon cross section around 1 GeV. In their calcula-
tion Wallace and Alexander use Glauber theory with a leading corrections forma-
lism[20] where eikonal, Fermi motion and kinematic corrections to the first order
Glauber theory are taken into account. In the nucleon-nucleon amplitudes only
the scalar (A) and spin flip (C) amplitudes (see eq. 14) were found to play an
important role. For single scattering the pp amplitude was taken directly
from phase shift analysis, while the pn amplitude was taken from a parameteri-
zation consistent with experimental scattering measurements:

$$A_{pn}(q^2) = \frac{ik_0\sigma_{pn}}{4\pi} \ (1 - i\alpha pn) \left[\frac{ae^{-cq^2} + be^{-dq^2}}{a+b}\right]^{\frac{1}{2}} \tag{23}$$

$$C_{pn}(q^2) = C_0 q \ e^{-C_1 q^2} \ e^{i\phi} \tag{24}$$

Here C_0, C_1 and ϕ were determined by a fit to new p-^{4}He polarization measure-
ments at 1.029 GeV[21]. The double and higher multiple scattering terms were
based on Gaussian approximations to the P-N amplitudes at small q^2 . Coulomb
effects were included and ^{4}He wave function was taken as the product of the
sum of Gaussian terms with the center-of-mass constraint. It provided a good
fit to the measured ^{4}He charge form factor. Including the spin and isospin
dependent Δ intermediate process the elastic scattering amplitude is then

$$|F|^2 = |F_0 + F_1 + F_\Delta|^2 + |G_0|^2 \tag{25}$$

where F_0 and G_0 are usual Glauber scalar and spin-flip amplitudes with

kinematic modifications in the single scattering term. F_1 is the leading order correction term[20] and F_Δ is the amplitude for the Δ intermediate process. Fig. 9 presents the fits of this calculation to five sets of p-^{4}He elastic scattering data around 1 GeV.[9],[10],[15],[21],[44] The Saclay A[10] and Saclay B[44] angular distributions represent the same run data with different normalizations. Recent results at LBL and ANL favor the Saclay A results. For the bottom curves the dashed curve is the Glauber plus leading corrections result $(|F|^2 = |F_0 + F_1|^2 + |G_0|^2)$ while the dot-dash curve is the Glauber result $(|F|^2 = |F_0|^2 + |G_0|^2)$. The Wallace and Alexander calculation provides a excellent fit to the recent p-^{4}He elastic scattering at 1 GeV in the interference region around $-t = 0.25(\text{GeV}^2/c^2)$. In particular the amplitude for the Δ intermediate process is of crucial importance in filling in the theoretical angular distribution in this region. Other calculations such as those of Auger et al[3] which do not include this process do not provide fits of comparable quality in the interference region. It would be most interesting to extend the Wallace and Alexander calculations to both the higher and lower energy p-^{4}He elastic scattering data, as a systematic test of the F_Δ contribution. A particularly good test would be provided by the 2.68 GeV data[15] whose $d\sigma/dt$ distribution is very similar to the Saclay A distribution at 1.05 GeV[2].

IV.   ELASTIC AND INELASTIC PROTON SCATTERING AT $\sim$ 1 GeV

A. Elastic Scattering

As an example of the type of nuclear structure information which may be obtained by elastic scattering data for $\sim$ 1 GeV protons on nuclei, several recent analysis[6],[22],[23] will be discussed which use this data to obtain nuclear neutron and mass distributions. Electron scattering experiments for $A \geqslant 12$ have indicated that the nuclear charge distribution, $\rho_c(r)$, is reasonably well represented by a Fermi function:
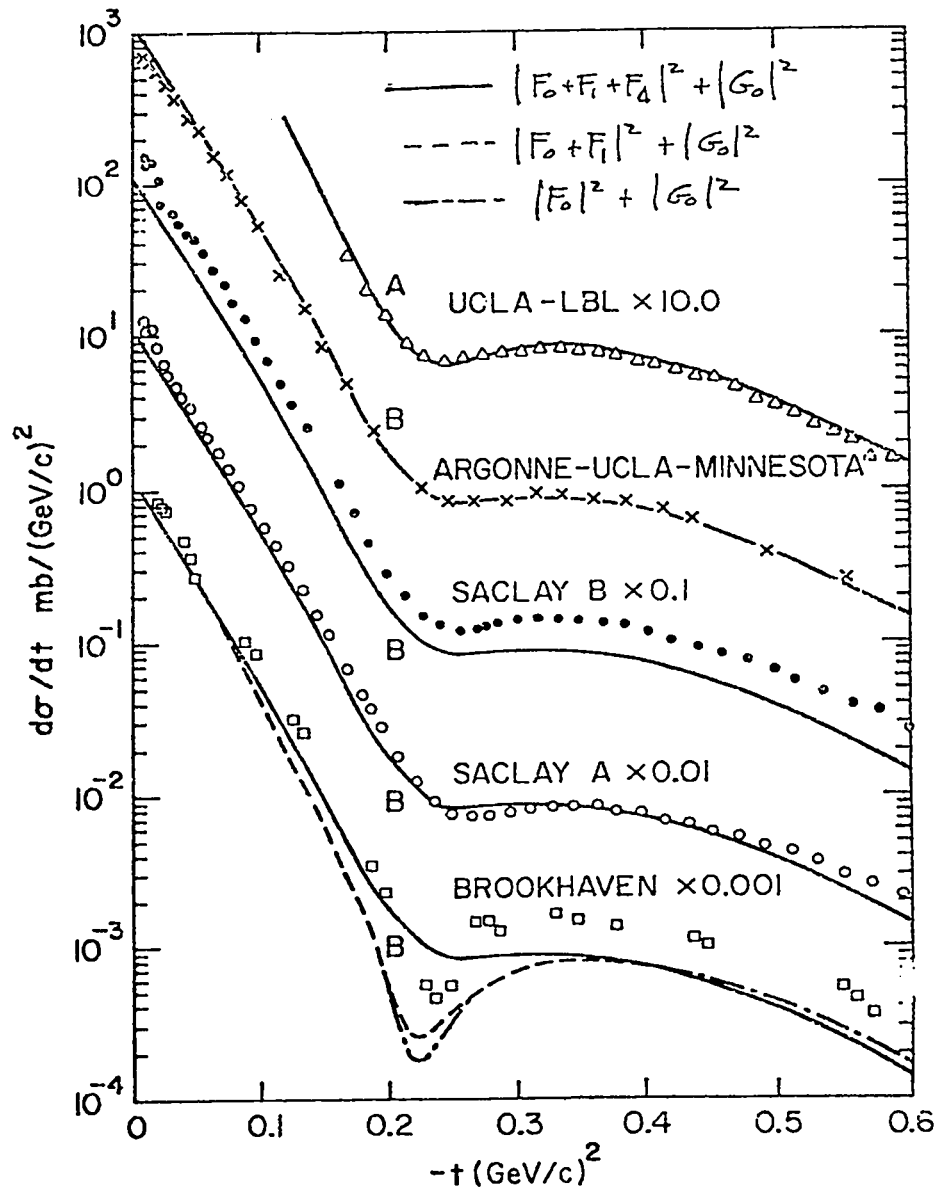
Fig. 9 - Comparison of the Wallace and Alexander Glauber calculation (ref. 19) which includes the Δ intermediate state process with experimental data for p-^{4}He scattering near 1 GeV: Δ ref. 15, x ref. 21, ● ref. 44, 0 ref. 10 and □ ref. 9.   The amplitudes F_0 and G_0 are the respective spin independent and spin dependent amplitudes in a first order Glauber calculation, F_1 is the amplitude representing corrections to the first order Glauber calculation (ref. 20), and F_Δ is the amplitude for the Δ intermediate state process.

$$\rho_c(r) = \rho_0[1 + \exp(\frac{r-R}{a_c}c)]^{-1}$$

where ρ_0 and a_c are nearly constant from nucleus to nucleus. In general the root-mean-square charge radius $< r^2 >_c^{\frac{1}{2}}$, $(< r^2 >_c^{\frac{1}{2}} \simeq \sqrt{\frac{3}{5}} R_c[1 + 7\pi^2/3(\frac{a_c}{R_c})^2]^{1/2}$ follows an $A^{1/3}$ law:

$$< r^2 >_c^{\frac{1}{2}} = r_{oc}A^{1/3} \tag{26}$$

where $r_{oc} = 1.02$ fm. However, some important exceptions have been found to Eq. 26. In the case of the Ca isotopes it has been found that $< r^2 >_c^{\frac{1}{2}}$ (^{48}Ca) is actually smaller than the $< r^2 >_c^{\frac{1}{2}}$ (^{40}Ca) by 0.015 fm (-0.5%) rather that being larger by 0.22 fm (+6.3%) as indicated by Eq. 26. Also, such results immediately raise the question of the behavior for the neutron distribution, $\bar{\rho}_n(r)$, (the bar represents the point neutron distribution $\rho_n(r)$ folded by the finite neutron size) and the nuclear matter distribution, $\bar{\rho}_M(r)$, where $(N + Z)\bar{\rho}_M(r) = Z\rho_c(r) + N\bar{\rho}_n(r)$. If one assumes that the matter distribution follows an $A^{1/3}$ rule then the neutron distribution in ^{48}Ca considerably exceeds the proton distribution:

$$\Delta_{48} = < \bar{r}^2 >_n^{\frac{1}{2}} - < r^2 >_c^{\frac{1}{2}} \cong 0.4 \text{ fm} . \tag{27}$$

Shell model calculations[26),27)] give values for Δ_{48} from 0.3 to 0.4 fm, but density dependent Hartree Fock calculations[28),29)] give values from 0.18 to 0.23 fm. In order to study these questions Alkhavoz et al[22)] measured the elastic scattering on $^{40,42,44,48}Ca$ of 1.044 GeV protons from the Saclay synchroton Saturne using the SPES-1 spectrometer facility[30)]. In their analysis of these data they used a Glauber calculation including the Coulomb interaction. The charge and neutron distributions were taken as parabolic Fermi distributions:

$$\rho_c(r) = C_c[1 + W_c(\frac{r}{R_c})^2][1 + \exp(\frac{r-R}{a_c}c)]^{-1} \tag{28}$$

$$\bar{\rho}_n(r) = C_n[1 + \bar{W}_n(\frac{r}{\bar{R}_n})^2][1 + \exp(\frac{r-\bar{R}_n}{\bar{a}_n})]^{-1} \tag{29}$$

where values of W_c, R_c and a_c were taken from electron scattering experiments at 250 MeV[25] while $\bar{W}_n$ was set equal to W_c; C_c and C_n are normalization constants. The proton-nucleon amplitudes $f_{pn}(q)$ were taken as spin independent and of the Gaussian form given by eq. 6. The parameters in these amplitudes were extracted from experimental data compilations. Thus the Glauber calculation has two free parameters $\bar{R}_n$ and $\bar{a}_n$, and their optimum values were obtained from a least squares fitting routine to the experimental data. Fig. 10 presents the Glauber fits to the experimental data for 1 GeV proton elastic scattering on ^{40,42,44,48}Ca. The dashed curves represent the calculated result when $\rho_c(r) = \bar{\rho}_n(r)$ while the solid curves represent the adjusted neutron distribution which gives the best fit to the experimental data. Fig. 11 presents the results of the Alkhavoz et al.[22] analysis in terms of $<r^2>_c^{\frac{1}{2}}$ (from ref. 25), $<\bar{r}^2>_n^{\frac{1}{2}}$ and $<\bar{r}^2>_m^{\frac{1}{2}}$ vs.A . Another Glauber analysis of the ^{40}Ca and ^{48}Ca data of Alkhavoz et al[22] has been reported by Varma and Zamick[23] where spin dependent proton-nucleon amplitudes were used. Fig. 12 presents their calculations where the solid curve represents the optimum fit to the ^{40}Ca and ^{48}Ca angular distributions. Another type of calculation has been reported by Ray and Coker[6], where proton-nucleus elastic scattering is calculated by solving the Schroedinger equation with relativistic kinematics using an optical potential derived using a "nuclear matter" approach. Fig. 13 presents their results for ^{40}Ca and ^{48}Ca. Table IV presents the $<r_n^2>^{\frac{1}{2}} - <r_p^2>^{\frac{1}{2}}$ results for the three analyses[6],[22],[23] and compares them with recent density dependent Hartree Fock (DDHF) calculations.[28],[29] The internal agreement of the three analyses is better than ±0.05 fm while the comparison with the DDHF calculations is quite good. Although more analyses must be performed on a larger set of medium energy proton elastic
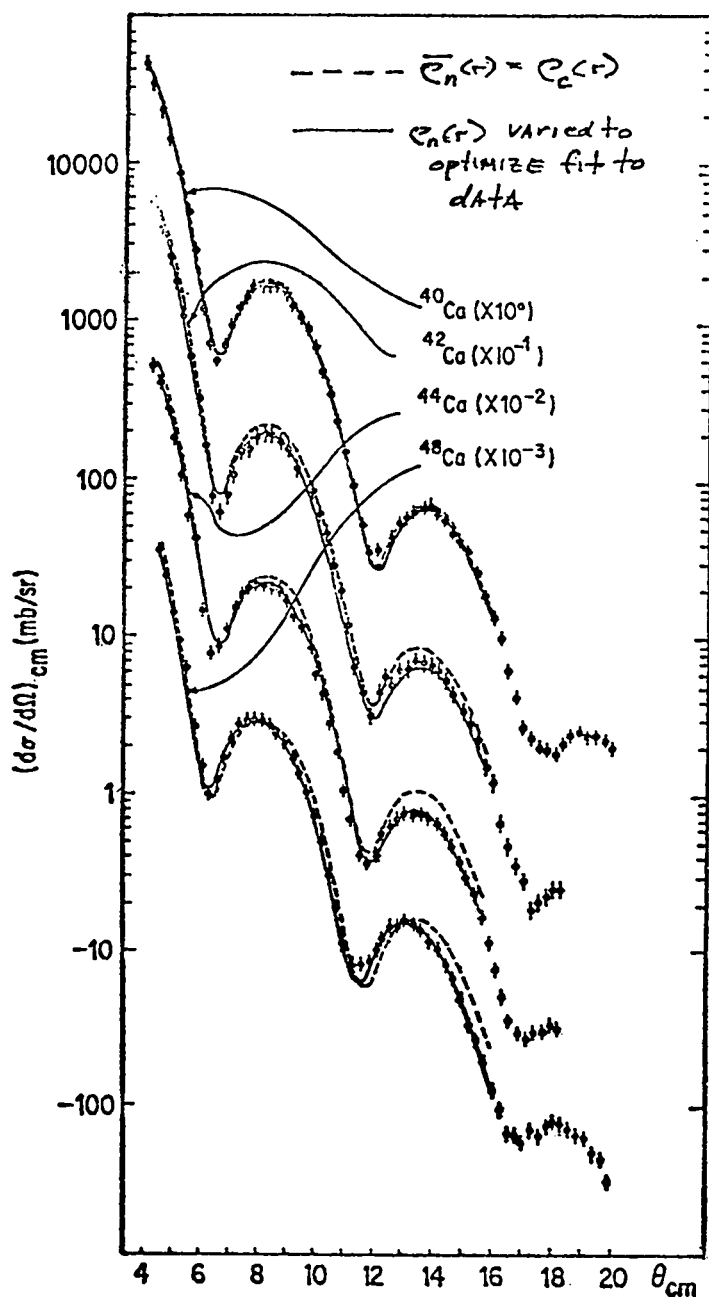
Fig. 10 - The proton elastic scattering data of Alkhazov et al (ref. 22) on
^{40,42,44,48}Ca at 1.044 GeV and their Glauber analysis of these data.
The dotted curves represent calculations where point neutron distribu-
tion folded by the finite neutron size, $\bar{\rho}_n(r)$, is set equal to $\rho_c(r)$.
The solid curves represent calculations where the parameters of $\bar{\rho}_n(r)$
are varied to optimize the fit to the experimental data.
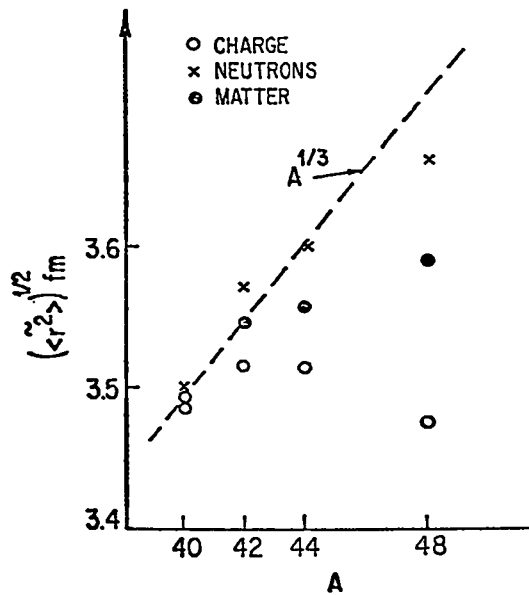
Fig. 11 - The values for $<\bar{r}^2>_n^{1/2}$ and $<\bar{r}^2>_m^{1/2}$ determined by the Alkhavoz et al (ref. 22) analysis of 1.044 GeV proton elastic scattering on $^{40,42,44,48}Ca$ plotted, versus A. The values for $<r^2>_c^{1/2}$ are taken from elastic electron scattering.

Fig. 12

Fits of the Glauber calculations by Varma and Zamick (ref. 23), which uses spin dependent nucleon-nucleon amplitudes, to the ^{40}C and ^{48}Ca 1.044 GeV proton elastic scattering data of Alkhavoz et al (ref. 22).
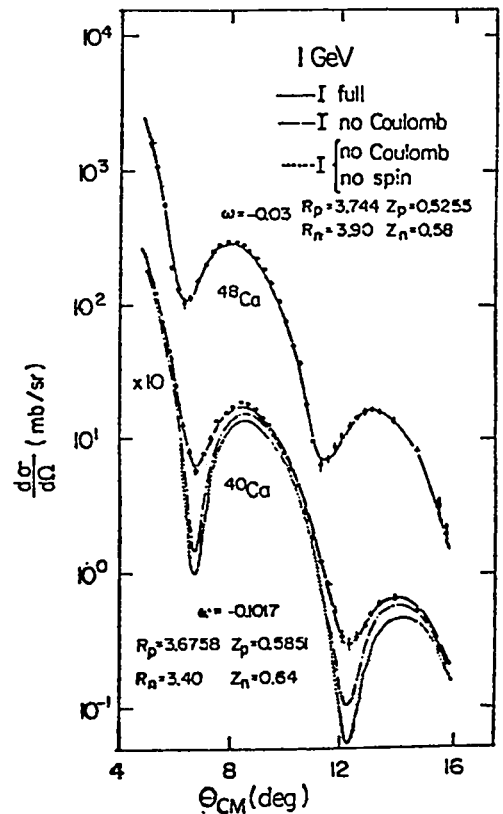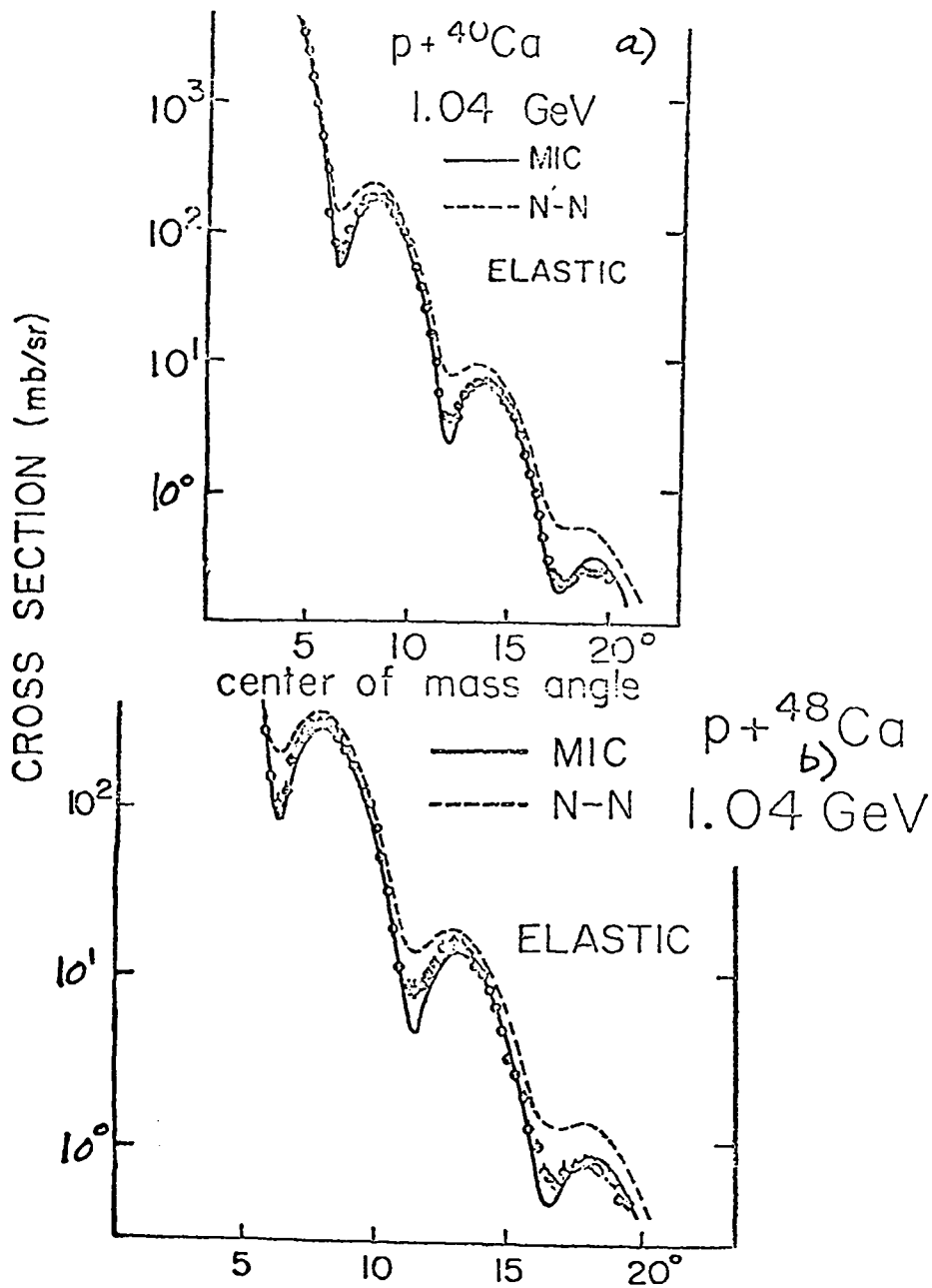
Fig. 13 - Fits of the calculations by Ray and Coker (ref. 6) to the ^{40}Ca and ^{48}Ca 1.044 GeV proton elastic scattering data of Alkhavoz et al ref. 22). In their calculations proton-nucleus elastic scattering is calculated by solving the Schroedinger equation with an optical potential and using relativistic kinematics. As is discussed in ref. 6 the solid curves (MIC) represent the results of these calculations using optical potentials derived in a "nuclear matter" approach developed by these authors, while the dashed curves (N-N) are calculated from optical potentials which are derived from an "impulse" approach.

- 183 -

Table IV. Nuclear Radii from the Analysis
of 1 GeV Proton Elastic Scattering Data

Nucleus	Analysis	$\langle r_n^2 \rangle^{\frac{1}{2}} - \langle r_p^2 \rangle^{\frac{1}{2}}$		
		from analysis of scattering data	from density dependent Hartree Fock calculations Negele[a]	Vautherin and Brink[b]
^{40}Ca	Alkhavoz et al.[c]	+0.014		
	Varma and Zamick[d]	-0.07	-0.04	-0.05
	Ray and Coker[e]	-0.026		
^{48}Ca	Alkhavoz et al.[c]	+0.185		
	Varma and Zamick[d]	+0.21	0.23	0.18
	Ray and Coker[e]	+0.171		

a) ref. 28
b) ref. 29
c) ref. 22
d) ref. 23
e) ref. 6

scattering data--which should be available in the near future--before the results as regards to the neutron and matter distributions can be regarded as definitive, proton-nucleus elastic scattering around 1 GeV holds great promise of providing reasonably accurate characterizations of these distributions.

B. Inelastic Scattering

In this paper I will briefly discuss the Glauber theory approach to proton inelastic scattering presented by Ahmad[31] which treats the initial and final state wave functions in terms of collective variables and calculates the angular distributions to one phonon levels. As at lower bombarding energies these are the states which are excited most strongly at medium energy. However, it should be mentioned that Glauber theory is rather easily developed for inelastic transitions to final states which differ from the initial state only by a simple particle transition. Examples would be the proton single particle states in ^{209}Bi, the neutron single hole states in ^{207}Pb, and the $4^-(g_{9/2} \, p_{1/2}^{-1})$ neutron particle-hole state in ^{208}Pb. The excitations of these levels would be interesting to study-- but quite difficult due to low cross sections--from a reaction mechanism and nuclear structure point of view.

Following Ahmad[31] we write the nuclear state ψ_i as:

$$\psi_i = \phi_0(\vec{r}_1, ---- \vec{r}_A) \, \psi_i^{coll} \tag{30}$$

where ϕ_0 and ψ_i^{coll} are the intrinsic and collective states of the target. Substituting in the general formula for Glauber scattering we obtain:

$$S_{f0} = \langle \psi_f^{coll} | e^{i\hat{\chi}(\vec{b})} | \psi_i^{coll} \rangle \tag{31}$$

$$e^{i\hat{\chi}(\vec{b})} = \langle \phi_0 | \prod_{j=1}^{A} [1 - \Gamma(\vec{b}-s_j)] | \phi_0 \rangle \tag{32}$$

where we may expand $\hat{\chi}(\vec{b})$ as previously in eqs. 10, 11 and 12.

$$\hat{\chi}(\vec{b}) = \hat{\chi}_0(\vec{b}) + \hat{\chi}_1(\vec{b}) + \text{----} \tag{33}$$

and

$$\hat{\chi}_0(\vec{b}) = iA \int \Gamma(\vec{b}-\vec{s})\hat{\rho}(r)d\vec{r} \tag{34}$$

$$\hat{\chi}_1(\vec{b}) = -\frac{1}{2} iA \int [(A-1)\hat{\rho}_2(\vec{r}_1,\vec{r}_2) - A\hat{\rho}(\vec{r}_1)\hat{\rho}(\vec{r}_2)]\Gamma(\vec{b}-\vec{s}_1)\Gamma(\vec{b}-\vec{s}_2)d\vec{r}_1 d\vec{r}_2 \tag{35}$$

Here we have assumed equal nucleon amplitudes and density distributions for neutrons and protons. Now the Tassie hydrodynamical operator is assumed:

$$\hat{\rho}(\vec{r}) = \rho_0(\vec{r}) + \sum_{LM} \rho_L(r) [b_{LM}Y_{LM}(\Omega) + b_{LM}^+ Y_{LM}^*(\Omega)] \tag{36}$$

where b_{LM} and b_{LM}^+ are one phonon creation and destruction operators respectively. Also the transition density $\rho_L(r)$ is given by:

$$\rho_L(r) = N_L \, r^{L-1} \frac{d\rho_0}{dr} \tag{37}$$

where N_L is the transition strength parameter. Now the phonon operators provide a coupling between the target ground state and the one phonon collective states, so that we obtain a result for the excitation of the one phonon state, L_f , (after considerable manipulation!):

$$\left(\frac{d\sigma}{d\Omega}\right)_{L_f} = \sum_{\substack{M_f = -L_f \\ L_f + M_f \text{ even}}}^{M_f = L_f} \left| k \int_0^\infty dbb \, J_{M_f}(qb) \, g_{L_f M_f}(b) \, \exp[i\chi_N(b)] \right|^2 \tag{38}$$

The $g_{LM}(b)$ is proportional to an integral over the nucleon-nucleon amplitude

f(q) and the transition form factor, $S_L(q)$, for the transition density $\rho_L(r)$

$$g_{LM}(b) \sim \int_0^\infty dq[q \ f(q) S_L(q) \ J_M(qb)] \tag{39}$$

$$\chi_N(b) = \chi_{00}(b) + \frac{1}{2} i \sum_{LM} g^2_{LM}(b) \tag{40}$$

where $\chi_{00}(b)$ is the function previously defined in our discussion of elastic scattering (eq. 11). With this formalism Ahmad[31] proceeds to fit inelastic proton scattering angular distributions at 1.04 GeV obtained by the Saclay group[35] at the SPES-1 spectrometer facility. In particular Ahmad uses transition densities related as closely as possible to these obtained in inelastic electron scattering. His results for the excitation of the 1.45 MeV 2^+ level in ^{58}Ni are shown in Fig. 14. Here Ahmad uses the same transition density as that obtained in inelastic electron scattering[36] where the simple Tassie form (eq. 37)--with $\rho_0(r) = \rho_c(r)$ --was found to fit the experimental data. The fit to the experimental data is reasonably good as regards to the positions and relative ratios of the maxima but the theoretical minima are quite a bit deeper than the experimental data. In the inelastic excitation of the 2.62 MeV 3^- level in ^{208}Pb Heisenberg and Sick[37] have found that the transition density obtained from the parameters of the ground state charge distribution do not fit the data very well, particularly at large q^2. Ahmad has used the transition density parameters obtained by Heisenberg and Sick[37] and has assumed the same form for neutrons and protons. His fit to the data is shown by the dashed curve in fig. 15a. The strength of the transition was set by value of the first maximum in the angular distribution and corresponds to a B(E3) value of 0.50 b^3. This is somewhat smaller than the B(E3) values obtained by inelastic electron scattering: $0.72 \pm 0.04 b^3$ Ziegler and Peterson[38],

$$\rho_2 = N_2 \, r^{-1} \, \frac{d\,\rho_c(r)}{d\,r}$$
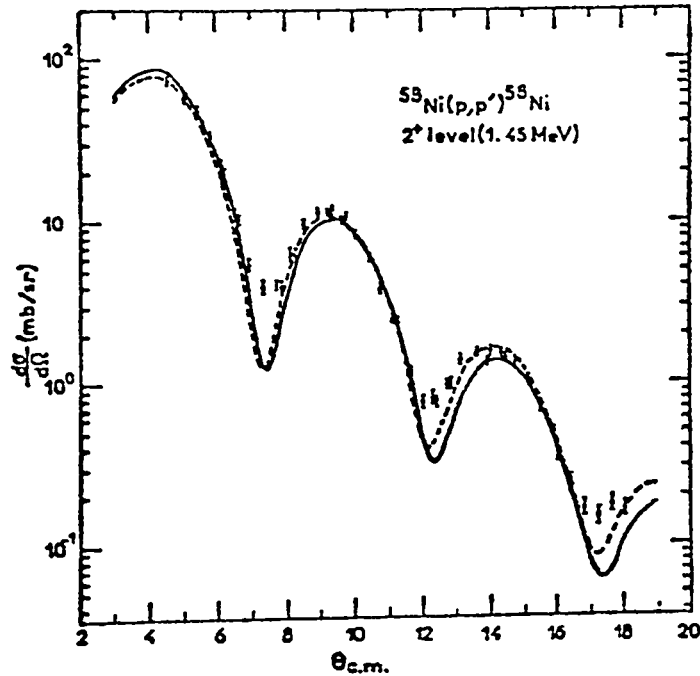
Fig. 14 - Theoretical fits by Ahmad (ref. 31) for the 1 GeV proton inelastic scattering data to the 1.45 MeV 2^+ state in ^{58}Ni (ref. 35). In his calculations Ahmad uses a transition density derived from inelastic scattering. The dotted curve represents a calculation which includes coupling to other inelastic states and an approximate two-body correlation effect, the solid curve represents a calculation which does not include these effects.

$0.624 \pm 0.024b^3$ Friedrich[39]; but close to the $B(E3)$ value of $0.58 \pm 0.04b^3$ determined by (α,α') experiments.[40] As is mentioned by Ahmad[31] some of the discrepancy here may be due to the fact that low q electron scattering experiments only determine the reduced transition probability in a model independent way when the Plane-wave-Born-approximation can be used; and this is not the case for heavy nuclei. The solid curve in fig. 15a represents a slightly better fit obtained with larger values of the parameters in the transition density. Fig. 15b shows the effect of Coulomb scattering in dampening the minima.

For the case of the inelastic proton scattering at 1.04 GeV to the 4.43 MeV 2^+ and 9.64 MeV 3^- levels in ^{12}C, Ahmad used inelastic charge form factors, $S_L(q)$, derived from inelastic electron scattering by Saudinos and Wilkin[32]:

$$S_L(q) = B_L q^L (1 - C_L q^2) \, e^{-\beta_L q^2} \qquad (41)$$

where $B_2 = 0.24$ fm^2, $C_2 = 0.13$ fm^2, $\beta_2 = 0.63$ fm^2 for the 2^+ level; and $B_3 = 0.134$ fm^3, $C_3 = 0.0$ fm^2, $\beta_3 = 0.77$ fm^2 for the 3^- level. The fits to the experimental data using these form factors are shown by the dotted and dashed curves in Figs. 16a and b respectively. For the 2^+ level the height of the first maxiumum and the relative height of the second maximum are reproduced by the data. (The position of the second maximum corresponds to a q^2 of about 7 fm^{-2}.) However the situation for the 3^- level is much worse. The height of the first maximum is over estimated in the calculation by about a factor of two; and a minimum is predicted which is not observed in the experimental data. If the theoretical curve is arbitrarily normalized to the experimental data (dashed curve in fig. 16b) the fit is reasonable out to $\theta_{cm} \approx 16°(q^2 \cong 4.4f^{-2})$. However, the discrepancies in the calculation for the excitation of the 3^- level are major; and the reason for them is not understood.
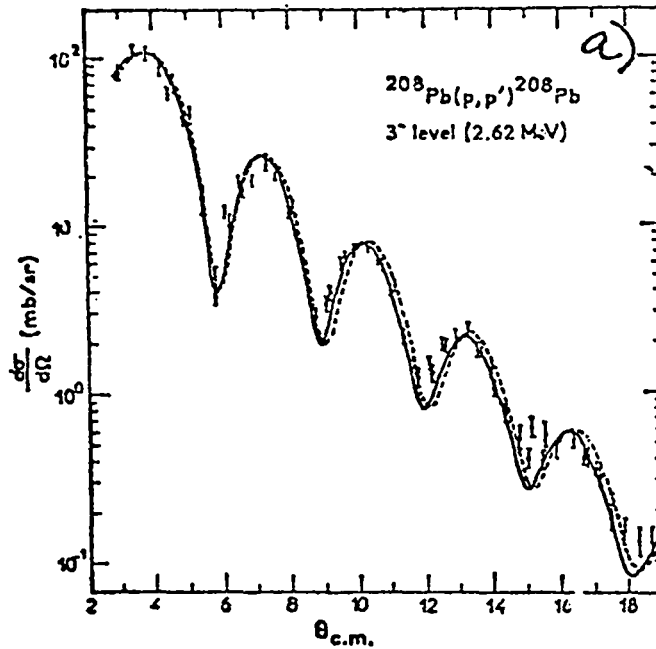
W_c=0.32; R_c=6.40 fm; a_c=0.54 fm

- - - W_{+r} = 0; R_{+r} = 6.414 fm; a_c = 0.56 fm.

-----W_{+r} = 0; R_{+r} = 6.55 fm; a_c = 0.58 fm.

Fig. 15 - a) Theoretical fits by Ahmad (ref. 31) for the 1 GeV proton inelastic
scattering data to the 2.62 MeV 3⁻ level in [208]Pb. The dashed curve
represents a calculation which uses the transition density of Heisenberg
and Sick (ref. 37) derived from inelastic electron scattering while
in the calculation represented by the solid curve the parameters of
this transition density are varied to obtain a slightly better fit
to the experimental data.
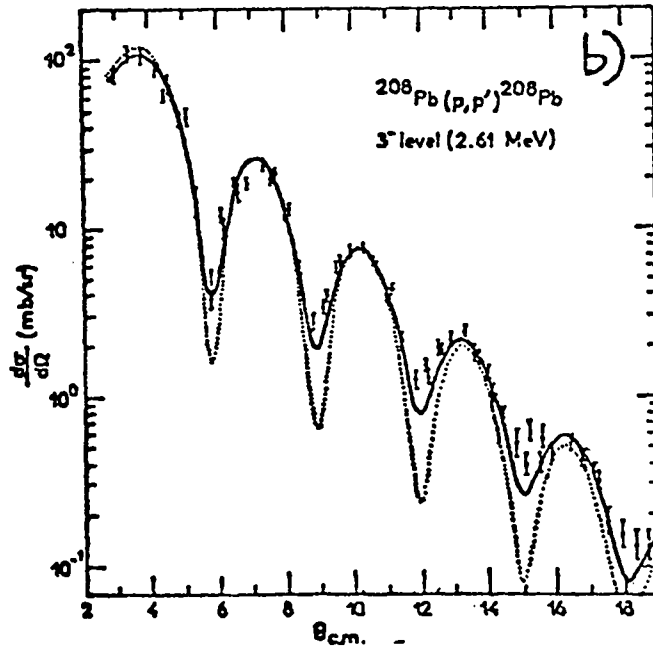
Fig. 15 - b) The solid curve represents the same calculation as in a) while
the dotted curve represents a calculation where the Coulomb interaction
was neglected. The B(E3) value for the 3⁻ transition derived from the
(p,p') scattering at 1 GeV is compared with B(E3) values derived from
inelastic electron scattering and from inelastic alpha scattering.

B(E3)

0.50 b^3 Ahmad analysis

0.72 ± 0.04 b^3 Ziegler and Peterson
        Phys. Rev. 165 (1968) 1337.   inelastic
                                     electron

0.624 ± 0.024 b^3 Friedrich, Nucl. Phys. A191   scattering
        (1972) 118

0.58 ± 0.04 Barnett and Philips
        Phys. Rev. 186 (1969) 1205.   (α,α')
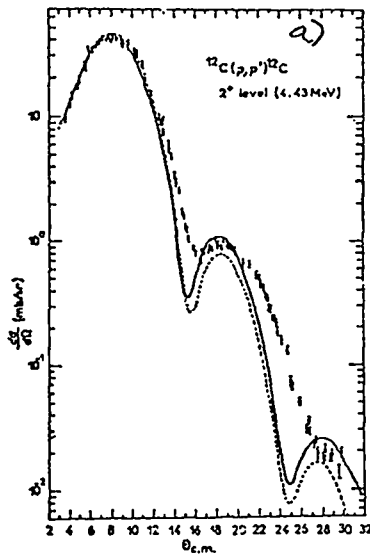
Fig. 16 - a) Theoretical fits by Ahmad (ref. 31) for the 1 GeV proton inelastic scattering data to the 4.43 MeV 2^+ level in ^{12}C. In his calculations Ahmad uses a transition form factor derived from inelastic electron scattering by Saudinos and Wilkin (ref. 32). The solid curve represents a calculation which includes coupling to other excited states and an approximate two-body correlation effect, the dashed curve represents a calculation which does not include these effects.
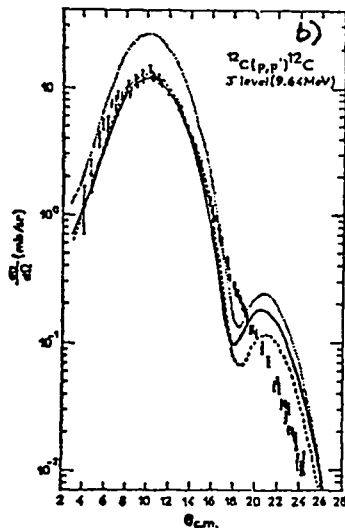
b) Theoretical fits by Ahmad (ref. 31) for the 1 GeV proton inelastic scattering data to the 9.64 MeV 3^- level in ^{12}C. The transition form factor used in these calculations is derived from inelastic electron scattering by Saudinos and Wilkin (ref. 32). The dotted curve represents a calculation which did not include coupling and two-body correlation effects, while the dashed curve is the dotted curve normalized to the experimental maximum in the data and the solid curve includes these two effects and is normalized to the experimental maximum.

Some points about inelastic proton scattering at energies around ~ 1 GeV not treated in the above discussion should be mentioned. One, the very large angular momentum brought into the nucleus by the incident wave (kR ≈ 30 ℏ at the nuclear surface) should allow the excitation of high spin collective levels difficult to excite at lower energies. Two, facilities such as HRS are able to measure the inelastic angular distributions out to quite large momentum transfer $q^2 \approx$ 1-1.5 GeV^2/c^2 or about 25-36 fm^{-2} with reasonable ease for the strong collective transitions. This may provide a good probe of the transition density form factors at much larger q^2 than can be easily studied in inelastic electron scattering.

I will now present some examples of the data which has been taken at the HRS facility. These data have just been analyzed and should be considered preliminary. Fig. 17 presents angular distributions for 790 MeV proton scattering to the 0^+ ground state and 4.44 MeV 2^+ level in ^{12}C. These angular distributions have been measured out to a q of about 4 fm^{-1}. Fig. 18 presents 800 MeV proton elastic scattering angular distributions on the even nickel isotopes ^{58}Ni, ^{60}Ni, ^{62}Ni and ^{64}Ni. The small but definite changes in the shapes of these angular distributions as a function of the neutron number should permit a study of the neutron distributions as was discussed with respect to the calcium isotopes. Fig. 19 presents angular distributions for 790 MeV proton scattering to the 0^+ ground state and 2.615 MeV 3^- level in ^{208}Pb. Note that the Blair phase rule holds quite well for these transitions.
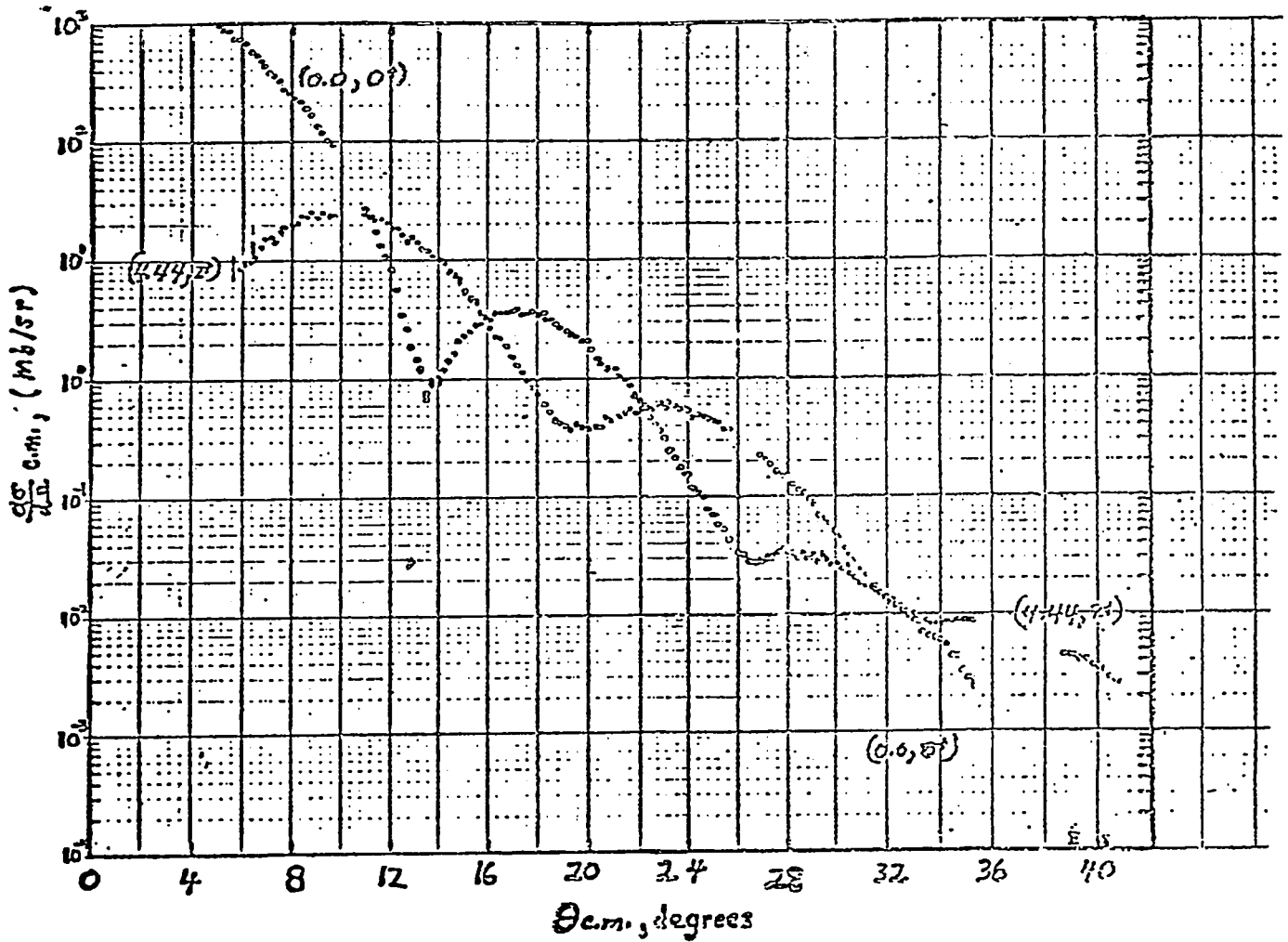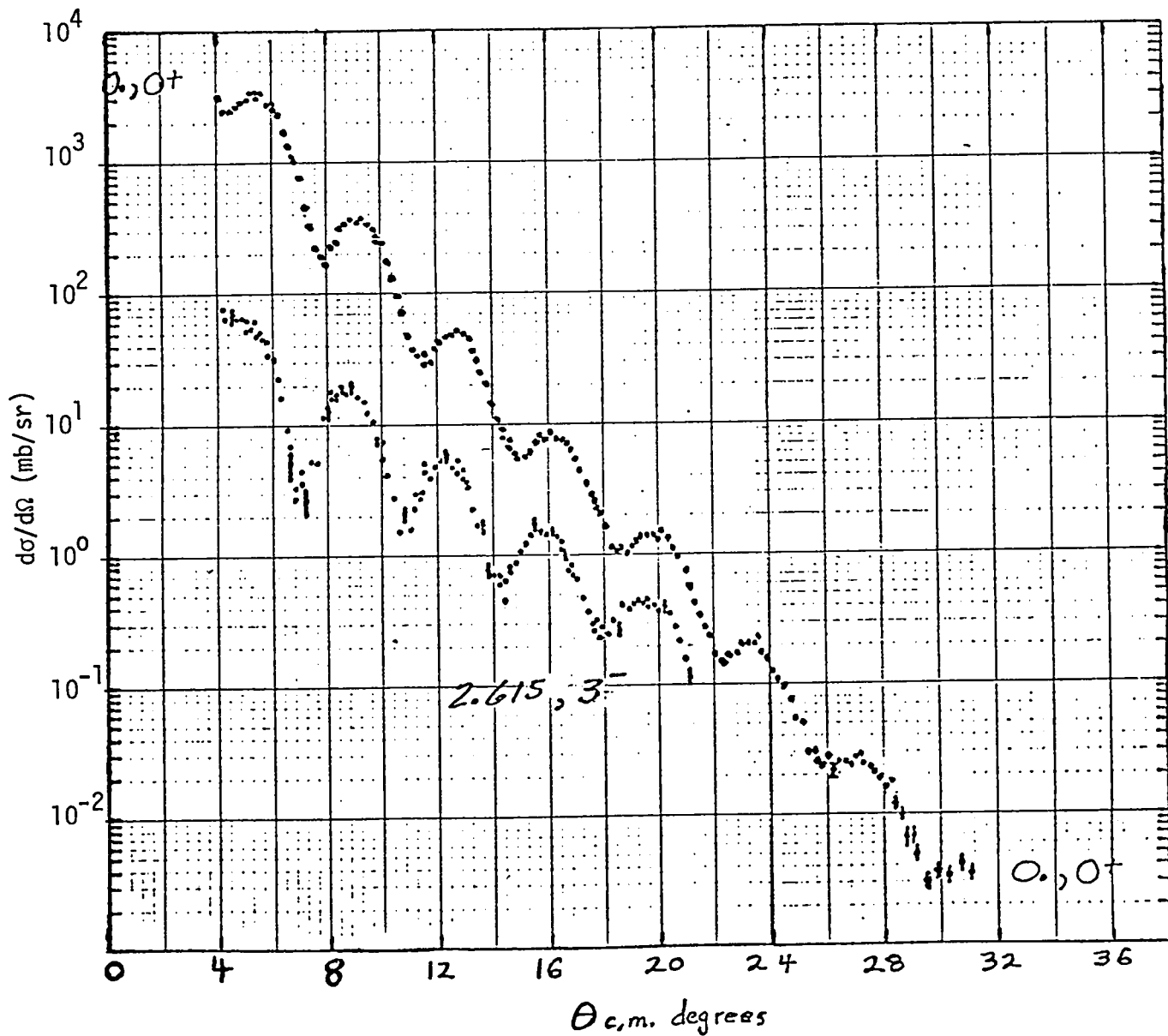
Fig. 17 - Angular distributions for 790 MeV proton scattering to the 0^+ ground
state and 4.44 MeV 2^+ level in ^{12}C. These are preliminary data from
the HRS facility courtesy of G. Blanpied.
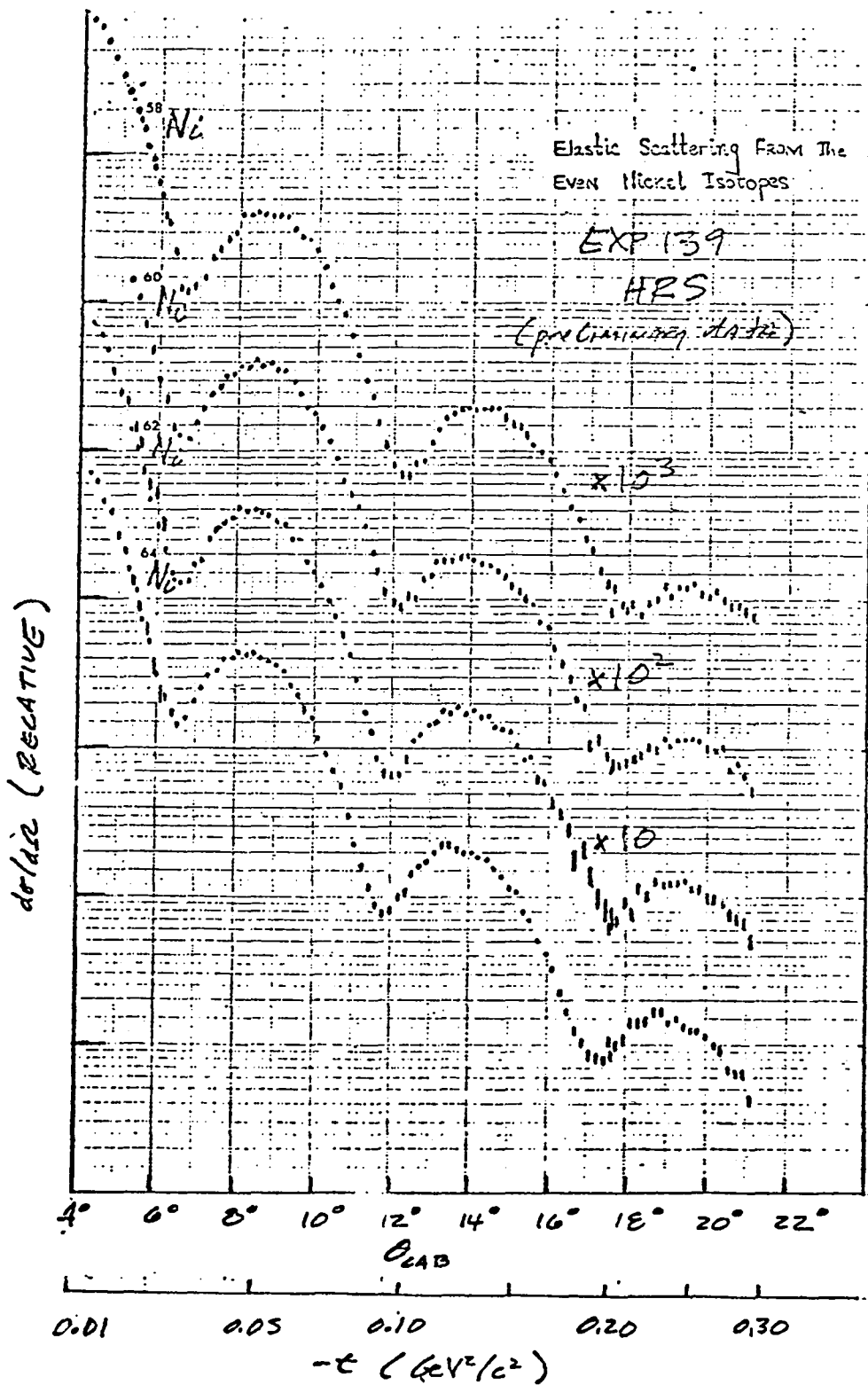
Fig. 18 - Angular distributions for 800 MeV elastic proton scattering on the even nickel isotopes 58Ni, 60Ni, 62Ni and 64Ni. These are preliminary data from the HRS facility courtesy of J. Spencer.

Fig. 19 - Angular distributions for 790 MeV proton scattering to the 0^+ ground state and 2.615 MeV 3^- level in ^{208}Pb. These are preliminary data from the HRS facility courtesy of G. Blanpied.

V. POLARIZATIONS STUDIES

Very few asymmetry measurements exist for polarized proton scattering on nuclei; at intermediate energies. Recently an Argonne-Minnesota-UCLA collaboration[21] has reported on polarization in p-^{4}He elastic scattering at 0.56, 0.80, 1.03, 1.27 and 1.73 GeV over a range of -t from 0 to 1.0 GeV^2/c^2. Fig. 20 presents their data. Considerable structure is observed in the polarization, P(-t), as a function of the incident proton energy. Last week at the LAMPF polarization Summer Study Session, Steve Young presented theoretical work by himself and C. W. Wong[41] which attempted to fit these data using a Glauber formalism. Also, Wallace and Alexander[19] present an excellent fit to the 1.03 GeV p-^{4}He polarization data[21] using their Glauber formalism which includes the Δ-intermediate state process.

In this section I would just like to point out the importance of polarization studies for the general study of proton elastic scattering at intermediate energies. The points to be emphasized are that spin effects must be understood before elastic scattering can be understood and that systematic studies of the polarization in elastic scattering are of utmost importance for this end. To give concrete examples to these points I would like to present some work by Ray and Coker[6] who looked at the dependence of elastic scattering angular distributions and polarizations on "reasonable" forms for the spin-orbit potential in a nucleon-nucleus optical model potential. They utilize three forms for the spin-orbit potential. The first is derived from the work of Blin-Stoyle,[42] the second is derived from the work of Kujawski and Vary,[5] while the third is derived from the form of the spin-orbit potential in the Dirac equation and called the Pauli-Dirac potential. The Blin-Stoyle and Pauli-Dirac spin-orbit potentials are taken to have only a real part while the Kujawski-Vary potential has both real and imaginary parts. In the Blin-Stoyle potential the strength

Handwritten annotations:
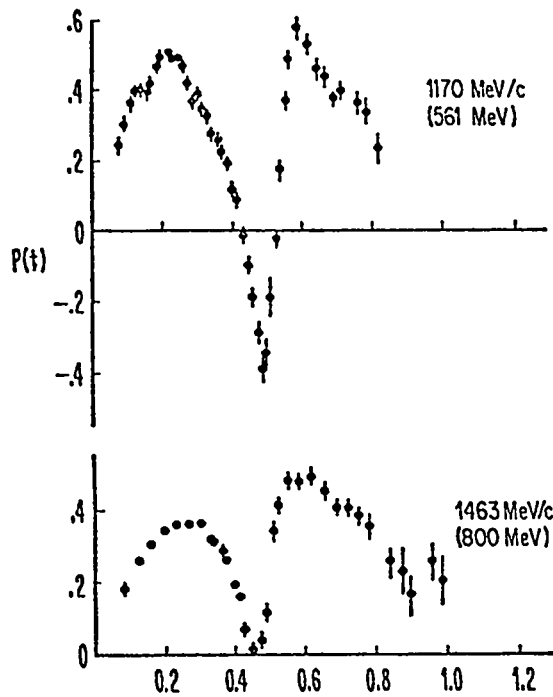
POLARIZATION

IN p-⁴He ELASTIC

SCATTERING

ARGONNE-MINNESOTA-UCLA
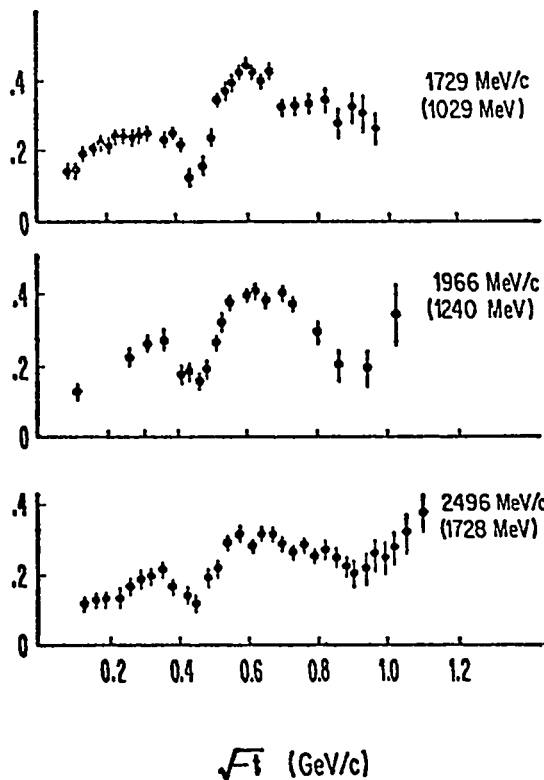COLLABORATION

KLEM ET AL. PHYS. REV. LETT.
38 (1977) 1272

Fig. 20 - Energy dependence of the polarization in p-⁴He elastic scattering for incident proton energies between 0.56 and 1.73 GeV, as measured by Klem et al ref. 21.

is adjusted to give magnitude agreement with the average of the other two forms of the spin-orbit term. Fig. 21 presents the proton elastic scattering on ^{40}Ca calculated with the three forms of the spin-orbit potential while Fig. 22 presents the polarization in ^{40}Ca proton elastic scattering calculated with these potentials. The correctness of any given calculation is not the point we want to emphasize here; rather we want to show both the sensitivity of elastic angular distributions to spin effects and the fact that different parameterizations of the spin effects give quite different results for the polarization in proton-nucleus elastic scattering.

To end this paper on a happy--and I believe exciting--note Fig. 23 presents polarization data for proton - ^{208}Pb elastic scattering at 800 MeV obtained in Exp. 311 at HRS. Similar polarization data has also been obtained on ^{12,13}C and ^{58,64}Ni targets. The structure shown by these data should be severe constraints on the parametrization of spin effects in the mechanism for proton-nucleus elastic scattering at intermediate energies; and similar asymmetry studies for proton inelastic scattering should deepen our understanding of the reaction mechanism and nuclear structure effects involved in those transitions.
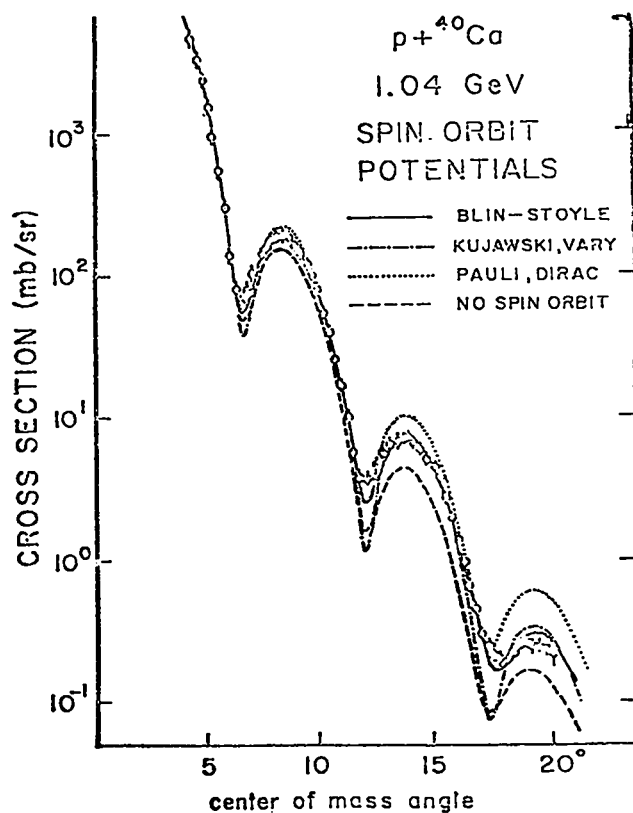
Fig. 21 - The effect of various prescriptions for the spin-orbit potential on the angular distribution for 1 GeV proton elastic scattering on ^{40}Ca as calculated by Ray and Coker (ref. 6).
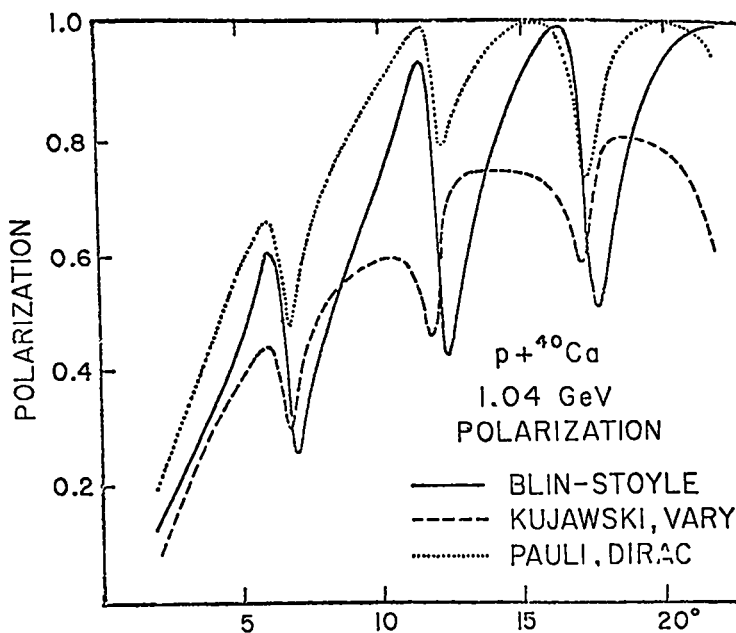
Fig. 22 - The effect of various prescriptions for the spin-orbit potential on the polarization in 1 GeV proton elastic scattering on ^{40}Ca as calculated by Ray and Coker (ref. 6).
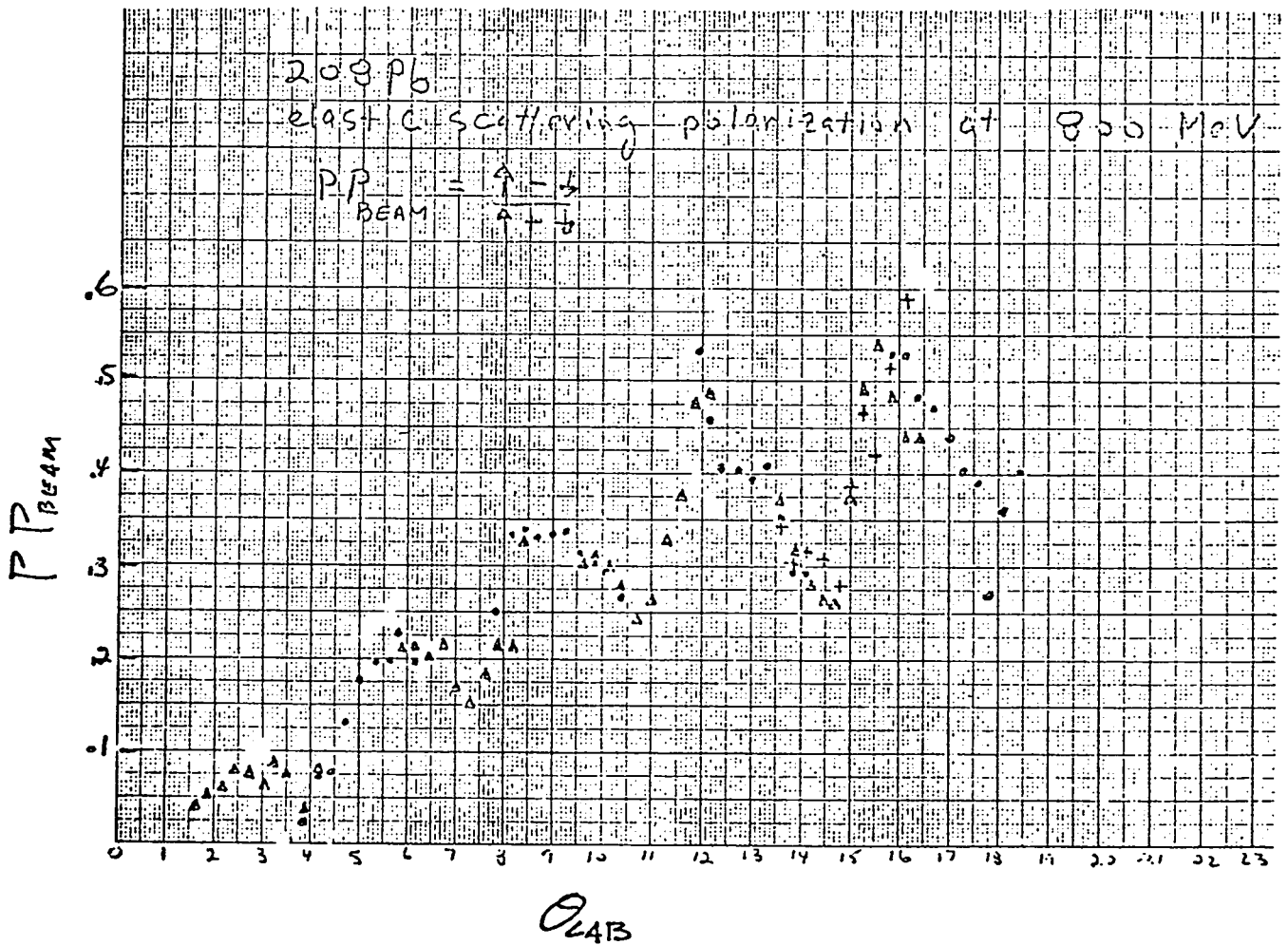
Fig. 23 - PP_{BEAM} measured for 800 MeV proton elastic scattering on ^{208}Pb. The beam polarization, P_{BEAM}, is believed to be 80%. These are preliminary data from the HRS facility courtesy of G. Hoffmann.

REFERENCES

1) R. J. Glauber, <u>Lectures in Theoretical Physics</u>, Boulder, 1958, ad. W. E. Brittin, vol. 1 (Interscience Publishers, New York, 1959) p. 315.

2) W. Cysz, and L. Lesniak, Phys. Lett. <u>24B</u>, 227 (1967); W. Cysz, in <u>High Energy Physics and Nuclear Structure</u>, edited by G. Alexander (North-Holland Publishing Co., Amsterdam, 1967).

3) J. P. Auger, J. Gillespie and R. J. Lombard, Nucl. Phys. <u>A262</u>, 372 (1976).

4) R. J. Glauber and G. Matthiae, Nucl. Phys. <u>B21</u>, 135 (1970).

5) E. Kujawski and J. P. Vary, Phys. Rev. <u>C12</u>, 1271 (1975).

6) L. Ray and W. R. Coker, 1 GeV Proton-Nucleus Scattering in a "Nucleon Matter" Approach (preprint).

7) R. J. Glauber and V. Franco, Phys. Rev. <u>142</u>, 1195 (1966).

8) E. Kujawski, Phys. Rev. <u>C1</u>, 1651 (1970).

9) H. Palevsky, J. L. Friedes, R. J. Sutter, G. W. Bennett, G. J. Igo, W. D. Simpson, G. C. Phillips, D. M. Corley, N. S. Wall, R. L. Stearns, and B. Gottschalk, Phys. Rev. Lett. <u>18</u>, 1200 (1967).

10) S. D. Baker, R. Beurtey, C. Bruge, A. Chaumeaux, J. M. Durand, J. C. Faivre, J. M. Fontaine, D. Garreta, D. Legrand, J. Saudinos, J. Thirion, R. Bertini, F. Brochard, and F. Hibou, Phys. Rev. Lett. <u>32</u>, 839 (1974).

11) E. Aslanides, T. Bauer, R. Bertini, R. Beurtey, A. Boudand, F. Brochard, G. Bruge, A. Chaumeaux, H. Catz, J. M. Fontaine, R. Frascavia, P. Gorodetzky, J. Guyor, F. Hibou, M. Matoba, Y. Terrien and J. Thirion, Contributions to the VI International Conference on High Energy Physics and Nuclear Structure, Santa Fe, New Mexico, June 9-14 (1975).

12) S. L. Verbeck, J. C. Fong, G. Igo, C. A. Whitten Jr., D. L. Hendrie, Y. Terrien, V. Perez-Mendez, and G. W. Hoffman, Phys. Lett. <u>59B</u>, 339 (1975).

13) E. T. Boschitz, W. K. Roberts, J. S. Vincent, M. Blecher, K. Gotow, P. C. Gugelot, C. F. Perdrisat, L. W. Swenson and J. R. Priest, Phys. Rev. <u>C6</u>, 457 (1972).

14) J. Fain, J. Gardes, A. LeFort, L. Meritet, J. F. Pauty, G. Peynet, M. Querrou, F. Vazeille, and B. Ille, Nucl. Phys. <u>A262</u>, 413 (1976).

15) J. V. Geaga, M. M. Gazzaly, G. J. Igo, J. B. McClelland, M. A. Nasser, A. Sagle, H. Spinka, J. B. Carroll, V. Perez-Mendez, and E. T. B. Whipple, Phys. Rev.

Lett. <u>38</u>, 1265 (1977).

16) M. A. Nasser, M. M. Gazzaly, J. Y. Geaga, B. Hoistad, G. Igo, J. B. McClelland, A. L. Sagle, H. Spinka, J. B. Carroll, V. Perez-Mendez, and E. T. B. Whipple, preprint 1977, submitted to Phys. Lett.

17) I. Berthot, G. Douhet, J. Gardes, L. Meritet, M. Querrou, A. Tetefort, F. Vazeille, J. P. Burg, M. Chemarin, M. Chevallier, B. Ille, M. Lambert, J. P. Marin, J. P. Gerber and C. Voltolini, Contributions to the VI International Conference on High Energy Physics and Nuclear Structure, Santa Fe, New Mexico, June 9-14 (1975).

18) R. F. Frosch, J. S. McCarthy, R. E. Rand and M. R. Yearian, Phys. Rev. <u>160</u>, 874 (1967).

19) S. J. Wallace and Y. Alexander, Phys. Rev. Lett. <u>38</u>, 1269 (1977).

20) S. J. Wallace, Phys. Rev. <u>C12</u>, 179 (1975); a related approach is reported by C. W. Wong, and S. K. Young, Phys. Rev. <u>C12</u>, 1301. (1975).

21) R. Klem, G. Igo, R. Talaga, A. Wriekat, H. Courant, K. Einsweiler, T. Joyce, H. Kaga, Y. Makdisi, M. Marshak, B. Mossborg, E. Peterson, K. Ruddick, and T. Walsh, Phys. Rev. Lett. <u>38</u>, 1272 (1977).

22) G. D. Alkhazov, T. Bauer, R. Beurtey, A. Boudad, G. Bruge, A. Chaumeaux, P. Couvert, G. Cvijanovich, H. H. Duhm, J. M. Fontaine, D. Garreta, A. V. Kulikov, D. Legrand, J. C. Lugol, J. Saudinos, J. Thirion, and A. A. Vorobyov, Nucl. Phys. A274, 443 (1976).

23) G. K. Varma and L. Zamick, preprint 1977.

24) L. B. R. Elton, Nuclear Sizes (Oxford 1961).

25) R. F. Frosch, R. Hofstader, J. S. McCarthy, G. K. Noldelec, K. J. Van, H. R. Yearian, B. C. Clark, R. Herman and R. G. Ravenhall, Phys. Rev. <u>174</u>, 1380 (1968).

26) L. R. Elton and A. Swift, Nucl. Phys. <u>A94</u>, 52 (1967).

27) C. J. Batty and G. W. Greenlees, Nucl. Phys. <u>A133</u>, 673 (1969).

28) J. W. Negele, Phys. Rev. <u>C1</u>, 1260 (1970) and Phys. Rev. <u>C9</u>, 1054 (1974).

29) D. Vautherin and D. M. Brink, Phys. Rev. <u>C5</u>, 626 (1972).

30) J. Thirion, P. Birien, and J. Saudinos, Note CEA N-1248 (1970).

31) I. Ahmad, Nucl. Phys. A247, 418 (1975).

32) J. Saudinos and C. Wilkin, Ann. Rev. Nucl. Sci. 24, 341 (1974).

33) H. J. Weber, Fortschrithe der Physik 24, 1 (1976).

34) L. J. Tassie, Austral. J. Phys. 9, 407 (1959).

35) R. Bertini, R. Beurtey, F. Brochard, G. Bruge, H. Catz, A. Chaumeaux, J. M.
Durand, J. C. Faiure, J. M. Fontaine, D. Garreta, C. Gustafsson, D. Hendrie,
F. Hibou, D. Legrand, J. Saudinos and J. Thirion, Phys. Lett. 45B, 119 (1973).

36) M. A. Duquay et al., Phys. Rev. 163, 1259 (1967).

37) J. H. Heisenberg and I. Sick, Phys. Lett. 32B, 249 (1970).

38) J. F. Zeigler and G. A. Peterson, Phys. Rev. 165, 1337 (1968).

39) J. Friedrich, Nucl. Phys. A191, 118 (1972).

40) A. R. Barnett, and W. R. Phillips, Phys. Rev. 186, 1205 (1969).

41) C. W. Wong and S. Young, preprint (1977) to be published.

42) R. J. Blin-Stoyle, Phil. Mag. 46, 973 (1955).

43) P. G. Manigal, R. D. Eandi, S. N. Kaplan, and G. J. Moyer, Phys. Rev. 137,
620 (1965).

44) E. Aslanides et al., Section Efficace Differentielle de Diffusion Elastique
^{4}He(p,p)^{4}He A Tp = 350, 650, 1050, 1150 MeV, communicated to Wallace by
D. Garreta.

INCLUSIVE REACTIONS AND HIGH MOMENTUM COMPONENTS IN NUCLEI

Sherman Frankel

Physics Department
University of Pennsylvania

When high energy physicists use 400 GeV protons at Fermilab to study nucleon structure, they really study physics in the .5-5 GeV region. The mass spectrum of hadronic states has typical spacings of .5 GeV and even the most massive particles weigh only 3-4 GeV. In inclusive cross-sections, the most significant parameter is the transverse momentum P_t which has been studied up to as high as ≈ 7 GeV/c but usually only out to 3 or 4 GeV/c.

Very high energy nuclear physics is the study of momentum in this same region but inside nuclei. Such studies have just started, although a small amount of data has existed in the literature, and we have as yet only reached internal momenta of k=1.5 GeV/c. The extension up to > 2.0 GeV/c is clearly feasible with modern detection techniques and accelerator intensities.

It is possible that at high momenta, we presently know more about internal structure of the nucleon than of the nucleus.

In this lecture I will try to summarize the activity in the last two years, both experimental and theoretical, to understand high momentum nuclear phenomena. Most of the data that is useful comes from the inclusive production of protons (p+A→p+A). Some of it comes from production of antiprotons (p+A→p̄+A) in nuclei at energies below threshold for free p-p interactions. Amazingly the initiation of inclusive reactions by composite particles like deuterons and alpha particles, although it might seem at first to add complications, and the study of the ejection of composite particle (d,t...) from nuclei, throws useful light on the mechanisms for all inclusive reaction.

We shall concentrate here on inclusive proton production by protons and review the data and the theoretical attempts to understand the data on the basis of different models. Next, we shall examine the different momentum distributions that enter into the models.

Finally, we return to discussion of problems and avenues for the present theory and to new experiments that could be designed to distinguish between or further probe present models.

Let me start by pointing out that we are dealing here with internal momenta generally above .5 GeV/c. The most important point to realize here is that if the CIA were to secretly cut off all nuclear wavefunctions at .5 GeV/c no nuclear experimentalist or theorist could tell the difference. Thus most of our conventional knowledge about Fermi momentum is of little use. Second if you were to measure the momentum spectrum in a high region, say around 1 GeV/c, you could not tell which excited state a nucleus was in. We should expect at these momenta that we are studying properties of <u>nuclear matter at high momentum</u>.

The second most important point is to recognize that the experiments to be described generally study <u>backward</u> production. This is the key ingredient. Consider p-p quasifree scattering. The forward particle scattering is dominated by p-p matrix elements slightly affected by the internal momentum of the struck proton. But it is the struck proton that <u>has</u> the momentum distribution we wish to study. It is the one emitted backward. This is because the <u>momentum transfer</u> is very small if the target nucleon of momentum k is nudged on to the mass shell and emerges with momentum q. It is very large if the projectile is turned around. A more qualitative way to estimate "clean" kinematic regions where observation of the target nucleon predominates is to calculate the appropriate values of t and u and look up the t dependence of the known p-p cross section. We use the word "backward" to mean that we predominantly examine the target nucleon.

(We recognize that this simple view prejudices us against the unlikely possibility that the mechanism is multiple scattering.)

Now let me turn to the first piece of data that led us to believe that there was interesting physics to be pursued at backward angles with high intensity proton beams. This cross section measurement, figure 1, was carried out by a Penn-Temple-LAMPF collaboration[1] in the line B tunnel. The data plotted are differential cross sections/nucleon at 180°. The pertinent conclusions are: 1) The cross sections have a Gaussian fall off, 2) the slopes are A-dependent, and 3) the magnitudes are A-dependent.

These features at first blush are confusing. They suggest an evaporation or statistical process (wrong); they suggest, since the cross sections/nucleon increase with A, that there is some multiple scattering or cooperative phenomenon (not likely).

Figures 2 and 3 show the cross sections/nucleon for deuteron and triton emission. The same features are present but the dependence of $d\sigma/d^3q$ on A is larger going from p to d to t.

Ralph Amado and I considered various models for a period of time in an attempt to study this data. The overriding physical fact was that quasifree scattering dominates the total cross section at these energies, and that for every forward going proton detected in traditional quasifree measurements, there had to be a backward proton. The first theoretical paper was that of R.D. Amado and R. M. Wolosyn.[2] This paper is the most important starting point. First, Amado and Woloshyn estimated the cross-sections on the basis of single scattering. Shadowing and final state interactions were neglected. The sum over the undetected final states was done by closure, assuming low mean excitations of the residual A-1 nucleus. This calculation relates the cross section to the ground state momentum distribution. (In a later paper[3] Amado and Woloshyn
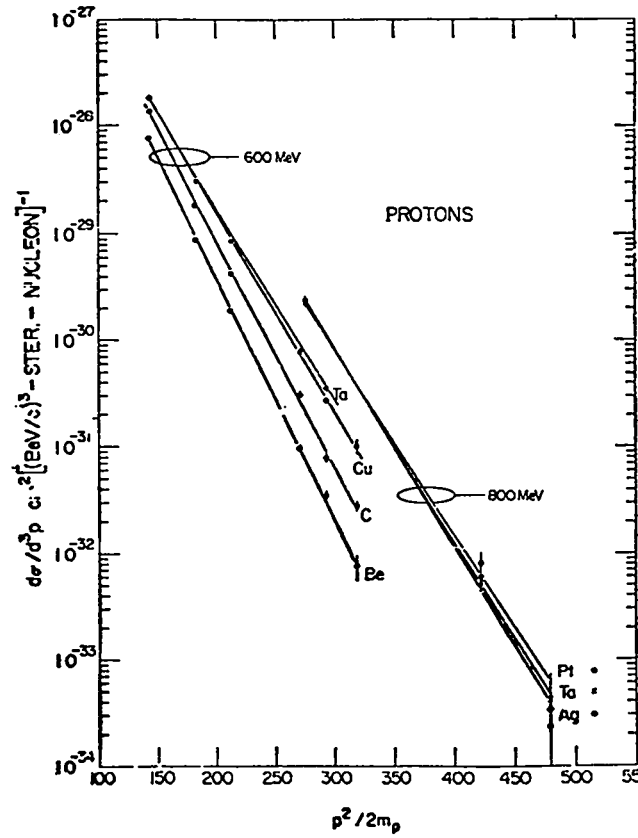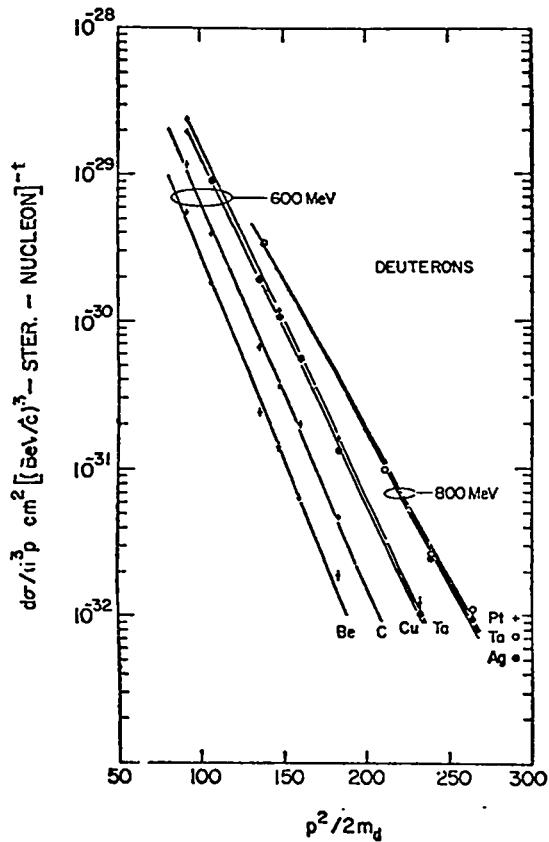
Figure 1.

Figure 2.
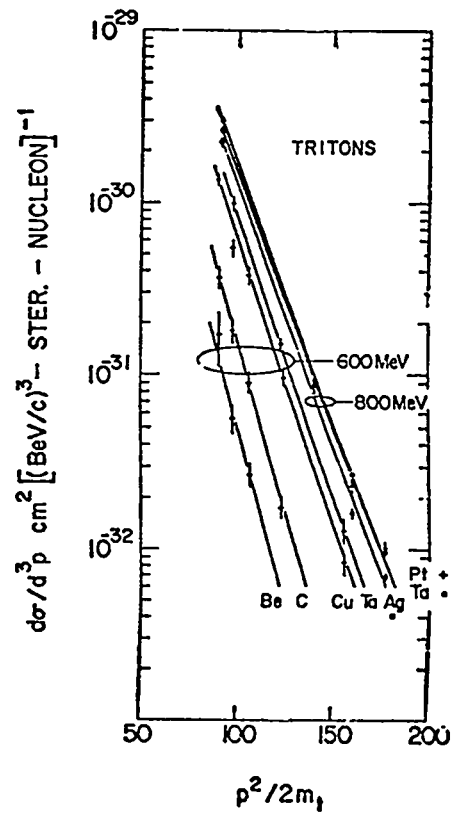
Figure 3.

showed this simple relation to be incorrect. We shall return to this later.)
The first test made by Amado and Woloshyn was to use a Fermi gas model of n(k)
at finite temperature, the parameters obtained by fits to ee' quasielastic data.
Figure 4 shows their result at 400 MeV; the Fermi gas misses by $\simeq 10^6$. The
important next ingredient introduced by Amado and Woloshyn was an estimate of
what the high momentum distribution might really look like above the usual Fermi
gas region. I will return to their ideas about n(k) later but for now let me
just say that they used the function $n(k) = N/\cosh^2(k/2k_0) \simeq e^{-k/k_0}$ at high
momenta. In order to determine k_0, they refit the ee' data. This was a
"headstrong" thing to do since it is very unlikely that low and high k regions
of n(k) are simply related. However, figure 4 shows that although they got poor
agreement with the fall off of $d\sigma/d^3q$, they fit magnitudes well.

As an experimentalist, I was unhappy with inserting n(k), since it came
from a very crude model, into the theoretical formula. It seemed best to me to
extract n(k) from the data. Also the Amado and Woloshyn calculation specified
elastic pp scattering which is not too good an approximation at 800 MeV and above.
The method used I call "quasi-two-body-scaling" (QTBS).[4] While it can be
"derived" from the Amado and Woloshyn expression for $d\sigma/d^3q$, I will avoid such
a derivation since it is in fact an incorrect way to proceed. To understand
it, we must first go back to the basic kinematics. After all we are studying
inclusive reactions in particular p+A→p+X, and we must at least understand the
kinematic constraints.

Figure 5 shows the relationships in the reactions p+A→q+p'+X. Here p is
the incident projectile's momentum, q that of the detected proton, p' that of
the undetected (forward going) proton, and X the remaining A-1 final state.
From the outset we make the assumption that $\vec{k}$ is the total momentum of the A-1
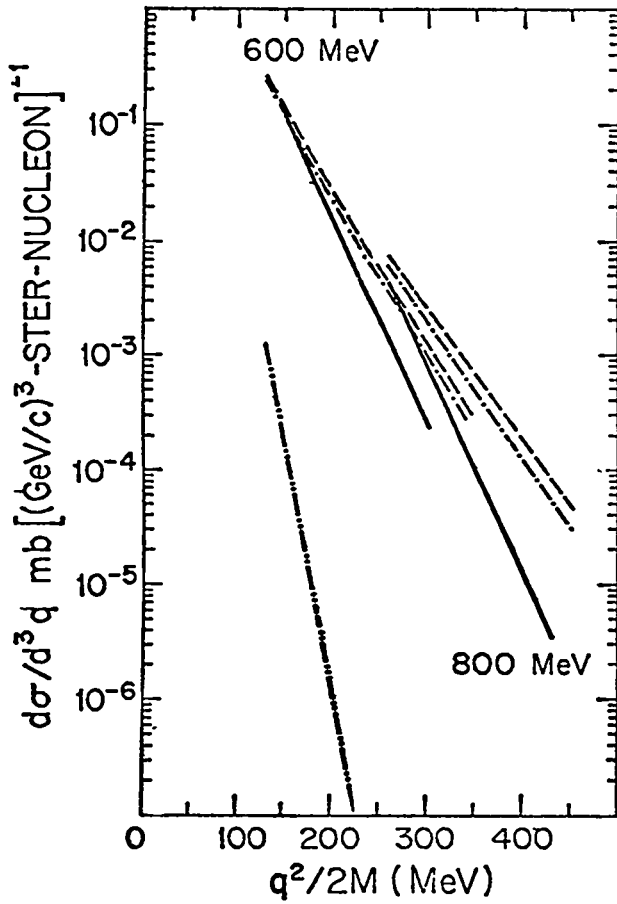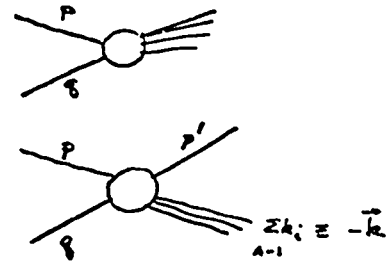nucleons and that this blob contains no fast nucleons. The only fast nucleon is

Figure 4.

Figure 5.

p'. This may not be the true final configuration, but it is the fundamental assumption of QTBS.

The <u>second assumption</u> is that the cross sections will fall very rapidly with the momentum transfer $\vec{k}$. It is trivial to see from this figure that, since (for large A) the magnitude of p' is fixed by p and q, the minimum value of $k = k_{min}$ is in the colinear configuration. Thus

1) $\quad k_{min} = |\vec{p}-\vec{q}| - |p'| = k_{min}(|p|,|q|,|\theta|,A)$

Figure 6 displays the details.

The <u>third assumption</u> is that the cross section is given by

2) $\quad \dfrac{d\sigma}{d^3q} = C(p,k_{min}) \dfrac{G(k_{min})}{|\vec{p}-\vec{q}|}$

That is, that the cross section is proportional to the "probability" $C(p,k_{min})$ of the interaction between the incoming projectile and the ejected nucleon (it may be an elastic cross section or inelastic inclusive cross section and depends on the energy of the projectile), and the probability of finding the final state of momentum k_{min}.

I would like now to express this scaling relationship in somewhat more detailed terms. Suppose we consider a momentum configuration in the ground state where a single nucleon has momentum $\vec{k}$, the remaining A-1 nucleons have total momentum $-\vec{k}$, <u>and</u> that this momentum is distributed over the A-1 nucleons almost equally so that the A-1 residual nucleons are in a configuration that overlaps strongly with the A-1 final state of low excitation. Then each nucleon has $k_i \simeq k/A-1$. In this case we can pretend that the A-1 nucleons act as a spectator and that we can talk about $\vec{k}_{min}$ as the momentum of the struck nucleon. Remember that the distribution of k_{min} is not a measurement of the <u>ground state momentum distribution n(k)</u>. More of this later.

INCIDENT PROJECTILE $\vec{p}$ UNOBSERVED SCATTERED PROJECTILE $\vec{p}'$

$\vec{q}$ $\vec{k}$

OBSERVED NUCLEON TARGET NUCLEON
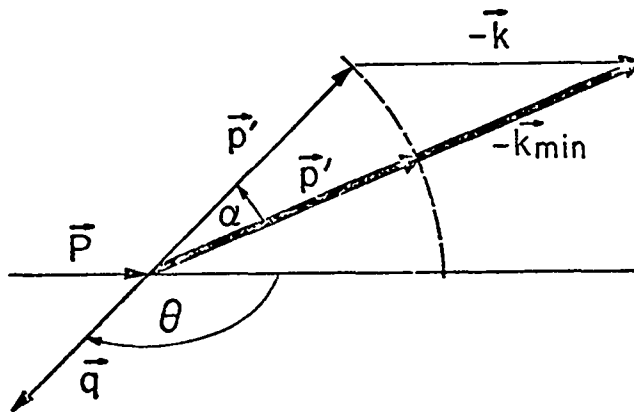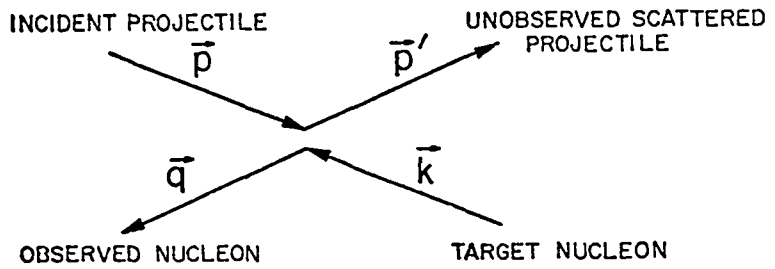
$$\begin{matrix} k_{max} \\ k_{min} \end{matrix} = |\vec{p} - \vec{q}| \pm |\vec{p}'| = \sqrt{p^2 + q^2 - 2pq \cos\theta} \pm \sqrt{(E_p + E_k' - E_q)^2 - m_p^2}$$

$$E_k' = m_q - (T + \epsilon + \Delta m)$$

$T =$ KINETIC ENERGY OF RECOILING NUCLEUS OF MASS A−Q

$\epsilon =$ EXCITATION ENERGY OF NUCLEUS

$\Delta m = (M_{A-Q} + M_Q) - M_A$

Figure 6.

What I then proceeded to do is to make the plausible assumption that C is slowly varying relative to G(k) and to plot $d\sigma/d^3q \ |\vec{p}-\vec{q}|$ vs k_{min} rather than q. Figure 7 shows this plot for the LAMPF 180° data.

The first feature to notice is that the 600 MeV data for ^{9}Be, ^{12}C, Cu, Ta now show identical shapes. There is also almost no variation in $d\sigma/d^3q$/nucleon with A. $G(k_{min})$ is a simple exponential and the data goes out to 1.4 GeV/c! For those who wish to consider the process as a single scattering, the proper A dependence is observed.

It then occured to me that if this scaling worked for protons, it should work for any particle. Figure 7 shows QTBS for p+A→(d,t)+A as well. Considering that C has been set = 1, the shapes are remarkably the same. I will not dwell on this except to say that study of $G(k_{min})$ for (p,d,α)+A→p,d,t,... ^{11}B + X shows the same kind of scaling. I shall concentrate on the Pin - Pout data since it is simplest.

Figure 8 shows PPA data at 90° and 3 GeV. It is an entirely different energy where, as opposed to $k \simeq q$ at 180°, $k \simeq q(\frac{q}{2m_p})$ at 90°. It is clear that QTBS works.

We wished to check the scaling further so a Penn-Wm & Mary-Virginia collaboration[5] went to SREL to study the reaction (p,d,α)+A→p+X. Here are unpublished results.

Figure 9 shows data for a carbon target. The left hand curves show conventional plots of $d\sigma/d^3q$/nucleon vs q^2 [slopes shown for α^{-1} in $d\sigma/d^3q = \exp(-\alpha\ q^2/2mp)$]. Note that slopes vary from 13.1 to 21.5 MeV while G(k) plotted to the right shows the scaling.

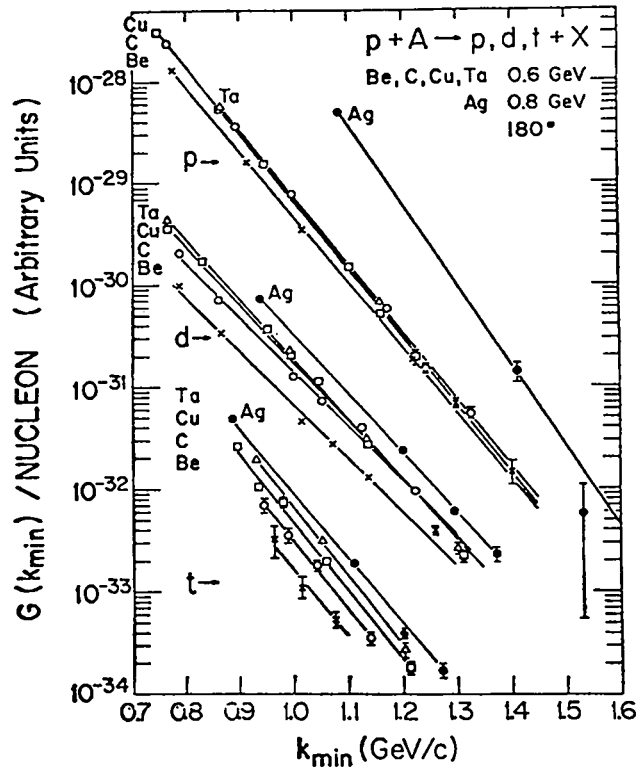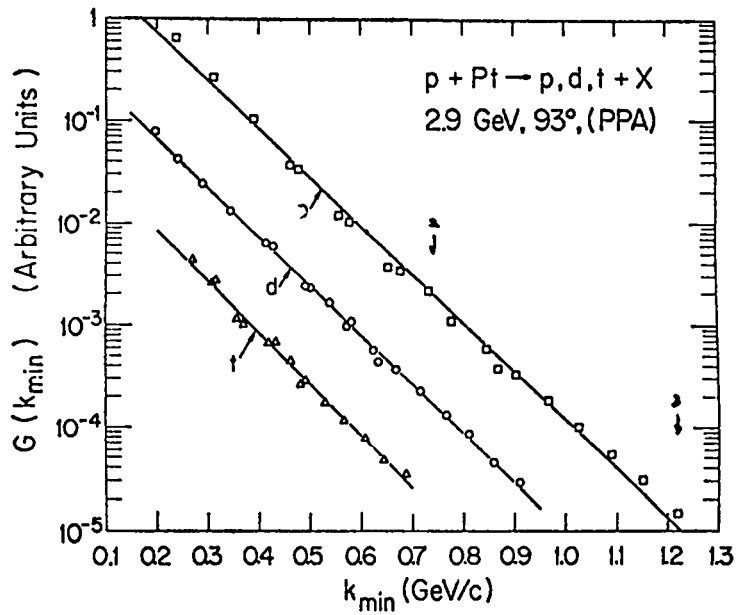Figure 10 shows Ta data. Remember that $C(p,k_{min}(A))$ is A-dependent and we have set C = 1.
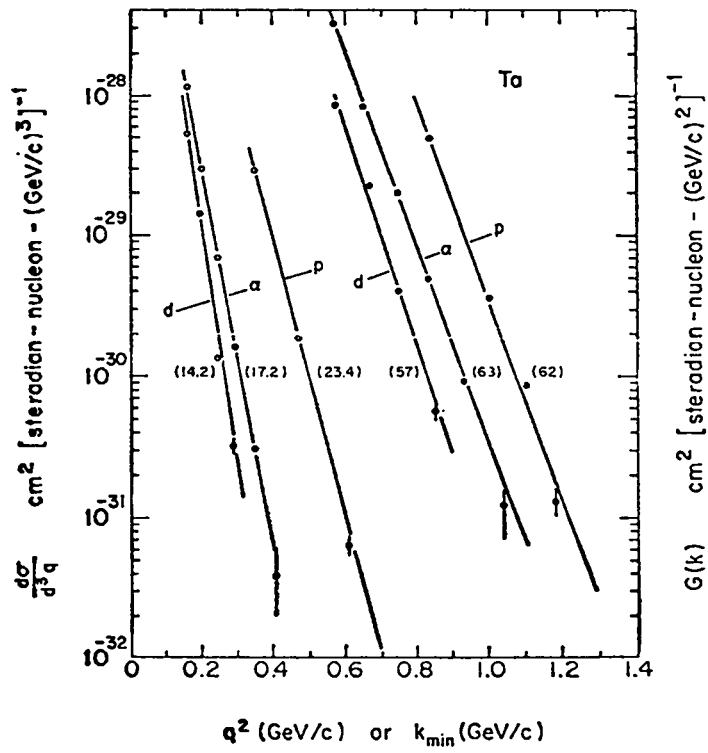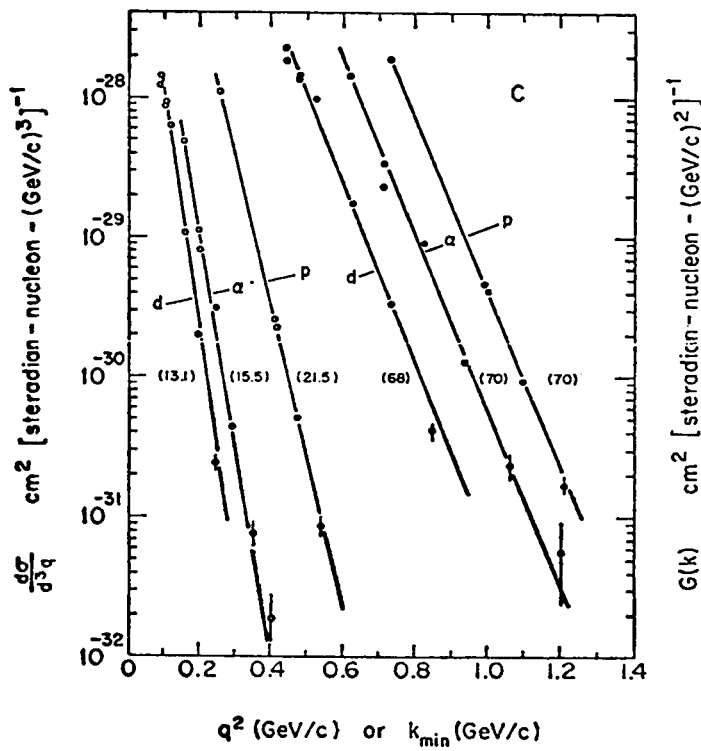
Figure 7.

Figure 8.

Figure 9.

Figure 10.

But I show these data mainly because of this _first_ study of ^{6}Li, shown in figure 11. _The important feature here is that the curves are the same shape to the elastic limit._ These data are crude but, we will see, very important to our understanding.

We now turn to the first HRS experiment #256 carried out last November[6] done by a Penn-HRS collaboration. The goal of this short 100 hour run was to make careful studies of data at other angles and up to the elastic limit in ^{6}Li.

Figure 12 shows yields as $d\sigma/d^3q$/nucleon vs $q^2/2m_p$. Figure 13 shows G(k) (C = 1) at 158°. Figure 14 shows G(k) C = 1 at 100°. Figure 15 shows only ^{6}Li and ^{181}Ta $d\sigma/d^3q$ vs $q^2/2m$. Figure 16 shows G(k) at both angles.

Conclusion: Not only does scaling appear to work but it works up to the elastic limit.

With these results at hand we then hoped to study $C(p,k_{min})$ in regions where we thought we could predict it accurately. Fortunately, Darragh Nagle gave us some unpublished data[7] over a large variety of values of θ, q, A that allow us to test the factorization for $C \neq 1$.

Figure 17 shows the cross section for p+Cu→p+X at 730 MeV. The cross sections look quite different. Figure 18 shows G(k) for C = 1. The shapes are more uniform. Figure 19 shows $d\sigma/d^3q$ $|\vec{p}-\vec{q}|$/C vs k_{min}. Note that these data go to much lower k_{min} than most early data, even into the Fermi gas region. The scaling appears to work. Figure 20 shows the lightest nucleus studied, ^{9}Be, now including a forward point at 75° showing $d\sigma/d^3q$ variation. (Note poor fit at 75°. For this forward angle the failure of assumption 2 (eq. 2) starts to enter; G(k) does not fall off faster than $d\sigma/dt$). Now let me overlay curves for Be....Ta. Figures 21 - 25 show these plots of G(k). _We now should be able to map out G(k) from .1→1.5 GeV/c._
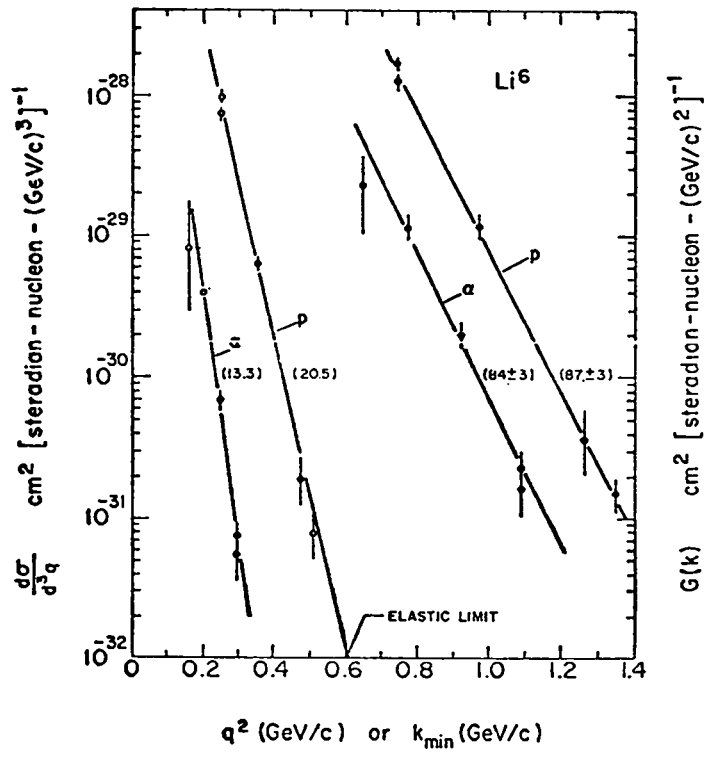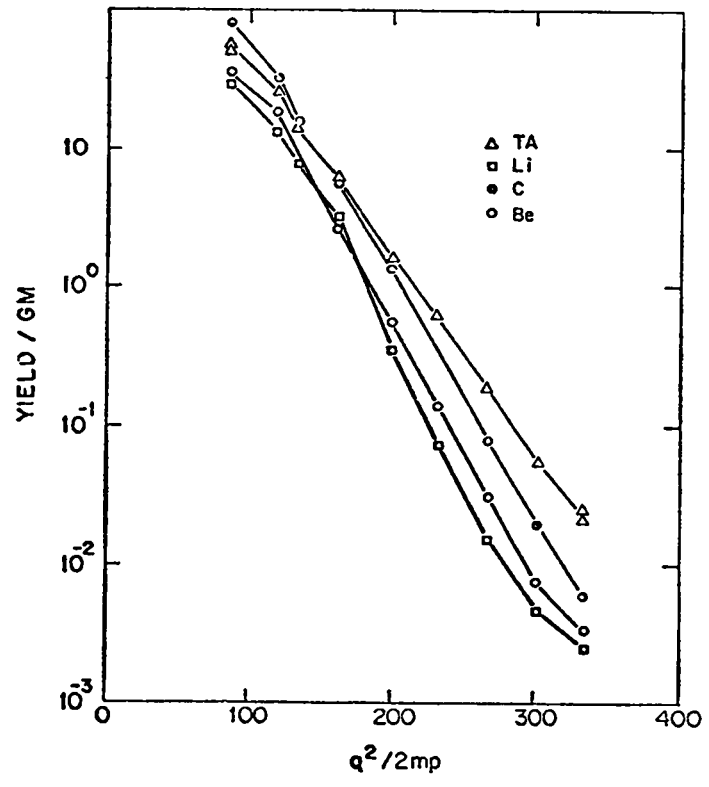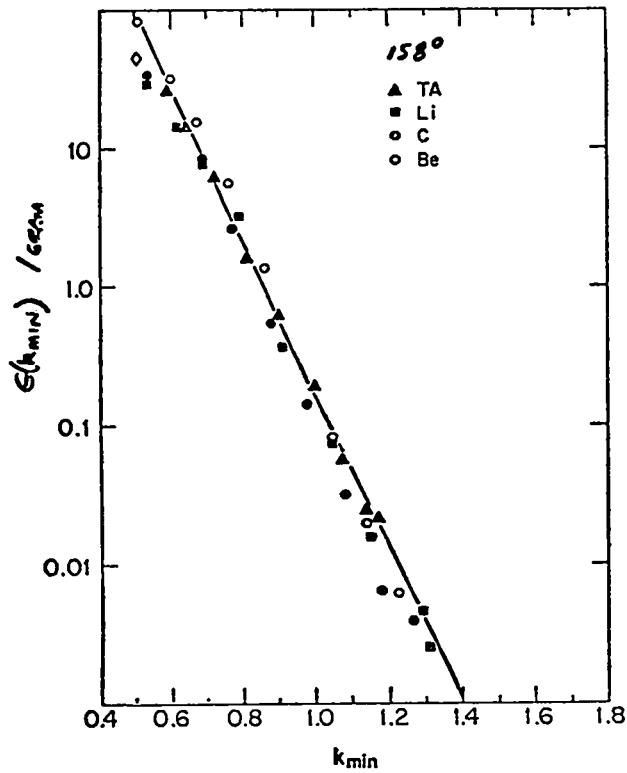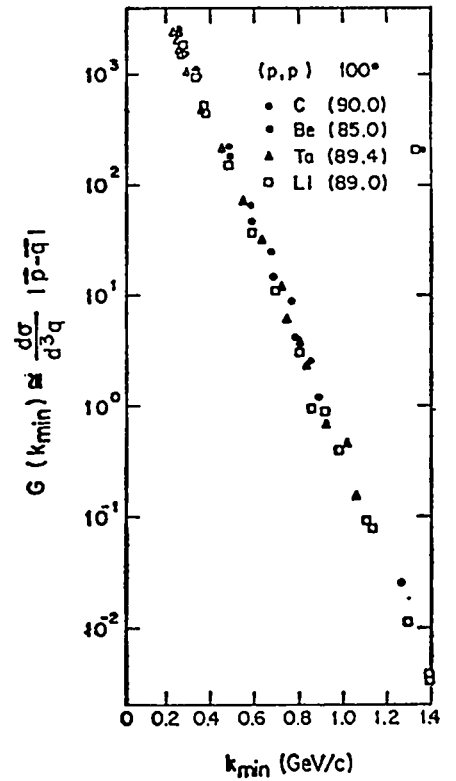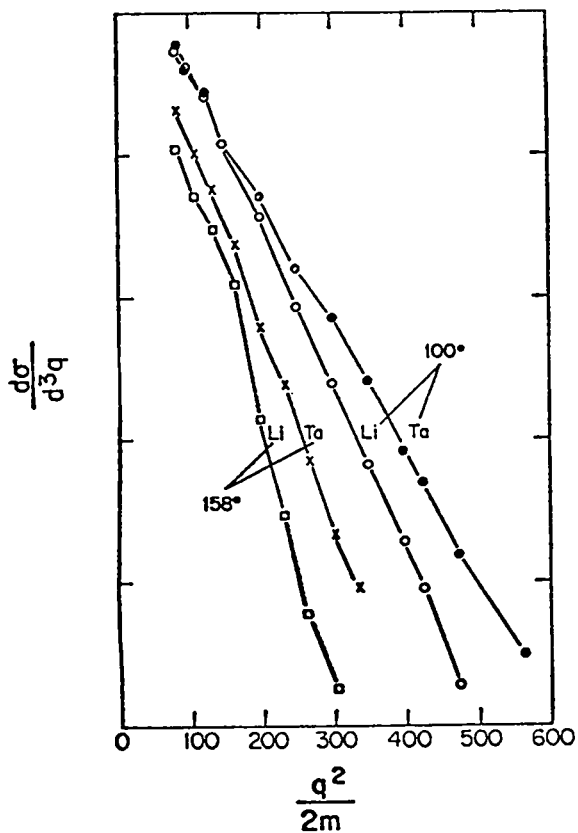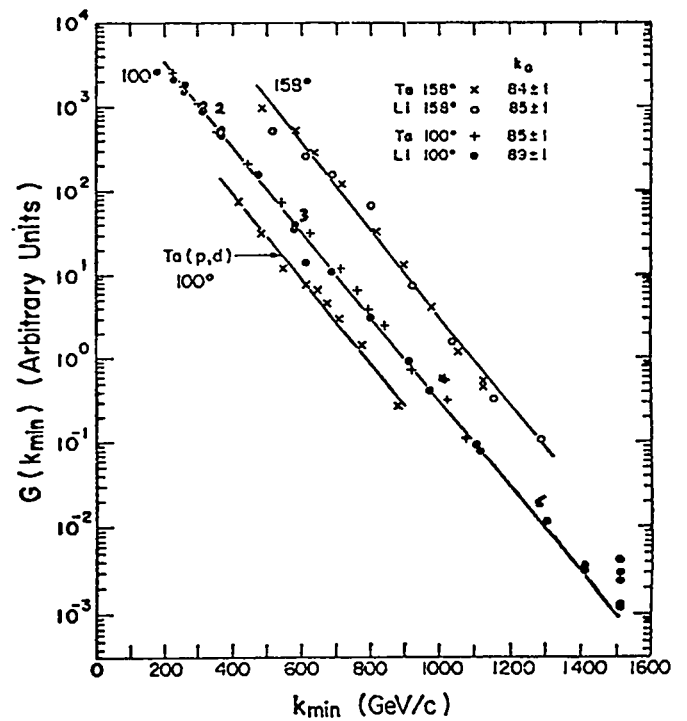
Figure 11.
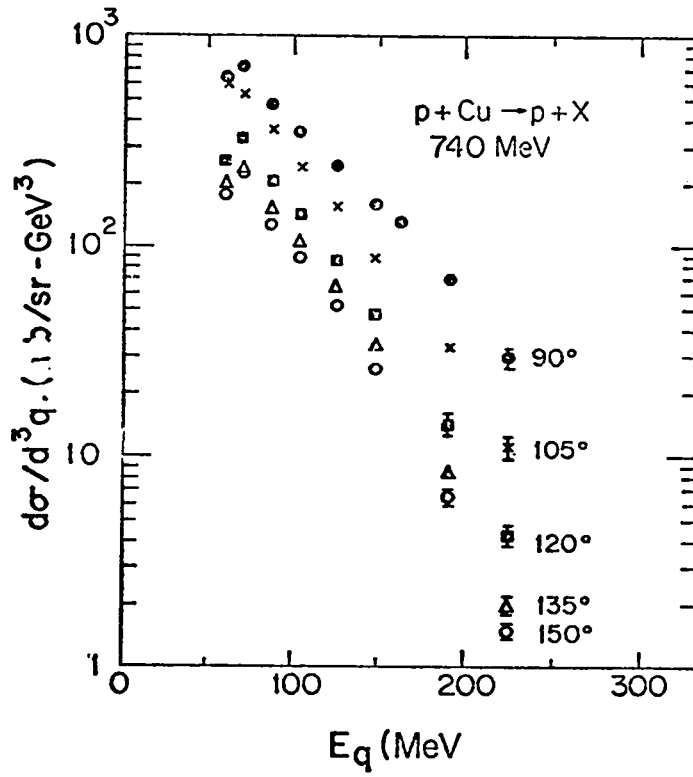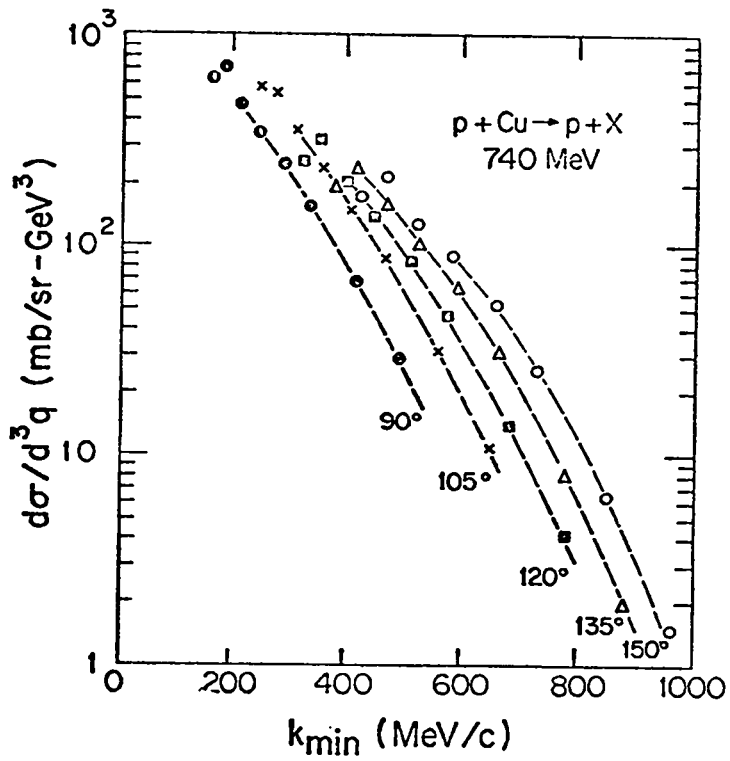

Figure 12.

Figure 13.

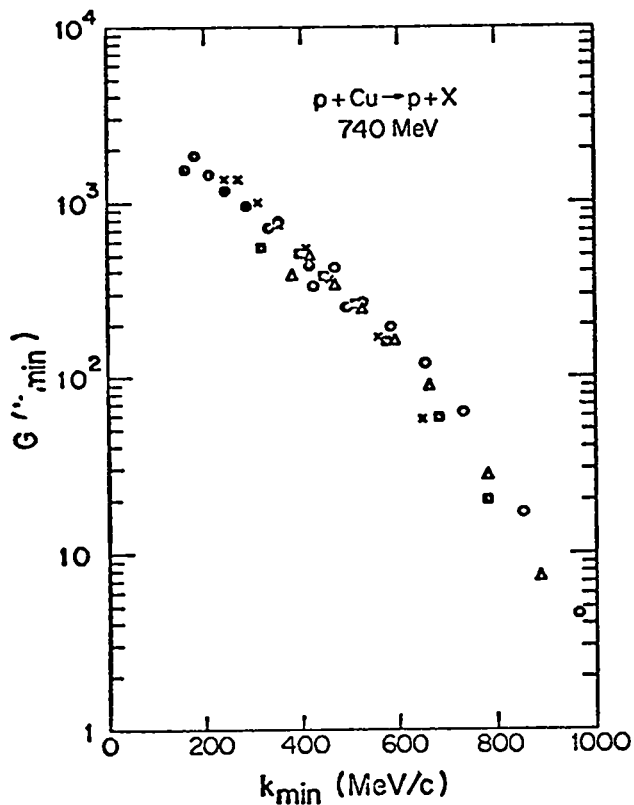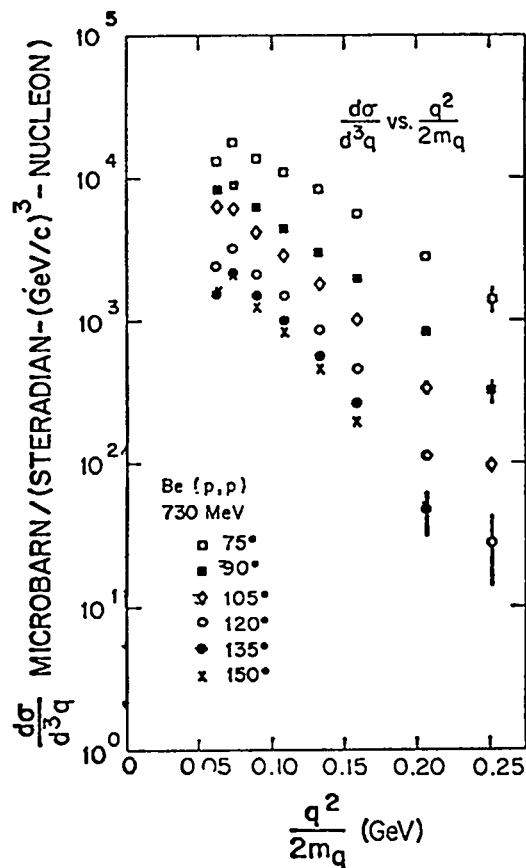Figure 14.

Figure 15.

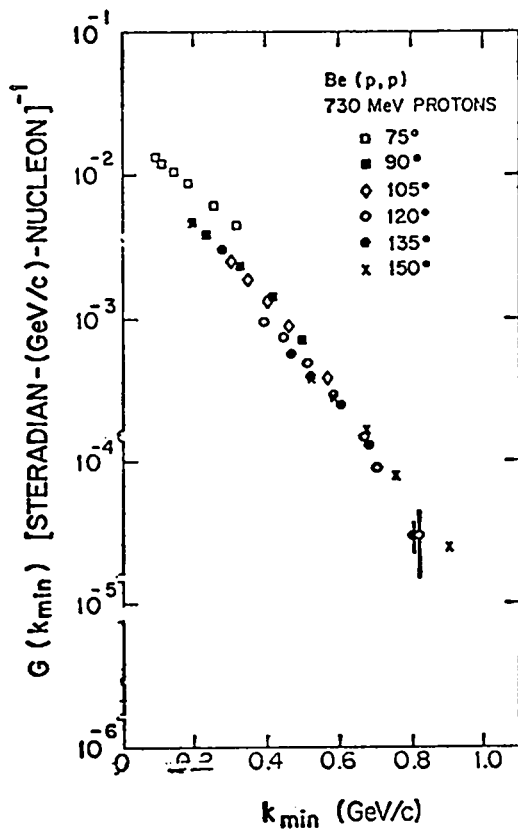Figure 16.

Figure 17.

Figure 18.
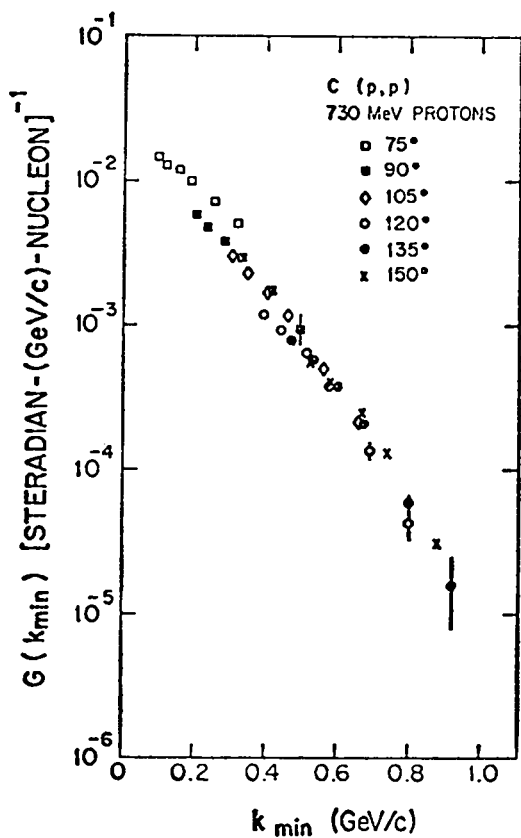
Figure 19.

Figure 20.
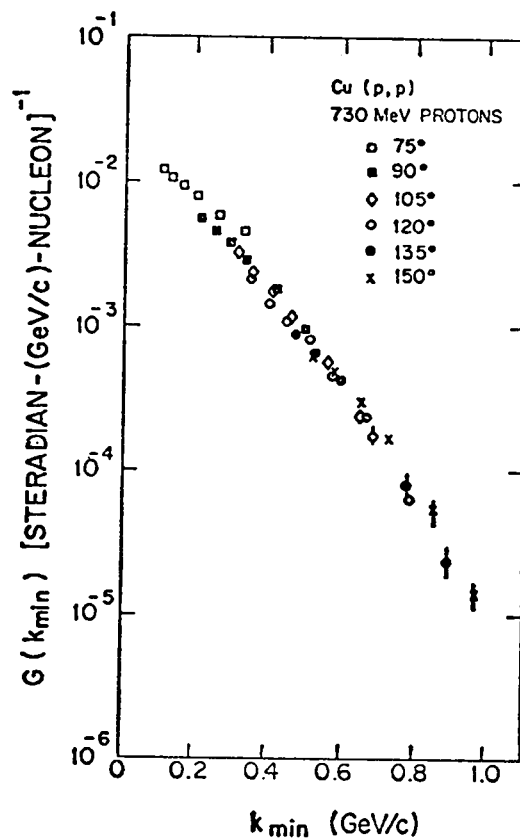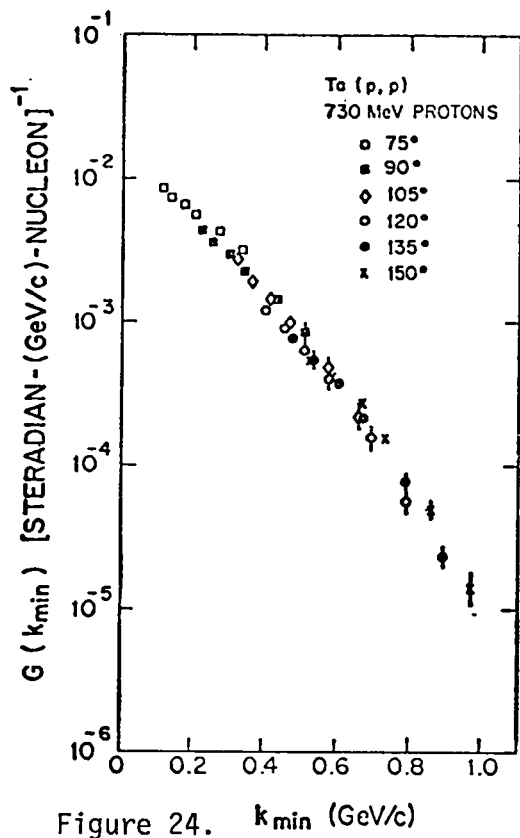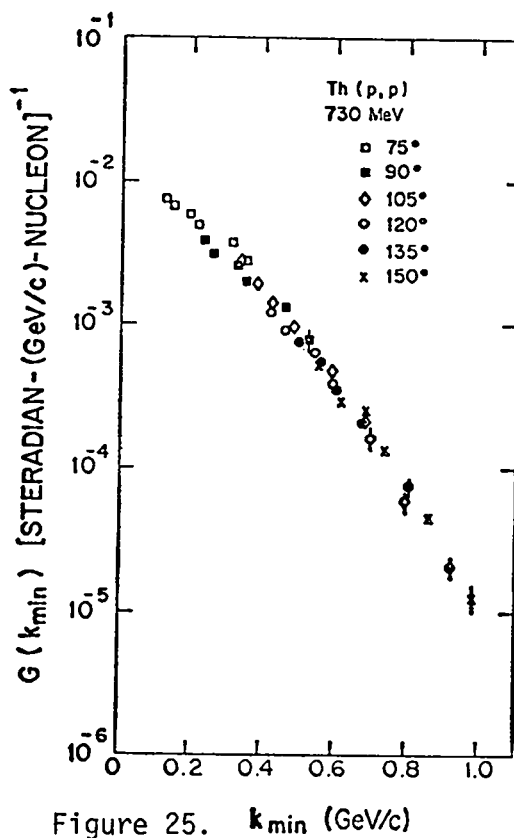

Figure 21.

Figure 22.

Figure 23.

Figure 24.

Figure 25.

A final check of the factorization comes from the study of antiproton producing at energies much below the free 6 GeV p+p→$\bar{p}$+X threshold. Clearly, equation (2) involves a C that is quite different (the threshold behavior of $\bar{p}$ production) from p-p scattering. Also, k_{min} is an entirely different function of p.

Figure 26 shows our plot of $G(k_{min}) \simeq \sigma/C_{\bar{p}}$ vs k_{min}. The data go out to k_{min} = .8 GeV/c. $G(k_{min})$ is exponential as before with about the same slope.

This completes the summary of the data and of scaling. I shall now briefly discuss two unpublished models, those of Weber and Miller[8] and Fujita[9] which have recently attempted to study the 180° LAMPF data.

Figure 27 shows the diagrams that describe the various models. In the Amado-Woloshyn model, the proton is off-shell, the observed proton having momentum q not k. The cross section is dominated by the differential p-p cross section at the upper vertex.

In the Weber and Miller model, the A-1 recoiling nucleus is off-shell. The momentum of the observed proton, q, is the internal momentum q. The cross section is dominated by the total cross section at the upper vertex.

Basically, to reproduce the high momentum parts of the cross section, Weber and Miller used a large σ_T but a rapidly (conventional) falling momentum distribution. Amado and Woloshyn use a tail to n(k) that falls off slowly.

In Fujita's cluster model, the A nucleus shakes off a cluster of N nucleons which are off-shell with momentum k given by a Gaussian momentum distribution that varies as $n(k) \simeq exp(-k^2/\nu N)$. The probability of cluster formation depends on permutations and combinations, and on a factor $(\frac{Vc}{V})^{N-1}$ which gives the probability of N nucleons occuring within a correlated volume, and a sticking probability = 1 of the cluster remaining together after p-N elastic scattering. Fujita must sum N from 1 to 4 to fit the 180° data.

Figure 26.

$$\sigma/c \text{ vs. } k_{min.}$$
$$\text{FOR } \bar{p} \text{ PRODUCTION}$$
$$\sigma \cong (S-S_T)^n$$

$+ (n=4) \ 98 \ \text{MeV/c}$

$(n=0) \ 71 \ \text{MeV/c}$

$(n=3) \ 90 \ \text{MeV/c}$

$\frac{p\sigma}{(\hat{q})^{n+1}}$ (ARBITRARY UNITS)

$k_{min.}$ (GeV/c)
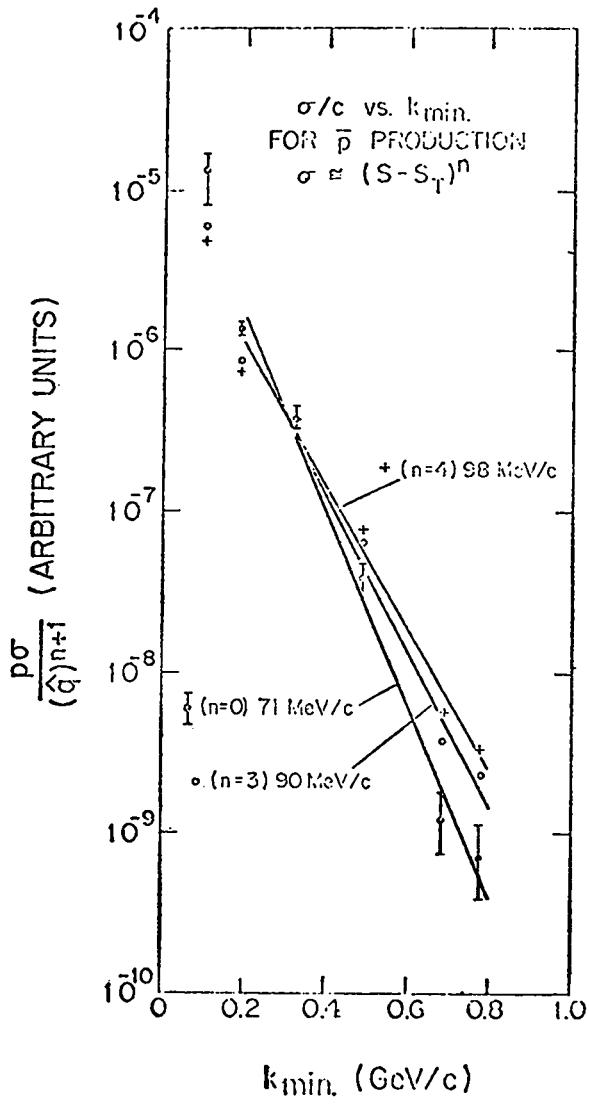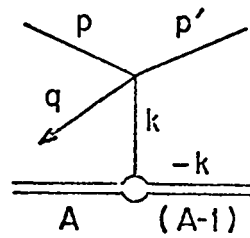
AMADO – WOLOSHYN
FRANKEL
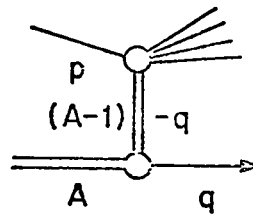
Figure 1

WEBER & MILLER
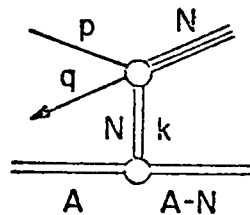(EXCHANGE)

Figure 3

FUJITA
CLUSTERS

Figure 4

Figure 27.

- 223 -

Figures 28a-b show the fits of Weber and Miller to various models. I do not have time to comment in detail on this paper.

Figures 29a-b show plots of Fujita.

The fundamental theorem to be enunciated is that at one angle and energy anything goes. These papers have not yet appeared in print but one will have to wait and evaluate them after they are applied to other angles, energies, etc. Perhaps in the discussion period we can talk more about such models.

However, I would like to point out a simple and elegant test[10] that separates the Amado and Woloshyn model from all other models. This experimental test uses a study of the polarization dependence of the cross section. From figure 27 we see that the Amado and Woloshyn model describes a scattering of the polarized proton and a proton of momentum k. Using QTBS makes it simpler; it is the scattering of a polarized proton from a proton of momentum k_{min}. Figure 30 shows our predictions of polarizations for an HRS experiment similar to our last. Notice that a) the polarizations are large, b) they vary in a characteristic way with angle and energy. Even if the magnitude is depressed by multiple scattering the general shapes can be verified by experiment.

On the other hand all other models give either zero or very small polarization P:

1) Weber and Miller model gives identically zero since no products of the upper vertex are detected (no polarization axis is therefore defined).

2) Evaporation of statistical models that do not remember the incident proton give zero.

3) Fujita's model sums over elastic scattering from at least N clusters of arbitrary spin. P should be small.

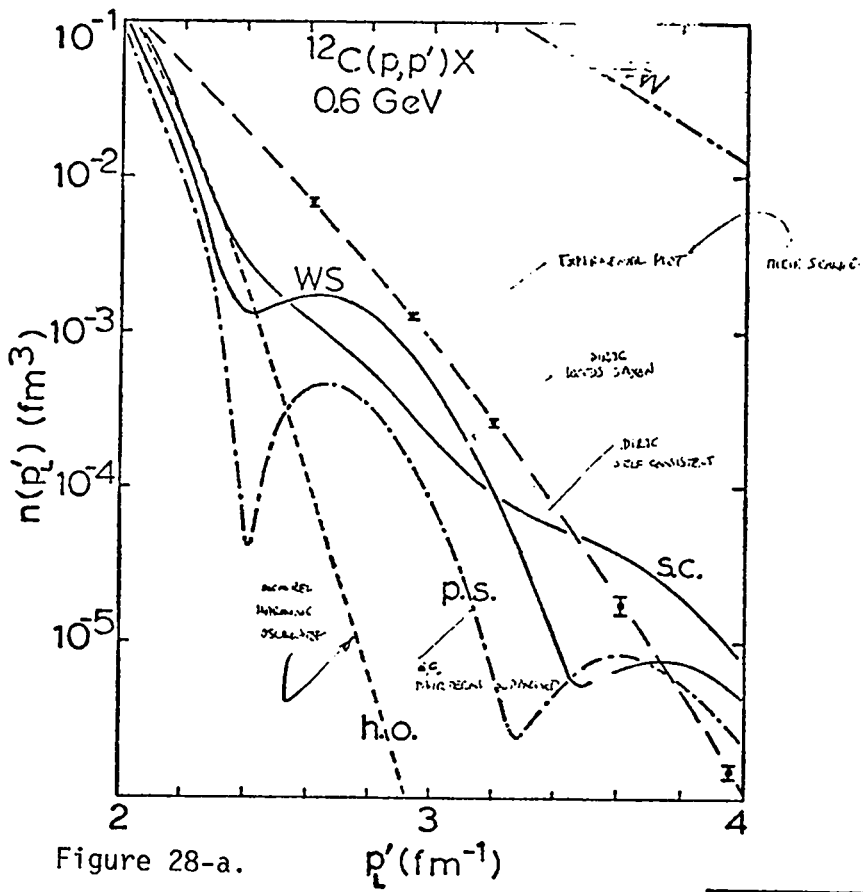4) At 800 MeV the polarization is very small at small angles so that we average small polarizations over n scatterings. Certainly there
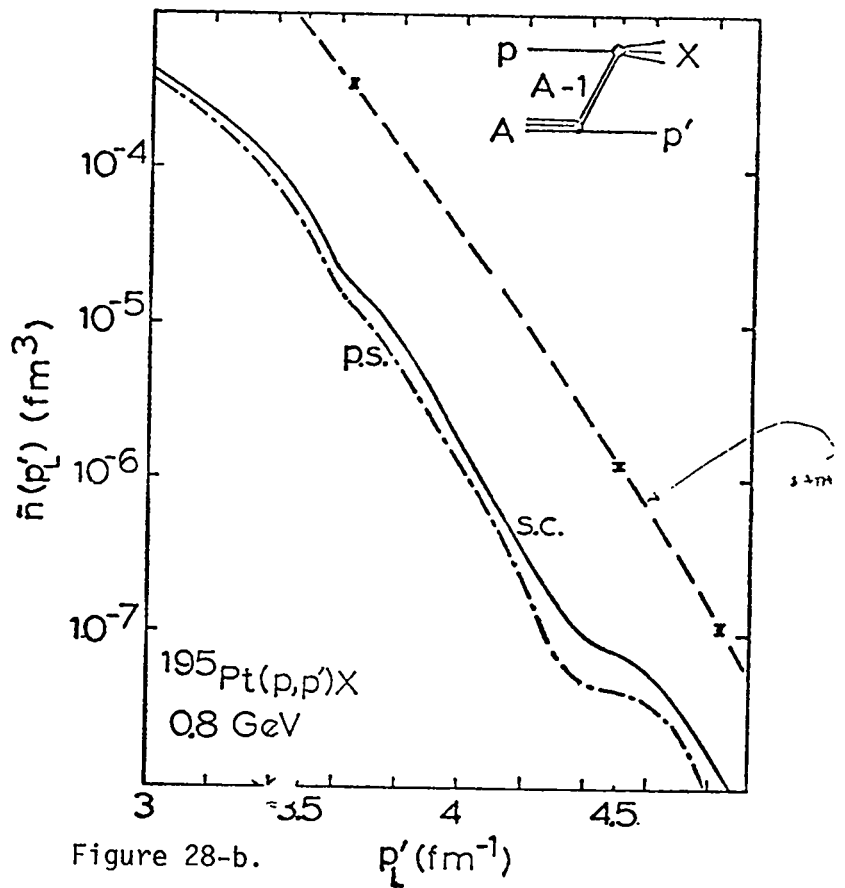
- 224 -

Figure 28-a.

Figure 28-b.
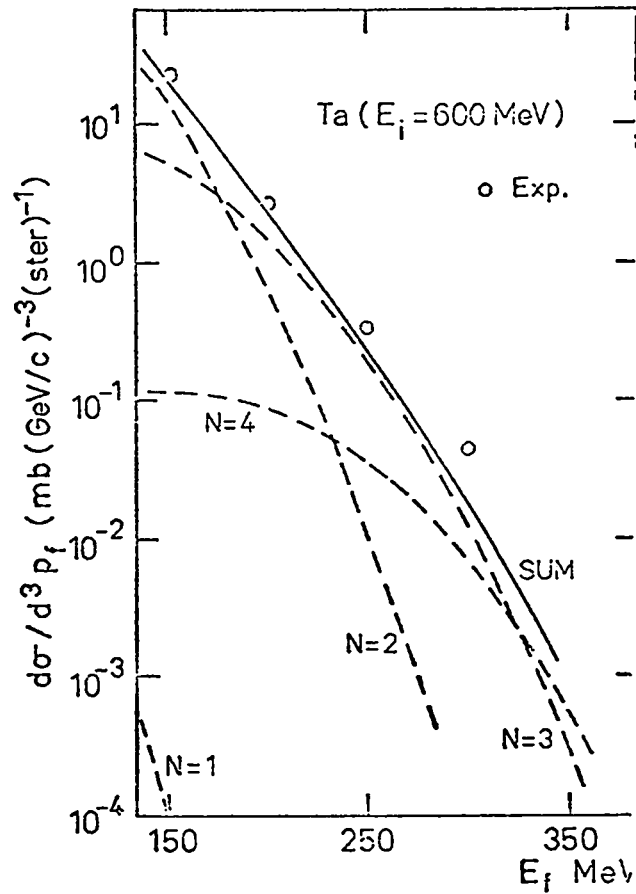
Figure 29-a.
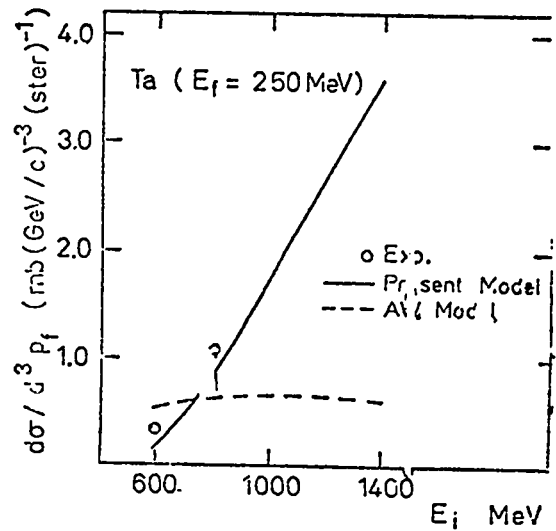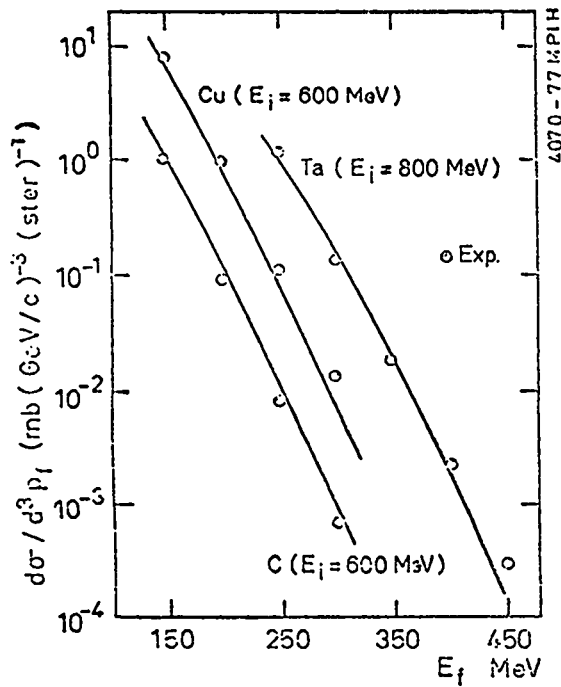
Figure 29-b.
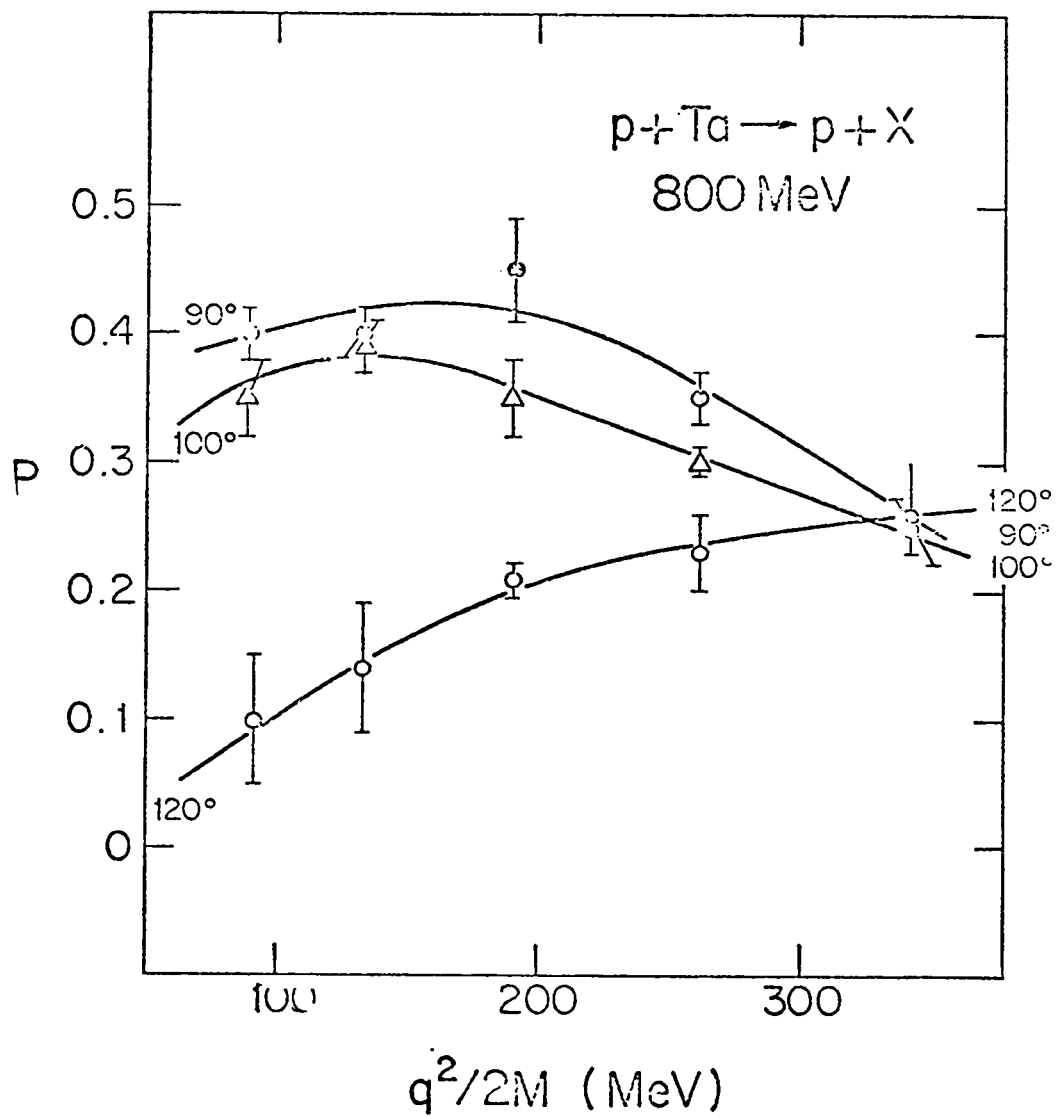
Figure 30.

is no reason for P at 120° to rise with q and P at 90° to fall with q on this model.

It would take 10 hours to measure P, with better accuracy than p-p scattering has achieved, at 90° and $\frac{q^2}{2m_p}$ = 200 MeV with the HRS.

Time does not allow me to describe p(polarized)+A→(d,t)+X which has many features that allow microscopic tests for the emission of composites.

Of course another way to test these models is with (p,2p) experiments since the products in coincidence with the backward proton are quite distinctive of the models. (Experiment 258, LAMPF).

Finally, I wish to turn to the very important work of Amado and Woloshyn on momentum distributions in nuclei.[11] They have been studying a very simple model whose advantage is that it is soluble. It is a one dimensional Boson model with δ function interactions between pairs of particles. It is not meant to be a description of nuclei. But I believe it contains the important features. At high momenta the internal momentum spectrum in this model in the assymptotic limit agrees with general model independent arguments that show that n(k) falls as $1/k^4$ and is dominated by two particle correlations. In this region the momentum k of the struck nucleon is shared by a single nucleon. At the low end of the spectrum the momentum k is distributed among the A-1 nucleons in a "coherent" manner. In this region n(k) falls as e^{-k/k_0}. Figure 31 shows the Amado and Woloshyn prediction.

Note that at q = λ the exponential region ends. As we move to the region of q ≃ 3λ, the sharing of k with a single nucleon dominates. For q = λ → q = 3λ the k is shared among 2,3,4... nucleons.

The purpose of showing this figure is not to predict shapes of ground state momentum distributions. Although this is a crude model, it does describe the two main regimes, characterized by a fall-off k_0 and a transition momentum
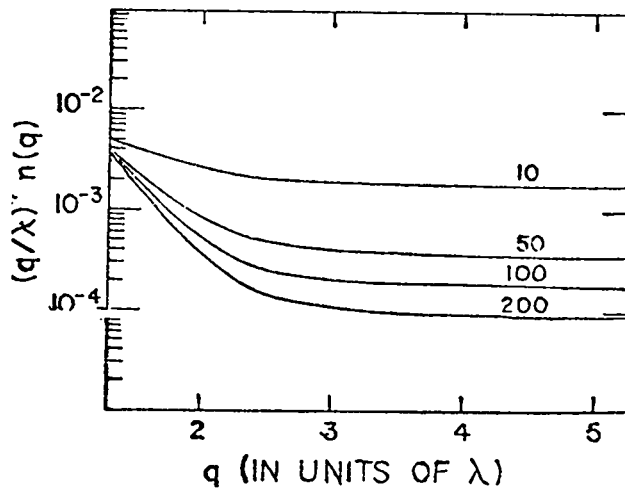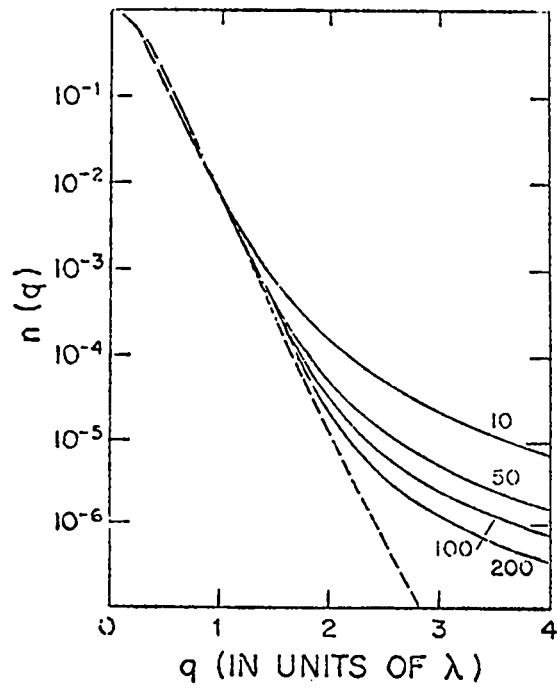
Figure 31.

$k_T = \lambda$. It also must be recognized that these regimes have very distinct momentum configurations that are dominant. The low region has the momentum configuration similar to that of quasi-two-body-scaling, the high region would have a single extra fast nucleon and A-2 nucleons of momentum << k.

I shall now show from our data that we can understand the scaling if $k_T \simeq 1.2$ GeV/c. The argument is subtle and must be carefully followed. The clue is in the elastic data of figures 13 and 14. Note that near the elastic limit the final state configuration is constrained by energy conservation to be exactly that of quasi-two-body-scaling. Therefore in this region, G(k) is exactly determined. We do not know that the recoil is coherent far from the elastic limit since at low k there is plenty of energy available to kick out 1,2,3 fast particles. Of course at very low k we expect that the internal nucleon of momentum k is nudged on to the mass shell. Little energy is lost by the projectile and the momentum transfers are low. It is plausible that in this region we would also be measuring G(k) for a coherent A-1 recoil. But, see figure 16, the function is everywhere the same. Therefore, we conclude that in the middle region, since G(k) does not change, the recoil is also coherent.

The tantalum data provides elegant confirmation. At a q corresponding to the elastic limit region in ^{6}Li where the whole Li$^{6-1}$ recoil is moving off coherently with about 400 MeV energy, the heavy Ta nucleus has essentially no kinetic energy. The forward going proton p' has 400 MeV of energy. Clearly there is enough energy for 1,2,3 extra fast nucleons to appear in the final state. But the G's for Ta and Li are the same! Thus we conclude that the recoils are coherent up to k = 1.2 GeV/c. Since G(k) falls exponentially and not with any sign of polynomial behavior, we conclude that $k_T \simeq 1.2$ GeV/c will allow us to account for the dominance of coherent recoils in the data.

Finally, we return to our last comment. How is G(k) related to the ground state momentum distribution? Amado and Woloshyn have shown[12] that $d\sigma/d^3q$ is after all not $\simeq$ n(k) in their first treatment.

Their derivation assumed a) that closure could be applied in a sum over final states, and b) that final state interactions could be ignored. They have now given an elegant demonstration that in fact final state interactions cancel the leading terms that produced $d\sigma/d^3q \rightarrow n(k)$ and that the closure approximation fails just when it is needed for the high momentum components $k > k_T$ where the final state does not have a large energy of excitation.

What does this all mean? Does it mean that QTBS originally "derived" using the Born approximation is invalid? The answer seems to be that 1) we can still retain the scaling relationship $k(q,\theta,A)$, 2) we can still retain the factorization into $C(p,k_{min}) \times G(k_{min})/|\bar{p}-\bar{q}|$ but that we must reinterpret the structure function $G(k_{min})$, which depends both on the ground state wave function and on the final state interactions as the integral of some "effective" distribution, $n_{eff}(k)$. As long as $n_{eff}(k)$ is still not very A dependent $G_{eff}(k_{min})$ will still retain its useful property as a "universal" scaling function, capable of describing quite different inclusive processes such as p-p scattering and $\bar{p}$ production.

Finally we conclude that all is well in this best of all possible worlds and that if it isn't, polarization and p,2p experiments will soon let us know what further we must do.

REFERENCES

1. S. Frankel, et al, Phys. Rev. Lett. 36, 642 (1976).

2. R. D. Amado and R. M. Woloshyn, Phys. Rev. Lett. 36, 1435 (1976).

3. R. D. Amado and R. M. Woloshyn, "Constraints on High Energy Scattering Amplitudes," to be published.

4. S. Frankel, Phys. Rev. Lett. 38, 1338 (1977).

5. H. Brody, S. Frankel, W. Frati, D. Yang, C. F. Perdrisat, J. C. Comiso, K. O. H. Ziock, "180° Production of Protons in High Energy p,d, and α Reactions in Nuclei", to be published. (UPR 0046N, Jan., 1977).

6. S. Frankel, W. Frati, G. Blanpied, G. Hoffman, T. Koslowski, C. Morris, M. Oothoudt, R. Ridge, H. A. Thiessen, O. VanDyck, C. Whitten, "Measurement of Differential Cross Sections in $p+A \to (p,d,t)+X$ from ^{6}Li to ^{181}Ta" (Submitted to International Conference on High Energy Physics and Nuclear Structure, Zurich, August, 1977).

7. D. R. F. Cochran, et al, LA-5083-MS, "Cross Sections for $p+\text{nucleus} \to \pi^+ -+$ for 740 MeV Protons," Informal Report, November, 1972.

8. H. Weber and L. D. Miller, preprint.

9. T. Fujita, accepted for Phys. Rev. Lett.

10. S. Frankel and R. M. Woloshyn, to be published.

11. R. D. Amado and R. M. Woloshyn, Phys. Lett. 62B, 253 (1976); R. D. Amado, Phys Rev. C 14, 1264 (1976); R. D. Amado and R. M. Woloshyn, Phys. Rev. C 15, 2200 (1977).

12. Amado and Woloshyn, "Constraints on High Energy Scattering Amplitudes", to be published.

APPENDIX A

R. D. AMADO AND R. WOLOSHYN MECHANISM FOR 180° PRODUCTION IN ENERGETIC PROTON-NUCLEUS COLLISIONS - PHYS. REV. LETT. 36, 1435 (1976)

Mechanism: Single Scattering of target nucleon by projectile $(p+A \to p'+q+S_k)$
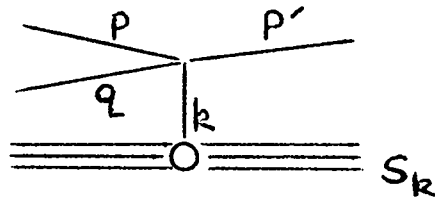
Assumptions:

a) Most states S_k have excitation energies ε that are low "compared with other energies in the problem" so that their excitation is neglected. Closure used to sum over final states.

b) Born approximation; no shadowing or final state interactions.

c) Assumes p-p matrix elements <u>slowly varying</u> so that in

$$\frac{d\sigma}{d^3q} = \frac{m^3_p}{pE_q} \frac{1}{2(2\pi)^3} \int \frac{d^3k}{E(\vec{p}+\vec{k}-\vec{q})} \; n_p(k)\Sigma|M_{pp}|^2 + n_n(k)\Sigma|M_{pn}|^2\delta[E_p+m_p-\bar{\varepsilon}-E_q-E(\vec{p}+\vec{k}-\vec{q})]$$

the matrix elements can be factored out of the integral and set equal to their on-shell values.

The momentum distributions $n_p(k)$ and $n_n(k)$ are normalized:

$$Z = 2\int\frac{d^3k}{(2\pi)^3} \; n_p(k) \qquad\qquad N = 2\int\frac{d^3k}{(2\pi)^3} \; n_n(k)$$

Momentum Distribution

Introduced new $n(k)$ $N_c/\cosh^2(\gamma_c k)$

Limiting (High k) Form $\simeq e^{-2\gamma_c k}$

<u>Calculations</u>

1) Used fits similar to those in E. J. Moniz et al. (Phys. Rev. Lett. <u>26</u>, 445 (1971) determining Fermi parameters for a <u>finite</u> temperature Fermi gas; fitted Frankel et al. data (Phys. Rev. Lett. <u>26</u>, 642 (1976) at 600 and 800 MeV for 180° production of protons.

2) Used same low energy quasi-elastic ee' data to determine N, γ and then attempted to predict Frankel et al. data, with <u>no</u> adjustable parameters.

<u>Conclusions</u>:

1) Conventional fit to Fermi gas gives cross-sections falling off <u>much</u> too rapidly and absolute value <u>much</u> too low.

2) New $n(k)$ falls off somewhat too slowly but correct order of magnitude and also gives roughly larger Ta than Cu and C cross-sections, as observed.

<u>Comments</u>:

This paper had courage to predict an entirely new $n(k)$ and gave crude fits to the data.

Amado and Woloshyn were exceedingly optimistic in attempting to suggest a single simple analytic function that would work for <u>both</u> the low momentum part of $n(k)$, in the Fermi gas region, and the high momentum part covered by the Frankel et al. data. First, these regions are probably quite different and not simply related. Second, a simple sinh or cosh function is too much to hope for. (This prompted Y. Alexander, E. F. Redish, and N. S. Wall, "Bound State Momentum Distribution" to re-examine data on p-p quasi-elastic scattering covering the same low momentum region covered in the e-e quasi elastic data. They concluded that the parameters N and γ, obtained from e-e, could not fit

the p-p data and that distortion effects had to be included to explain the p-p

data.) Thus we are not too surprised by the poor match to the high k data (γ

is wrong) A & W also attributed differences to $d\sigma/d^3q$ with A to differences

in γ. (These poor fits prompted S. Frankel (Phys. Rev. Lett. 38, (1977), to

extract n(k) from the data directly.)

QUASI-TWO BODY SCALING - A STUDY OF HIGH MOMENTUM COMPONENTS

IN NUCLEAR MATTER

S. Frankel, Phys. Rev. Lett. <u>38</u>, (1977)

<u>Method</u>   This paper started with the integrated form of the A & W equation

1) $$\frac{d\sigma}{d^3q} = C(p,k_{min}) \frac{G(k_{min})}{|\vec{p}-\vec{q}|}$$

2) $$G(k_{min})-G(k_{max}) = \int_{k_{min}}^{k_{max}} n(k)kdk \qquad [|\vec{p}-\vec{q}| \text{ comes from doing } \theta\text{- integration}]$$

(Since k_{max} is always $>> k_{min}$ the second turn is completely negligible up to within a few MeV of the elastic limit.)

3) $$C(k_{min},q) = C(s,t)$$

contains all the kinematic factors and information on the p-p elastic scattering cross section dσ/dt Frankel assumes C=1 throughout the paper.

The kinematic configuration for k is shown graphically below
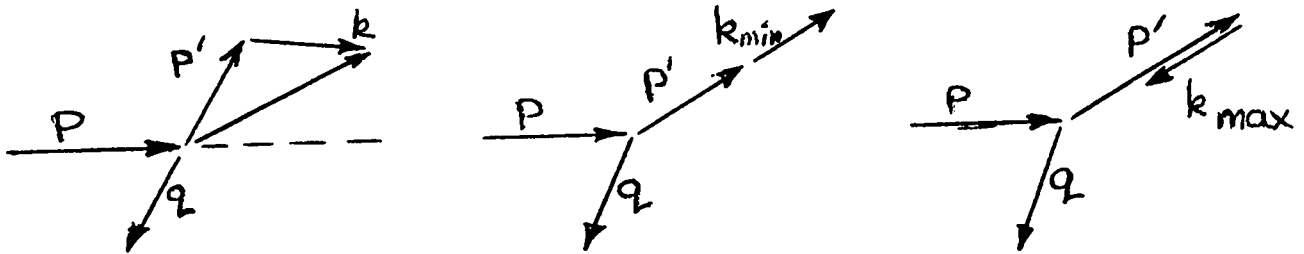
$$k_{min} = |\vec{p}-\vec{q}| - |\vec{p}'|$$

$$= \sqrt{p^2+q^2-2pq\cos\theta} - \sqrt{(Ep+m_p-\bar{\epsilon}-T(k)-Eq)^2-m_p^2}$$

Note that $T_k = \sqrt{k^2+m_{A-1}^2} - m_{A-1}$ is the kinetic energy of the recoiling nucleus $\bar{\epsilon}$ is the average energy of excitation.

(Note a) The closure approximation neglects the variations in ε and uses an

average $\bar{\varepsilon}$ for all final states. In consistency, we use this ε in

k_{min}; its effect is to produce a simple __shift__ dk $= \frac{\varepsilon E'}{p'}$ p' is relative)

so it can be largely ignored.

b) k_{min} is now a defined function of A (this was neglected by A & W).

Data Studied:

S. Frankel et al. LAMPF   600, 800 Gev p,d,t at 180°

P. Piroué et al. PPA   2.9 Gev p, d, t at 93°

Yu. D. Bayukov et al. (Soviet)   1.2-5.0 Gev p, d at 137°

Conclusions:

1) The A dependence in the shape of the cross section vanishes when k

is corrected for its dependence on A. Be...Ta have same G(k)

2) The magnitude of $d\sigma/d^2q$/nucleon now is independent of A

3) G(k) is a simple exponential $\approx e^{-k/k_o}$

MOMENTUM DISTRIBUTIONS IN THE NUCLEUS

R. D. AMADO AND R. M. WOLOSHYN

Physics Letters, 62B, 253 (1976)

Studies Form Factor F(q)

$$F(q) = \int \psi^2(r_1 \ldots r_A) e^{i\vec{q}\cdot\vec{r}} d^3 r_i \ldots A \, \delta(\Sigma r_i)/A$$

$$F(q) = \int \phi^*(k_1 \ldots k_A) \, \phi(\vec{k}_1 + \vec{q}, k_2 \ldots k_A) \, d^3 k_i \ldots \delta(\Sigma k_i)$$

Form factor is overlap between state ϕ and same state with one particle of

momentum k given the extra transfer $\vec{q}$.

Studies Momentum Distribution n(k)

$$n(k) = \int \phi^2(k, k_2 \ldots k_A) \, d^3 k_2 \ldots A^{\delta(\Sigma k_i)}$$

$$n(k) = \int \psi^*(\frac{r_1 + r'}{2} \ldots r_A) \, \phi(\frac{r_1 - r'}{2} \ldots r_a) e^{i\vec{k}\cdot\vec{r}} d^3 r_i \ldots A \, d^3 r' \delta(\Sigma r_i)/A$$

Form Factors are in assymptotic limit. Since form factor describes probability

of k+q remaining inside nucleus, A-1 nucleons must acquire momentum -q, each

q/A; this takes A-1 scatterings, i.e. A-1 interactions of Schrodinger equation.

Starts with homogeneous Schrodinger equation

$$\chi = -\frac{1}{B + q^2/2m} V\chi = -G_0 V\chi$$

for $B \ll q^2/2m$ - $G_0 \to \frac{1}{q^2}$

$$F(q) \simeq (\frac{\tilde{v}(q)}{q^2})^{A-1} \qquad \tilde{v} \text{ is Fourier transfer of V in scattering.}$$

This is a polynomial fall off, A dependent. Pauli principle and form of $\tilde{v}$ changes actual fall off. By large momentum we mean q/A very large. In study of high momentum elastic scattering, even in ^{6}Li $q/A \leq \frac{2 \text{ Gev/c}}{6} \simeq .3$ Gev/c. This theory then predicts large differences in ^{6}Li and ^{181}Ta form factors. Form Factor q/A not large. To study this use one dimensional model δ function interaction between pairs, go still $\simeq \frac{1}{q^2}$ in this model.

$$F(q) = \prod_{n=1}^{A-1} (1 + \frac{q^2}{q_0^2 r^2})^{-1} \qquad\qquad q/A \gg q_0$$

$$F(q) = \frac{\pi q}{q_0} \sinh^{-1} \frac{\pi q}{q_0} \rightarrow q e^{-q/q_0} \qquad\qquad q/A \ll q_0$$

Particle Momentum Distribtution

Similar arguments n(k) - Since only one other nucleon needs to recoil with -k

for very high p only one iteration $[\frac{\tilde{v}(k)}{k^2}]$

Cannot solve exact equation but Hartree solution obtain

$$n(k) = N/\cosh^2 q/Q_0 \rightarrow N e^{-2q/q_0}$$

Conclusions: There are now three regions in n(k)

1) Fermi-gas region - region of low energy nuclear physics <k = .2 Gev/c determined by "average" nuclear potential details of low lying states n(k) for each bound state known up to .2 Gev/c.

2) Experimental Region - Region of "coherent recoil"

3) Assymptotic region "polynomial tail" k>k critical.

Comments

Key theoretical questions: what is size of k_{crit}

what is physical basis for k_{crit}

Important experimental questions: can the assymptotic region be observed?

what is k_{crit} and A dependence?

FUJITA "CORRELATED CLUSTERS" AND INCLUSIVE SPECTRA OF ENERGETIC PROTONS AT 180° IN PROTON NUCLEUS COLLISIONS (PREPRINT)

<u>Model</u>: Proton elastically scatters from a quasi cluster having internal momentum distribution

Problem of finding cluster: $G_N = \binom{A}{N} \dfrac{1}{A^{N-1}} \left(\dfrac{V_c}{V}\right)^{N-1} \xi$

Combinations

Prob. within
correlated vol.

Sticking prob.

$$\frac{d\sigma}{d^3q} = \sum_N G_N \frac{1}{pE_q E_{cc} Nm_p} |M_{p+cc}|^2 \overline{W_N(k)} \frac{d^3k}{(2\pi)^3} \frac{1}{8\pi^2} \delta[E_p + Nm_p - E_q - E_{cc} - \bar\varepsilon]$$

$$E_{cc} = \sqrt{(Nm_p)^2 + (\vec{p}+\vec{k}-\vec{q})^2} = \sqrt{(Nm_p)^2 + p_{cc}^2}$$

E_q detected, E_p incident, E_{cc} recoil cluster.

Used p-p elastic cross section to replace p-N, i.e., p-cluster elastic cross

section. Finds $V_c \to \ell_c = .6$ fermi where mean ℓ used for $V = 1.4$ f.

$\xi = 1$ to fit data, no breakup of cluster

use $W_n(k) = \left(\frac{4\pi}{N\nu}\right)^{3/2} e^{-k^2/N\nu} \qquad \nu = .84 \ f^{-2}$

ie Gaussian internal momentum distribution of cluster with fall-off N-dependent

(this comes from Gaussian wavefunction).

<u>Results</u>:

Fits 180° data only with N = 1,2,3,4

C, Cu, Ta   600 MeV   Ta 800 MeV

claims dependence on E_p given correctly by model but not by A & W.

Comments:

1) Only tested at 180° should have tested at 90°; why not deuterons?

2) Elastic p-cc = p-p clearly wrong; if cluster does stick together (ξ = 1) this cannot be true, and p-cc dσ cannot track p-p with energy.

3) Extends A & W to 1.4 GeV where it doesn't apply and misinterprets it.

NUCLEAR STRUCTURE FROM PION-NUCLEUS SCATTERING [†]

George Walker

Department of Physics
Indiana University

I. INTRODUCTION

The study of nuclear structure usually implies the testing of the validity of various proposed nuclear models by comparison with experiment. Current well-established pictures such as the shell and collective models concentrate on different nuclear degrees of freedom. The predictions of these models with respect to ground state properties, excitation energies, and transition rates have been studied extensively for the past two - three decades using projectiles whose reaction mechanism with the nucleus is "better understood" than the pion-nucleus interaction. In such a situation how can one expect that the pion can contribute significantly to our knowledge of nuclear structure? Isn't it more likely that our present knowledge of nuclear structure will aid in clarifying some details of pion-nucleus reaction mechanisms? The answer to the second question is probably yes, initially, but after using structure information available from other sources to study the pion-nucleus interaction, the pion can be used to obtain information about the nucleus not easily obtainable from other probes.

Inelastic scattering and charge exchange are examples of reactions that should allow one, at an early stage, to study both nuclear structure and the pion-nucleus reaction mechanism in separable way. It is important, from the beginning, to compare results of pion-nucleus inelastic scattering with results obtained from electron and proton inelastic scattering to the same final nuclear states. Pion-nucleus inelastic scattering and charge exchange experiments are more sensitive to the details of the pion-nucleus reaction mechanism than elastic scattering and so the reaction mechanism can be studied by comparison

with other inelastic scattering experiments involving more thoroughly studied probes. In addition, because of the particular kinds of states predicted to be strong in the nuclear response to the pion some additional states of interest to structure theorists may be located for the first time.

In the next section the theoretical formalism for inelastic scattering is discussed and the current calculational procedures and uncertainties are summarized. In section III a brief summary of selected theoretical results obtained by various groups is given. In this section are also included some studies of the sensitivity of the results to changes in variation of the input parameters in the formalism. In the final section the pion predictions are compared with inelastic scattering results for electron, proton, and kaon (plus) projectiles.

Before ending this introductory section, we wish to encourage those models of the nucleus and reaction mechanism formalisms which introduce ex-plicitly meson degrees of freedom and nucleon isobars. Of course such models contain many uncertainties associated with the appropriate vertex functions in the many-body environment. However, particularly at intermediate energies, such approaches appear quite natural in terms of accentuating unfamiliar but perhaps central degrees of freedom (such as intermediate or pre-existing Δs). As with other more established models, experiments using several probes can be used to provide input parameters for the meson-baryon couplings. Such models may bring us closer to a "fundamental theory" of the nuclear many body problem involving a relativistic field theory of interacting mesons and baryons.

II. INELASTIC SCATTERING

The differential cross section for inelastic scattering (o →n) in the distorted wave impulse approximation is given by

$$\frac{d\sigma_{no}}{d\Omega} = \frac{(2\pi)^4}{\hbar^4} \frac{E_\pi(k_i)E_A(k_i)E_\pi(k_f)E_A(k_f)}{[E_\pi(k_i) + E_A(k_i)][E_\pi(k_f) + E_A(k_f)]} \frac{k_f}{k_i} |T_{no}(\underset{\sim}{k}_f, \underset{\sim}{k}_i)|^2 \tag{1}$$

where k_i and k_f are the initial and final relative momenta.

The transition matrix for the inelastic process $T(\underset{\sim}{k}_f, \underset{\sim}{k}_i)$ can be written symbolically as

$$T_{no} = \int \chi^+_{E_\pi(k_f)} \Phi^+_n \, t \, \chi_{E_\pi(k_i)} \Phi_o \tag{2}$$

where $\chi_{E_\pi(k_i)}$ ($\chi^+_{E_\pi(k_f)}$) is the initial (final) distorted wave function for the pion, Φ_o and Φ_n are the initial and final many body nuclear wave functions, respectively, and t is the transition operator. In general the transition operator is a function of both the pion and nucleus co-ordinates. Its particular form may vary depending, for example, on whether the nuclear degrees of freedom are expressed in terms of single nucleon or collective variables.

The nuclear structure information is contained directly in Φ_n and Φ_o and to a certain degree in t itself. Before proceeding to compare theory and experiment for inelastic scattering with the goal of obtaining information about Φ_n and Φ_o one must have confidence in the basic assumptions and other input parameters in the DWIA. Questions that need to be investigated are

1) The adequacy of a one step theory. To what extent is a coupled channel or multistep reaction mechanism necessary?

2) The appropriateness of the distorted waves adopted. How sensitive is $\frac{d\sigma}{d\Omega}$ to different distorted waves giving equivalent fits to elastic scattering?

3) Is the free t a reasonable form to choose for the transition operator? How sensitive are the results to the particular off-shell extrapolation chosen for t? How do binding, Pauli-blocking and other effects of the many-body environment modify t and thus yield different results for the inelastic scattering?

Later in this talk we shall present some results indicating the sensitivity of the inelastic scattering predictions to some of the uncertainties mentioned above.

If the nuclear wavefunctions are described in terms of collective degrees of freedom as in the rotational model then a macroscopic approach is used to obtain the transition operator and the differential cross section. This procedure is often used to study the low-lying $T = 0$ normal parity states in nuclei such as ^{12}C. Most of the available experimental data on inelastic scattering is for just such states because of their strong excitation and separation from other excited states.

A summary of the approach using collective degrees of freedom follows. One begins with the familiar form for the pion-nucleus optical potential

$$V(r) = \frac{\hbar^2 c^2}{2E} \{-Ab_0 k^2 \rho(r) + Ab_1 \underset{\sim}{\nabla} \cdot [\rho(r)\underset{\sim}{\nabla}]\}$$

(3)

where b_0 and b_1 contain the S and P wave pion-nucleon input data, A is the number of nucleons and ρ is the nuclear density. In general the potential would have spin and isospin dependent terms. The form shown is appropriate for a $J = T = 0$ ground state. The effect of deformation is provided by writing $\rho(r,a) \to \rho(r,a(\theta))$ where

$$a(\theta) = a_0 [1 + \underset{LM}{\Sigma} \beta_L Y_M^L (\theta)]$$

(4)

The deformation parameter, β_L, is the basic parameter of "nuclear structure" to be determined from experiment. Using a Taylor series expansion allows one to obtain

$$\rho(r,a) = \rho(r,a_0) + \underset{LM}{\Sigma} \beta_L F(r)Y_M^L(\theta)$$

(5)

where

$$F(r) = a[\frac{\partial \rho}{\partial a}]_{a_0}$$

(6)

The density, $\rho(r,a)$, given by eq. (5), is inserted into the expression, eq. (3) for $V(r)$. The potential, $V(r)$, is then used for both elastic and inelastic scattering. We have

$$V(r) = V°(r) + \sum_{LM} V'_{LM}(r,\theta)$$

(7)

where

$$V'_{LM}(r,\theta) = \beta_L \frac{\hbar^2 c^2}{2E} \{-Ab_0 k^2 F(r) Y^L_M(\theta) + Ab_1 \underset{\sim}{\nabla} \cdot [F(r) Y^L_M(\theta) \underset{\sim}{\nabla}]\}$$

(8)

As an example, consider the transition from a $J = 0$ ground state to a non-spin-flip state where $J = L$. Then one obtains

$$T_{LM,00} = \int d^3 r \, \chi_f^{(-)}(k_f,r) <LM|V'|00> \chi_i^{(+)} (k_i,r)$$

(9)

where

$$<LM|V'|00> \simeq \beta_L \{-b_0 k^2 F(r) Y^{L*}_M(\hat{r}) + b_1 \underset{\sim}{\nabla} \cdot [F(r) Y^{L*}_M(\hat{r}) \underset{\sim}{\nabla}] \}$$

(10)

Edwards and Rost [1] carried out calculations of this type for 120-280 MeV inelastic pion scattering on ^{12}C leading to the lowest 2^+ and 3^-, T = 0 states. They found that, except at large angles, their calculation give good agreement with experiment for a value of $\beta_L \simeq .55$ which was consistent with results obtained using other probes. More recently Sparrow [2] has used the collective model approach to study the sensitivity of inelastic scattering results to the inclusion of spin-flip and to the difference in the neutron and proton matter density for ^7Li. Sparrow found that, in general the results were not sensitive to the inclusion of the spin-flip amplitude. The most significant sensitivity (roughly 50% changes) was obtained for the neutron-proton matter density studies for charge exchange transitions to non-analogue states. The collective model has been most recently used to compare predictions with the 50 MeV data on ^{12}C leading to the ground state, 2^+ (4.44 MeV), and 3^- (9.64 MeV) states. [3] If free pion-nucleon input parameters for b_0 and b_1 are adopted, along with

standard values of β_2 and β_3 there is considerable disagreement between theory and experiment.[3] However, using the same deformation parameters, if one uses phenomenological values of b_0 and b_1 fitted to the elastic 50 MeV data, acceptable agreement between theory and experiment is obtained.[3] By including second order terms arising from the Pauli exclusion principle, and short range correlations as well as true pion absorption other authors (see the lectures by G. Brown and B. Jennings at this Summer School) have shown that acceptable agreement between theory and experiment is possible using micro-scopically motivated parameters in the transition potential.[4,5,6]

Several researchers have studied inelastic scattering using single nucleon degrees of freedom (the shell model).[7-10] In these studies a large number of final nuclear excited states have been considered. In the following the procedures and results are briefly summarized. The single-nucleon transition operator is needed, in general, in a region of kinematic variables not given by the free pion-nucleon amplitude. One way of circumventing this difficulty is to assume a separable transition operator of the form

$$t_{E(k_i)}(k', k) = \sum_{\substack{lm \\ \mathscr{J}\mathscr{T}}} P_{l\mathscr{J}} P_{\mathscr{T}} \, t^E_{l\mathscr{J}\mathscr{T}}(k', k) \frac{4\pi}{2l+1} Y^*_{lm}(\Omega_{k'}) Y_{lm}(\Omega_k),$$

where (11)

$$\frac{2l+1}{4\pi} t^{E(k_i)}_{l\mathscr{J}\mathscr{T}}(k', k) = \frac{(\lambda_{l\mathscr{J}\mathscr{T}}/2\pi^2) v_{l\mathscr{J}\mathscr{T}}(k) v_{l\mathscr{J}\mathscr{T}}(k')}{1 + [\lambda/(2\pi)^3] \int v^2_{l\mathscr{J}\mathscr{T}}(t) dt/[E(t) - E(k_i) - i\varepsilon]}$$

(12)

The separable form factor, $v_{l\mathscr{J}\mathscr{T}}(k)$, may be obtained, under certain conditions from a knowledge of the complex fixed-scatterer phase shift, $\delta_{l\mathscr{J}\mathscr{T}}(k)$ at all energies via the relation

$$\lambda_{l\mathscr{J}\mathscr{T}} v^2_{l\mathscr{J}\mathscr{T}}(k) = \frac{-4\pi\hbar^2 \sin\delta_{l\mathscr{J}\mathscr{T}}(k)}{2kE(k)} \exp\left[\frac{-1}{\pi} P \int_0^\infty \frac{\delta_{l\mathscr{J}\mathscr{T}}(t) t \, dt}{E(t) - E(k)} \frac{\hbar^2}{E(t)}\right]$$

(13)

The general form of the transition operator can be written as

$$t_L^{\frac{1}{2}}(k',k) = \sum_{l,m} \frac{4\pi}{(2l+1)^2} \left(\left[\tfrac{1}{3}(l+1)\{ t_{l,\mathcal{J}=l+\frac{1}{2},\mathcal{J}=\frac{1}{2}}(k',k) + 2t_{l,\mathcal{J}=l+\frac{1}{2},\mathcal{J}=\frac{1}{2}}(k',k)\} \right. \right.$$

$$+ \tfrac{1}{3}l\{ t_{l,l-\frac{1}{2},\frac{1}{2}}(k',k) + 2t_{l,l-\frac{1}{2},\frac{1}{2}}(k',k)\} \right] + \left[\tfrac{1}{3}(l+1)\{ t_{l,l+\frac{1}{2},\frac{1}{2}}(k',k) - t_{l,l+\frac{1}{2},\frac{1}{2}}(k',k)\} \right.$$

$$+ \tfrac{1}{3}l\{ t_{l,l-\frac{1}{2},\frac{1}{2}}(k',k) - t_{l,l-\frac{1}{2},\frac{1}{2}}(k',k)\} \right] I \cdot \tau$$

$$+ \tfrac{1}{3}[2t_{l,l+\frac{1}{2},\frac{1}{2}}(k',k) + t_{l,l+\frac{1}{2},\frac{1}{2}}(k',k) - 2t_{l,l-\frac{1}{2},\frac{1}{2}}(k',k) - t_{l,l-\frac{1}{2},\frac{1}{2}}(k',k)]\sigma \cdot L_\pi$$

$$+ \tfrac{1}{3}[t_{l,l+\frac{1}{2},\frac{1}{2}}(k',k) - t_{l,l+\frac{1}{2},\frac{1}{2}}(k',k) - t_{l,l-\frac{1}{2},\frac{1}{2}}(k',k) + t_{l,l-\frac{1}{2},\frac{1}{2}}(k',k)](I \cdot \tau)(\sigma \cdot L_\pi))$$

$$\left. \times Y_{lm}^*(\Omega_{k'}) Y_{lm}(\Omega_k). \right.$$

(14)

Eq. (14) makes manifest the spin and isospin dependence of the pion-nucleon transition operator. We now assume a closed shell nuclear ground state and a final nuclear configuration mixed particle-hole state. It is standard to make a partial wave decomposition of the momentum space distorted waves and to express the pion partial wave functions in terms of spherical Bessel functions using the procedure discussed in reference 11. Adopting the assumptions and techniques summarized above allows one to write the square of the transition amplitude as

$$\frac{1}{(2\pi)^6} \frac{2}{9} \sum_{J_z} \left| \sum_{j_p j_h} \alpha_{j_p j_h} \sum_{\substack{l\ l_3 l_4 \\ l' l n n' \\ m'm}} a^*_{n'l'} a_{nl} \begin{pmatrix} l & l_3 & l' \\ 0 & 0 & 0 \end{pmatrix} \begin{pmatrix} l & l_4 & l \\ 0 & 0 & 0 \end{pmatrix} (-1)^l \right.$$

$$\times [(2l_3+1)(2l_4+1)][(2l+1)(2l'+1)(2J+1)]^{\frac{1}{2}}[(2j_p+1)(2j_h+1)(2l_p+1)(2l_h+1)]^{\frac{1}{2}}(i)^{l_3-l_4}$$

$$\times \left[\begin{pmatrix} J & l_3 & l_4 \\ 0 & 0 & 0 \end{pmatrix} \begin{Bmatrix} l_p & j_p & \frac{1}{2} \\ j_h & l_h & J \end{Bmatrix} \begin{pmatrix} l_p & l_h & J \\ 0 & 0 & 0 \end{pmatrix} (-1)^{j_h+\frac{1}{2}} \begin{Bmatrix} J & l & l' \\ l & l_3 & l_4 \end{Bmatrix} [A_{\Delta T=0}^{\Delta S=0} + B_{\Delta T=1}^{\Delta S=0}] \right.$$

$$+ \sqrt{6} \sum_{\bar{J}} \begin{pmatrix} J & l_3 & l_4 \\ 0 & 0 & 0 \end{pmatrix} \begin{Bmatrix} l_p & \frac{1}{2} & j_p \\ l_h & \frac{1}{2} & j_h \\ \bar{J} & 1 & J \end{Bmatrix} (2\bar{J}+1)(2l+1)^{\frac{1}{2}} \begin{pmatrix} l_p & l_h & \bar{J} \\ 0 & 0 & 0 \end{pmatrix} (-1)^{l_p}$$

$$\left. \times \begin{Bmatrix} l & l_4 & l \\ l & l_3 & l' \\ 1 & \bar{J} & J \end{Bmatrix} [C_{\Delta T=0}^{\Delta S=1} + D_{\Delta T=1}^{\Delta S=1}] \right] \int x^2 dx\, R_{l_p}(x) R_{l_h}(x) j_{l_3}(k_{\pi'} x) j_l(k_{nl} x)$$

$$\times \left[(-1)^{m'} \begin{pmatrix} J & l & l' \\ -J_z & -m & m' \end{pmatrix} Y_{l'm}(\Omega_{k'}) Y_{lm}^*(\Omega_{k_l}) \right]^2 ,$$

(15)

where

$$A_{\Delta T=0}^{\Delta S=0}(k',k) \equiv [l\alpha + (l+1)\beta] + 2[l\gamma + (l+1)\delta],$$

(16a)

$$B^{\Delta S=0}_{\Delta T=1}(\ell',\ell) \equiv \left[l\alpha+(l+1)\beta\right]-\left[l\gamma+(l+1)\delta\right],$$

(16b)

$$C^{\Delta S=1}_{\Delta T=0}(\ell',\ell) \equiv \left[^-\sqrt{l(l+1)}\alpha+\sqrt{l(l+1)}\beta\right]+2\left[^-\sqrt{l(l+1)}\gamma+\sqrt{l(l+1)}\delta\right],$$

(16c)

$$D^{\Delta S=1}_{\Delta T=1}(\ell',\ell) \equiv \left[^-\sqrt{l(l+1)}\alpha+\sqrt{l(l+1)}\beta\right]-\left[^-\sqrt{l(l+1)}\gamma+\sqrt{l(l+1)}\delta\right],$$

(16d)

where

$$\alpha \equiv f^k_{\substack{\mathscr{J}=\frac{1}{2}\\ \mathscr{J}=l-\frac{1}{2}}}(\ell',\ell),\quad \beta \equiv f^k_{\substack{\mathscr{J}=\frac{1}{2}\\ \mathscr{J}=l+\frac{1}{2}}}(\ell',\ell),\quad \gamma \equiv f^k_{\substack{\mathscr{J}=\frac{3}{2}\\ \mathscr{J}=l-\frac{1}{2}}}(\ell',\ell),\quad \delta \equiv f^k_{\substack{\mathscr{J}=\frac{3}{2}\\ \mathscr{J}=l+\frac{1}{2}}}(\ell',\ell).$$

(17)

The off-shell transition operator f(k',k) is assumed to have the separable form

$$f^k_{l\mathscr{J}\mathscr{T}}(\ell',\ell) = \frac{v_{l\mathscr{J}\mathscr{T}}(\ell')v_{l\mathscr{J}\mathscr{T}}(\ell)}{v^2_{l\mathscr{J}\mathscr{T}}(k)}f^k_{l\mathscr{J}\mathscr{T}},\qquad f^k_{l\mathscr{J}\mathscr{T}} \equiv \frac{e^{i\delta_l}\sin\delta_l(k)}{\pi kE(k)}\hbar^2$$

(18)

where $f^k_{l\mathscr{J}\mathscr{T}}$ is the fixed scatterer on-shell pion-nucleon scattering amplitude and the off shell form factors, the $v(k)$ are obtained from the phase shifts via eq. (13). The $\alpha_{j_p j_h}$ are the admixture amplitudes of the pure particle-hole states obtained for the configuration mixed particle-hole state. The a_{nl} are the expansion coefficients for the Bessel function expansion of the pion distorted waves. The ΔS and ΔT labels on A to D indicate the S and T values of the final nuclear state reached via that part of the transition operator assuming a major closed shell ground state. The expressions A through D are very convenient for estimating the relative size of cross sections for various final nuclear states. For example, if the P_{33} phase shift is the only non-negligible contributor in a given region of energy, inspection of C and D allows one to predict that $\Delta S = 1$, $\Delta T = 0$ states will be approximately four times stronger in the nuclear excitation spectrum than $\Delta S = 1$, $\Delta T = 1$ states. We shall see presently that detailed calculations support this simple estimate. In the next section results are presented using the formulae and procedures given in this section.

III. CALCULATIONAL RESULTS AND STUDIES OF UNCERTAINTIES

In figures 1 and 2 results are presented for (π,π') on ^{16}O at 69.5 and 180 MeV respectively.[10] The details of the calculations including the residual interaction used for diagonalizing the particle-hole states and the pion optical potential parameters are given in reference 10. In figures 1 and 2 solid lines denote T = 1 states and dashed lines represent T = 0 states. For both pion energies the calculations predict that at forward angles (low momentum transfer) the T = 1, $J^\pi = 1^-$, giant dipole state will dominate the spectrum. At higher values of the momentum transfer high spin 3^- and 4^- states are predicted to dominate the spectrum. (This result simply reflects the fact that larger angular momentum transfers L are dominant for large momentum transfer q $[L \approx qR_{nuc}]$. Similar results have been noted earlier in inelastic electron scattering.[12-14] As will be discussed in the next section the high spin 4^-, T = 0 state predicted to be dominant at high q for pions is not strongly excited in electron and kaon inelastic scattering but does show up in inelastic proton scattering due to exchange effects. The location of such states, because of their spin and isospin character, is of considerable interest in nuclear structure physics. (Note that the predicted 4:1 ratio for the 4^-,T = 0 to 4^-, T = 1 cross section is essentially reproduced in the detailed calculations.) We have recently found that this ratio is quite insensitive to appreciable variations in the P_{33} amplitude.

The sensitivity of predictions to the optical potential used to generate the distorted waves has been the subject of considerable study. In figure 3 typical results[8,15] are shown and compared with experimental data for 150 MeV inelastic scattering to the 2^+ (4.43 MeV) and 3^- (9.64 MeV) states of ^{12}C. The solid curve was generated using distorted waves derived from a momentum space optical potential due to Landau and Tabakin while the dashed curve was
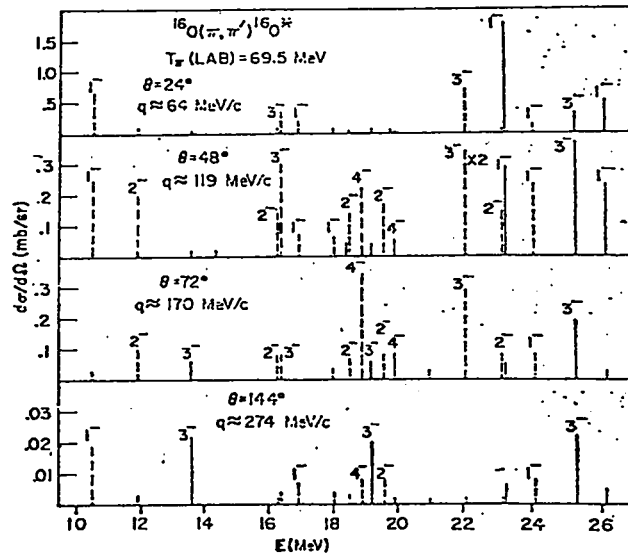
Fig. 1 Pion - ^{16}O inelastic scattering differential cross sections as a function of the final nuclear excitation energy E. The initial lab kinetic energy of the pion T_π(lab) is 69.5 MeV. The differential cross sections are shown for four different scattering angles (momentum transfers). Solid lines correspond to T = 1 final nuclear excited states while T = 0 states are represented by dotted lines. The spin and parity J^π of the more prominently excited states is indicated. Only states with appreciable cross sections are included. (Figure taken from ref. 18).
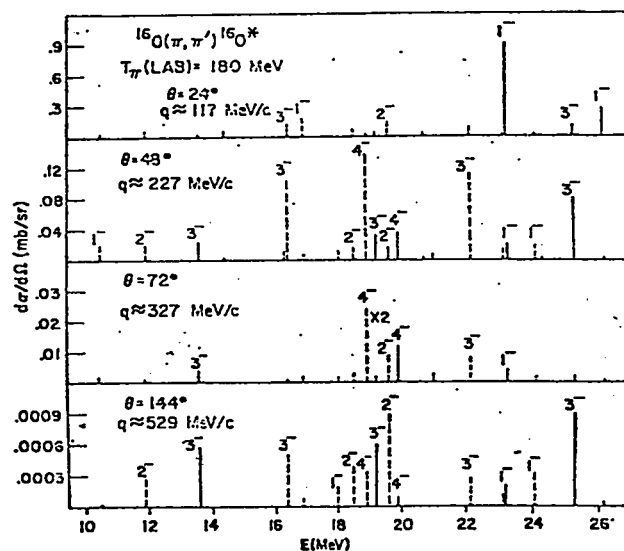

Fig. 2 Inelastic scattering cross sections as in fig. 1 except T_π(lab) is 180 MeV. (Figure taken from ref. 18).

- 252 -

obtained using a Laplacian optical potential. The data is from reference 17.
In figures 4 and 5 results obtained[18] using a Kisslinger optical potential
(solid line) and the Laplacian optical potential (dashed line) are compared
for a 3^-, T = 0 state and the 4^-, T = 0 state predicted to be dominant at large
momentum transfer in ^{16}O. The results of these studies indicate that while
the predictions do vary at large angles depending on the optical potential
adopted, the variations are not large and do not qualitatively change the shape
of the angular distribution. Of course a plane wave calculation is not suf-
ficient, some optical potential definitely must be used primarily because of
the large absorptive part of the optical potential. The typical effect of
absorption is shown for the 4^-, T = 0 state in figure 6 where a plane wave
calculation (dashed line) is compared with a distorted wave calculation (solid
line). The DWIA calculation is smaller by about an order of magnitude, near
the cross-section peak, than the PWIA prediction.

One of the major uncertainties in inelastic scattering calculations is
the appropriate form for the required off-shell pion-nucleon t matrix. Three
standard forms are

$$< k' \, |t(\tilde{w}_0)| \, k> = a(\tilde{w}_0) + b(\tilde{w}_0)\underset{\sim}{k}' \cdot \underset{\sim}{k}$$

(Kisslinger Model) $\qquad\qquad$ (19a)

$$= a'(\tilde{w}_0) + b'(\tilde{w}_0)(\underset{\sim}{k}'-\underset{\sim}{k})^2$$

(Laplacian Model) $\qquad\qquad$ (19b)

$$= \underset{\alpha}{\Sigma} \, < k_0 \, |t(w_0)| \, k_0> \frac{g_\alpha(k')g_\alpha(k)}{g_\alpha^2(k_0)}$$

(separable model) $\qquad\qquad$ (19c)

The sensitivity of the inelastic scattering predictions for the 2^+ (4.43 MeV)
state in ^{12}C is shown in figure 7 for the three off-shell t matrices given by
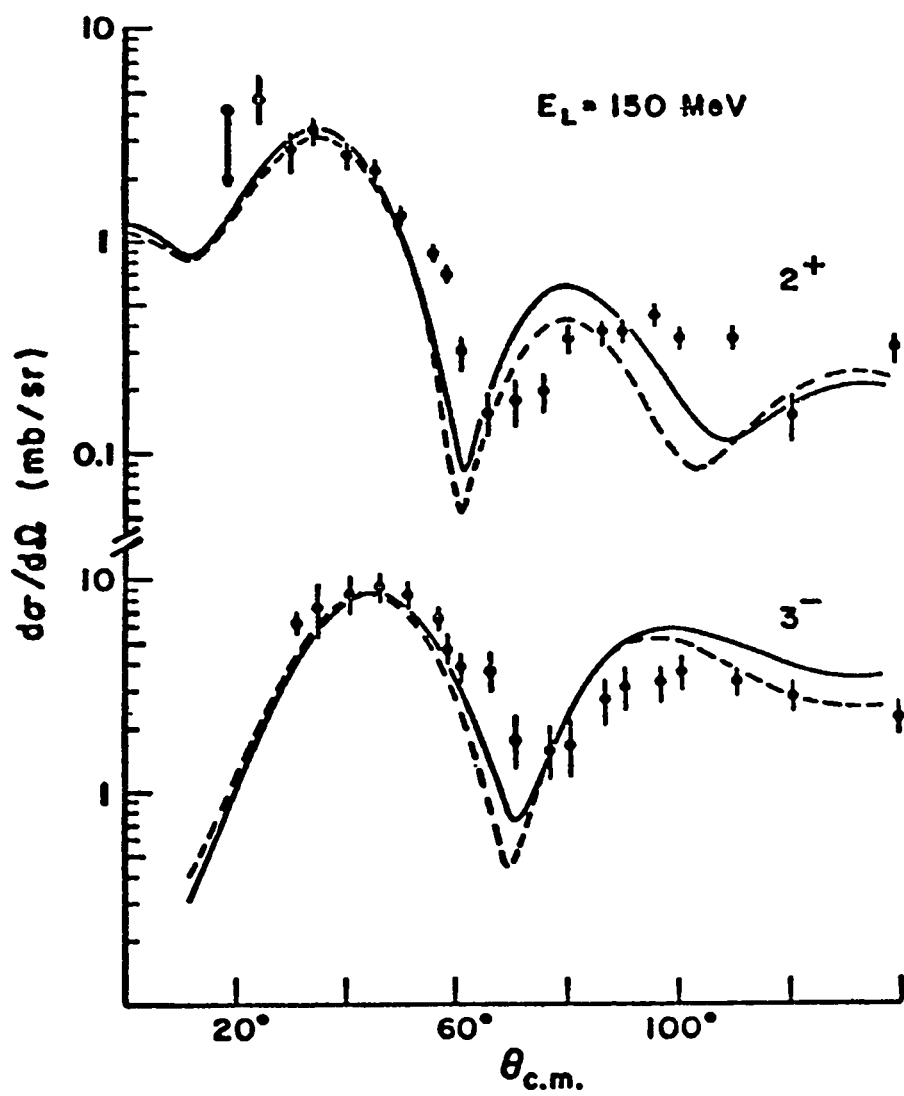eq. (19). The Landau-Tabakin separable form factor was used to generate the

Fig. 3   Pion - ^{12}C inelastic scattering cross sections using the same pion-nucleus transition potential but different distorted waves. The solid curve (dashed curve) uses distorted waves generated from the Landau-Tabakin momentum space optical potential (Laplacian optical potential). (Figure taken from ref. 15).
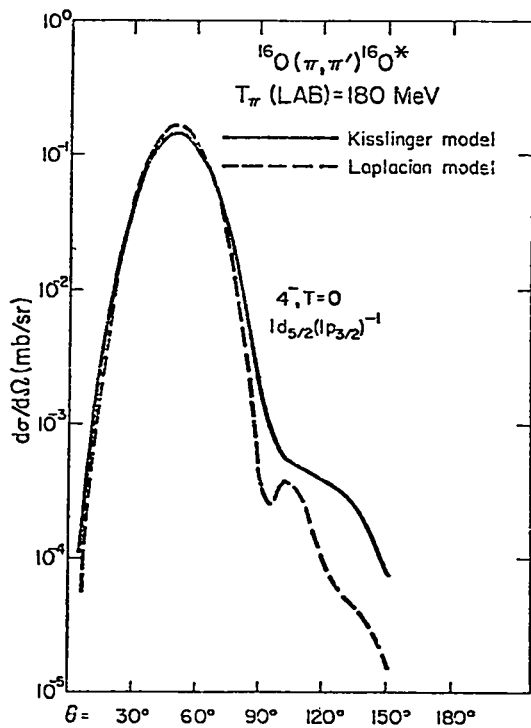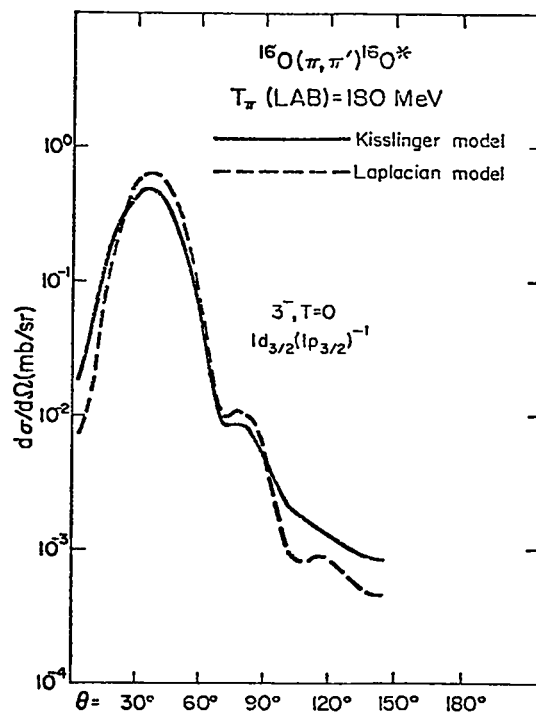
Figure 4

A comparison of the pion - ^{16}O inelastic scattering angular distribution for the 4^-, T = 0, $1d_{5/2}(1p_{3/2})^{-1}$ final nuclear state calculated using distorted waves generated from the Kisslinger optical potential (solid line) and the Laplacian optical potential. (Figure taken from ref. 18).

Figure 5

Same as figure 4 except the comparison is shown for inelastic scattering leading to a pure particle-hole 3^-, T = 0, $1d_{3/2}(1p_{3/2})^{-1}$ final nuclear state.
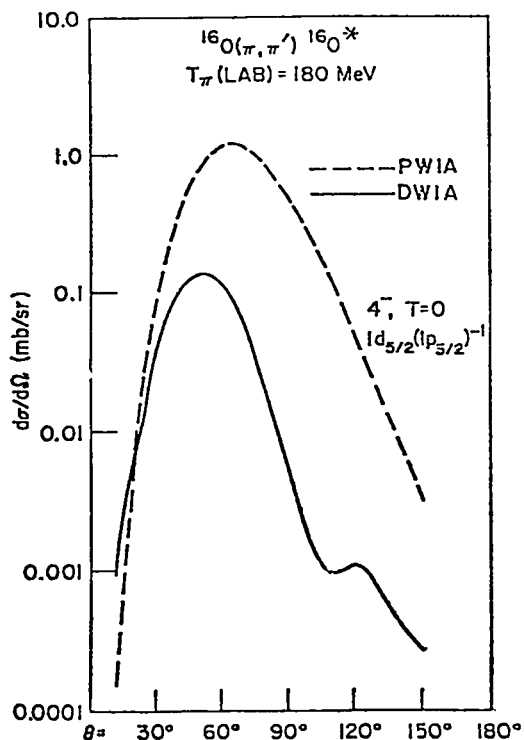
Figure 6

A comparison of the pion - ^{16}O inelastic scattering angular distribution for the 4^-, T = 0, $1d_{5/2}(1p_{3/2})^{-1}$ final nuclear state calculated in the plane wave impulse approximation (dotted line) and in the distorted wave impulse approximation (solid line). (Figure taken from ref. 18).
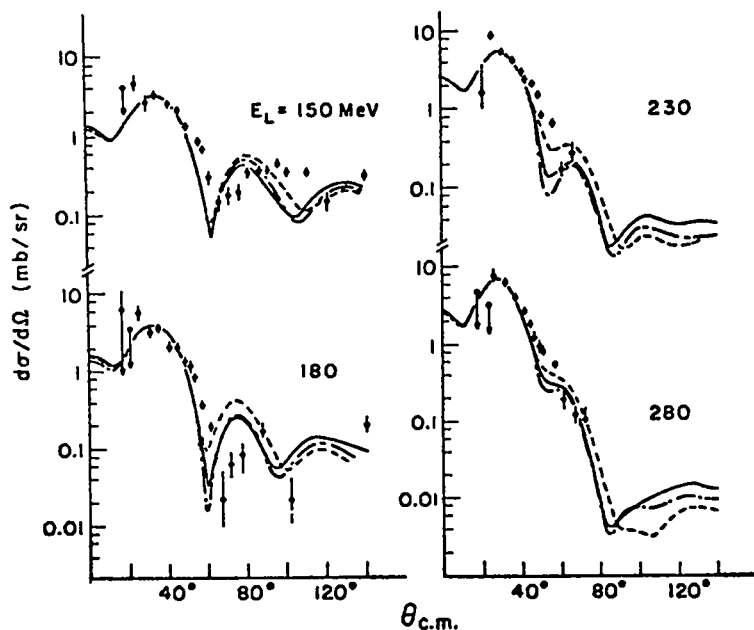
Fig. 7   The sensitivity of inelastic scattering to different forms for the pion-nucleon off-shell transition matrix. The three transition potentials are constructed using the same 2^+ (4.43 MeV) collective rotational form factor but three different off-shell models of the pion-nucleon collision matrix. The pion-nucleon off-shell models used are the Landau-Tabakin (solid curve), the Kisslinger (dashed curve), and the Laplacian (dashed-dot curve) extrapolations. (Figure taken from ref. 15).

- 256 -

solid curve, the Kisslinger form factor generated the dashed curve, and the Laplacian model generated the dashed-dot curve.[8,15] The results indicate that at large angles there can be 50% difference in the predictions depending on the off-shell extrapolation adpoted. However up to the first minimum in the differential cross section the predictions are quite similar.

Changes in the effective shape of the nuclear form factor given in the collective model can cause more significant changes in the inelastic predictions than the uncertainties discussed above. The effect of changing the peak of the form factor, $F(r)$, by .5 fermi is shown in figure 8[8,15]. The solid (dashed) curve is obtained by using the original 2^+ collective rotational form factor (shifting the form factor by substituting $F(r + .5F)$ for $F(r)$).

In general we find that the sensitivity of calculations to the ambiguities in the appropriate distorted waves and off-shell pion nucleon t matrix is not severe and thus for example, the pion can be used as a probe for studying high spin $T = 0$ states in nuclei.

Charge exchange (π^-, π^0) experiments may be useful for locating the $T_>$ giant dipole states in $T \neq 0$ nuclei. The results of a typical charge exchange calculation for ^{48}Ca is shown in figure 9. Details of the calculation are given in reference 10. Because $|T_z|$ increases by one in the process only the $T_>$ states are present in the spectrum. For ^{48}Ca the $T_>$ dipole resonance states with non-spin-flip strength concentrated near 11 MeV are predicted to be prominent at low momentum transfer. At large momentum transfer high spin states dominate as usual.

It is difficult to identify the $T_>$ states in inelastic scattering and therefore charge exchange reactions of the type (n,p), $(\mu^- + p_{nuc} \to \nu + n_{nuc})$, and (π^-, π^0) are motivated. By doing pion charge exchange on nuclei like ^{12}C where there is considerable data from other probes one can eliminate some
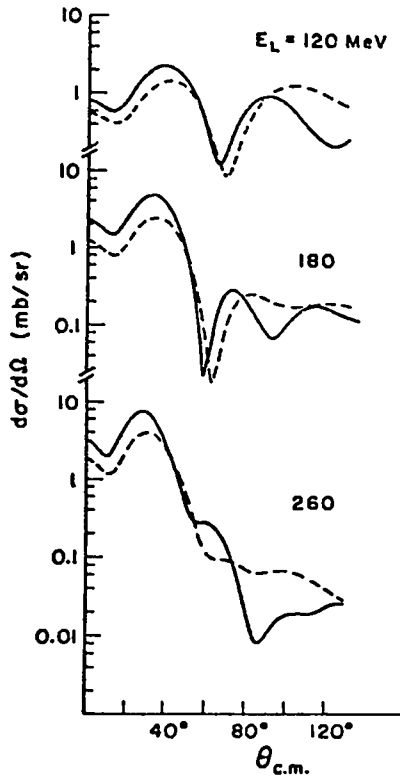
Figure 8

The sensitivity of pion-nucleus inelastic scattering to the location of the collective rotational form factor peak. The dashed curve is the inelastic differential cross section calculated using a form factor obtained by shifting the peak of the 2^+ form factor to a smaller radius [F(r)→ F(r + .5F)]. The solid curve is obtained using the original 2^+ form factor. The Landau-Tabakin off-shell extrapolation is used in constructing the pion-nucleus transition potential. (Figure taken from ref. 15).
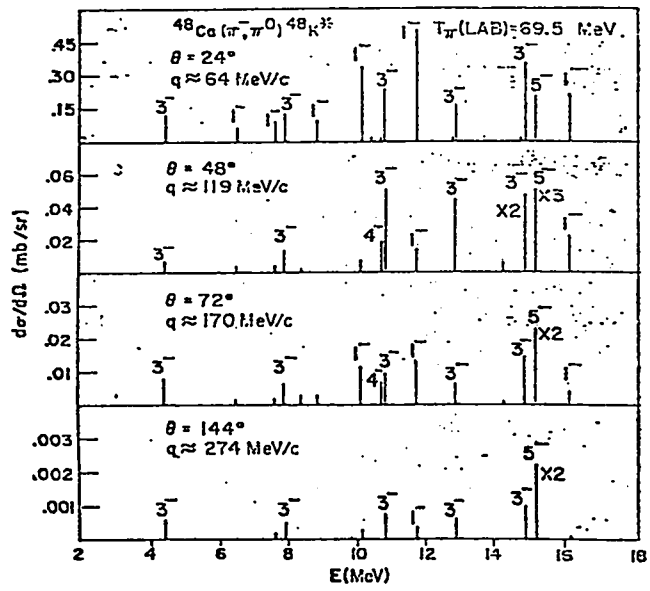
Figure 9

^{48}Ca (π^-,π^0) ^{48}K* differential cross sections for T_π(lab) = 69.5 MeV are shown as a function of the excitation energy of the final T = 5, ^{48}K* nucleus (relative to the ground state of ^{48}Ca) for four different scattering angles. All states shown have T = 5, only states with appreciable cross section are shown in the figure. (Figure taken from ref. 18).

of the uncertainties in the (π^-,π^0) reaction mechanism. The (π^-,π^0) reaction has the advantage over muon capture of allowing one to vary the momentum transfer delivered to the nucleus.

IV. COMPARISON WITH ELECTRON, PROTON, AND KAON RESULTS

Historically inelastic electron scattering has been a rich source of nuclear structure information. The electromagnetic probe has a well-known interaction with the nucleon. The interaction is weak and therefore inelastic scattering from the nucleus can be treated using the single photon exchange mechanism.[19] The electron interacts with the nuclear charge, convection current, and magnetization current densities. For medium energy electrons large momentum transfer implies large angle scattering. At large angles the transverse form factor dominates because it contains an extra $\tan^2 \theta/2$ factor missing from the longitudinal form factor. Since the neutron and proton magnetic moments are of different sign the isovector magnetic moment dominates the transverse multipole contribution and thus high spin T = 1 states dominate at large momentum transfer.[20] A typical experimental excitation spectrum is compared with the theoretical prediction in figure 10.[14] For our discussion today an important point is that at high momentum transfer the 6⁻, T = 1 state of ^{28}Si is predicted to dominate the nuclear response to the electron. For pions the 6⁻, T = 0 state would be the dominant spike. Thus in this regard the two probes yield complementary information.

Often, although the shape of the angular distribution is correctly given by the theory for inelastic electron scattering, the overall magnitude of the cross section may be off by factors of two. This is usually attributable to the use of approximate nuclear wavefunctions but is unclear for high spin states which may be affected, for example by exchange current contributions.
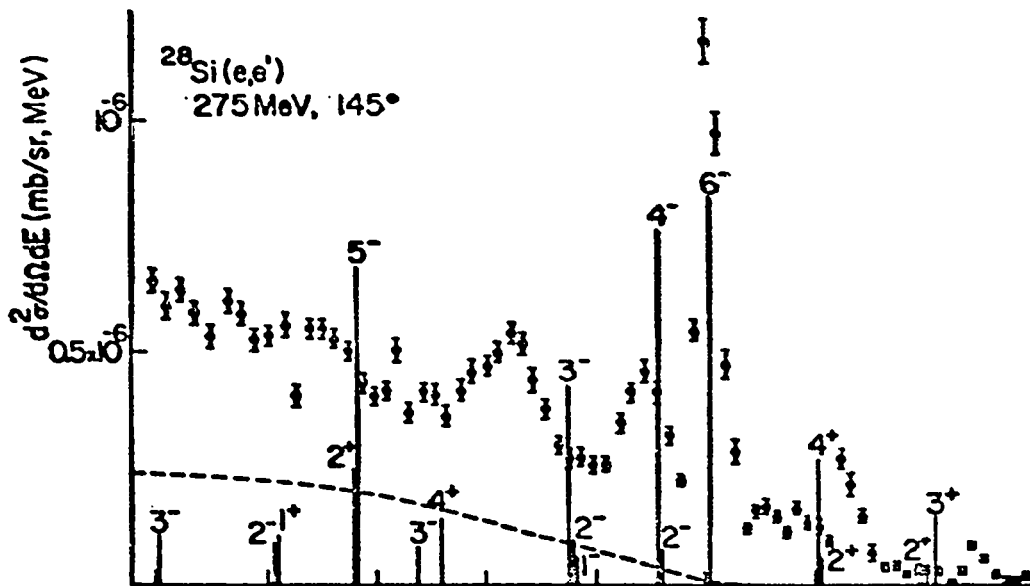
Fig. 10a   The cross section $d^2\sigma/d\Omega dE$ for inelastic electron scattering from ^{28}Si
at E_e = 275 MeV, θ = 145° unfolded for radiative processes. The non-
negligible cross sections predicted by the p-h model (T = 1 states)
for q = 525 MeV/c are shown as spikes (arbitrary overall scale). The
dashed line is the computed quasi-elastic spectrum;

Fig. 10b   Same as (a), except E_e = 200 MeV and theoretical cross sections
computed for q = 275 MeV/c. (Figure taken from ref. 14).

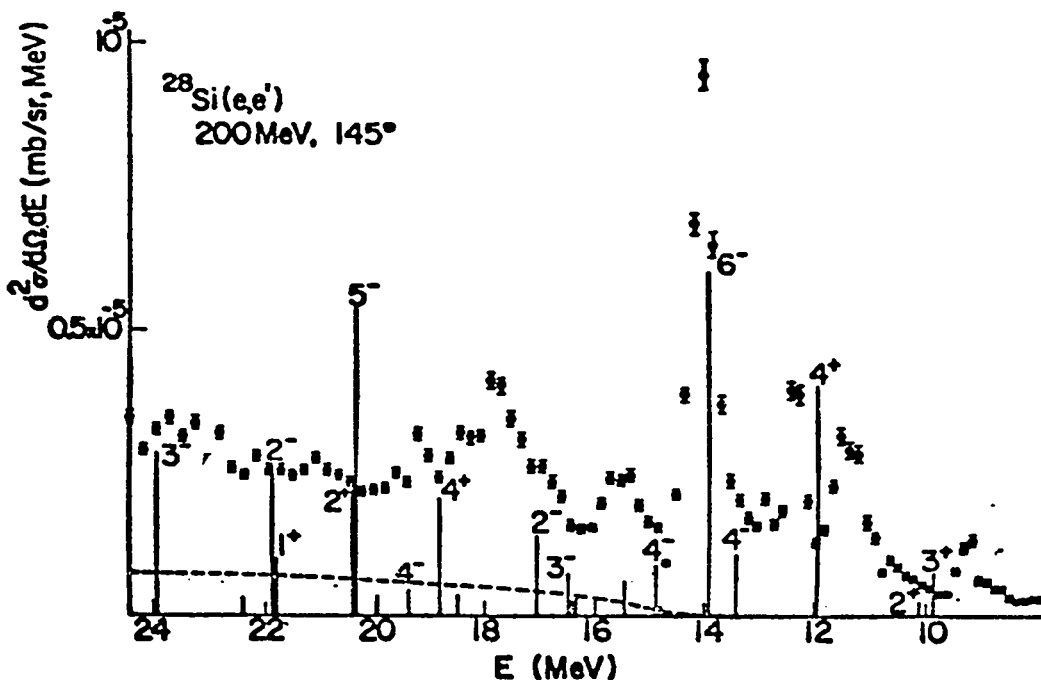One must be careful in pointing to a disagreement between theory and experiment at high momentum transfer as yielding evidence for short-range correlations. There are usually more complicated reaction mechanisms, such as multistep processes which can effect the large momentum transfer region. An example is provided by the $^{16}O(\gamma,p)^{15}N_{g.s.}$ results by Mathews et al[21]. The experimental angular distribution at large momentum transfer is not reproduceable by a one step theory using conventional nuclear wavefunctions. Londergan et al[22] have shown that the contribution of an intermediate Δ (1232) isobar mechanism (see figure 11) is quite large for photon energies above 150 MeV and at large momentum transfer. Inclusion of the mechanism results in qualitative agreement between theory and experiment without introducing a substantial high momentum tail in the nuclear wavefunction. Often it should be possible to differentiate between nuclear structure effects and reaction mechanism uncertainties by working at fixed energy loss and momentum transfer and varying the energy of the incoming electromagnetic probe. In general the reaction mechanism effects will be energy dependent while the structure effects are not.

Let us now turn our attention to other strongly interacting probes such as the proton and kaon (plus). The proton-proton total cross section is a rapidly decreasing function of energy from 20 to ~ 200 MeV (with a minimum of ~ 20 mb), the pion^{+}-proton total cross section is a rapidly increasing function of energy for low to medium energies reaching its peak of ~ 200 mb at 200 MeV, and, finally the kaon^{+}-proton total cross section is quite flat below 200 MeV and is relative weak, ~ 12 mb. The different energy dependences summarized above means that these three strong probes should have significantly different mean free paths in the nucleus as a function of energy and that the characteristic energy dependence of such complications as multistep processes should be quite different for each probe.
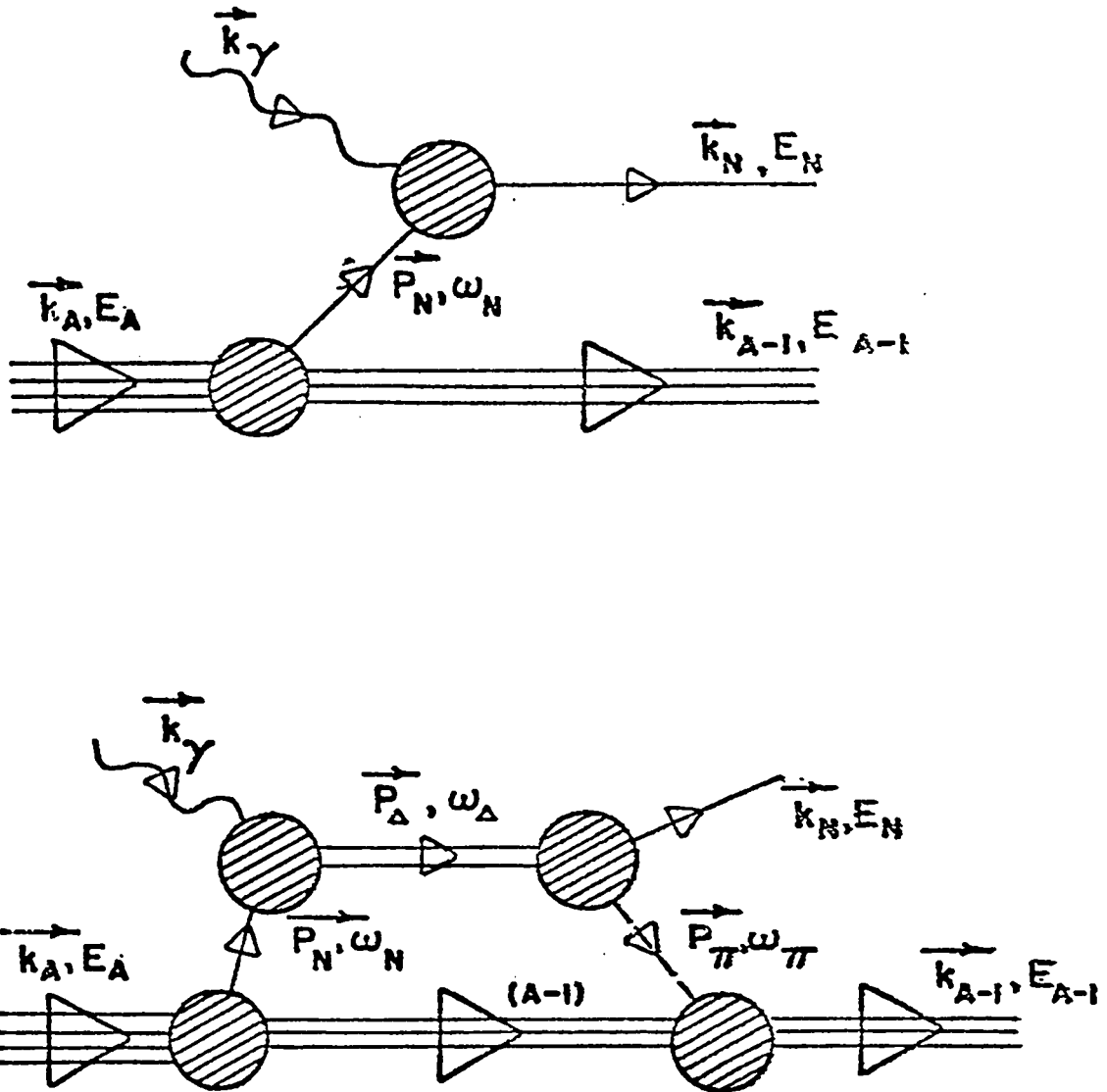
Fig. 11   Diagrammatic representation of two mechanisms for photoproton emission, with initial photon momentum $\vec{k}_\gamma$ and nuclear momentum $\vec{k}_A$ leading to final proton momentum $\vec{k}_N$ (a) Direct, or one-step, process (b) Two-step contribution due to isobar formation. A nucleon (proton or neutron) is converted by the photon into a Δ (1232), which propagates and then decays into a proton plus pion, the pion being absorbed by the residual nucleus. (Figure taken from ref. 22).

Proton inelastic scattering is complementary to both inelastic electron and pion scattering. Previous calculations[23] predicted that high spin T = 1 states would dominate the nuclear response to the proton at high momentum transfer (as in inelastic electron scattering). Recently Picklesimer and Walker have used the 50 - 400 MeV differential cross section and polarization data to obtain a nucleon-nucleon transition matrix[24]. The transition operator obtained is a sum of spin and isospin-dependent central, two-particle spin-orbit, and tensor complex local interactions with Yukawa radial shapes. The derived N - N transition operator can be employed in standard DWBA computer codes and is appropriate for use in medium energy proton-nucleus reaction calculations. It can be used in microscopic polarization predictions and is appropriate for explicitly calculating exchange effects. This interaction has been used to make predictions for inelastic proton scattering on ^{16}O and ^{28}Si.[24] In addition to again predicting that T = 1 high spin, spin-flip states would be strongly excited at large q, the recent calculations have predicted that through the exchange term (which we find to be quite important even at medium energies for large momentum transfer) high spin, spin-flip T = 0 states should also be important (as in inelastic pion scattering). Thus the proton results will be useful to compare with both inelastic electron and pion scattering. The part of the nucleon-nucleon interaction responsible for exciting these high spin states is a two particle tensor interaction which we find to have a relatively short range. Recent experimental results[25] from IUCF on $^{28}Si(p,p')$ $^{28}Si^{*}$ are shown in figure 12. The 6^{-}, T = 1 and 6^{-}, T = 0 states are seen to be dominant at high q as predicted. The excellent energy resolution available at IUCF was crucial in being able to identify these states. Calculations based on the DWIA and PWIA are in good agreement with the experimental results.

The kaon $^{(+)}$ - nucleus interaction is weak, short range, S wave, spin independent, and relatively independent of energy, at low to medium energies.[26]

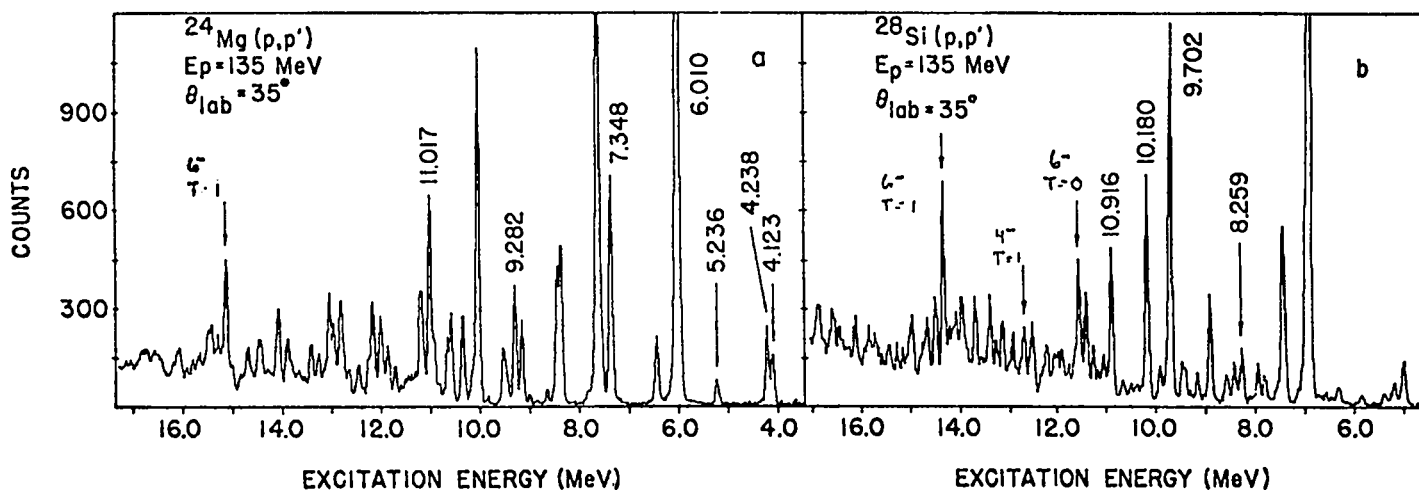Fig. 12 Representative spectra for the reactions ^{28}Si, ^{24}Mg(p,p') taken with 135 MeV protons. Some of the peaks used for energy calibration are identified by their excitation energies. The peaks labeled by arrows are high spin states predicted to be dominant at large momentum transfer by the DWIA. (Figure taken from ref. 25).

Thus the kaon-nucleus interaction should be simple and it should be an excellent probe for studying nuclear structure via inelastic scattering and knockout reactions. The facility at Brookhaven would seem to be an attractive laboratory in which to carry out such experiments. Because the elementary kaon (plus)-nucleon interaction, at low-medium energies, is independent of spin and only appreciable in the two particle isospin one channel, one predicts that $\Delta T = 0$, $\Delta S = 0$ states will dominate the nuclear response to kaon scattering at all momentum transfers (unlike any of the other probes discussed!) Thus many of the anticipated kaon results will also be complementary to results obtained with pion, electron and proton results.

CONCLUSIONS

We have used inelastic pion scattering as an easy example of how pion reactions can be used now to study nuclear structure and the pion-nucleus reaction mechanism in a separable manner by also using results available from other probes. High spin states that characteristically peak at large momentum transfer have been the focus of our study. Where experimental results are available such states have dominated the spectrum as predicted at large q and their angular distribution has been relatively easily obtainable. In the simple shell model these stretched high spin states are pure particle-hole states and thus are attractive to study from a nuclear structure perspective. The location in energy of high spin $T = 0$ and $T = 1$ states is attractive to determine because the $T = 1$, $T = 0$ energy difference can be related back to the spin and isospin dependence of the appropriate nucleon-nucleon G matrix. We have argued that often reaction mechanism effects can be differentiated from nuclear structure effects by working at fixed momentum transfer and projectile energy loss and varying the energy of the incoming probe. It was pointed out that the pion-, proton-,and kaon-proton elementary interactions have quite different energy

dependences and thus the associated multistep reaction mechanisms will also have a different energy dependence characteristic of the probe involved. At high momentum transfer pions appear to selectively excite high spin $T = 0$ states, electrons excite high spin $T = 1$ states, protons excite high spin $T = 1$ states through the direct term and high spin $T = 0$ states through the exchange term, and kaons (plus) excitè high spin (no spin-flip) $T = 0$ states. Thus the different probes complement each other nicely in both nuclear structure and reaction mechanism studies via inelastic scattering. Therefore we propose that such experiments (including polarization studies for the protons) should play an important role in medium energy facilities experimental programs. In order to ensure that the experiments needed to take advantage of the complementarity of the various probes are actually carried out (for a variety of reactions of which inelastic scattering is only a simple example) perhaps workshops or symposiums should take place that bring together active researchers at the various major facilities (and other interested researchers) with the expressed purpose of planning some major programs involving several of the medium energy probes.

REFERENCES

†   Work supported in part by the National Science Foundation.

1)   G.W. Edwards and E. Rost, Phys. Rev. Lett. 26 (1971) 785.

2)   D.A. Sparrow, Nucl. Phys. A276 (1977) 365.

3)   S.A. Dytman et al, Phys. Rev. Lett. 38 (1977) 1059.

4)   M. Thies, Phys. Lett. 63B (1976) 43.

5)   N.J. DiGiacomo et al, Phys. Lett. 66B (1977) 421.

6)   G. Brown and B. Jennings, Lectures at this Summer School and to be published.

7)   H.K. Lee and H. McManus, Nucl. Phys. A167 (1971) 257.

8)   T.-S.H. Lee and F. Tabakin, Nucl. Phys. A226 (1974) 253.

9)   A.T. Hess and J.M. Eisenberg, Nucl. Phys. A241 (1975) 493.

10)   M.K. Gupta and G.E. Walker, Nucl. Phys. A256 (1976) 444.

11)   L.A. Charlton, Phys. Rev. C8 (1973) 146.

12)   J.W. Donnelly and G.E. Walker, Ann. of Phys. 60 (1970) 209.

13)   I. Sick et al, Phys. Rev. Lett. 23 (1969) 1117.

14)   T.W. Donnelly et al, Phys. Lett. 32B (1970) 545.

15)   T.-S.H. Lee, Ph.D. thesis, University of Pittsburgh, (1974), unpublished.

16)   R.H. Landau, S.C. Phatak and F. Jabakin, Ann. of Phys. 78 (1973) 299.

17)   F. Binon et al, Nucl. Phys. B17 (1970) 168.

18)   M.K. Gupta, Ph.D. Thesis, Indiana University, (1976), unpublished.

19)   T. DeForest, Jr. and J.D. Walecka, Advan. Phys. 15 (1966) 1.

20)   T.W. Donnelly and G.E. Walker, Ann. of Phys. 60 (1970) 209.

21)   J.L. Mathews et al, Phys. Rev. Lett. 38 (1977) 8.

22)   J.T. Londergan, G.D. Nixon, and G.E. Walker, Phys. Lett. 65B (1976) 427.

23)   P.J. Moffa and G.E. Walker, Nucl. Phys. A222 (1974) 140; P.J. Moffa, Ph.D. thesis, Indiana University, (1974), unpublished.

24) A. Picklesimer and G.E. Walker, to be submitted for publication.

25) G.S. Adams et al, Phys. Rev. Lett <u>38</u> (1977) 1387.

26) G.E. Walker, to be submitted for publication.

SUMMER SCHOOL PARTICIPANTS

Kirk Allbright
University of Texas

John Allred
University of Houston

James Amann
Carnegie-Mellon

Hans Arnold
Instituus Boor Kern

Anthony Attard
University of Indiana

Andrew Bacher
Indiana University

B. L. G. Bakker
Amsterdam

Richard J. Barrett
LASL

Hans A. Bethe
Cornell University

Balram S. Bhakar
LASL

Christopher Wayne Bjork
University of Wyoming

Charles Bordner
University of Wyoming

Richard L. Boudrie
University of Colorado

Thomas Bowles
Argonne National Laboratory

David Bowman
LASL

Kenneth G. Boyer
University of Texas

Wilfred J. Braithwaite
University of Texas

Juliet Brosing
Florida State University

G. E. Brown
State University of New York

George R. Burleson
New Mexico State University

Robert Burman
LASL

R. F. Carlson
University of Redlands

Tuan W. Chen
New Mexico State University

Sidney A. Coon
University of Arizona

Martin Cooper
LASL

Wayne Cornelius
Texas A & M University

A. J. Cox
University of Redlands

C. L. Critchfield
LASL

Mike Devereux
New Mexico State University

Nick DiGiacomo
University of Colorado

D. C. Dodder
LASL

Radhameham Doss
Carnegie-Mellon

William Drogoset
Rice University

J. P. Egger
Neuchatel

Guy T. Emery
Indiana University

Werner Fabian
State University of New York

Sherman Frankel
University of Pennsylvania

Donald F. Geesaman
Argonne National Laboratory

David Giebink
University of Texas

J. Ginocchio
LASL

Paul Glodis
UCLA

Kazuo Gotow
Virginia Polytech. Institute

Steven J. Greene
University of Texas

R. H. Heffner
LASL

Richard G. Helmer
E G & G, Idaho

John Hoftiezer
Rice University

Roy Holt
Argonne National Laboratory

George Igo
LASL

H. E. Jackson
Argonne National Laboratory

Randolph H. Jeppensen
University of Montana

Mikkel Johnson
LASL

Nick King
LASL

David J. Ernst
Texas A & M University

Richard D. Felder
Bonner Nuclear Laboratory

William A. Friedman
University of Wisconsin

B. F. Gibson
LASL

Shalev Gilad
Tel-Aviv University

Charles Glashausser
LASL

Charles D. Goodman
Oak Ridge Laboratory

Charles M. Grassl
University of Wyoming

Wick Haxton
LASL

Leon Heller
LASL

Peter Herczeg
LASL

Kenneth Hogstrom
Cancer Research/Treatment Center (UNM)

Jozica Hudomalj-Gabithch
T. W. Bonner Nuclear Laboratory

Hikaru Inoue
Hiroshima University

Byron Jennings
State University of New York

Kenneth Johnson
Temple University

Arthur Kerman
MIT

W. M. Kloet
LASL

Rubin H. Landau
Oregon State University

Mel Leon
LASL

Steve Luckstead
Washington State University

Behzad Maghami
Florida State University

E. L. Mathie
University of British Columbia

William McHarris
Michigan State

Gerald A. Miller
University of Washington

R. Mischke
LASL

Murray Moinester
LASL

John Moses
LASL

Shoji Nagamiya
Lawrence Berkeley Laboratory

Ray Nix
LASL

G. Pauletta
UCLA

R. J. Peterson
University of Colorado

Philip Pile
Indiana University

Glen A. Rebka
University of Wyoming

Dennis Roeder
LASL

Al Rosenthal
University of Colorado

T. S. Harry Lee
Argonne National Laboratory

Jerry Lisantti
University of Idaho

Dave Madland
LASL

T. Masterson
University of British Columbia

Robert J. McCarthy
University of Arizona

Kirk McVoy
University of Wisconsin

Bob Miracky
LASL

Gordon L. Moake
Indiana University

Joseph Morganstern
SACLAY

Gordon S. Mutchler
T. W. Bonner Nuclear Laboratory

Koji Nakai
Lawrence Berkeley Laboratory

Y. Nogami
McMaster University

Charles F. Perdrisat
William & Mary University

Mark Pickar
Indiana University

W. Plumlee
UCLA

Robert P. Redwine
LASL

Philip G. Roos
University of Maryland

Prof. Dr. Erwin Rossle
University Freiburg, Germany

Ernest Rost
University of Colorado

Viktor Rostokin
Moscow Physics Eng. Institute

Norio Saito
Central Research Lab of Hitac

Scott Sandford
LASL

Ralph E. Segel
Northwestern University

Ryoich Seki
California State University

Joseph Sherman
Carnegie-Mellon

R. R. Silbar
LASL

Elton Smith
LASL

Greg Smith
University of Colorado

J. E. Spencer
LASL

Daniel Strottman
State University of New York

L. W. Swenson
Oregon State University

Michikatsu Takai
Hamamatsu Univ. School of Medicine

Willard Talbert
LASL

Henry A. Thiessen
LASL

Jim Thomas
LASL

Andrew M. Thomson
University of Minnesota

Marios Tsangarides
Indiana University

Tony Turkevich
University of Chicago

Vlado Valkovic
Rice University

Olin B. Van Dyck
LASL

R. VanWageningen
National Laboratory V.U.

Steve Verbeck
New Mexico State University

H. Verheul
Vrije University

E. Alan Wadlinger
University of Virginia

George Walker
Indiana University

Steven J. Wallace
University of Maryland

John B. Walter
University of Wyoming

Aaldert H. Wapstra
Inst. Kernphysisch Onderzoek

Weddigen
Ges. Fuer Kernforschung

William R. Wharton
Carnegie-Mellon

Charles Whitten
UCLA

Suzanne Willis
Yale University

Yoshihige Yamazaki
LASL

Mary Anne Yates-Williams
LASL

Stephen K. Young
LASL

Marco Zaider
LASL

Ben Zeidman
Argonne National Laboratory